

DTIC FILE COPY

①

SECURITY CLASSIFICATION OF THIS PAGE

REPORT DOCUMENTATION PAGE				Form Approved OMB No. 0704-0188	
1a. REPORT SECURITY CLASSIFICATION UNCLASSIFIED			1b. RESTRICTIVE MARKINGS NONE		
2a. SECURITY CLASSIFICATION AUTHORITY			3. DISTRIBUTION/AVAILABILITY OF REPORT APPROVED FOR PUBLIC RELEASE; DISTRIBUTION UNLIMITED.		
2b. C					
4. PE AD-A217 467			5. MONITORING ORGANIZATION REPORT NUMBER(S) AFIT/CI/CIA-88-197		
6a. NAME OF PERFORMING ORGANIZATION AFIT STUDENT AT UNIVERSITY OF MISSOURI-COLUMBIA		6b. OFFICE SYMBOL (If applicable)	7a. NAME OF MONITORING ORGANIZATION AFIT/CIA		
6c. ADDRESS (City, State, and ZIP Code)			7b. ADDRESS (City, State, and ZIP Code) Wright-Patterson AFB OH 45433-6583		
8a. NAME OF FUNDING/SPONSORING ORGANIZATION		8b. OFFICE SYMBOL (If applicable)	9. PROCUREMENT INSTRUMENT IDENTIFICATION NUMBER		
8c. ADDRESS (City, State, and ZIP Code)			10. SOURCE OF FUNDING NUMBERS		
			PROGRAM ELEMENT NO.	PROJECT NO.	TASK NO.
					WORK UNIT ACCESSION NO.
11. TITLE (Include Security Classification) (UNCLASSIFIED) EFFECTS OF THE MEASUREMENT CONFIGURATION ON THE SIMULATION OF LIGHTNING-AIRCRAFT INTERACTION					
12. PERSONAL AUTHOR(S) RANDY JOSEPH JOST					
13a. TYPE OF REPORT THESIS/DISSERTATION		13b. TIME COVERED FROM _____ TO _____		14. DATE OF REPORT (Year, Month, Day) 1988	
				15. PAGE COUNT 480	
16. SUPPLEMENTARY NOTATION APPROVED FOR PUBLIC RELEASE IAW AFR 190-1 ERNEST A. HAYGOOD, 1st Lt, USAF Executive Officer, Civilian Institution Programs					
17. COSATI CODES			18. SUBJECT TERMS (Continue on reverse if necessary and identify by block number)		
FIELD	GROUP	SUB-GROUP			
19. ABSTRACT (Continue on reverse if necessary and identify by block number)					
DTIC ELECTE D JAN 31 1990 S E					
90 01 31 013					
20. DISTRIBUTION/AVAILABILITY OF ABSTRACT <input checked="" type="checkbox"/> UNCLASSIFIED/UNLIMITED <input type="checkbox"/> SAME AS RPT. <input type="checkbox"/> DTIC USERS			21. ABSTRACT SECURITY CLASSIFICATION UNCLASSIFIED		
22a. NAME OF RESPONSIBLE INDIVIDUAL ERNEST A. HAYGOOD, 1st Lt, USAF			22b. TELEPHONE (Include Area Code) (513) 255-2259		22c. OFFICE SYMBOL AFIT/CI

© Copyright by Randy Joseph Jost 1988
All Rights Reserved

EFFECTS OF THE MEASUREMENT CONFIGURATION ON THE
SIMULATION OF LIGHTNING-AIRCRAFT INTERACTION

A Dissertation

Presented to
the Faculty of the Graduate School
University of Missouri-Columbia

Submitted in Partial Fulfillment
of the Requirements for the Degree of
Doctor of Philosophy

by

RANDY JOSEPH JOST, MSEE

Donald L. Waidelich

Dissertation Supervisor

August 1988



Accession For	
NTIS GRA&I	<input checked="checked" type="checkbox"/>
DTIC TAB	<input type="checkbox"/>
Unannounced	<input type="checkbox"/>
Justification	
By _____	
Distribution/	
Availability Codes	
Dist	Avail and/or Special
A-1	

EFFECTS OF THE MEASUREMENT CONFIGURATION ON THE
SIMULATION OF LIGHTNING-AIRCRAFT INTERACTION

by

Randy Joseph Jost, MSEE

Dr. Donald L. Waidelich

Dissertation Supervisor

ABSTRACT

Many factors affect the validity of results obtained during lightning simulation and testing. One influence is that due to the configuration of the test setup. Although there have been some attempts to define the magnitude of these configuration effects, there has not been a comprehensive investigation of them. This dissertation presents the results of a comprehensive investigation into the effects of the measurement configuration on the testing of aircraft with simulated lightning. An extensive series of experiments were carried out to characterize the effects of the configuration on the test results. The simulations were carried out using a simplified Lightning Test Object. Extensive measurements were taken using the swept frequency continuous wave, current injection, and shock-excitation methods for exciting the test object. Transfer functions of different measurement configurations using these methods were computed. A comparison of these transfer functions

shows that the effects of the measurement configuration can significantly affect the transfer function representing the measured system. A method is proposed whereby the effect of the measurement configuration can be eliminated or minimized. Results of the investigation are summarized and recommendations for further research are made. Removal of the configuration effects from the results should lead to more accurate measurements which can be used to further refine prediction techniques for lightning-aircraft interaction. The combination of more accurate prediction and simulation techniques will lead to better protection of aerospace platforms from the effects of lightning, while minimizing the penalties of that protection.

ACKNOWLEDGMENTS

The successful completion of a PhD program is due to many individuals, least of which is the author. In my own case, I owe thanks to many individuals for the completion of this effort. First and foremost, I owe a large debt, which may take forever to pay, to my wife, Vickie, and my children - Tom, Halie, Bradley and Emelia. They are the ones who sacrificed the many, many hours they could have had with their husband and father. I also owe much, if not everything, to my parents, whose dedication to the ideas of education, hard work and bettering oneself inspired me to do as much as I could, the best I could.

Although I appreciate the efforts of all the members of my PhD committee, special mention goes to two of the individuals. First, to my advisor, Dr. Donald L. Waidelich, whose example as an educator, scholar, and engineer has given me a goal to aim for. His patience and measured guidance throughout the seemingly interminable length of this effort is greatly appreciated. I also appreciate the help, guidance, and wisdom of Dr. Wes Sherman. In addition, I thank him for being an individual whose friendship has always stood out, like the sun in the storm clouds, and has been as strong and deep as the ocean. Despite what he says or thinks, he has ALWAYS been there when needed.

Thanks are due to Mr. Larry Walko and Captain Harry Burket of the Atmospheric Electrical Hazards Group, Flight Dynamics Laboratory, Air Force Wright Aeronautical Laboratories (AFWAL/FIESL). Thanks are also due to Art Serrano, Marty Risley, Jean Reazer, Vic McNier and Gary Webb of Technology/Scientific Services, Inc. These many individuals unselfishly contributed their time, efforts and suggestions to this research work, in the often unsung, but always important, support positions. Their efforts made it possible for this work to be accomplished in a timely manner, while facing severe budgetary and time constraints.

Mention must be made of Dr. John J. D'Azzo, chairman of the Department of Electrical Engineering at the Air Force Institute of Technology, and my many colleagues there. Their encouragement often kept me going when I needed a boost.

Thanks also to Dr. Brent M. Strong and Lt. Michael L. Martin. Your encouragement and aid kept me going.

Last, but most assuredly not least, an extra special thanks to Jim and Pat Hebert. Words alone can not express my appreciation to them. Thanks for the help, suggestions, encouragement and, most important, friendship. In those immortal words, that's one down and one to go!

TABLE OF CONTENTS

	Page
ABSTRACT	ii
ACKNOWLEDGMENTS	iv
LIST OF ILLUSTRATIONS	viii
LIST OF TABLES	xviii
LIST OF ACRONYMS	xix
 INTRODUCTION	 1
Motivation	4
Problem Statement and Scope	11
Assumptions	12
Approach	14
Dissertation Overview	15
 CHAPTER	
I. BACKGROUND	19
Overview	19
The Phenomenology of Lightning	19
Atmospheric Electricity Threats	34
Defining the Lightning Threat To Aircraft	37
Lightning-Aircraft Interaction Processes	46
The Effects of Lightning on Aircraft	53
II. MEASUREMENT OF ELECTROMAGNETIC LIGHTNING THREATS	76
Overview	76
Basic Instrumentation System	76
Measurement of Electromagnetic Quantities	85
Sensors for Lightning Measurement	97
Signal Transmission Lines	111
Signal Conditioning	115
Data Collection, Processing and Display	117

	Page
III. PREDICTION OF LIGHTNING INTERACTION WITH AIRCRAFT	124
Overview	124
The Lightning-Aircraft Interaction Process	127
Modeling of the Interaction Process	154
Models for Prediction of External Interaction Processes	157
Models for Prediction of Coupling Processes	180
Models for Prediction of Internal Interaction Processes	187
IV. LIGHTNING SIMULATION AND CONFIGURATION EFFECTS	198
Overview	198
Simulation of the Lightning-Aircraft Interaction Event	199
Lightning Simulation Waveforms	205
Simulator Design	214
Simulation Test Techniques	247
Simulation Test Techniques for Direct Effects Testing	249
Simulation Test Techniques for Indirect Effects Testing	251
Configuration Effects	265
V. GROUND LIGHTNING SIMULATION TEST RESULTS	283
Overview	283
CV-580 Airborne Test Program	284
Current Injection Tests	298
CV-580 Ground Simulation Tests	299
AFIT LTO Current Injection Tests	307
Swept-Frequency Continuous Wave Tests	325
The UH-60A Black Hawk SFCW Tests	325
The Boeing F-14A SFCW Tests	345
The AFIT LTO SFCW Tests	356
Shock-Excitation Tests	381
Early Work Using Shock-Excitation Test Techniques	381
AFIT LTO Shock-Excitation Tests	386
VI. SUMMARY, CONCLUSIONS AND RECOMMENDATIONS	414
APPENDIX I - Sensor Data Sheets	429
BIBLIOGRAPHY	452
VITA	468

LIST OF ILLUSTRATIONS

Figure		Page
I-1	Probable Charge Distribution in a South African Thunderstorm.	21
I-2	Stepped-leader Initiation and Propagation.	24
I-3	Return Stroke Initiation and Propagation.	24
I-4	Dart Leader and Subsequent Return Stroke.	27
I-5	Diagrammatic Representation of Lightning Model.	27
I-6	Stepped-Leader Attachment to an Aircraft.	31
I-7	Charging Processes Affecting Inflight Aircraft.	36
I-8	The Double-Exponential Waveform.	36
I-9	Single Stroke Threat Definition Waveforms.	43
I-10	Single Stroke Threat Definition Waveform Parameters.	44
I-11	Severe Threat Lightning Current Waveform.	45
I-12	Illustration of the Aircraft-Lightning Interaction Process.	45
I-13	Illustration of Typical Lightning Strike Zones, Large Aircraft.	54
I-14	Illustration of Typical Lightning Strike Zones, Small Aircraft.	55
I-15	Distribution of Materials in a F/A-18A Aircraft, Top View.	61
I-16	Distribution of Materials in a F/A-18A Aircraft, Bottom View.	62
I-17	Distribution of Materials in an AV-8B Aircraft.	63
I-18	Composite Structures on the Boeing 767.	64
I-19	The All Carbon Composite Lear Fan 2100.	64

Figure		Page
II-1	Basic Instrumentation System.	77
II-2	Electrically Small Electric Dipole Sensor In Free Space.	90
II-3	Electrically Small Magnetic Dipole Sensor In Free Space.	92
II-4	Electrically Small Inductive Current Sensor In Free Space.	94
II-5	Typical Dipole Sensor Configurations.	99
II-6	Hollow Spherical Dipole (HSD) D-dot Sensor.	99
II-7	Asymptotic Conical Dipole (ACD) D-dot Sensor.	101
II-8	Parallel Plate Dipole (PPD) E-Field Sensor.	101
II-9	Electric Field Mills.	104
II-10	Typical Circular Parallel Mutual-Inductance (CPM) Sensor Geometry.	106
II-11	I-dot One-turn Insertion Unit Current Sensor.	106
II-12	Current Shunt For Measurement of Current.	108
II-13	Distribution of Signals in a Multi-Gap Loop (MGL) B-dot Sensor.	108
II-14	Cylindrical Moebius Loop (CML) B-dot Sensor.	110
II-15	Attenuation of Coaxial Cable as a Function of Frequency.	113
II-16	Composite Waveform Derived from Three Recorders to Yield Data Spanning Several Time Bases.	119
III-1	Block Diagram of Lightning-Aircraft Interaction Process.	128
III-2	The Steps in the Lightning-Aircraft Interaction Process for Indirect Effects.	129

Figure		Page
III-3	Approximate Source and Termination Impedances for Inflight Lightning Strike.	131
III-4	Transmission Line Model of Lightning Channel and Aircraft.	133
III-5	Illustration of Coupling Mechanisms.	136
III-6	Most Common Coupling Mechanisms.	138
III-7	Magnetic Field Coupling Through Apertures.	140
III-8	Electric Field Coupling Through Apertures.	140
III-9	The Aperture Coupling Problem.	142
III-10	Illustration of an Unintentional Antenna as a Coupling Mechanism to the Aircraft Interior.	145
III-11	Example of Joint Resistance that Concentrates Current, Resulting in High IR Voltages.	145
III-12	Comparative Susceptibility of Common Devices to Energy Deposition.	155
III-13	Field Component Positions About the Unit Cell of the FD-TD Lattice.	155
III-14	A B-52 Model in a 30x30x30 THREDE Grid.	177
III-15	A B-52 Model in a 50x43x59 THREDE Grid.	178
III-16	Lumped Parameter Network Model Used for SGEMP Study of a FLTSATCOM Satellite.	181
III-17	Partial Circuit Model Representation for Composite Space Shuttle Vehicle Lightning Test.	182
IV-1	Voltage Waveforms A and B.	207
IV-2	Voltage Waveforms C and D.	207

Figure		Page
IV-3	Current Waveforms.	208
IV-4	Typical Double-Exponential Voltage Waveforms.	211
IV-5	Damped Sinusoidal Test Current Waveform.	213
IV-6	Simplified Single-Stage Impulse Generators.	216
IV-7	Transformed Generator Circuit for Laplace Analysis.	220
IV-8	Marx's Original Voltage Multiplication Circuits.	220
IV-9	Basic Circuit of a Four-Stage Impulse Generator.	226
IV-10	Circuits of a Four-Stage Impulse Generator.	227
IV-11	Illustration of the Four Microfarad, 200 Kilovolt Generator with Flat Ground Plane Return Path.	234
IV-12	Side View of a Flat Plate EMP Simulator.	234
IV-13	Coaxial Return Path Around the AFIT Lightning Test Object.	235
IV-14	Coaxial Return Path Around a CV-580 Aircraft.	236
IV-15	Quasi-Coaxial Return Path Systems.	238
IV-16	Coaxial/Conformal Return Path Around a UH-60A Helicopter.	239
IV-17	F-14A Return Path Arrangements.	240
IV-18	Effect of Return Path on Field Distribution Around Test Vehicle.	241
IV-19	Comparison of Induced Voltages Due to Various Conductor Arrangements.	246
IV-20	Lightning Simulation Test Configuration Used for Current Injection Technique.	253

Figure		Page
IV-21	Shock-Excitation Test Setup Used at McDonnell Aircraft Company.	256
IV-22	Block Diagram of the Swept Frequency Continuous Wave Instrumentation System.	260
IV-23	Swept Frequency Continuous Wave Instrumentation System Setup.	262
IV-24	AFIT Swept Frequency Continuous Wave Test Setup.	263
V-1	Sensor Locations on CV-580 Aircraft During the 1985 Data Gathering Season.	287
V-2	Illustration of the Techniques Used to Correct Sensor Data for Nonlinearity in the Measurement System.	290
V-3	Time-Domain Surface Current Waveforms Recorded by the Surface Current Sensors on the CV-580, During a Lightning Strike to the Aircraft Nose.	293
V-4	Lightning Strike to the Right Wing of the CV-580.	294
V-5	Transfer Functions at the Four Surface Current Sensors from the Right Wing Lightning Strike to the CV-580.	295
V-6	Injected Current Waveforms from the Pulse Simulation Unit, and Resulting Transfer Functions at the Left Wing Current Sensor.	302
V-7	Input Waveform and Response from Fast Rise Time Generator Using Coaxial Return Path.	304
V-8	Transfer Functions at the Four Surface Current Sensors. Results from the Fast Rise Time Generator and Coaxial Return Path.	305
V-9	Transfer Functions at the Four Surface Current Sensors. Results from the Fast Rise Time Generator and Flat Plate Return Path.	306
V-10	Current Injection Test Setup for AFIT Current Injection Tests with LTO.	311

Figure		Page
V-11	Unipolar, Double-Exponential 20kA Current Waveform Used in AFIT Current Injection Tests.	311
V-12	Representative Oscillatory Current Waveforms.	313
V-13	Sensor Locations During Current Injection Tests.	315
V-14	Block Diagram of the Data Acquisition System Used During the AFIT Lightning Simulation Tests.	317
V-15	20 kA Unipolar Current Injection Data, Solid Panel. (External Magnetic Field.)	318
V-16	20 kA Unipolar Current Injection Data, Solid Panel. (External Electric Field.)	320
V-17	External Magnetic Field Responses for Current Injection Tests, Solid Panel, Location A1.	321
V-18	External Electric Field Responses for Current Injection Tests, Solid Panel, Location A1.	322
V-19	Measurement System Used for the UH-60A SFCW Tests.	328
V-20	Illustration of Breakout Box Connections During the UH-60A SFCW Tests.	329
V-21	Representative Transfer Functions of Major UH-60A Measurement Components.	331
V-22	Measured Transfer Functions Resulting from the Application of the Threat Waveform to the UH-60A.	332
V-23	Measured Transfer Functions Resulting from the Application of the Threat Waveform to Measurement System Only.	333
V-24	Transfer Function from UH-60A SFCW Tests - Simulated Rotor-to-Wheel Strike Measured at CAP.	335

Figure		Page
V-25	Transfer Function from UH-60A SFCW Tests - Simulated Tail-to-Wheel Strike Measured at CAP.	336
V-26	Transfer Function from UH-60A SFCW Tests - Simulated Rotor-to-Wheel Strike Measured at GCU.	337
V-27	Transfer Function from UH-60A SFCW Tests - Simulated Tail-to-Wheel Strike Measured at GCU.	338
V-28	Defined MIL-STD-1757A Threat Waveform Used in UH-60A SFCW Tests.	340
V-29	Boeing Generator and Measurement System Used for the F-14A SFCW Tests.	347
V-30	Excitation Source for the Boeing F-14A SFCW Tests.	350
V-31	Results of Measurements Made Under a Graphite-Epoxy Panel on the F-14A.	352
V-32	Predicted Versus Measured Voltage Drop Across a Graphite-Epoxy Panel.	354
V-33	Predicted Versus Measured Voltage Transient on the FCSE Throttle Actuator Wire.	354
V-34	Basic Test Setup Used During AFIT SFCW Tests.	357
V-35	Sensor Locations Used in AFIT LTO SFCW Tests.	359
V-36	SFCW Field Measurement on LTO With Solid Panel.	361
V-37	Various Coaxial Return Path Configurations Used in AFIT SFCW Tests.	363
V-38	SFCW Transfer Function of Magnetic Field Measured With Configuration Depicted in Figure V-37a.	364
V-39	SFCW Transfer Function of Magnetic Field Measured With Configuration Depicted in Figure V-37b.	365

Figure		Page
V-40	SFCW Transfer Function of Magnetic Field Measured With Configuration Depicted in Figure V-37c.	366
V-41	SFCW Transfer Function of Magnetic Field Measured With Configuration Depicted in Figure V-37d.	367
V-42	Configurations Used to Make SFCW Measurements on LTO While in Shock-Excitation Configurations.	370
V-43	SFCW Transfer Functions Made With LTO and Solid Panel.	371
V-44	SFCW Transfer Functions Made With LTO and Composite Panel #1.	373
V-45	SFCW Transfer Functions Made With LTO and Composite Panel #2.	374
V-46	SFCW Transfer Functions Made With LTO and No Panel, Aperture Down.	375
V-47	SFCW Transfer Functions Made With LTO and No Panel, Aperture Up.	376
V-48	Comparison of SFCW Transfer Functions Made With LTO Terminated With Open, and Using Two Composite Panels.	378
V-49	Comparison of SFCW Transfer Functions Made With LTO Terminated With Open, and Using Solid and Composite Panels.	379
V-50	Comparison of SFCW Transfer Functions Made With LTO Terminated With Open, and Using No Panels in Aperture.	380
V-51	Relationship of Changes in Electrical Field to Arc Attachment Sequence.	382
V-52	Comparison of Electric Field, Induced Voltage and Driving Current for the Double Arc Case.	384
V-53	Comparison of Electric Field, Induced Voltage and Current on the Cylinder.	385
V-54	Basic AFIT Shock-Excitation Test Setup.	388

Figure		Page
V-55	Sensor Locations for Shock-Excitation Tests.	391
V-56	Typical Shock-Excitation Responses.	393
V-57	External B-Dot Sensor Shock-Excitation Response for Solid Panel Configuration.	395
V-58	Resulting Magnetic Field Calculated From the Response of Figure V-57.	395
V-59	Magnetic Field Lines Around LTO Due to Current Flowing on the Cylinder.	397
V-60	External Electric Field Response of LTO With Solid Panel Due to Shock-Excitation.	399
V-61	External Magnetic Field Response of LTO With Solid Panel Due to Shock-Excitation.	399
V-62	External Magnetic Field Transfer Function of LTO With Solid Panel Due to SFCW Excitation.	400
V-63	External Magnetic Field Transfer Function of LTO With Solid Panel Due to 20 kA Unipolar Current Pulse Excitation.	403
V-64	External Magnetic Field Transfer Function of LTO With Solid Panel Due to 20 kA Oscillatory Current Pulse Excitation.	404
V-65	External Magnetic Field Transfer Function of LTO With Solid Panel Due to 100 kA Oscillatory Current Pulse Excitation.	405
V-66	External Magnetic Field Transfer Function of LTO With Solid Panel Due to Shock-Excitation.	406
V-67	External Electric Field Transfer Function of LTO With Solid Panel Due to 20 kA Unipolar Current Pulse Excitation.	407

Figure		Page
V-68	External Electric Field Transfer Function of LTO With Solid Panel Due to 20 kA Oscillatory Current Pulse Excitation.	408
V-69	External Electric Field Transfer Function of LTO With Solid Panel Due to 100 kA Oscillatory Current Pulse Excitation.	409
V-70	External Electric Field Transfer Function of LTO With Solid Panel Due to Shock-Excitation.	410

LIST OF TABLES

Table	Page
I-1. Data for a Normal Cloud-to-Ground Lightning Flash Bringing Negative Charge to Ground	26
I-2. Typical Values for a Multi-Stroke Lightning Event	40
V-1. Current Pulse Characteristics	348

LIST OF ACRONYMS

Acronym		Page
ACD	- Asymptotic Conical Dipole Sensor	100
AEHP/ADP	- Atmospheric Electricity Hazards Protection / Advanced Development Program	39
AFIT	- Air Force Institute of Technology	14
AFWAL	- Air Force Wright Aeronautical Laboratories	284
AFWL	- Air Force Weapons Laboratory	85
CAP	- Caution Advisory Panel	334
CML	- Cylindrical Moebius Loop Sensor	107
CPM	- Circular Parallel Mutual-Inductance Sensor	103
DNA	- Defense Nuclear Agency	345
DFT	- Discrete Fourier Transform	330
EFIE	- Electric Field Integral Equation	166
EMC	- Electromagnetic Compatibility	187
EMI	- Electromagnetic Interference	59
EMP	- Electromagnetic Pulse	9
FAA	- Federal Aviation Administration	214
FD	- Finite Difference	172
FDTD	- Finite Difference Time-Domain	172
FEM	- Finite Element Method	191
FFT	- Fast Fourier Transform	276
FRG	- Fast Rise Time Generator	301
GCU	- Ground Control Unit	334
GTD	- Geometrical Theory of Diffraction	191

Acronym		Page
HP	- Hewlett-Packard	346
HSD	- Hollow Spherical Dipole Sensor	100
IEE	- Institution of Electrical Engineers	3
IEEE	- Institute of Electrical and Electronics Engineers	2
LPN	- Lumped Parameter Network	179
LRU	- Line Replaceable Unit	334
LTA	- Lightning Transient Analysis	251
LTO	- Lightning Test Object	14
MFIE	- Magnetic Field Integral Equation	167
MGL	- Multi-Gap Loop Sensor	107
MMIC	- Monolithic Microwave Integrated Circuits	153
MOM	- Method of Moments	168
NASA	- National Aeronautics and Space Administration	15
NOAA	- National Oceanic and Atmospheric Administration	175
NEMP	- Nuclear Electromagnetic Pulse	41
PPD	- Parallel Plate Dipole Sensor	102
PSU	- Pulse Simulation Unit	300
RFI	- Radio Frequency Interference	9
SAE	- Society of Automotive Engineers	3
SEM	- Singularity Expansion Method	185
SFCW	- Swept Frequency Continuous Wave	14
SGEMP	- System Generated Electromagnetic Pulse	180
VHSIC	- Very High Speed Integrated Circuit	67

INTRODUCTION

Lightning is a commonplace, everyday phenomenon with which all people are familiar. It is a phenomenon that was recognized and recorded in ancient times in the art and literature of myth. Lightning has always been recognized as a phenomenon associated with great power. The ancient Greeks considered their pantheon of gods to be headed by Zeus, the god of lightning.

By the early 1700's, several investigators were coming to the conclusion that there was a similarity between lightning and the electric sparks produced by experiments in electricity. In 1743, Benjamin Franklin began his investigations and experiments on the subject of electricity. The publication in 1751 of his book "Experiments and Observations on Electricity" contains Franklin's conclusion that lightning and electricity are the same phenomenon. He is also known as the inventor of the lightning rod, the first lightning protection system.

Over the ensuing years work was carried out concerning the phenomenology of lightning and its origin. Also, work was taking place to apply this knowledge to the protection of property and life, much of it based upon Franklin's pioneering efforts with lightning rods. Yet, in a 1941 paper on the lightning discharge, Bruce and

Golde [1941] made the statement that

The power engineer has become aware of many investigations of lightning phenomena carried out independently by physicists and meteorologists. A survey of the relevant, very extensive, literature shows, however, that very little attempt has been made to correlate the data of various authors and of different methods of investigation or to translate the results of these investigations into terms applicable to the problem confronting the engineer.

Today, this is not a true statement. Shortly after this article was published, a flood of articles appeared addressing this point, not only with respect to power engineering, but other areas of engineering also.

Consider the area of power engineering. The results of an eight year study of lightning currents and protection against them for transmission systems were published by Hansson and Waldorf in 1944. A few of the notable studies on the interaction of lightning with power systems include those by Golde [1945, 1954] and Griscom et al. [1965]. In 1975 the IEEE published a bibliography of publications pertaining to lightning protection [IEEE, 1975]. In fact, in one publication alone, the IEEE Transactions on Power Apparatus and Systems, there were 63 lightning-related articles in the years 1975-1984. Good review articles on lightning protection of electrical power systems are given by Whitehead [1977] and Rusck [1977].

The power industry has invested much time and money in investigating the interaction of lightning with power generation and distribution systems, and developing protection schemes against the destructive effects of lightning. In addition, many organizations including the IEEE, SAE, IEE and others have devoted much effort to providing adequate standards for lightning protection of transmission systems.

The power industry is not alone in worrying about the effects of lightning. For instance, the telecommunications industry is concerned with many of the same problems as the power industry. The protection of overhead lines and underground cables is as important to the phone company as it is to the power company. There are some differences, because the impedances of the phone lines limit the currents conducted on them. However, signal interference and noise are more important in a communication system. In addition, the line equipment tends to be more sensitive to large, transient signals. Also, the broadcast industry uses some of the largest lightning rods known to exist: broadcast towers for radio and television antennas. Boyce [1977] gives a good overview on the protection of telecommunications systems from lightning.

The space program is concerned not only with the direct impact of lightning on its vehicles and equipment, but also with lightning-like effects due to related phenomena. For instance, a series of conferences, jointly sponsored by the Air Force and NASA, were held in the mid 70's through the early 80's concerning the topic of spacecraft charging [1976, 1978, 1980, 1982, 1983] and its effects on space systems. This charging is analogous to the effect of corona discharge, also known as St. Elmo's fire.

These are just a few representative industries that are concerned about the hazards of lightning and related phenomena. This dissertation will concentrate on the lightning threat to aircraft and methods that have been developed to model, predict and simulate that threat.

Motivation

Lightning poses an increasingly dangerous threat to future military and commercial aircraft and comprehensive proven lightning qualification test techniques are necessary to ensure the safety of flight. A variety of test analysis, simulation, and prediction techniques have been developed, but very little has been done to investigate or validate their effectiveness. Lightning presents a formidable threat to present and future

aerospace vehicles. A look at past Air Force lightning strike experiences emphasizes the danger lightning poses to aircraft. Corn reports the following U.S. Air Force statistics as of February 1979 [Corn, 1979].

"More than half of all Air Force weather-related aircraft mishaps are caused by lightning strikes. The USAF financial loss incurred in such mishaps exceeds 21 million dollars in the past five years, and includes two aircraft with eight lives in 1978 alone. In the past ten years seven USAF aircraft losses have been confirmed as lightning-related, two others ascribed to lightning as a likely cause, and over 150 serious mishaps reported. Imputed mechanisms include pilot disorientation and instrument failure (F101, F106), flight control failure after high current penetration (F-111F), fuel tank explosion, dual engine flameout with electrical failure (F-4), fuel tank burn-through and explosion (C-130E), and failure of unprotected nonmetallic rotor blades (HH-33). A total of 773 documented USAF lightning strikes were reported in this period. A probable lightning-associated fuel ignition caused the loss of an Imperial Iranian Air Force 747 aircraft on 9 May 1976 near Madrid, Spain."

Similar reports of lightning strike experience and lightning-caused mishaps to both military and commercial aircraft are given by Fisher and Plumer [1977], Clifford [1980], Rasch and Glynn [1984], and Corbin [1984].

Lightning research has typically been performed in three arenas: Lightning characterization (phenomenology), lightning susceptibility testing (analysis, simulations, and predictions) and hardening techniques (protection). Phenomenology considers the origin of the threat, while the second of these considers lightning in terms of the threat that it poses. One of the important end products

of the characterization and susceptibility testing research is better protection methods for aerospace vehicles.

Lightning produces two different types of effects when it interacts with an aircraft, missile, satellite or some other platform or object: direct effects and indirect effects. Direct effects include those associated with pitting and burning which can cause loss of structural integrity or catastrophic fuel tank explosions. Indirect effects are those which are electromagnetically induced, such as voltage and current transients on flight critical avionics systems. To understand and protect against these potentially harmful effects, many studies on how lightning interacts with commercial and military vehicles have been carried out. The importance of these studies is emphasized by considering some of the factors that motivated the initiation of these studies.

For commercial aircraft, lightning is an important flight consideration. Commercial aircraft usually avoid bad weather if possible, but often that is not possible because of schedules and changing weather patterns. Two general trends in commercial aviation have increased the interest in protection from lightning's effects. The first of these is the increasing use of composite materials in aircraft construction [Leonard and Mulville, 1980]

and the second is the on-going development in advanced aircraft flight control systems.

Most of the current commercial fleet consists of all metal aircraft. However, composite structures are desirable because of weight savings. This can translate directly into cost savings due to increased cargo weight that can be carried, or reduced fuel consumption. Metal aircraft skins provide substantial shielding, and they are inherently better protected from lightning's indirect effects and more resistant to its direct effects. Many experts believe that aircraft with metal skins are adequately protected and that current design procedures are adequate for them [Corbin, 1984]. Composite structures are less resistant to both direct and indirect effects. They are more susceptible to burning, pitting, and delamination resulting from direct lightning strikes. They provide additional avenues for energy from lightning to couple to the aircraft interior because of diffusion through the skin and the greater difficulty of obtaining a good bond between joints, panels, etc. [Blake and Corbin, 1980].

A second area of concern is raised because of the increased use of digital flight control and avionics systems. New aircraft are very dependent upon digitally based systems. For instance, older systems used hard-

wired flight control systems. These were relatively immune to indirect effects. Newer systems use computers as integral parts of flight control systems. These systems are susceptible to logic upset from indirect effects. Communication and navigation systems have the same problem. With the increased emphasis on systems sharing computer resources, such as bus structures, central processing units, and memories, there is the possibility for upset in one system to affect other systems.

In military aircraft, all of the above factors are present, and several additional factors are of concern. Not only are composite structures important for future aircraft, but extensive retrofit of composite components is being considered to keep current planes flying longer. In digital flight control systems and avionics there are the same considerations as with commercial aircraft. In addition, there is a premium on high performance, which requires many specialized systems with varying sensitivities to digital upset.

Additional military requirements include all weather capability and large numbers of flights in short periods of time. Unique mission requirements raise the possibility of having to fly regardless of the minor damage that might be caused by lightning. Also, military

aircraft contain specialized equipment, such as electronic countermeasures (ECM) gear, weapons systems with electro-triggered explosives, etc. There are many types of aircraft and each requires balanced protection from lightning, as well as radio frequency interference (RFI) and electromagnetic pulse (EMP) effects. This protection does not come free. There are costs in terms of money, weight, and performance, and these costs must be balanced against the need for adequate protection of the crew and cargo of aerospace vehicles.

Finally, there are applications to other areas such as protection of ground equipment, vehicles, and structures. Lightning studies can enhance our basic knowledge of the lightning interaction event and provide for protecting objects from its damaging effects.

In the study of lightning interaction with objects there is difficulty in using real lightning for studies. It is not possible to schedule lightning strikes on demand, or to always have a test object ready for a lightning strike. Since the occurrence of lightning is a "random event," and the voltage and current levels produced by natural lightning strikes are statistically distributed, there is a problem of repeatability and verification to establish the validity of results. Finally, the processes and mechanisms of natural lightning

are still areas of active characterization research.

One active area of lightning characterization research is to determine how the measurement configuration affects the measurement results. Much of the statistical database used for lightning characterization is based on measurements obtained from tall metal towers. Rustan and Axup [1984] and Melander [1984] have shown that the characterization of the tower affects the results, and hence the validity, of the measurements taken. These effects must be considered for the results to be valid for comparison with data taken in other locations around the world. Because of these factors, it has been recognized that there is a need for accurate simulations of the effects of the lightning event and its interactions with objects under test. This need is especially critical in the area of lightning protection, and verification of that protection, as well as setting the standards to be used for that protection [Clifford et al., 1982].

Many techniques have been developed to analyze, simulate and predict the lightning-aircraft interaction event. However, little has been done to characterize configuration simulation effects and to investigate how to relate ground simulation to the actual airborne event. Most investigations in the past have been satisfied to create a uniform field distribution around the aircraft

through the use of a return path. It was felt that this would be a sufficiently accurate representation of the actual airborne event or at least would give conservative results. Yet, the requirement of providing necessary protection at minimum expense demands a more precise knowledge of the lightning-aircraft interaction event. It is only by having and using this knowledge that decisions can be reached that properly optimize the tradeoffs between cost and safety.

Problem Statement and Scope

The purpose of this dissertation is to examine the current methods of simulating lightning interaction with aircraft and to better define how the lightning test set-up configuration affects the accuracy of the transient circuit measurements and test results. In addition, we wish to investigate how to remove configuration effects so that ground simulation data can be related to actual lightning strike interactions. Several methods of predicting the response of an aircraft to a lightning strike are examined to determine their sensitivity to configuration effects.

There are several problems with the current state of lightning simulation. This dissertation, is limited to the examination of the simulation of lightning interaction

with aircraft. The problems can be characterized by how accurately the ground simulation data relate to the actual airborne event. Other areas to be examined include: (1) What parameters of the test configuration affect the accuracy of the results? (2) How can the responses of measurement systems be corrected to give a true representation of the response of the aircraft to a simulated lightning strike? (3) Which assumptions commonly made in lightning simulation testing are true and how do these assumptions affect the validity of the simulation test results? (4) How can current simulation techniques be improved?

Assumptions

The primary motivation for this dissertation is that ground simulations, as usually performed today, are not an accurate representation of the airborne lightning-aircraft interaction event. The circuit transient measurements made on the ground are not identical to those that are measured during the airborne event. This is primarily attributed to the configuration effects of the simulator and measurement setup used during ground-based simulation tests.

A motivating assumption for this dissertation is that it may be possible to analytically relate the ground

simulation to actual airborne events. This may be possible by the proper application of analysis techniques to remove the effects of the measurement configuration, leaving only the actual interactions that would be observed during inflight measurements.

The assumption most commonly made in lightning simulation tests is linearity. Most of the results of research in current literature are based upon linearity arguments. This is especially true with regard to lightning qualification and protection specifications development. An important determination to be made is when the assumption of linearity is valid. This dissertation will utilize the linearity of Maxwell's equations [Jackson, 1975]. What must be determined is the validity of the direct linear scaling of current and voltage transient levels, as well as their derivatives, dI/dt and dE/dt . This is a matter of concern because of the wide variance between the lower simulation current and voltage levels commonly used and the higher threat levels actually experienced by aircraft struck by severe lightning. Linear extrapolation is used to relate the results of low level simulation tests to the much higher levels encountered in the actual severe lightning threat. Another matter for investigation is a determination of how much extrapolation is valid. While an extrapolation of 2:1 may be valid, there is no assurance that an

extrapolation of 10:1 or 100:1 will give correct results.

To concentrate on the configuration effects and their influences on the analysis, simulation, and prediction of aircraft lightning interactions, a simplified lightning test object (LTO) was built by the Air Force Institute of Technology (AFIT) machine shop. Thus, to perform the research in this dissertation, two assumptions with regard to the test object are required. The first assumption is that the LTO shape and dimensions are sufficiently related to that of the fuselage of an aircraft that conclusions drawn from the study of the LTO are representative of what can be said about an actual aircraft. The other assumption is that the LTO is sufficiently symmetrical to allow measurements over part of the structure to be representative of measurements on other parts.

Approach

The general approach of the dissertation work was to investigate and compare the results of several methods of analyzing, predicting, and simulating lightning interaction with an aircraft. Analysis methods focused on those based on the direct application of Maxwell's equations to the electromagnetic interaction problem. Simulation methods examined were the Swept Frequency Continuous Wave (SFCW), Current Injection, and Shock-

Excitation techniques. Methods for predicting lightning's airborne interactions with aircraft were investigated. Finally, these results were compared with data measured from actual inflight lightning strikes to specially instrumented CV-580 and NASA F-106 lightning research aircraft, to help determine the validity of the modeling and simulation techniques.

Dissertation Overview

In Chapter I the necessary background on the lightning threat and its definition are covered. In Chapter II, methods of measuring lightning level electromagnetic quantities are developed. Methods of lightning interaction analysis and prediction are examined in Chapter III. In Chapter IV a detailed examination of lightning simulation and configuration effects is presented. This chapter contains a description of procedures that may be employed to remove the configuration effects from lightning simulation tests. Experimental work with the lightning simulation test object is reported and the results of using these correction techniques with several experimental configurations is given in Chapter V. Chapter VI summarizes the conclusions and accomplishments resulting from this research and includes a list of recommendations for further work in this area.

REFERENCES - INTRODUCTION

C.E.R. Bruce and R.H. Golde, "The Lightning Discharge," Journal of Institution of Electrical Engineers, Part II, Vol. 88, 1941, pp. 487-520.

E. Hansson and S.K. Waldorf, "An Eight-Year Investigation of Lightning Currents and Preventive Lightning Protection on a Transmission System," Transactions of the American Institute of Electrical Engineers, Vol. 63, May 1944, pp. 251-258.

R.H. Golde, "The Frequency of Occurrence and the Distribution of Lightning Flashes to Transmission Lines," Transactions of the American Institute of Electrical Engineers, Vol 64, 1945, pp. 902-910.

R.H. Golde, "Lightning Surges on Overhead Distribution Lines Caused by Indirect and Direct Lightning Strokes," Transactions of the American Institute of Electrical Engineers, Vol 73, Part III-A, June 1954, 437-447.

S.B. Griscom, R.W. Caswell, R.E. Graham, H.R. McNutt, R.H. Schlomann and J.K. Thorton, "Five-Year Field Investigation of Lightning Effects on Transmission Lines," IEEE Transactions on Power Apparatus and Systems, PAS-84, No. 4, April 1965, pp. 257-280.

IEEE Power Engineering Society, Substations Committee, Transmission Substation Subcommittee, "Bibliography of Publications Pertaining to Lightning Protection," IEEE Transactions on Power Apparatus and Systems, PAS-94, No. 4, July/August, 1975, pp. 1241-1247.

E.R. Whitehead, "Protection of Transmission Lines," in Lightning. Vol. 2: Lightning Protection, ed. R.H. Golde, (New York: Academic Press, 1977), pp. 697-745.

S. Rusck, "Protection of Distribution Lines," in Lightning. Vol. 2: Lightning Protection, ed. R.H. Golde, (New York: Academic Press, 1977), pp. 747-771.

C.F. Boyce, "Protection of Telecommunication Systems," in Lightning. Vol. 2: Lightning Protection, ed. R.H. Golde, (New York: Academic Press, 1977), pp. 793-829.

Spacecraft Charging Technology - 1976, NASA Technical Memorandum TM-X-73537, U.S. Air Force Academy, Colorado Springs, CO, October 27-29, 1976.

Spacecraft Charging Technology - 1978, NASA Conference Publication 2071, U.S. Air Force Academy, Colorado Springs, CO, October 31 - November 2, 1978.

Spacecraft Charging Technology - 1980, NASA Conference Publication 2182, U.S. Air Force Academy, Colorado Springs, CO, November 12-14, 1980.

Spacecraft Charging - Proceedings of the Air Force Geophysics Laboratory Workshop on Natural Charging of Large Structures in Near Earth Polar Orbit, AFGL-TR-83-0046, September 14-15, 1982.

Spacecraft Environmental Interaction Technology, NASA Conference Publication 2359, U.S. Air Force Academy, Colorado Springs, CO, October 4-6, 1983.

P.B. Corn, "Lightning as a Hazard to Aviation," Proceedings of American Meteorological Society's 11th Conference on Severe Local Storms, Kansas City, MO, October 2-5, 1979, pp. 301-306.

F.A. Fisher and J.A. Plumer, Lightning Protection of Aircraft, NASA Reference Publication 1008, October 1977. Chapter 3.

D.W. Clifford, "Aircraft Mishap Experience From Atmospheric Electricity Hazards," AGARD Lecture Series No. 110, Atmospheric Electricity-Aircraft Interaction, AGARD LS-110, June 1980, pp.2-1--2-17.

N.O. Rasch and M.S. Glynn, "Lightning Interaction with Commercial Air Carrier Type Aircraft," Proceedings of 1984 International Aerospace and Ground Conference on Lightning and Static Electricity, Orlando, FL, June 26-28, 1984, pp.21-1--21-11.

J.C. Corbin, "The Risk Factor in Aircraft Lightning Protection," Proceedings of 1984 International Aerospace and Ground Conference on Lightning and Static Electricity, Orlando, FL, June 26-28, 1984, pp.20-1--20-5.

R.W. Leonard and D.R. Mulville, "Current and Projected Use of Carbon Composites in United States Aircraft," AGARD Conference Proceedings No. 283, AGARD CP-283, June 1980, pp.1-1--1-19.

C.L. Blake and J.C. Corbin, "Electrical/Electromagnetic Concerns Associated with Advanced Composite Materials in Aerospace Systems," AGARD Conference Proceedings No. 283, AGARD CP-283, June 1980, pp.20-1--20-7.

P. Rustan and P. Axup, "Analysis of Lightning Current Measurements," Proceedings of 1984 International Aerospace and Ground Conference on Lightning and Static Electricity, Orlando, FL, June 26-28, 1984, pp.24-1--24-7.

B.G. Melander, "Effects of Tower Characteristics on Lightning Arc Measurements," Proceedings of 1984 International Aerospace and Ground Conference on Lightning and Static Electricity, Orlando, FL, June 26-28, 1984, pp.34-1--34-12.

D.W. Clifford, K.E. Crouch and E.H. Schulte, "Lightning Simulation and Testing," IEEE Transactions on Electromagnetic Compatibility, EMC-24, No. 2, May 1982, pp.209-224.

J.D. Jackson, Classical Electrodynamics, 2nd ed., John Wiley and Sons, New York, 1975, pp.10-13.

CHAPTER I

BACKGROUND

Overview

This dissertation requires a basic understanding of the lightning event, the threat it poses to aircraft and how this threat has been simulated in ground lightning effects testing. This chapter will present the necessary background on the phenomenology of lightning and discuss the hazards to aircraft due to atmospheric electricity. The lightning event is characterized and the threat posed by lightning's interaction with aircraft is covered. Finally, the threat and its characterization are related to the simulation process.

The Phenomenology of Lightning

Lightning has been defined as "...a transient, high-current electric discharge whose path length is generally measured in kilometers." [Uman, 1969]. Lightning occurs when a region of the atmosphere attains an electric charge differential between itself and some other point that is large enough to cause a breakdown of the intervening atmosphere. That point may be on the ground (the typical cloud-to-ground flash) or at some other point in the atmosphere (a cloud-to-cloud flash).

The atmospheric electrical system is an extremely complex system. It consists of a "background" electrical field plus intermittent phenomena which influence the local field. The local phenomenon which most influences the local electrical field is lightning. The most common producer of lightning is the thundercloud, known to meteorologists as the cumulonimbus cloud. A typical South African thunderstorm cloud with a probable charge distribution is shown in Figure I-1. The solid black circles indicate locations of equivalent point charges, with typical values of $P = +40$ Coulombs, $N = -40$ Coulombs and $p = +10$ Coulombs. Uman [1969] reports that Malan found these values would give the observed electric field intensity in the vicinity of the thunderstorm.

What is the mechanism for this charge distribution? This is still an unanswered question and is an area of ongoing research. Wahlin [1986] lists more than a half dozen possible candidates for the charging processes which occur in a thunderstorm.

For the purpose of this dissertation, we are more interested in the actual lightning phenomenon and the threat it poses to aircraft, than in its origin. To this end, we will focus on the lightning event, its chronology and characteristics. Characterization of the actual lightning event provides us with the necessary information

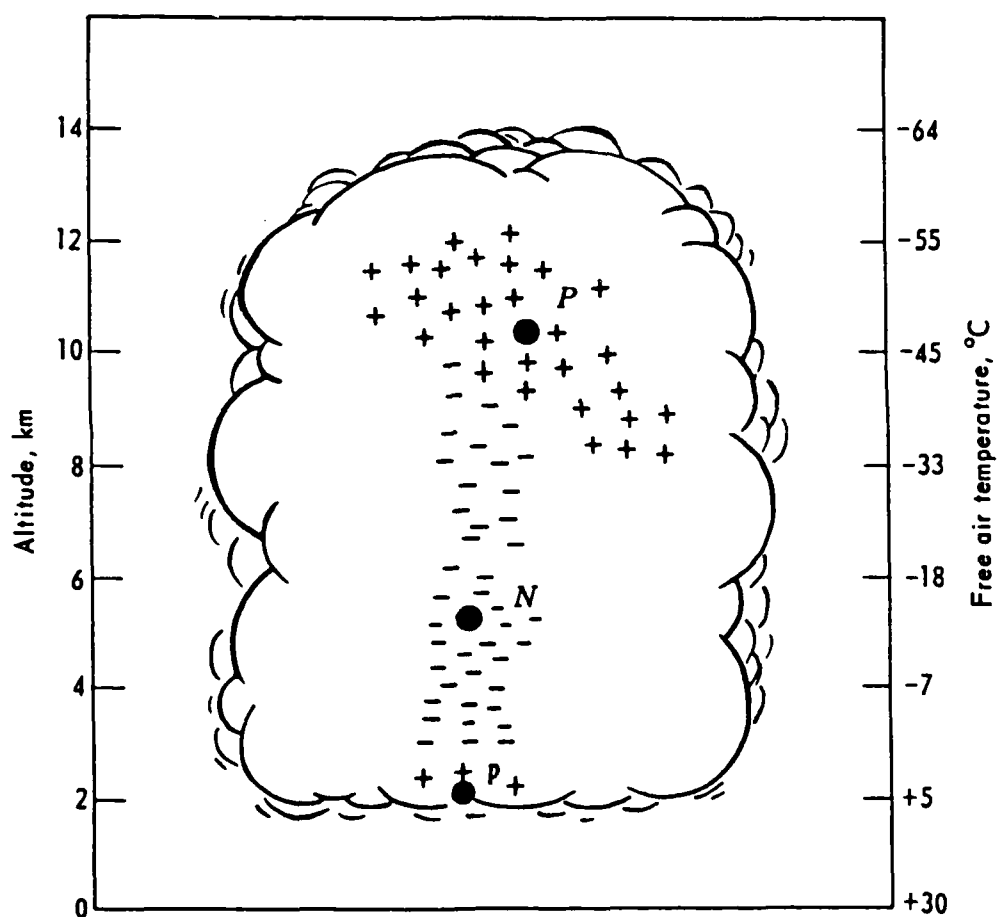


Figure I-1. Probable charge distribution in a South African thunderstorm [Uman, 1969].

to simulate its effects and to predict its interaction with aircraft.

Much of what is known about lightning's electrical characteristics comes from many years of measurements made on specially instrumented towers which were struck by lightning. Work by Berger [1975] in Switzerland, Garbagnati [1982] in Italy and Eriksson [1978] are notable in this respect. More recently, lightning strikes to specially instrumented lightning research aircraft, such as the NASA F-106B [Fisher and Plumer, 1983; Fisher, 1986] and the FAA CV-580 [Reazer, 1986], have greatly increased the available database of measurements of lightning strikes to aircraft. From these measurements, researchers have derived a statistical model of a typical lightning event.

The typical lightning event is well outlined in several standard works, among them Malan [1963], Uman [1969], Fisher and Plumer [1977], and Berger [1977]. The total lightning event or discharge, called a flash, is made up of one or more component discharges called strokes. In a cloud-to-ground lightning strike there are typically 3 to 4 strokes per flash, with the total flash lasting about 200 milliseconds. Cloud-to-cloud strikes often consist of many more and faster pulses, but of less intensity than in the cloud-to-ground lightning flash.

Because the cloud-to-ground event is considered to pose the most severe threat to aircraft, we will concentrate on the characteristics of this particular lightning event.

In a typical cloud-to-ground lightning flash, the first lightning stroke begins with a weakly glowing stepped leader, propagating from the cloud to the ground (Figure I-2). This stepped leader carries with it the very high voltage potential caused by the accumulation of charges in the cloud. As the stepped leader approaches the ground or some other object, the electric field caused by this voltage potential becomes very large, causing an upward moving oppositely charged ground leader to propagate upward to meet the oncoming stepped leader. This is the basis of the attachment process. When the stepped leader and the ground initiated leader make contact, a conducting channel is established. The source of the clap of thunder associated with the lightning strike is typically located a hundred meters or more above the ground at the point where the two leaders meet. The meeting of the two leaders is followed by the very luminous return stroke (Figure I-3).

The return stroke wavefront propagates up the channel established by the leader at a velocity averaging about one-third the speed of light. During the time the return stroke is flowing, currents in the channel may reach

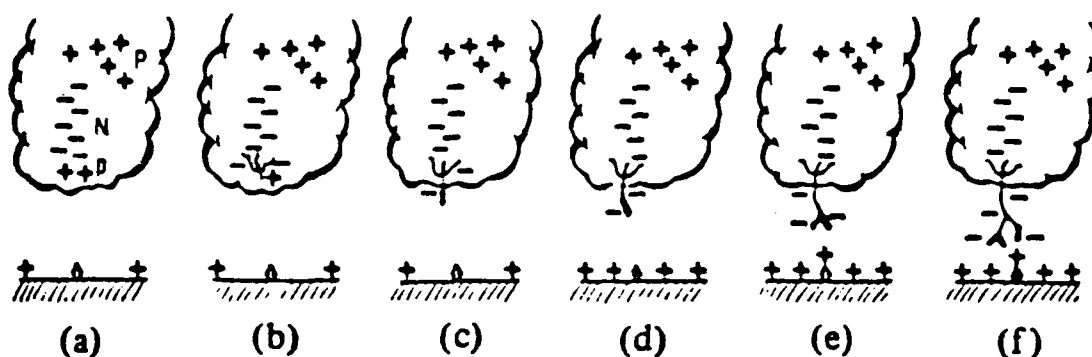


Figure I-2. Stepped-leader initiation and propagation. (a) cloud and ground charge distributions prior to lightning. (b) discharge called "preliminary breakdown" in lower cloud. (c)-(f) stepped-leader progression toward the ground. Adapted from Uman and Krider [1982].

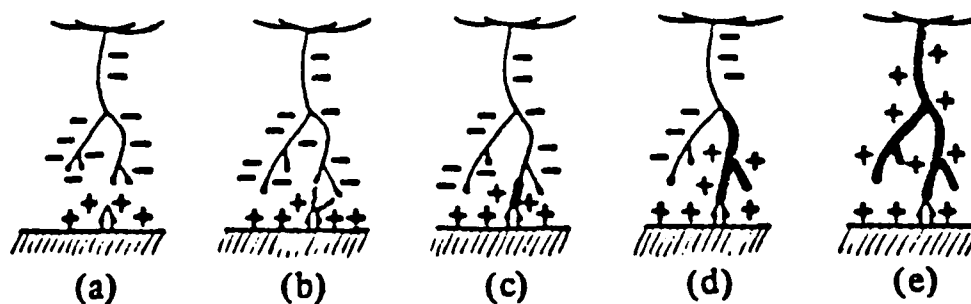


Figure I-3. Return stroke initiation and propagation. (a) Final stage of the stepped-leader descent. (b) Initiation of upward moving discharges. (c)-(e) Return-stroke propagation from ground to cloud. Adapted from Uman and Krider [1982].

values as high as 200 kA, though 20 kA is considered to be the median value of peak current in the channel. The time from zero current to peak current is typically on the order of a few microseconds. After about 50 microseconds, the currents fall to approximately half the peak value, and continuing currents of the order of hundreds of amps may flow for milliseconds or longer [Uman and Krider, 1982].

When the return stroke current has stopped flowing, the lightning flash may be ended. If sufficient charge remains in the cloud, subsequent strokes may take place. If this process begins in less than 100 milliseconds, a dart or continuous leader will flow down the ionization channel established by the first stroke in the flash. Because there is still the remnants of the previous channel, there is less resistance to channel formation, the channel is much less jagged and the leader travels considerably faster than the initial stepped leader. This dart leader will start any subsequent return strokes (Figure I-4). Generally, the subsequent return strokes carry much less charge than the first return stroke, and peak currents are reduced accordingly. Typical values for the components of a normal cloud-to-ground lightning discharge, as compiled by Uman, appear in Table I-1.

Table I-1

Data for a normal cloud-to-ground lightning flash bringing negative charge to ground. Values are intended to provide a feel for the physical parameters of lightning flashes.

SOURCE: After Uman [1969].

	Min.	Typical	Max.
Stepped Leader			
Length of step, m	3	50	200
Time interval between steps, μsec	30	50	125
Velocity of propagation, m/sec *	1.0×10^5	1.5×10^5	2.6×10^6
Charge deposited on leader channel, coulombs	3	5	20
Dart Leader			
Velocity of propagation, m/sec *	1.0×10^6	2.0×10^6	2.1×10^7
Charge deposited on leader channel, coulombs	0.2	1	6
Return Stroke ***			
Velocity of propagation, m/sec *	2.0×10^7	8.0×10^7	1.6×10^8
Current rate of increase, kamp/ μsec **	<1	10	>80
Time to peak current, μsec **	<1	2	30
Peak current, kamp **		10-20	110
Time to half of peak current, μsec	10	40	250
Charge transferred, excluding continuing current, coul	0.2	2.5	20
Channel length, km	2	5	14
Lightning Flash			
Number of strokes per flash	1	3-4	26
Time interval between strokes in absence of continuing current, msec	3	40	100
Time duration of flash, sec	10^{-2}	0.2	2
Charge transferred, including continuing current, coul	3	25	90

* Velocities of propagation are generally determined from photographic data. Since many lightning flashes have a nonvertical component, values stated are probably low.

** Current measurements made at the ground.

*** First return strokes have slower average velocities of propagation, slower current rates of increase, longer times to current peak, and generally larger charge transfer than subsequent return strokes in a flash.

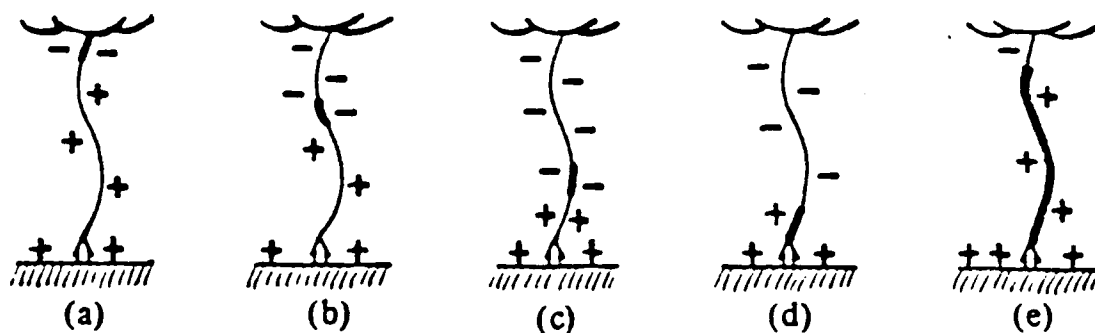


Figure I-4. Dart leader and subsequent return stroke.
 (a)-(c) Dart leader deposits negative charge on defunct first-stroke channel.
 (d)-(e) Return-stroke propagates from ground to cloud.
 Adapted from Uman and Krider [1982].

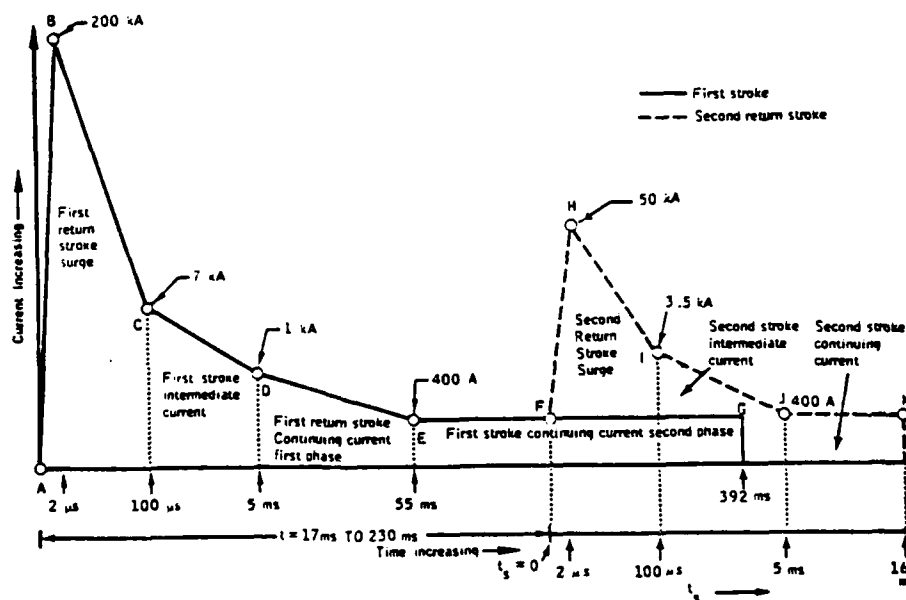


Figure I-5. Diagrammatic representation of lightning model.
 [Fisher and Plumer, 1977].

An important point to consider is that these parameters are derived from cloud-to-ground lightning measurements, typically made on top of specially instrumented metal towers. When discussing the airborne event, we must be aware that the situation is somewhat different. Cloud-to-ground strikes are believed to produce more severe lightning effects than intracloud and intercloud lightning strikes. Tower measurements have shown cloud-to-ground lightning parameters to be more severe than those measured during the in-flight strikes to a CV-580 aircraft. Rustan and Hebert [1985] reviewed the results of three in-flight lightning characterization programs and found that the rate at which aircraft are struck by lightning decreases at lower altitudes, but the intensity of the electrical parameters increases. As altitude increases, the number of intracloud and intercloud strikes increases while the intensity of the strike decreases. This means that in flying in or near an active thunderstorm, an aircraft is more likely to be struck at higher altitudes, but the intensity of such a strike is likely to be less than at lower altitudes. Therefore, the likelihood of a severe strike is higher at low altitudes.

Knowledge of the electrical parameters of the lightning flash is needed as they form the basis of determining (1) what kind of damage may occur to an object

struck by the lightning; (2) what parameters of the lightning event must be simulated and (3) how the lightning-aircraft interaction event may be modeled and simulated.

For instance, one model of the lightning flash that has been widely disseminated in the aerospace industry is diagrammed in Figure I-5. This model is the Space Shuttle Lightning Protection Criteria waveform [1975]. Though there is only an infinitesimal chance that an actual lightning event would fit this model exactly, it is reported to reproduce the effects of an actual lightning strike and is considered to be an accurate model for producing the typical worst case threat that an aerospace vehicle might face. This waveform has several components which correspond to the worst case parameters of various phases of the lightning event. Modeling of the lightning threat is discussed in more detail later in this dissertation.

When simulating the lightning flash, the question of what can be realistically produced must be considered. It is not economically feasible to build a simulator which can simulate the entire lightning flash at once. Normally, one or more parts of the lightning flash is simulated, focusing on just a few of the flash's physical effects on the object under test. A knowledge of the

electrical parameters of the lightning flash allows the designer to build a system which can simulate the desired aspects of the lightning flash for any given test.

To focus more on the subject of this dissertation, we next consider the interaction of lightning with aircraft. When considering the lightning event and its relationship to an aircraft in the vicinity of the event, we see many similarities to what has been previously discussed. The process of attachment and propagation of the channel proceeds as before (Figure I-6). In addition, there are several factors that must be considered to develop an accurate picture of what happens when an aircraft is struck by lightning.

The first factor that must be addressed is the fact that the aircraft is a moving object. When the relative speeds of the channel propagation versus the aircraft's forward progress are considered, 10^5 meters/sec vs. 10^2 meters/sec, it would appear that the aircraft can almost be considered to be standing still with respect to the channel. In reality, since the flash occurs over a relatively long period of time, milliseconds, the lightning channel may be swept over various sections of the aircraft. Therefore, the aircraft must be appropriately protected not only at the initial entry/exit points, but also along each of the sections over which the

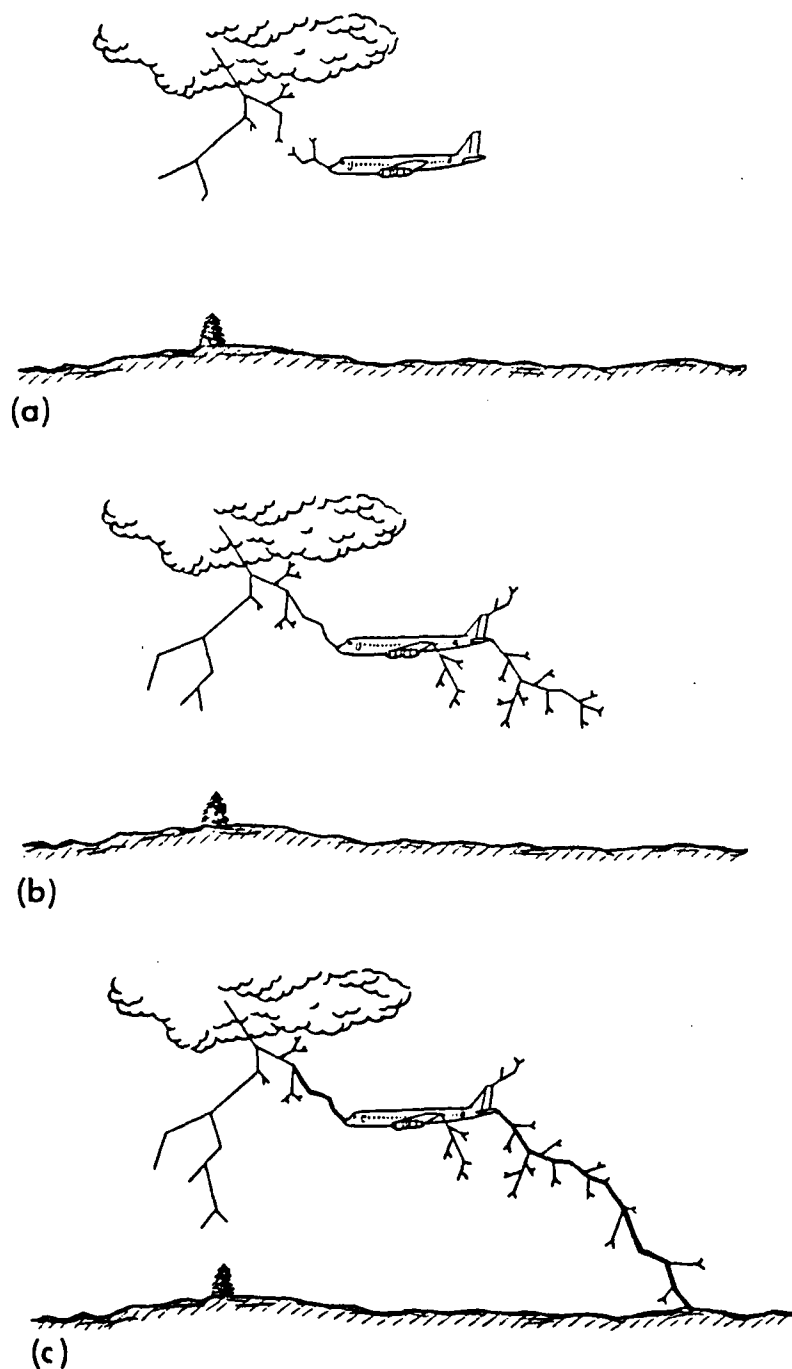


Figure I-6. Stepped-leader attachment to an aircraft.
(a) Stepped-leader approaching aircraft
(b) Stepped-leader attachment and continued propagation from an aircraft
(c) Return stroke through the aircraft

lightning channel may be swept due to the movement of the aircraft. Aircraft post-lightning strike incident reports often describe a path of damage along the aircraft's fuselage in which the lightning jumped from place to place, normally attaching to rivet heads as the lightning was swept across the aircraft due to its movement.

Another factor that has been widely debated in recent literature is the concept of the aircraft triggering the lightning channel which attaches to it. This is of more than academic interest, because it directly affects the design of the aircraft's protection scheme. Although the issue has not been totally resolved, it is known that the presence of the aircraft does influence the initiation of the attachment process [Fisher and Plumer, 1977]. Through various mechanisms, to be discussed later in this chapter, the aircraft moving through the atmosphere develops a static charge on it. This moving, charged body can influence the electric field distributions existing in the atmosphere. Some say this charge is enough to attract a lightning flash that may not have occurred were the aircraft not present.

In a paper by Clifford and Kasemir [1982], this question is addressed. When examining data compiled from strike reports, it is apparent that many strikes are occurring near clouds which do not exhibit typical

thunderstorm behavior, including noticeable lightning. The authors state that it is quite probable that high electrical fields can exist in clouds that are not electrically active. Thus, it is possible that aircraft can initiate or trigger lightning strikes in clouds that have produced no natural lightning. This is the probable cause of what pilots refer to in several aircraft lightning incident reports as a "bolt from the blue."

Further evidence that aircraft can trigger lightning bolts is the lightning strike experience of the NASA F-106 lightning research aircraft. When flying high in the clouds near active thunderstorm cells, this aircraft experienced many direct strikes. An analysis of the UHF radar data of direct strikes to the aircraft strongly indicated that the direct strikes were triggered by the aircraft itself [Mazur, et al., 1983].

Regardless of why or how the aircraft becomes involved in a lightning strike, it is appropriate to develop the criteria for the lightning threat that aircraft will face. Although the phenomenology of lightning has been briefly discussed, the interaction of lightning with an aircraft must be examined to determine the potential threat this interaction presents. Examining the threat allows us to determine what to model, simulate and protect against.

Atmospheric Electricity Threats

When considering the hazards due to atmospheric electricity, we can divide them into two categories: static discharges due to aircraft charging and lightning [Melander, 1985]. Although the focus of this dissertation is on the lightning threat, the effects of static discharges is briefly discussed to complete the discussion of the atmospheric electricity hazards faced by aircraft.

One reason to examine static charging is that static charging may alter the electrostatic environment around the aircraft. As previously noted, debate still continues as to whether this is enough to trigger an actual strike, although evidence is accumulating that it does.

Another reason to be concerned about static charging is that it can adversely affect aircraft operation. The most noticeable effect of static charging is interference in communication and navigation systems due to broadband, low-frequency electromagnetic radiation or noise. This radiation is due to ionization processes (corona discharges) which can occur once the potential on the aircraft reaches the breakdown potential of the surrounding air. This effect is similar to the phenomenon known as St. Elmo's fire, where visible corona currents are discharged from the masts of ships. Other sources of

danger include arcing and sparking from discharges. These arcs and sparks can cause direct damage to the aircraft when they occur in fuel tanks and fuel distribution systems.

Static electrification of the aircraft can occur in many ways. Three major causes are frictional electrification, engine charging, and exogenous charging (Figure I-7) [Nanevich, 1980].

Frictional or triboelectric charging is commonly known as precipitation static or P-static. This occurs when precipitation particles strike the aircraft. As the uncharged particles impact the aircraft, a charge separates from the particle and accumulates on the aircraft. This leaves the aircraft with an excess of positive or negative charges, depending on the form of precipitation, thereby changing the potential of the aircraft with respect to its environment. According to Fisher and Plumer [1977], the P-static charging process can raise the aircraft to a potential of 50 kV, or more, with respect to its surroundings.

Engine charging occurs due to poorly understood chemical and electrical processes occurring in the engine combustion chamber. As the engine exhaust leaves a jet aircraft, it carries with it a predominantly positive

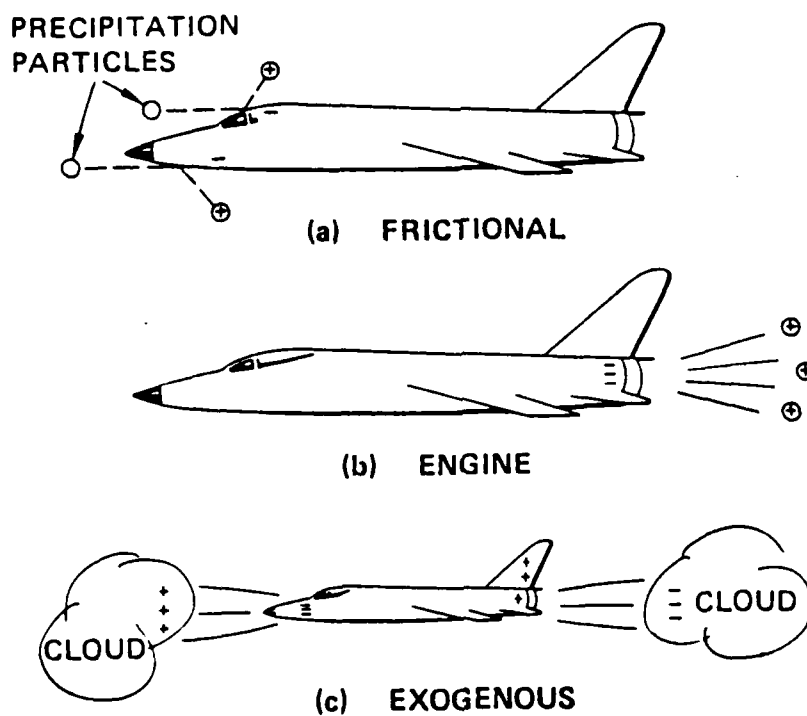


Figure I-7. Charging processes affecting in-flight aircraft [Nanevicz, 1980].

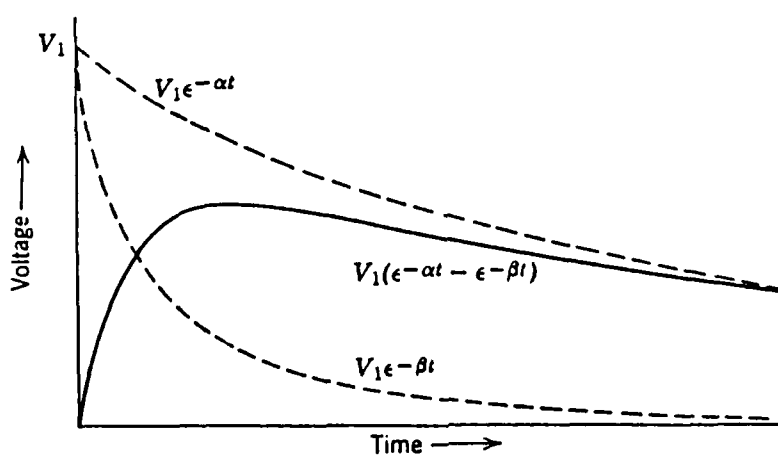


Figure I-8. The double exponential waveform. [Greenwood, 1971]

charge. This leaves the aircraft with an equal and opposite charge, causing a potential difference that may reach tens to hundreds of thousands of volts. This effect is also experienced by spacecraft and satellites when they expel exhaust jets to maneuver or stabilize their attitude [Garrett, 1980]. This is one of the mechanisms causing spacecraft charging.

Finally, exogenous charging occurs when a vehicle flies in a region of electric field, such as between two clouds having regions of opposite charge or between two oppositely charged regions of the same cloud.

Although these processes produce notable effects that must be protected against, they are generally not of the magnitude of the lightning threat. In the next section we will consider the specific threat of lightning and how it will be defined for our purposes of simulation and testing.

Defining the Lightning Threat to Aircraft

There are many ways to "define" the threat to aircraft. One common way is to give the historical, anecdotal evidence concerning the number of strikes, when they occurred, under what conditions, the damage done, etc. Many studies are of this type [Plumer, 1972; Clifford, 1980; Corbin, 1983; Rasch et al., 1984] and are

very important, because they provide information about the phenomenology associated with the aircraft-lightning interaction event. However, this viewpoint does not describe the actual aircraft-lightning interaction event and does not give us the information needed to develop quantitative models or simulation techniques for research and testing purposes.

Another common way to define the lightning threat is to characterize the electrical parameters of the lightning event. This approach has the benefit of developing the actual parameters needed to simulate the lightning threat and produce its effects in test objects.

Because the lightning flash is a phenomenon that varies greatly in its basic electrical parameters, there is a need for a statistical basis to define the threat. According to Melander [1985], a moderate threat is one caused by "the expected levels from a typical lightning flash. Severe lightning is defined as a reasonable worst-case level expected to occur during the service life of an aircraft."

Much research has taken place to define these threat values. Although cloud-to-ground, intercloud and intracloud discharges are involved with strikes to aircraft, the cloud-to-ground discharge is considered to

be the more severe, though less frequent, threat. Most of the data available on lightning level currents has been derived from cloud-to-ground strikes measured on tall instrumented towers at ground level. Rustan and Axup [1984] and Melander [1984] have shown that the characterization of the tower affects the results, and hence the validity, of the measurements taken. This is a clear example of how the measurement configuration affects the measurement process and these effects must be taken into consideration for the measurement results to be valid.

Because there are many types of lightning discharges that can affect aircraft, no one set of measurements will represent all possible discharges. Instead, the lightning threat is defined to be representative of the broad range of values for the many types of strikes. Ideally, experts seek to define a threat that is conservative. By conservative, we mean that protection from this defined threat will protect the aircraft from any possible threat, to some limit of statistical probability. For the purposes of this study, the threat as developed in the Air Force's Atmospheric Electricity Hazards Protection Advanced Development Program (AEHP/ADP), defined in the Boeing report by Melander [1985], will be used.

The parameters that were chosen to represent the threat were those that have a large impact on the aircraft and its systems. These parameters included waveform rise times and fall times, maximum rate of rise of the current (dI/dt), the value of the peak current, and the amount of energy transferred through the channel. Of these, the maximum dI/dt , peak current and energy transferred, also known as the action integral, are used to define the threat.

The defined threat must represent the significant electrical parameters produced by both single and multiple stroke flashes. If a single stroke threat is defined, then the multiple stroke threat can be built up from the single stroke threat by including such factors as the duration of the induced transient, the time interval between strokes, the number of strokes in the flash and the total duration of the flash. A range of typical values for a multiple stroke flash is given in Table I-2.

Table I-2

Typical values for a multi-stroke lightning event.

Variable	Range
Transient Duration	50 - 500 μ sec
Inter-stroke Time Interval	10 - 100 msec
Duration of Lightning Flash	0.01 - 2 sec
Number of Strokes	1 - 24

The waveform that is used for the single stroke lightning threat model is given by

$$I(t) = I_0(e^{-\alpha t} - e^{-\beta t})$$

This is a double exponential waveform (Figure I-8) and was first suggested by Stekolnikov [1941] and by Bruce and Golde [1941], and is still the most common model of the source waveform for lightning and nuclear electromagnetic pulse (NEMP) work.

One of the major advantages of this waveform is its simplicity, its ease of generation by physically realizable pulsed power generators and the good fit it makes to existing data collected on lightning strikes. However, in simulation of lightning level currents, we will see that other waveforms are also used for testing. It is important to realize that all simulation waveforms are a compromise between accurately representing the electrical parameters of the lightning strike and being physically realizable within economic and engineering constraints. In reality, these simulation waveforms are often considered as ideal for analytical purposes, but are only rarely achieved in actual aircraft lightning simulation tests.

This single stroke waveform represents the current from the initial lightning strike flowing in an

unperturbed arc channel. To use this threat for analysis of lightning's interaction with an aircraft, a coupling model representing the interaction of channel geometry and the aircraft is needed. The threat current waveform is then applied to the modified channel and aircraft.

Figure I-9 shows the single stroke moderate and severe threat current waveforms and spectra, while Figure I-10 gives currently suggested values for the parameters of the single stroke threat waveforms and spectra as given by Melander [1985]. Peak values for the moderate and severe threat are given as 20kA and 200kA respectively. These values were derived from studies by Berger [1975] and Cianos and Pierce [1972] based upon their ground level measurements made on specially instrumented towers.

The severe threat waveform is of major interest, as it is the one most often used to determine whether aircraft pass qualification tests. As such, we should consider its definition in greater detail. Figure I-11 shows the severe threat lightning current waveform with its defining parameters. This waveform was defined by reviewing existing lightning data and statistically quantifying the waveform parameters. For instance, measured lightning current amplitudes were plotted on log normal probability charts and straight line curve fitting was applied to the plots. The assumption of a normal

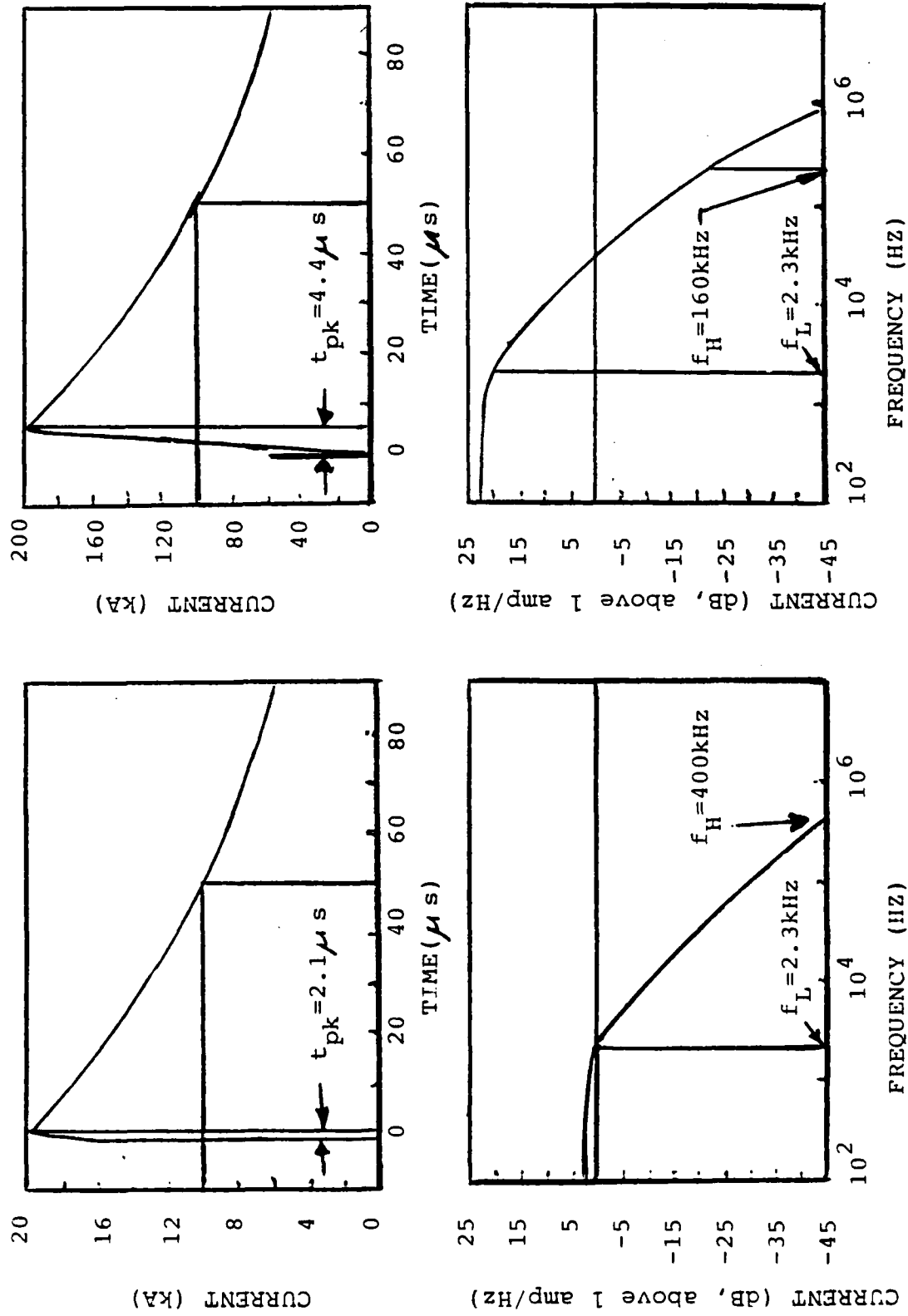


Figure I-9. Single Stroke Threat Waveforms. [Melander, 1985].

WAVEFORM

$$I(t) = I_0(e^{-\alpha t} - e^{-\beta t})$$

	<u>Moderate</u>	<u>Severe</u>
I_0 (kA)	20.6	216
α (10^3 sec^{-1})	14.3	15.0
β (10^6 sec^{-1})	2.5	0.95
t_{pk} (10^{-6} sec)	2.1	4.44
$t_{1/2}$ (10^{-6} sec)	50	50

SPECTRUM

$$I(f) = I_0(1/[\alpha + j2\pi f] - 1/[\beta + j2\pi f])$$

	<u>Moderate</u>	<u>Severe</u>
DC Limit	1.4 amps/Hz	14 amps/Hz
Upper Turning Frequency	400 kHz	160 kHz
Lower Turning Frequency	2.3 kHz	2.3 kHz

LIGHTNING PARAMETERS

	<u>Moderate</u>	<u>Severe</u>
Peak Current (kA)	20	199
Peak Rate-of-Rise (amp/sec)	5.00×10^{10}	2.02×10^{11}
Action Integral ($\text{amp}^2\text{-sec}$)	1.50×10^4	1.53×10^6

Figure I-10. Single Stroke Threat Definition Waveform Parameters for Damage Effects.
[Melander, 1985].

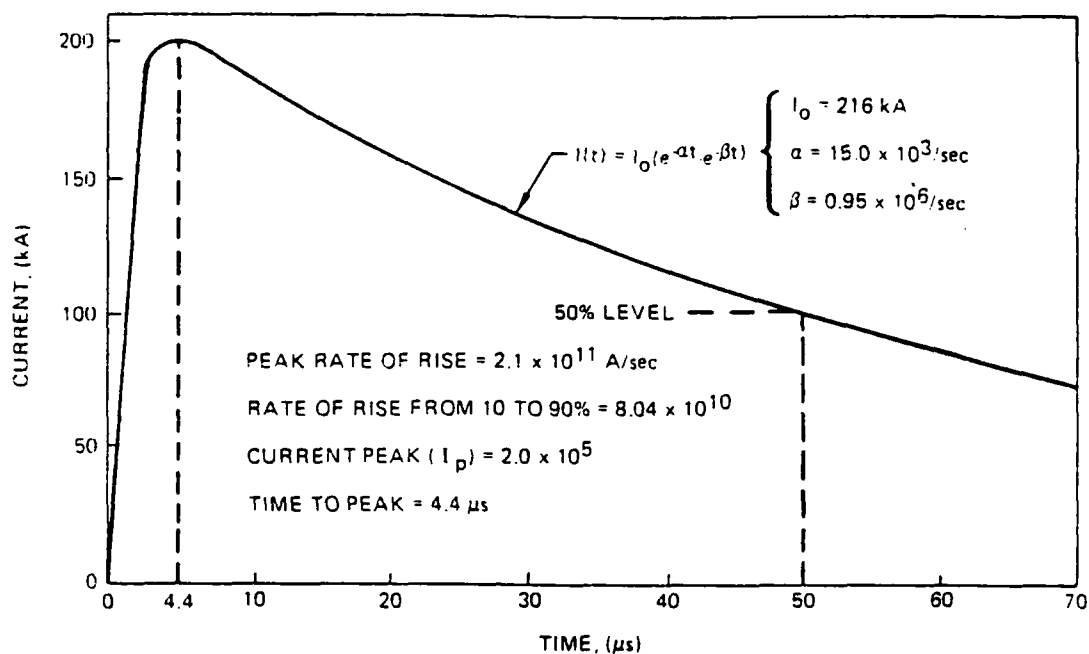


Figure I-11. Severe Threat Lightning Current Waveform. [Melander, 1985]

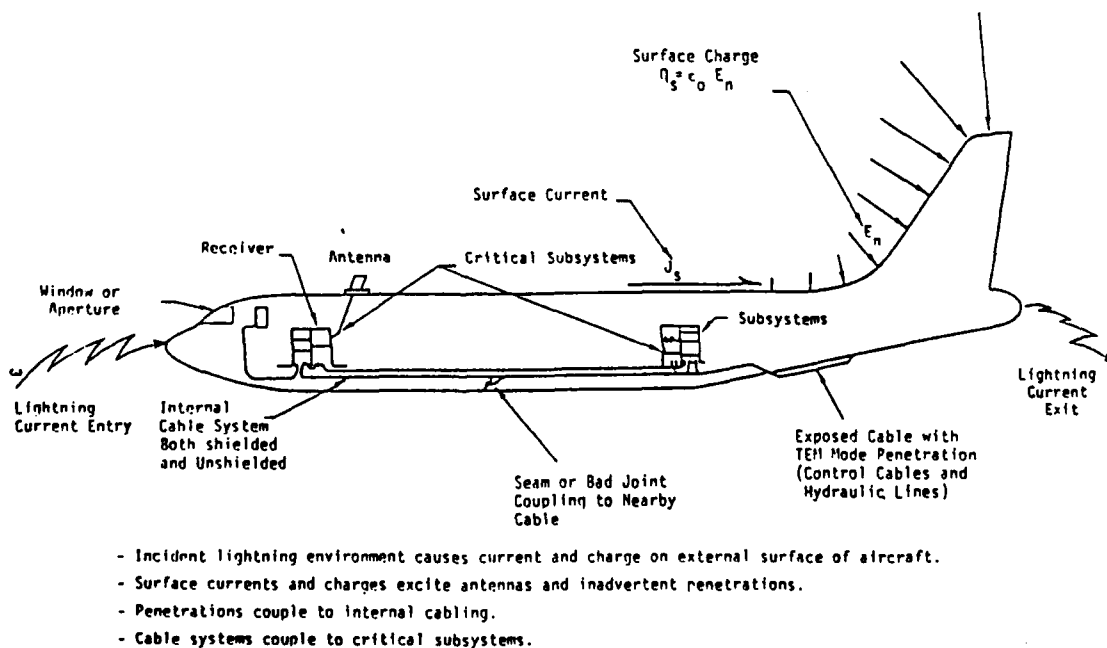


Figure I-12. Illustration of the Aircraft-Lightning Interaction Process [Perala et al., 1982].

probability density distribution is verified when the data fits a straight line, as was seen when this procedure was carried out. However, most of the measured data fell near the midrange and much less frequently near the extremes. Because of this, the tails of the distribution function are known with less certainty [Ketterling, 1987].

Once the threat is defined, suitable simulation waveforms can be constructed. To be truly representative of the threat, these simulation waveforms must produce the same effects that an actual threat would produce. Thus, it is appropriate to examine the lightning-aircraft interaction process and how lightning affects aircraft. Additional information concerning appropriate lightning waveforms for simulation purposes is given in chapter IV.

Lightning-Aircraft Interaction Processes

At this point it is appropriate to discuss the overall lightning-aircraft interaction process. We will break the overall process down into smaller steps and briefly discuss the individual steps. In Chapter III, we will examine each portion of the interaction process in greater detail. Finally, we will look at aircraft strike zones, as a knowledge of where an aircraft is most likely to be struck will help define how that strike interacts with the aircraft.

We need all this information because a knowledge of the interaction that lightning has with an aircraft will help determine the importance of configuration effects in the simulation process. Just as the tower effects must be removed from tower measurements so the results of electrical parameter characterizations are valid, the configuration effects of the simulation system must be removed from simulation measurements to make any results comparable to those measured in different simulation facilities or to actual in-flight measurements.

The lightning-aircraft interaction process consists of several parts, not all of which may be of importance during a particular event. Because the indirect effects problem is typically the most involved, we will focus on that process. The direct effects problem may be considered to be a subset of the indirect effects process, and a somewhat simpler problem, although this is not always true. The indirect effects problem consists of an external process, a coupling process and any internal processes occurring within the aircraft due to the coupling (Figure I-12). Breaking out the component parts of these processes, the interaction process can be described by the following general steps:

1. The current in the lightning channel attaches to the aircraft or passes very close to the aircraft.

2. The current from the channel causes a current and charge distribution on the aircraft skin and structure.
3. The aircraft skin current and charge distribution produces magnetic and electric fields around the aircraft.
4. The electric and magnetic fields around the aircraft may couple into the aircraft.
5. Fields coupled into the aircraft can induce currents and voltages directly into electrical and electronic systems in the aircraft, or onto cables and wiring which then can carry the energy to individual subsystems or components.
6. Depending on the amount of energy delivered to the subsystem or component, damage or upset may occur.

The determination of what takes place during a given event is quite complicated because of the many simultaneous processes that occur. What makes this a tractable problem is that the external, coupling, and internal processes can usually be treated as separate events. Although these processes are not independent from a theoretical viewpoint, they can usually be treated separately because the mutual coupling between the processes is often considered to be weak [Perala et al., 1982]. That is, changes in the voltages and currents that can be induced on internal wiring do not tend to perturb the external charge and current distribution on the aircraft skin.

Conceptually, each of these processes is relatively easy to understand. Let us take each one of these steps

in turn and discuss the processes occurring. First, let us consider the attachment of the lightning channel to the aircraft. Depending on where and how the channel attaches to the aircraft (or even if it merely passes nearby the aircraft), we will have different current and charge distributions on the aircraft. If we have a nose-to-tail strike, the current flow will follow the body of the aircraft, and structures along the long dimension of the aircraft will be preferentially excited. In a wing-to-wing strike, different types of resonances will be set up.

Once a current and charge distribution is set up on the aircraft, electric and magnetic fields will be produced around the aircraft. The fields are constrained by the geometry of the aircraft and boundary conditions related to the materials associated with that structure. It is important to remember that these fields are generated by a transient phenomenon. However, we can often use quasi-static approximations to simplify the work of describing these fields.

When we have a description of the electric and magnetic fields surrounding the aircraft, we can consider the coupling problem from the exterior to the interior of the aircraft. We can draw upon a large body of research concerning the coupling of fields through apertures. In addition, we must examine other possible mechanisms for

the entry of energy into the aircraft. One important process is that of diffusion, which becomes very important when considering magnetic fields or non-metallic structures.

In an analogous process, fields that penetrate the interior of the aircraft may couple into and onto the wiring and cables of the many systems that exist within the aircraft. These coupled fields may develop significant voltages and currents within these systems. These voltages and currents may travel over the entire aircraft, generating effects far removed from the location where the interaction occurred.

Finally, if sufficient energy is delivered to vulnerable components and sub-systems, up-set and damage may occur to critical avionics and flight-control systems. The amount and type of damage will be dependent upon the susceptibility of that particular component. This susceptibility is related to the amount of energy deposited or absorbed by that component. Thus, knowledge of this quantity is key to determining the extent of possible damage. To assist in this determination, a quantity known as the action integral has been defined.

The action integral is related to the energy deposited or absorbed in a system. However, the actual

energy deposited can not be defined without a knowledge of the resistance of the system. For instance, the instantaneous power dissipated by a resistor is given by i^2R and is expressed in watts. To determine the total energy dissipated or absorbed (expressed in watt-seconds or joules), the power must be integrated over time. By specifying the integral of $[i(t)]^2$ over the time interval of interest, a quantity is defined for any resistance value of interest. For lightning, this quantity is defined as the action integral and is given by

$$\int [i(t)]^2 dt$$

over the time the current of interest flows.

Each of the above processes is relatively straight forward. What makes the overall lightning-aircraft interaction process so difficult to analyze is the large number of possible interactions that can occur, and the high probability that no two of those possibilities will ever be repeated. Thus, all possibilities must be considered and all those that pose a threat that exceeds some predefined hazard criterion must be protected against.

We will conclude this simplified discussion of lightning-aircraft interaction by discussing the concept of strike zones. Strike zones are locations on the

aircraft where the lightning flash will attach or where substantial amounts of electrical current may be conducted between attachment points. The locations of these zones on any aircraft are dependent on the aircraft's geometry and operational factors, and often vary from one aircraft to another.

Strike zones are of interest for many reasons. First, they indicate areas of the aircraft's skin and structure that most likely will suffer the effects of direct or swept lightning attachment. Second, the direct and indirect effects that the aircraft will experience strongly depend on the entry and exit points, and how the lightning moves between those two locations. Third, strike zones provide guidance in designing adequate protection for the aircraft, helping to minimize the weight penalty incurred with that protection by better defining the area to be protected and the type of protection needed. Finally, the effect on skin current and charge distributions of different attachment points will affect the interaction process.

Lightning strike zones have been defined [SAE, 1978] as follows:

Zone 1

Zone 1A: Initial attachment point with low possibility of lightning arc channel hang on.

Zone 1B: Initial attachment point with high possibility of lightning arc channel hang on.

Zone 2

Zone 2A: A swept stroke zone with low possibility of lightning arc channel hang on.

Zone 2B: A swept stroke zone with high possibility of lightning arc channel hang on.

Zone 3

Zone 3: All of the vehicle areas other than those covered by zone 1 and zone 2 regions. In zone 3, there is a low possibility of any attachment of the direct lightning channel. Zone 3 areas may carry substantial amounts of electric current, but only by direct conduction between some pair of direct or swept stroke attachment points.

Again, it should be pointed out that these zones are dependent upon aircraft geometry and operational factors. Examples of typical strike zones are given in Figures I-13 and I-14.

The Effects of Lightning on Aircraft

To complete the background information on the lightning threat, it is worth while to examine the effect of lightning on an aircraft, its systems and components. This knowledge is useful to the thrust of this dissertation because it gives us insight into what must be simulated, and how effective that simulation is. The usefulness of a particular simulation technique will depend on what is to be simulated. For instance, if a simulated lightning strike produces the same damage that a real lightning strike does, that simulation may be used in

LIGHTNING STRIKE ZONES

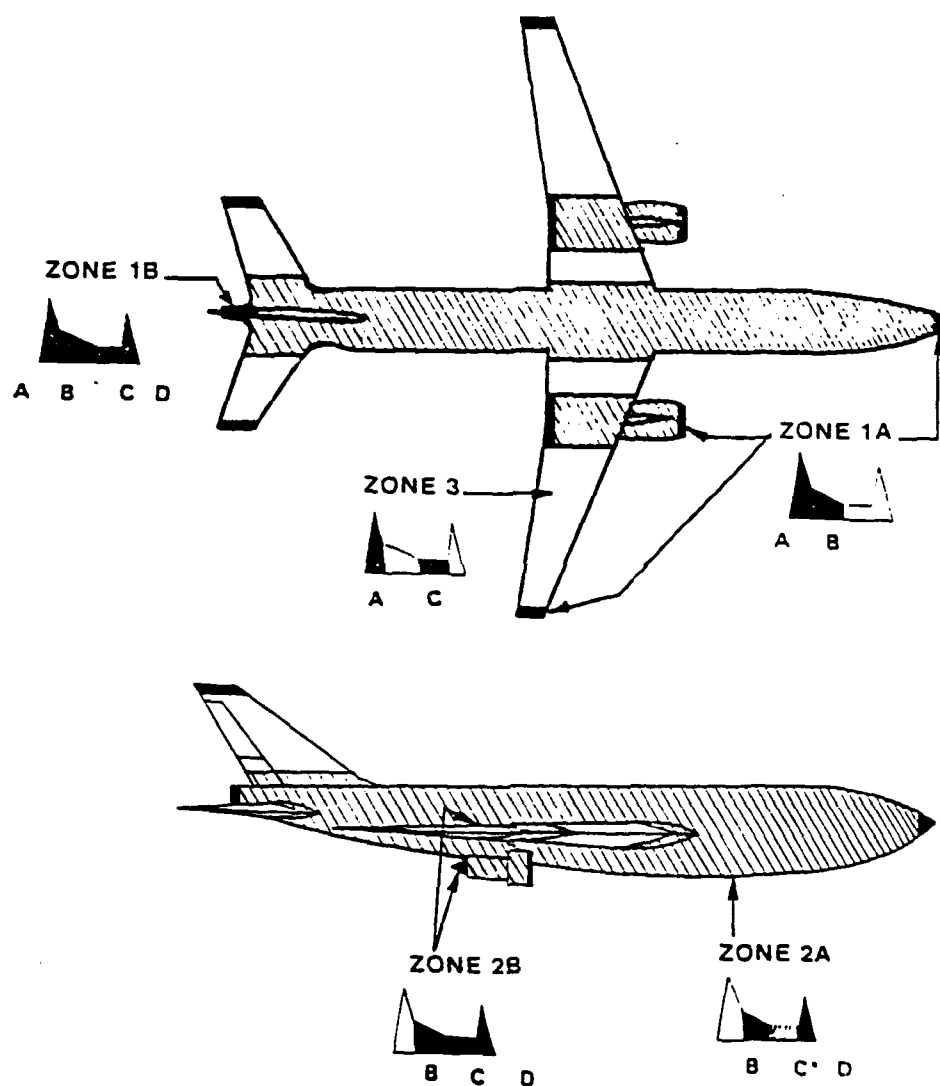


Figure I-13. Illustration of Typical Lightning Strike Zones, Large Aircraft [Rasch, 1984].

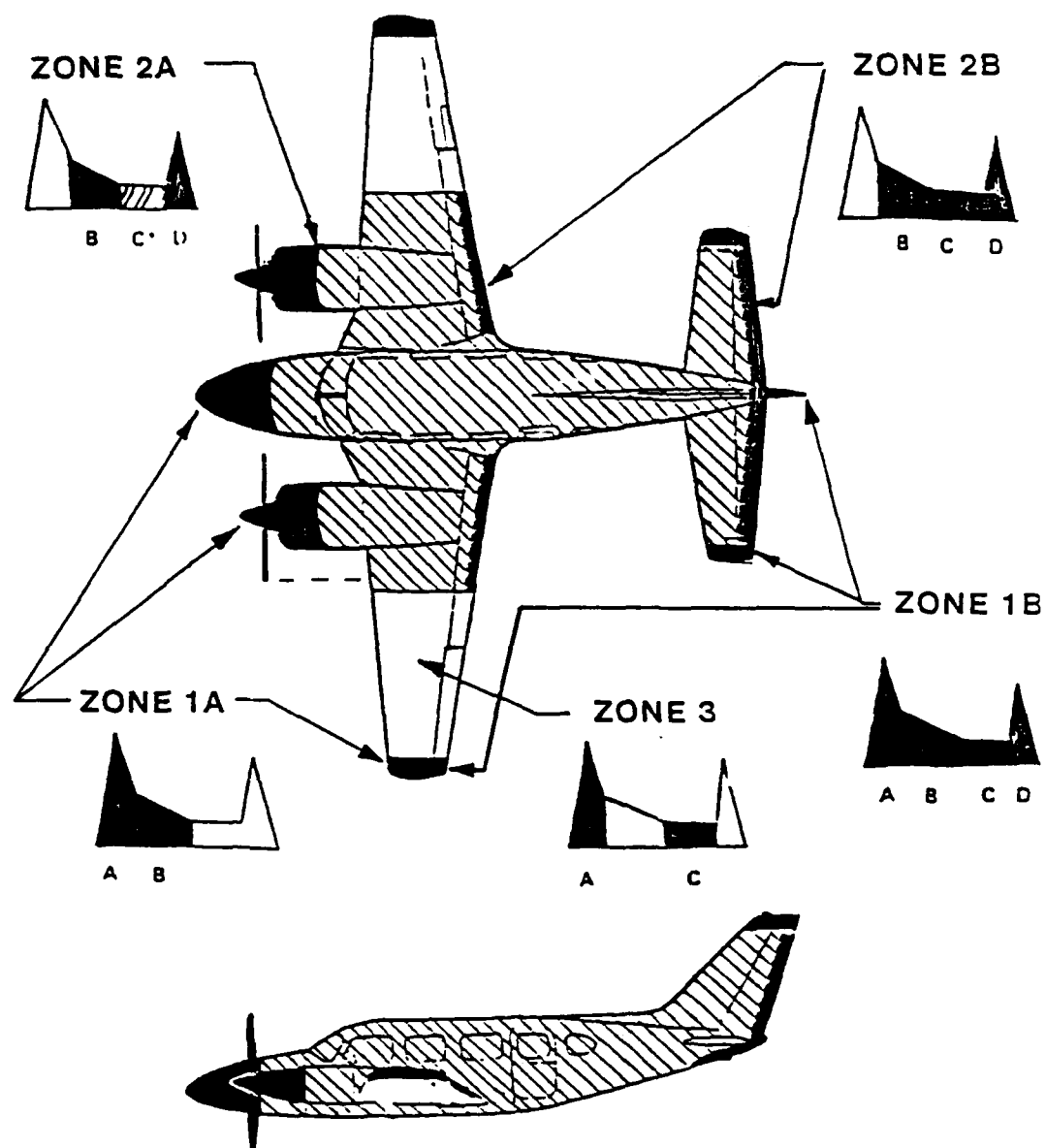


Figure I-14. Illustration of Typical Lightning Strike Zones, Small Aircraft [Rasch, 1984].

damage assessment studies. However, that same simulation technique may be inadequate to show the results of electromagnetically coupled energy interacting with a flight control system. Thus, we must know what effects we are trying to simulate.

The effects of lightning on an aircraft are generally divided into two categories: direct effects and indirect effects. Direct effects include the physical damage produced at points of arc attachment, due to current flow between points of arc attachment or to current flow between arc entry and exit points. Direct effects may include the effects due to both high current and high voltage interacting with hardware. Indirect effects are those electromagnetically induced by the coupling of fields to wires or avionics equipment.

Many effects of lightning may be attributed to either direct or indirect causes. For instance, fuel vapor ignition or engine outages may be caused by either direct or indirect effects, or a combination of both. It is often difficult to draw a clear line between direct and indirect effects because of multiple causes of effects.

Other than these types of effects, physiological effects on the crew such as flash blindness and loss of consciousness from electrical and acoustical shock are of

concern. These effects are usually temporary, lasting perhaps up to 30 seconds or longer, but have the potential of being very serious if loss of aircraft control comes at a critical time. For the purpose of this dissertation, we will not consider these effects any longer, as they do not play a role in the simulation process that we will discuss.

The direct effects of lightning are such things as: the melting and pitting of metallic skins; the puncturing, splintering or splitting of nonmetallic structures, such as radomes; the welding and roughening of bearings and movable structures, such as the hinges on flaps; the deformation of metallic structures due to magnetic force; and other physical damage. In most cases, this damage occurs at the point of attachment or exit of the leader, or at some part of the conducting path between these two points.

The primary causes of these effects are due to the fact that as an electric current passes through a material, a certain amount of energy is converted to heat because of the electrical resistance of the conducting material. The process is much more complicated than this, because the resistance of the material will change as the material heats up, and the current that we are dealing with is transient in nature. If we neglect the resistance

changes due to heating effects, the Joule heating in a material is given by

$$H = \int_0^t RI^2(t) dt$$

where:

H = Heat developed in the material (Joule)

R = Electrical resistance (Ohm)

t = Time (sec)

I(t) = Electrical current as a function of time (Amp)

If the electrical current is injected into the material by way of an electric arc, the situation becomes even more complicated. Heat is developed in the material due to normal Joule heating and at the arc attachment/metal interface. The end result of these processes is the metal structure can experience melting and burn through if the arc or current flows for a sufficiently long time. Other factors such as type of material, geometry and construction techniques will determine how this process proceeds.

Another type of direct effect is that due to magnetic force. If two parallel wires have current flowing through them in the same direction, they will experience a mutual attraction. If the structure near an attachment point is considered to be a large number of parallel conductors with current flowing through them, then forces can occur

which tend to draw these conductors closer together. This magnetic force is proportional to the square of the current producing it and the damage will be related to the magnetic forces and to the response time of the affected structure. If the structure is not rigid enough, or the current is sufficiently high, pinching, crimping, or buckling may occur in the structure. James and Phillpott [1971] examined this problem and determined that an arc rising in a few microseconds to a peak current of 200 kA will have a diameter of about 2 mm and its maximum magnetic field will be about 40 Tesla, producing a magnetic pressure approaching $6.3 \times 10^8 \text{ N/m}^2$ (150,000 lbs/in.²).

Indirect effects are those caused by the electromagnetic field resulting from the current flowing through or on an aircraft due to a lightning strike. These fields can couple to the electrical system of the aircraft and their effects may be seen at locations distant from the location of the current. In many ways, these indirect effects can be likened to the effects seen in systems due to heavy electromagnetic interference (EMI) or radio frequency interference (RFI) problems.

Indirect effects are becoming more and more important with the introduction of aircraft that are more susceptible to these effects. This vulnerability comes

about because of two trends in the aircraft industry. The first trend is the increasing use of nonmetallic structures, while the second trend is the use of sophisticated avionics based upon low voltage solid state technology.

Non-metallic structures such as composite wings, rudders, body panels, etc. are becoming increasingly common on aircraft. For instance, Figures I-15 through I-19 [Leonard and Mulville, 1980; Corbin, 1982] show the distribution of non-metallic structures on representative types of vehicles. As time progresses, the use of composite structures will move beyond the simple replacement of existing subsections to the creation of aircraft which are essentially non-metallic, like the Lear Fan 2100.

One of the reasons for this increasing use of composite structures is their higher strength/density and stiffness/density ratios compared to available metal alloys. Carbon composites are especially notable in this respect [Leonard and Mulville, 1980]. Another major advantage of composite materials is their demonstrated weight savings. This directly translates into a combination of fuel savings, increased range and/or increased cargo-carrying capability.

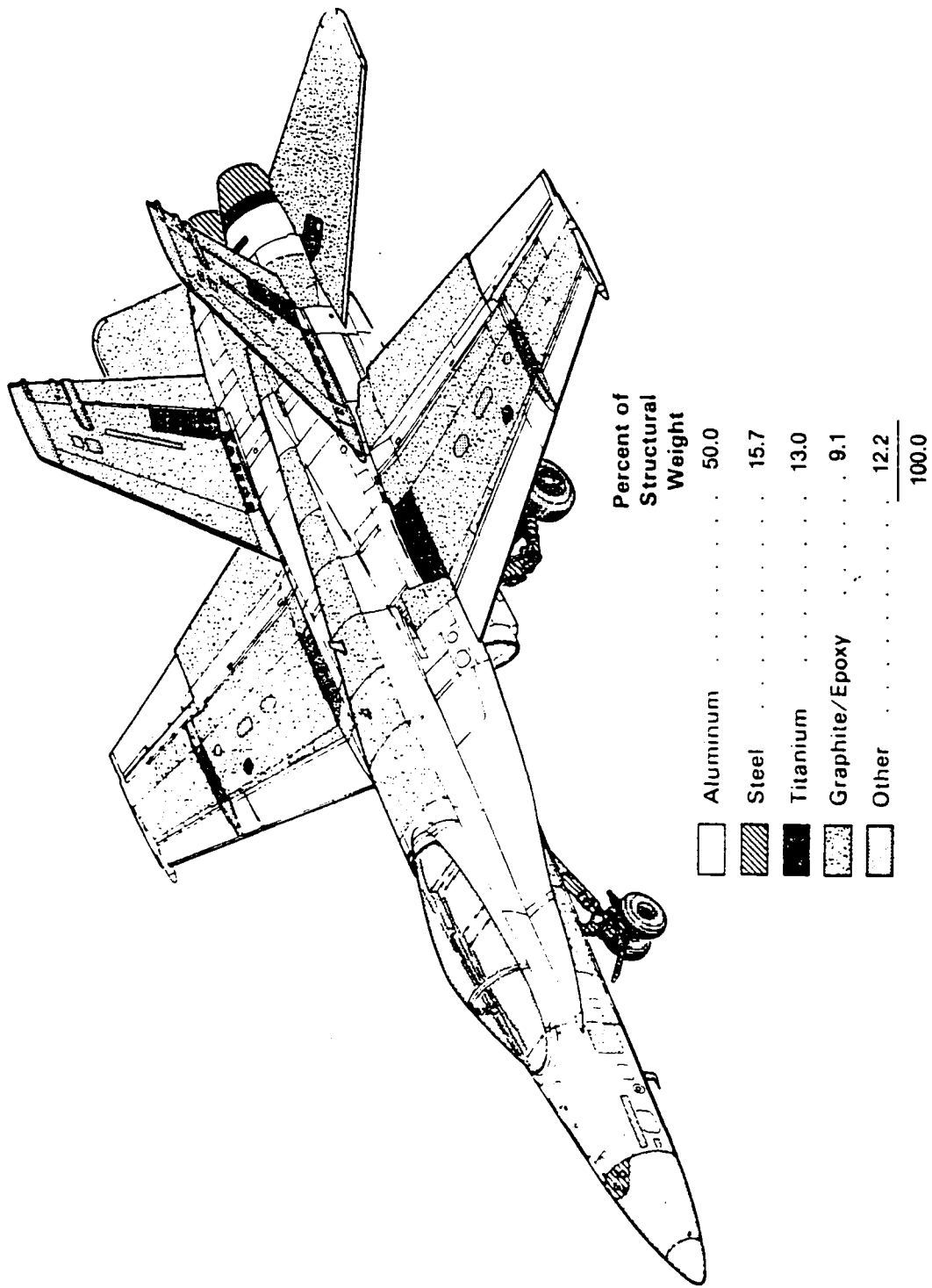


Figure I-15. Distribution of Materials in a F/A-18A Aircraft, Top View. [Rasch, 1982].

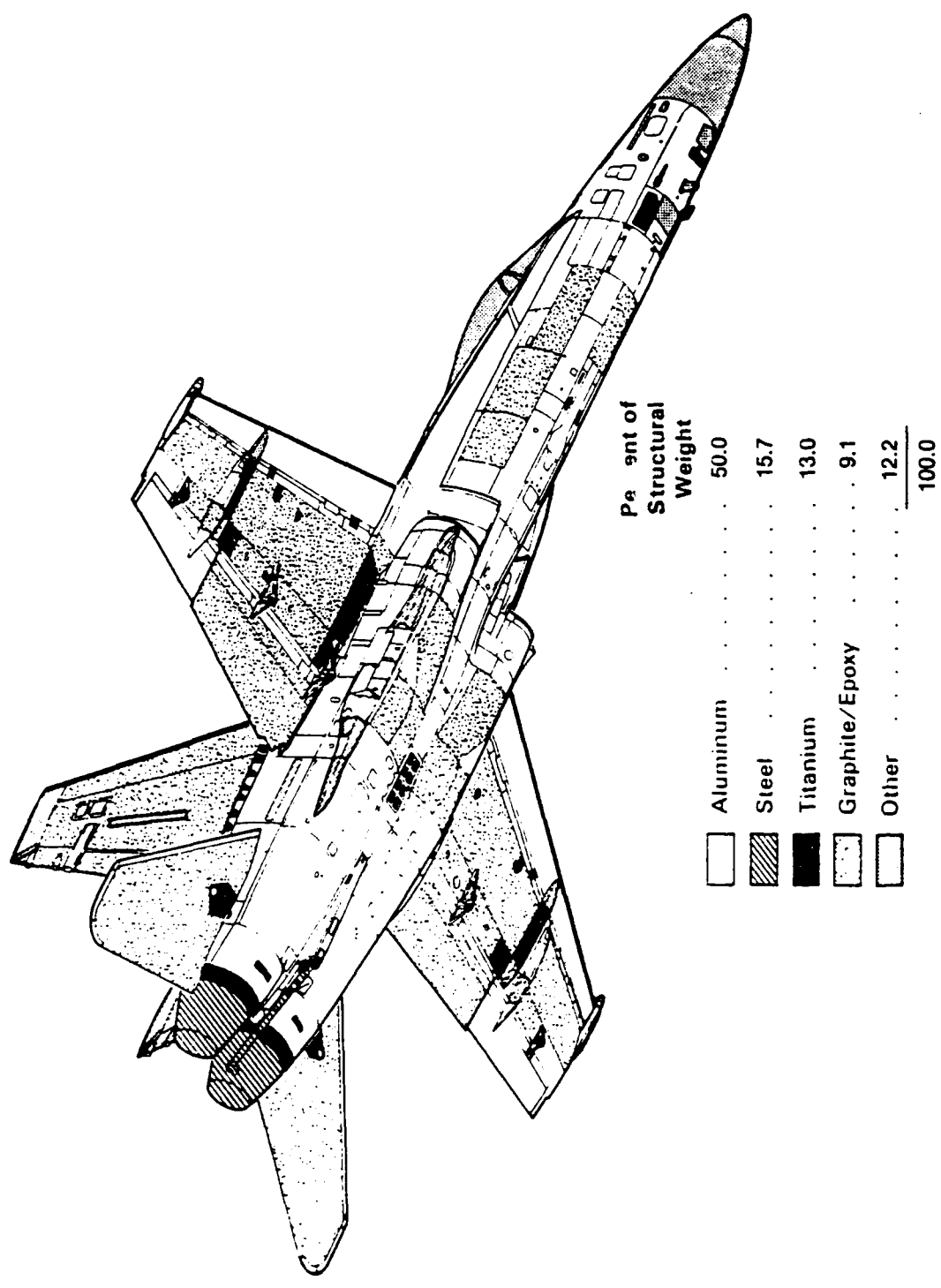


Figure I-16. Distribution of Materials in a F/A-18A Aircraft, Bottom View. [Rasch, 1982].

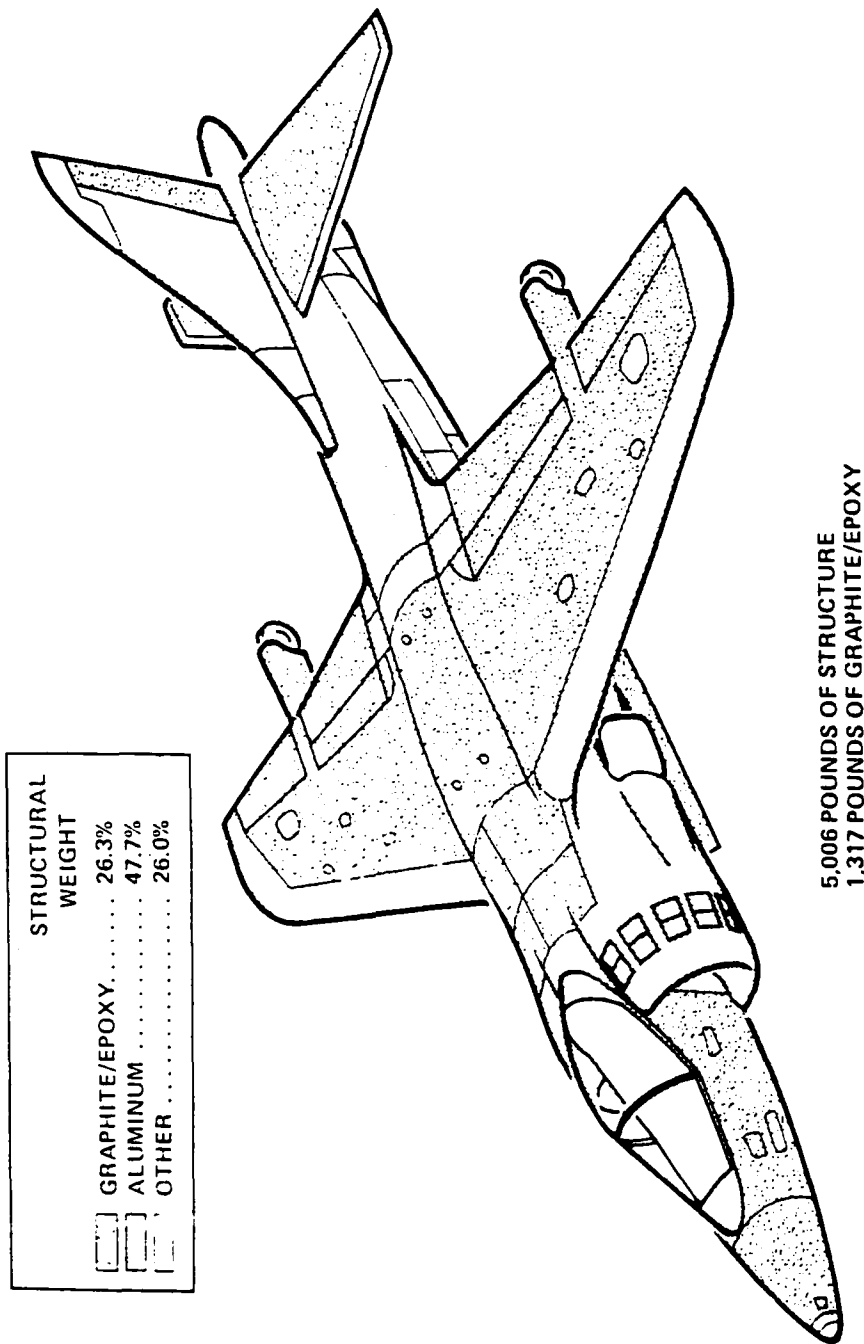


Figure I-17. Distribution of Materials in an AV-8B Aircraft.
[Rasch, 1982].

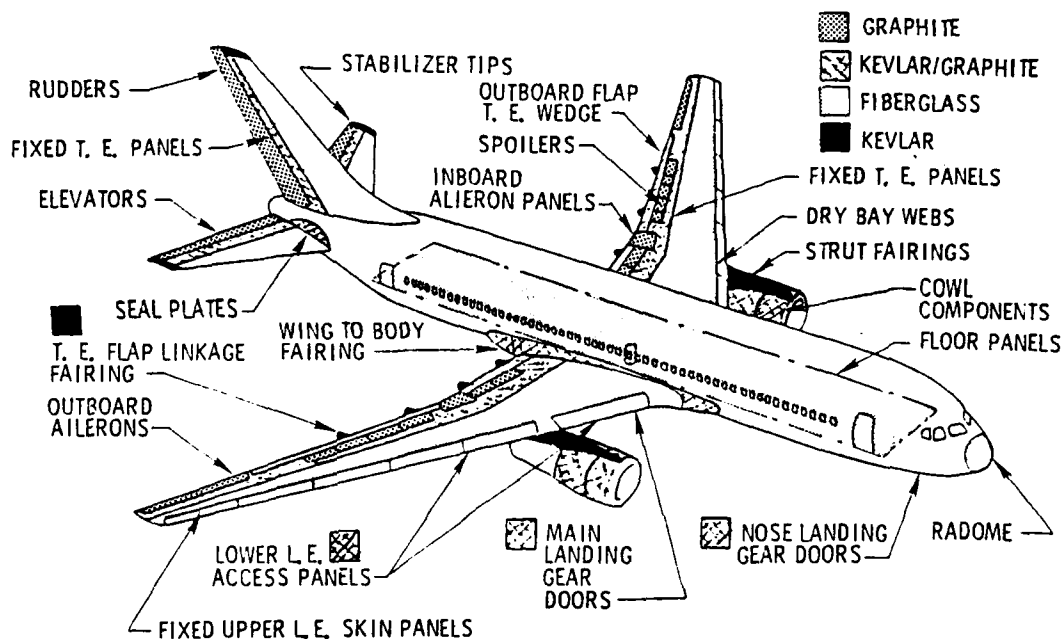


Figure I-18. Composite Structures on the Boeing 767
[Leonard and Mulville, 1980].

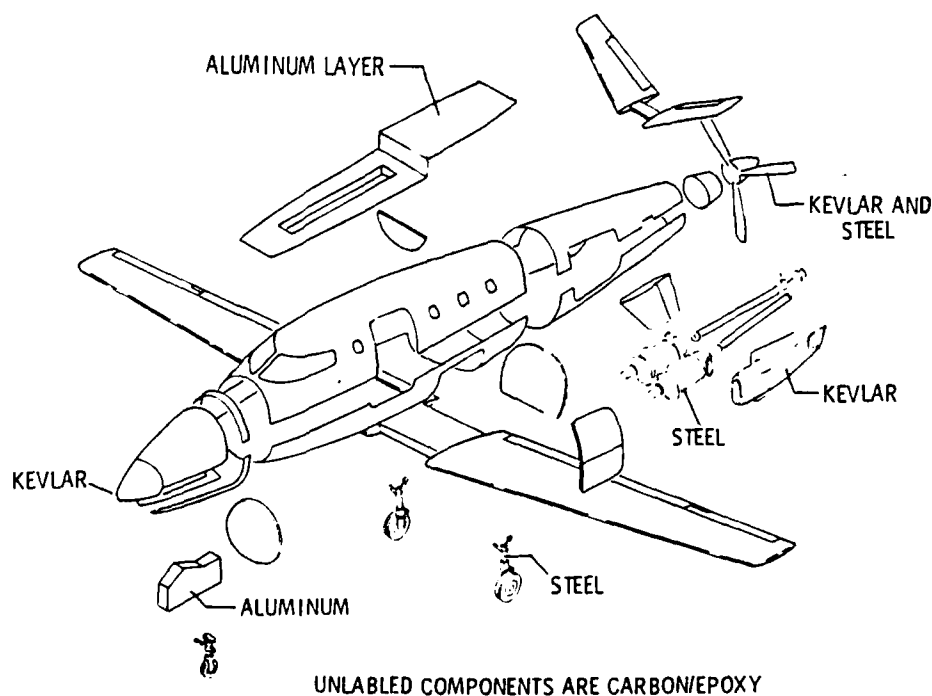


Figure I-19. The All Carbon Composite Lear Fan 2100
[Leonard and Mulville, 1980].

To offset the obvious advantages of composite materials, there are major concerns about the impact of incorporating these materials into aircraft systems. One area of concern is the proper functioning of the aircraft's electrical and electronic systems and subsystems. For instance, an all-metal aircraft provides a readily available return path for signal and power. The metal skin also provides a relatively unbroken counterpoise system for aircraft antennas. Another area of concern is how the aircraft will operate in the presence of high electromagnetic fields due to on-board generators, such as radars and electronic warfare systems, and external sources, such as nuclear electromagnetic pulse and lightning.

Metal skins on the aircraft provide a low resistance, high conductivity structure for carrying the currents of a direct lightning strike, and dissipating the charge due to precipitation static. In addition, the unbroken metal skin provides an electromagnetic shield of 20 dB or more between the exterior electromagnetic environment and internal electronics enclosed by the skin. However, materials such as boron, graphite, Kevlar, etc., allow the direct propagation or diffusion of exterior fields into the interior of the aircraft. These diffusion fields can be of a magnitude where they produce voltages and currents at levels which can cause upset or damage to mission

critical electronic systems.

Even if the diffusion of fields through composite structures is not important, the joints in composite sections are likely to be poor electrically, not only allowing substantial field penetration, but providing high impedance paths where I^2R (heating) losses can cause physical damage to the joint. Although there are methods of decreasing the vulnerability of the aircraft, they come at the expense of increased weight, which can partially negate the benefits of the use of composites.

Compounding the potential problems caused by increased field levels from composite structures, the ever expanding use of solid state components and the growing complexity of on-board avionic systems increases the susceptibility of the aircraft to upset or damage. Older avionics systems were inherently "harder" to electromagnetic upset, because there were fewer systems, and those systems that were on board operated at higher voltages because of the technology employed.

Solid state components are desirable for their greater reliability and decreased weight and volume. These desirable characteristics are especially evident with integrated circuits. However, many logic families operate at lower voltages, and with smaller noise margins

than discrete components, making them even more susceptible to upset and damage. The push to increasingly denser integrated circuits utilizing very high speed integrated circuit (VHSIC) technology accelerates this susceptibility.

Another trend is the greater complexity of on-board systems. Today's systems tend to be strongly interconnected, using common busses for control and data communication between interacting systems. Much of the on-board instrumentation sends its readings to a central computer, which routes the information to appropriate subsystems. Not only are there the usual electronic systems such as communications, navigation, autopilot systems, system monitoring, etc., but manufacturers are incorporating all-digital flight control systems into the latest aircraft.

Older aircraft used combinations of mechanical and hydraulic systems to control their flight characteristics. Newer aircraft now use a fly-by-wire approach, where flight control surfaces are controlled by computer and the interconnecting links are electrical. In fact, the latest test aircraft are inherently unstable, and can only fly with the aid of constant computer monitoring and control of adjustable flight surfaces.

Lightning protection for flight-critical and mission-critical subsystems is normally designed in terms of safety margins since it is impractical and too costly to design the aircraft such that no energy is coupled into its circuits. Instead, protection is designed so that in the worst case the lightning-aircraft interaction produces transients lower than those necessary to upset or damage the components. The safety margin is defined as the difference between the electrical levels necessary to upset or damage the components and the worst case, maximum level of coupled electromagnetic energy allowed by design.

Because of these many trends and the need to provide sufficient safety margin for critical equipment, it has become more important than ever that aircraft be sufficiently hardened against electromagnetic upset and damage. This requires the necessary protection being incorporated during the design phase, and that the appropriate qualification and surveillance testing take place to verify adequate hardening of the aircraft from factory roll out to retirement.

We will conclude this chapter with an example of the type of mishap that lightning causes, illustrating the concepts of direct and indirect effects, as well as strike zones. This incident was reported in an article by

Clifford [1980], and illustrates a "typical" lightning incident.

In 1975 an Air Force F-4 fighter flying at 37,000 feet and 0.86 Mach experienced an in-flight explosion that resulted in separation of the left wing and loss of the aircraft. According to verbal reports, the crew had reported visual sighting of lightning ahead and was attempting to contact the area controller when they heard a loud explosion. The aircraft went into a roll to the left and the pilot tried to correct and assess the damage but the high G forces caused him to lose consciousness. The second crew member ejected immediately after hearing fragments of statements from the pilot to "leave the aircraft." The pilot remained with the aircraft until an altitude of 5,000 feet before he regained consciousness and successfully ejected. The left wing impacted into a swamp miles from the point of aircraft impact, but the fliers were safely recovered. Recovery of the left wing and parts of the right wing allowed the accident investigation team to determine that ignition of fuel vapors occurred in the right integral fuel tank. The ignition front propagated into the left wing tank, rupturing the center rib panel separating the tanks. The pressure rose in the left tank, resulting in an explosion that separated the left wing from the aircraft.

Positive evidence of a lightning strike was found on the aircraft. Attachment points were found on the navigation lights on both wing tips, both stabilators, and the rudder. The left wing navigation light showed one attachment point. The right wing light had three attachment points on the tips, and there were two on the rudder, one at the top rear tip, and the second on the trailing edge near the bottom. All of these attachment points showed the typical characteristics of pitting and molten metal.

Although the aircraft was lost because of a fuel vapor explosion, this incident is of interest to aircraft electrical and electronic engineers because the possible ignition sources in such cases include electrical equipment such as fuel quantity probes or electrically actuated valves or pumps in the fuel volume. In this particular incident, the accident investigation board determined that the most probable cause of ignition was fuel probe arcing or breakdown.

This particular incident is illustrative of the validity of the strike zone concept. Also, it shows the complex interplay between direct effects and indirect effects. It is to avoid incidents such as these that simulations are carried out. The knowledge gained from these simulations is used to design protection systems

that minimize the possibility of such occurrences, while simultaneously minimizing the costs of such protection.

These simulations are of value only if the results of them can be used to accurately assess the potential danger and the validity of protection schemes. We can maximize that accuracy by eliminating the perturbing effects of the measurement system and configuration from the simulation and validation process. In the next few chapters, this measurement and simulation process will be described and the method of error elimination will be explained and illustrated.

REFERENCES - CHAPTER I

M.A. Uman, Lightning, (New York: McGraw-Hill, 1969), p. 1.

L. Wahlin, Atmospheric Electrostatics, (New York: John Wiley & Sons, 1986), pp.37-58.

K. Berger, et al., "Parameters of Lightning Flashes," *Electra*, Vol. 80, 1975, pp. 23-37.

E. Garbagnati and G. Lopipard, "Lightning Parameters - Results of 10 Years of Systematic Investigation in Italy," *Proceedings of 1982 International Aerospace and Ground Conference on Lightning and Static Electricity*, Oxford, England, March 24-26, 1982.

A. Eriksson, "Lightning and Tall Structures," *Transactions of South African Institute of Electrical Engineers*, Vol. 69, Pt. 8, August, 1978, pp. 238-252.

B. Fisher and J. Plumer, "Lightning Attachment Patterns and Flight Conditions Experienced by the NASA F-106B Airplane," *Proceedings of 1986 International Aerospace and Ground Conference on Lightning and Static Electricity*, Fort Worth, TX, June 21-23, 1983, pp. 26-1--26-15.

B. Fisher, P. Brown and J. Plumer, "Summary of NASA Storm Hazards Lightning Research, 1980-1985," *Proceedings of 1986 International Aerospace and Ground Conference on Lightning and Static Electricity*, Dayton, OH, June 24-26, 1986, pp.4-1--4-16.

J. Reazer and A. Serrano, "Spatial and Temporal Description of Strikes to the FAA CV-580 Aircraft," *Proceedings of 1986 International Aerospace and Ground Conference on Lightning and Static Electricity*, Dayton, OH, June 24-26, 1986, pp.15-1--15-11.

D.J. Malan, Physics of Lightning, (London: English Universities Press, 1963), pp. 58-67.

F.A. Fisher and J.A. Plumer, Lightning Protection of Aircraft, NASA Reference Publication 1008, NASA RP-1008, (Washington, D.C.: Government Printing Office, October 1977), pp. 1-27.

K. Berger, "The Earth Flash," in Lightning. Vol. 1: The Physics of Lightning, edited by R.H. Golde. (New York: Academic Press, 1977), pp.119-190.

M.A. Uman and E.P. Krider, "A Review of Natural Lighting: Experimental Data and Modeling," IEEE Transaction on Electromagnetic Compatibility, EMC-24, No. 2, May 1982, pp. 79-112.

Space Shuttle Program Lightning Protection Criteria Document, JSC-07636, Revision A, National Aeronautics and Space Administration, Lyndon B. Johnson Space Center, Houston, TX, November 4, 1975, p. A-5.

P. Rustan and J. Hebert, "Lightning Measurements on an Aircraft Flying at Low Altitude," Proceedings of the Second International Conference on the Aviation Weather System, June 19-21, 1985, pp. 220-225.

D.W. Clifford and H.W. Kasemir, "Triggered Lightning," IEEE Transaction on Electromagnetic Compatibility, EMC-24, No. 2, May 1982, pp. 112-122.

V. Mazur, B. Fisher and J. Gerlach, "Conditions conducive to Lightning Striking an Aircraft in a Thunderstorm," Proceedings of 1983 International Aerospace and Ground Conference on Lightning and Static Electricity, Fort Worth, TX, June 21-23, 1983, pp. 90-1--90-7.

B.G. Melander, "Atmospheric Electricity Hazards Threat Environment Definition," by Boeing Military Airplane Company. Air Force Wright Aeronautical Laboratory Technical Report, AFWAL-TR-85-3052, Wright-Patterson AFB, OH, August 1985, p. 2.

J.E. Nanevich, "Static Charging Effects on Avionic Systems," AGARD Lecture Series No. 110, Atmospheric Electricity-Aircraft Interaction, AGARD LS-110, June 1980, p. 12-2.

H. Garrett, "Spacecraft Charging: A Review," in Space Systems and Their Interactions with Earth's Space Environment, Edited by H. Garrett and C. Pike, Progress in Astronautics and Aeronautics, Vol 71, 1980, p. 178.

J.A. Plumer, "Data From the Airlines Lightning Strike Reporting Project," Proceedings of 1972 International Aerospace and Ground Conference on Lightning and Static Electricity, Las Vegas, NV, December 12-15, 1972, pp. 282-289.

D.W. Clifford, "Aircraft Mishap Experience From Atmospheric Electricity Hazards," AGARD Lecture Series No. 110, Atmospheric Electricity-Aircraft Interaction, AGARD LS-110, June 1980, pp. 2-1--2-17.

J.C. Corbin, "Lightning Interaction with USAF Aircraft," Proceedings of 1984 International Aerospace and Ground Conference on Lightning and Static Electricity, Fort Worth, TX, June 21-23, 1983, pp. 66-1--66-6

N.O. Rasch and M.S. Glynn, "Lightning Interaction with Commercial Air Carrier Type Aircraft," Proceedings of 1984 International Aerospace and Ground Conference on Lightning and Static Electricity, Orlando, FL, June 26-28, 1984, pp. 21-1--21-11.

P. Rustan and P. Axup, "Analysis of Lightning Current Measurements," Proceedings of 1984 International Aerospace and Ground Conference on Lightning and Static Electricity, Orlando, FL, June 26-28, 1984, pp. 24-1--24-7.

B.G. Melander, "Effects of Tower Characteristics on Lightning Arc Measurements," Proceedings of 1984 International Aerospace and Ground Conference on Lightning and Static Electricity, Orlando, FL, June 26-28, 1984, pp. 34-1--34-12.

I.S. Stekolnikov, "The Parameters of the Lightning Discharge and the Calculation of the Current Waveform," Elektrichestvo. 3, 1941, pp. 63-68.

C.E.R. Bruce and R.H. Golde, "The Lightning Discharge," Journal of Institution of Electrical Engineers, Part II, Vol. 88, 1941, pp. 487-520.

N. Cianos and E.T. Pierce, "A Ground Lightning Environment for Engineering Usage," Stanford Research Institute Technical Report 1, August 1972.

G. Ketterling, Final Report, Atmospheric Electricity Hazards Protection Program, Part V. Qualification and Surveillance Test and Analysis Procedures, by Boeing Military Airplane Company. Air Force Wright Aeronautical Laboratory Technical Report, AFWAL-TR-87-3025, Part V, Wright-Patterson AFB, OH, June 1987, p. 2-5.

R.A. Perala, T. Rudolph and F. Eriksen, "Electromagnetic Interaction of Lightning with Aircraft," IEEE Transaction on Electromagnetic Compatibility, EMC-24, No. 2, May 1982, pp. 173-203.

Society of Automotive Engineers. "Lightning Test Waveforms and Techniques for Aerospace Vehicles and Hardening," Report of the SAE Committee AE4L, June 20, 1978.

J.A. Plumer, "Further Thoughts on Location of Lightning Strike Zones on Aircraft," Supplement to NASA Conference Publication 2128, Proceedings of Lightning Technology Symposium, Hampton, VA, April 22-24, 1980, pp. 81-98.

T. James and J. Phillpott, "Simulation of Lightning Strikes to Aircraft," Culham Laboratory Report CLM-R111, Abingdon, Oxfordshire, U.K. 1971.

R.W. Leonard and D.R. Mulville, "Current and Projected Use of Carbon Composites in United States Aircraft," AGARD Conference Proceedings No. 283, AGARD CP-283, June 1980, pp. 1-13--1-19.

J. Corbin, "An Overview of the Electrical/Electromagnetic Impact of Advanced Composite Materials on Aircraft Design," from A Compendium of Lightning Effects on Future Aircraft Electronic Systems, N. Rasch, ed. Department of Transportation, Federal Aviation Administration, Report No. DOT/FAA/CT-82/30, February 1982, pp. 100-104.

CHAPTER II

MEASUREMENT OF ELECTROMAGNETIC LIGHTNING THREATS

Overview

This chapter discusses the instrumentation used to measure the effects on an aircraft, or some other test object, of simulated lightning and actual strikes. These measurements include: the magnetic (current) and electric (voltage) field distributions on the outer surfaces/skins of the aircraft; the voltage and current transients induced in internal electronic circuits, and the currents which flow onto the aircraft. The instrumentation includes: external and internal sensors; data transmission lines; data conditioning equipment; collection and recording devices; and display subsystems. The basic electromagnetic and physical principles which influence the operation of each of the subsystems is discussed in terms of how they may affect the measurements which are made in airborne characterization programs and lightning simulation tests.

Basic Instrumentation System

The basic lightning measurement system has several component pieces which are displayed in block form in Figure II-1. This section presents the functional purpose and relationships of these subsystems.

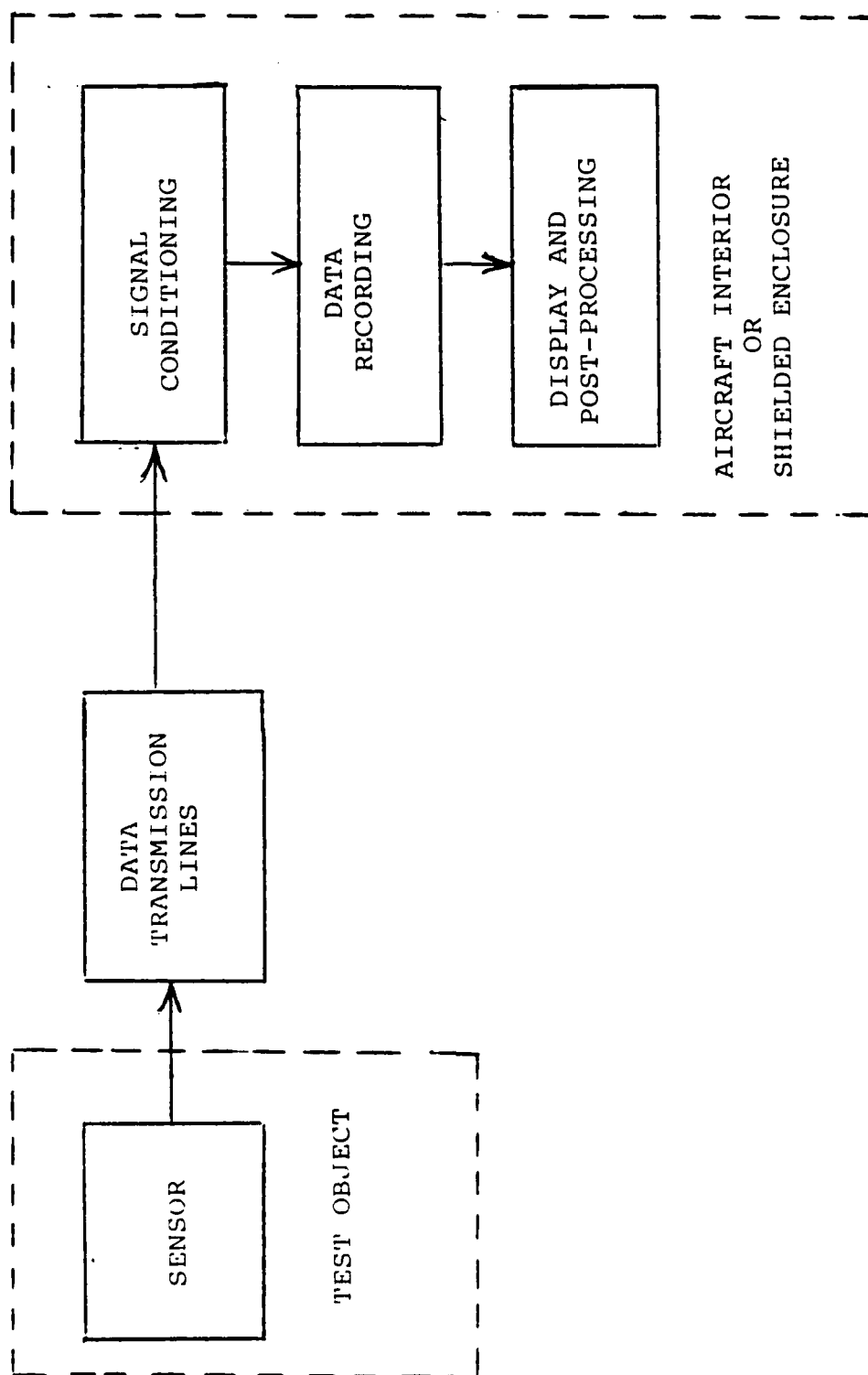


Figure II-1. Basic Instrumentation System

The front end of the basic instrumentation system is the sensor or transducer. In lightning characterization and lightning simulation tests, the sensors are placed on the outside of the aircraft or test object to measure magnetic and electric field distributions and currents which flow onto the aircraft or test object. The purpose of the sensor is to interface the measurement system to the signal to be measured. In general terms, it often acts as a translation device to convert the electromagnetic phenomenon to be measured into a signal that can be transmitted, processed, recorded and displayed by the instrumentation system. An important characteristic of the sensor is the actual quasi-static and transient electromagnetic field quantities must be translated into electrical signals before they may be processed. In succeeding sections, the basic operating principles of the sensors and other subsystems are presented.

Often the signal to be measured originates in a hostile environment or location. It is also possible that the signal to be measured is dangerous to the instrumentation system or its users. Also, locating the equipment of the measurement system near the sensor will alter the local electromagnetic environment. Because of these and other reasons, once the electromagnetic phenomenon is detected at the measurement location, it

must be transmitted to another place where the processing, recording and display subsystems can be safely and practically located. As much as possible, the data transmission link should be transparent to the signals moving through it. This implies that the bandwidth of the transmission system should be broad enough to allow the signal to pass through unaltered.

In airborne characterization programs, this means transmitting the transduced signal from the sensor on the outside of the vehicle to the interior of the aircraft. Typically, shielded coaxial transmission lines, such as triax, are used for this purpose. Using shielded connectors, the triax is connected from the sensor to the conditioning equipment, with the outer shield grounded to the aircraft's interior approximately every 2 feet. This procedure is used to minimize ground loop phenomenon and prevent stray fields from perturbing the transduced signal during transmission.

In ground simulation tests, electromagnetic compatibility problems can arise from inductive mutual coupling with the intense electromagnetic fields present on and around the aircraft if the transmission lines are not carefully designed. For many years data transmission was performed using shielded, twisted pairs. Twisted pair transmission lines consist of two wires which are tightly

twisted together to minimize inductive mutual coupling. Also, great care has to be taken to isolate the extremely high voltages and currents present on the aircraft from personnel and other equipment during the course of the test. Because of these disadvantages, twisted pair cable is not the transmission line of choice.

In recent years considerable improvement in the isolation and transmission of the detected signals has been accomplished through the use of fiber optic transmission lines. At or near the sensor's location, the electrical signal produced by the sensor is converted into light, which is then transmitted via dielectric fiber optic cables to the location of the conditioning equipment. There it is converted back to an electrical signal to be processed. The bandwidth of the fiber optic converters and transmission line must be broad enough, and the calibration accurate enough, to allow the signal originally detected by the sensor/transducer to be converted, transmitted and reconverted without the introduction of error or the alteration of the detected signal.

In ground simulation tests the signal is usually transmitted to an instrumentation van or a specially designed, electromagnetically shielded room. In either case, care must be taken to shield the rest of the

measurement and processing equipment from the intense electromagnetic environment created by the operation of high voltage and high current lightning simulation generators. These noise signals will introduce error if they are allowed to enter the signal processing chain at any point.

After the detected signal has been reconverted or is otherwise connected to the signal conditioning equipment, this subsystem processes the measured data. It is important to note that signal conditioning can take place at many locations in the measurement system. In a typical system, there will be many types of signal conditioning. Signal conditioning may include the attenuation of too large signals by resistive dividers or current shunts, or the amplification of weaker signals through solid state amplifiers. It may also include the hardware integration of the output signal of a derivative sensor before it is recorded. These actions are generally referred to as pre-processing and they usually occur in real time while the signal is actually being detected. Most fiber optics receivers and transmitters are capable of converting and reconvertng electrical signals which are approximately 2 volts peak-to-peak. The measured signals are amplified or attenuated to meet this criteria. Weak signals are amplified to 2 volts while large signals are attenuated to this level.

Once the data is pre-processed, it is collected for storage and further processing. For many years this data was recorded photographically in an analog form on an oscilloscope or magnetically on an analog recorder. In recent years, this has been replaced almost totally by digital systems which sample and record the data at set sample rates or discrete frequencies.

While digital sampling allows great flexibility in processing, storage and display, it requires care to ensure that data is faithfully preserved. The sample rate must be fast enough to prevent aliasing or the folding of the high frequency components of the signal onto the low frequency components. This minimum sampling rate is at least twice as fast as the reciprocal of the highest frequency, or put another way, if the signal to be sampled has a bandwidth B , then the minimum sampling frequency, ω_s , is equal to $2B$. This minimum frequency is called the Nyquist sampling frequency. Thus, for a digitized signal with an upper frequency of 10,000 Hz, we can take the bandwidth to be $2\pi \times 10^4$ rad/sec and the Nyquist sampling frequency should be at least

$$\omega_s = 2B = 4\pi \times 10^4 \text{ rad/sec}$$

Since $\omega_s = 2\pi/T$, where T is the sampling interval, the required sampling interval is $2\pi/\omega_s = 50 \mu\text{sec}$.

The sampling rate must also be fast enough to capture all of the transient phenomena of interest. Otherwise, quick changes in the data may not be recorded. Despite these potential problems, digitized data is extremely attractive and is widely used in conjunction with small and medium sized computers to process lightning simulation and characterization data. There are many storage formats; most are based on magnetic storage technology. These include magnetic disks or diskettes for digital data and magnetic tape for analog signals as well as digital data.

Finally, the data may be processed and is displayed. While the raw data may be displayed, it is common to format the results into a form that yields the most insight into what has been measured. Of course, this depends on what is being observed.

The ultimate configuration developed is dependent upon the specific signal to be measured and what is to be done with the measurements. For the quick determination of a low level voltage, a voltmeter may be the only instrumentation system needed. If the types of signals to be measured are the operating parameters resulting from a laser activated fusion experiment, the instrumentation system will be quite different.

The instrumentation described here could be used for the measurement of many different electromagnetic based phenomena. For example, measurement of NEMP waveforms, ionizing radiation, optical effects, or any other high speed, short-time transient phenomenon could be measured with the basic system outlined here. In each case, selection of suitable components will determine the success of collecting the needed data from the phenomenon to be measured.

Many factors determine the suitability of an instrumentation system in measuring a particular type of phenomenon. For instance, the type of sensors used, the parameters of the instrumentation subsystems such as bandwidth, power handling capability, etc., and the type of data processing and display. Regardless of the system components chosen, the instrumentation scientist/engineer must design the system carefully and be aware of how each component works. Particular attention must be paid to how the component may perturb the detected signals and add errors to the resulting data. These perturbations make up part of the errors known as configuration effects. In later chapters we will see how these errors affect the validity of the measured data and how they may be removed. For this chapter, the emphasis will be on the basic principles of operation of those components needed to measure, process, store and display lightning level

electromagnetic quantities, whether simulated or natural.

Measurement of Electromagnetic Quantities

The ultimate signals we are interested in are the fields, voltages and currents that are developed on and within the aircraft. In this section we will examine the basic principles which govern the operation of sensors that measure electromagnetic field quantities. After developing the necessary background on the measurement of electromagnetic quantities, various sensors used for the measurement of lightning level quantities are discussed.

Excellent reviews on the theory and operation of electromagnetic sensors are given in a series of papers by Baum [1978, 1980, 1981, 1982]. In addition, Baum, under the auspices of the Air Force Weapons Laboratory (AFWL) at Kirtland Air Force Base, Albuquerque, New Mexico, has been instrumental in publishing several series of notes on EMP and lightning related topics. These notes comprise a valuable collection of information on sensors, simulators, instrumentation, data collection and reduction techniques, and basic phenomenology.

The physical quantities that we are interested in

measuring are related by Maxwell's equations:

$$\nabla \times \mathbf{E} = -\partial \mathbf{B} / \partial t \quad (1)$$

$$\nabla \times \mathbf{H} = \partial \mathbf{D} / \partial t + \mathbf{J} \quad (2)$$

$$\nabla \cdot \mathbf{D} = \rho \quad (3)$$

$$\nabla \cdot \mathbf{B} = 0 \quad (4)$$

the constitutive relationships:

$$\mathbf{D} = \epsilon \mathbf{E} \quad (5)$$

$$\mathbf{B} = \mu \mathbf{H} \quad (6)$$

$$\mathbf{J} = \sigma \mathbf{E} \quad (7)$$

and the current continuity equation:

$$\nabla \cdot \mathbf{J} + \partial \rho / \partial t = 0 \quad (8)$$

While these equations, with the appropriate boundary conditions, will describe the mathematics and physics of sensor operation, they do not give a feel for what the sensor should do for us. In line with the development of Baum [1978], we will quote a definition of a sensor as a special type of antenna that has the following properties:

- 1) It is an analog device which converts the electromagnetic quantity of interest to a voltage or current (in the circuit sense) at some terminal pair for driving a load impedance, usually a constant resistance appropriate to a transmission line (cable) terminated in its characteristic impedance.
- 2) It is passive.

- 3) It is a primary standard in the sense that for converting fields to volts and current, its sensitivity is well known in terms of its geometry; i.e., it is "calibrated by a ruler." The impedances of loading elements may be measured and trimmed. Viewed another way it is in principle as accurate as the standard field (voltage, etc.) in a calibration facility. (A few percent accuracy is typically easily attainable in this sense.)
- 4) It is designed to have a specific convenient sensitivity (e.g., $1.00 \times 10^{-3} \text{ m}^2$) for its transfer function.
- 5) Its transfer function is designed to be simple across a wide frequency band. This may mean "flat" in the sense of volts per unit field or time derivative of field, or it may mean some other simple mathematical form that can be specified with a few constants (in which case more than one specific convenient sensitivity number is chosen).

In addition to the above characteristics, the sensors utilized typically must operate in one or more measurement environments and should be linear. These environments may be broken up into two broad categories or regions. These are the source region and outside the source region. Sensors used outside the source region are also used in measuring the response of a system to the fields propagating away from the source region.

The source region can be considered to be that area that is intimately associated with the generation of the electromagnetic phenomenon to be measured. In this region we must be concerned with a multitude of factors that affect the validity of measurements. Environmentally,

this region can be harsh and demanding due to the processes associated with generating the electromagnetic phenomenon. Usually the parameters that must be measured are modified by nonlinearities and other complications.

For instance, when measuring the electromagnetic fields produced by nuclear weapons, in the source region the sensor must withstand factors such as blast, heat, ionizing and non-ionizing radiation, weapon fragments, etc. When considering the measurement of lightning generated electromagnetic fields, many nonlinearities are associated with the lightning arc and corona. In addition, we must take the conductivity of the air into account in the source region. This effect is more pronounced the closer the sensor is located to the source, and affects some sensors more than others. Finally, the sensor must be able to withstand the effects of a direct lightning strike.

Away from the source region, we are not as affected by these nonlinearities. Also, the propagation medium (the air) tends to be more uniform. Finally, the sensor is in a more benign environment in terms of the source of the electromagnetic quantities. This does not negate the fact that the sensor must withstand other environmental effects that may be as severe. For example, a sensor mounted on the external surface of an aircraft must

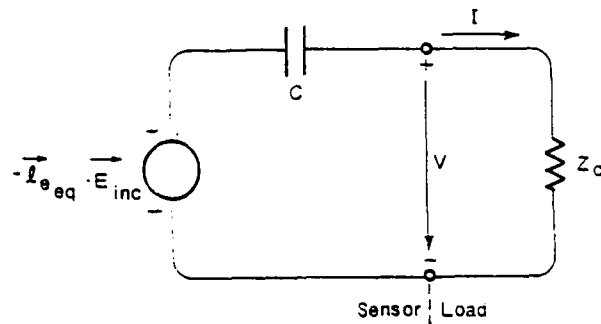
withstand the temperature extremes, vibration, mechanical stress and other effects of flight.

The response of the internal systems of the aircraft to ambient or induced fields can usually be measured by the same types of sensors as used to measure fields outside the source region. For instance, to measure the field that penetrates apertures on the aircraft, an appropriate loop or dipole antenna could be used.

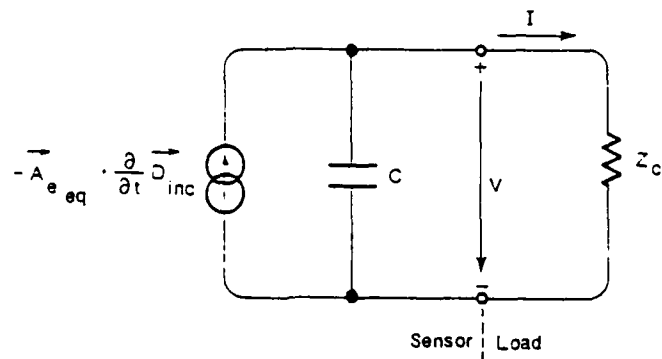
When discussing the many sensors that have been developed for the measurement of electromagnetic quantities, we can also subdivide them into categories based upon the specific electromagnetic quantity to be measured. These quantities are the electric and magnetic fields, voltage, current and charge density.

Electric field and charge density measurements are usually made with an electric dipole sensor. According to Baum [1982], the basic form of such a sensor is two separate conductors connected to a terminal pair. The topology and equivalent circuit representations for such a sensor is given in Figure II-2.

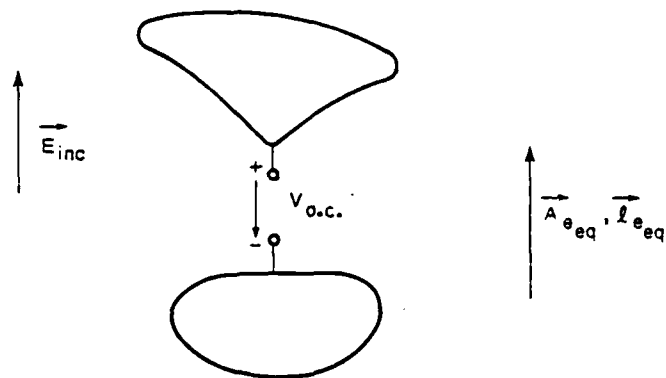
Recalling the desired properties of a sensor, we want a convenient sensitivity that is easily found from the sensor's geometry. For a load impedance that is large



(a)



(b)



(c)

Figure II-2. Electrically Small Electric Dipole Sensor In Free Space. (a) Thevenin Equivalent Circuit. (b) Norton Equivalent Circuit. (c) Electric Dipole Sensor. [Baum et al., 1980]

compared to the source impedance (capacitance), we have the Thevenin equivalent circuit representation. The sensitivity is related to an equivalent length, l_{eq} , and the output voltage of the sensor can be related to the incident electric field and is given by

$$V_o = l_{eq} \cdot E_{inc} \quad (9)$$

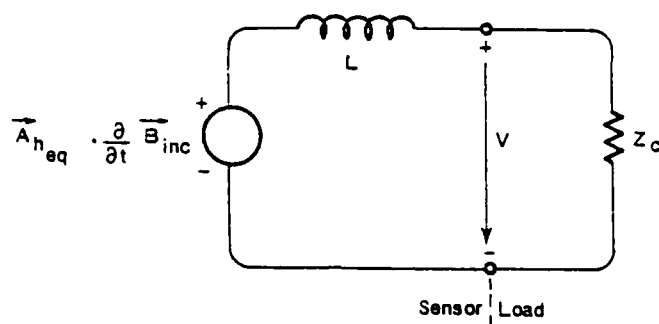
If the load impedance is small compared to the source impedance (capacitance), we have a Norton equivalent circuit representation. The sensitivity is related to the equivalent area, A_{eq} , and the output current of the sensor can be related to the incident current density and is given by

$$I_o = A_{eq} \cdot \partial D / \partial t \quad (10)$$

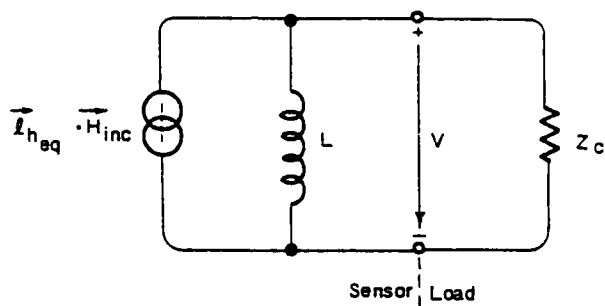
For electrically small sensors, the equivalent length and area are related by the capacitance of the dipole element and the permittivity of the medium around the sensor. This relationship is given by

$$A_{eq} = l_{eq} (C/\epsilon) \quad (11)$$

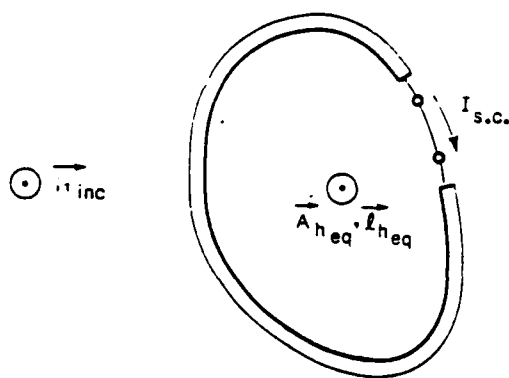
Magnetic dipole sensors are used to measure the magnetic field and current density. As shown in Figure II-3, these sensors take the form of a loop broken to connect to a terminal pair.



(a)



(b)



(c)

Figure II-3. Electrically Small Magnetic Dipole Sensor In Free Space. (a) Thevenin Equivalent Circuit. (b) Norton Equivalent Circuit. (c) Magnetic Dipole Sensor (Loop). [Baum et al., 1980].

For a load impedance that is small compared to the source impedance (inductance), we again have a Norton equivalent circuit representation. The sensitivity is related to an equivalent length, l_{eq} , and the magnetic field can be found from

$$I_o = l_{eq} \bullet H_{inc} \quad (12)$$

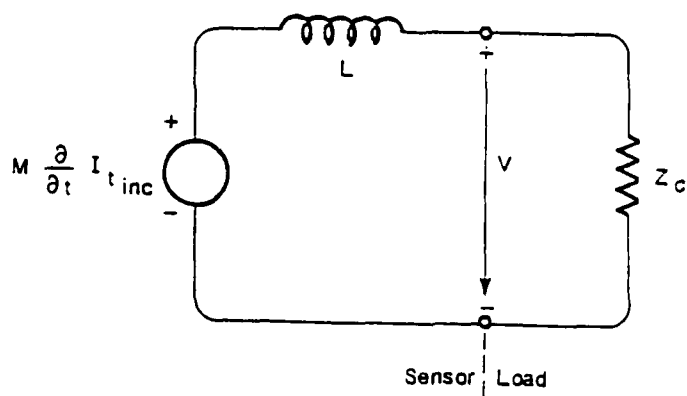
For a load impedance that is large compared to the source impedance (inductance) we have a Thevenin equivalent circuit representation. The sensitivity is related to an equivalent area, A_{eq} , and the time rate of change of the magnetic flux is given by

$$V_o = A_{eq} \bullet \partial B / \partial t \quad (13)$$

Again, for an electrically small sensor, the equivalent area and length are related by the inductance of the loop (magnetic dipole) and the permeability of the region surrounding the loop. This relationship is given by

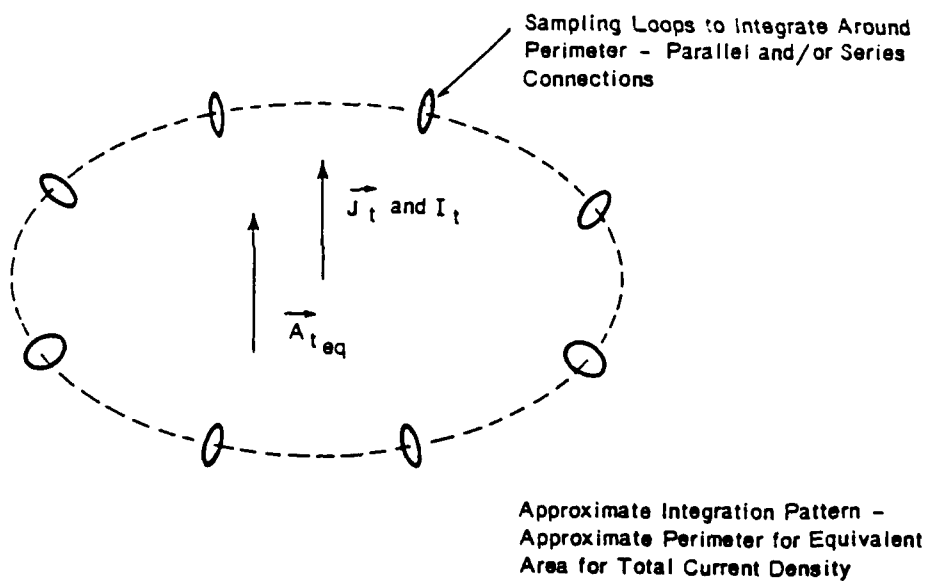
$$A_{eq} = l_{eq} (L/\mu) \quad (14)$$

Current sensors can be developed that are based upon the measurement of the fields produced by the current flowing through a specified surface. The topology of this is shown in Figure II-4, and is represented by a toroidal structure. The toroid represents a surface over which the magnetic field is integrated and the toroid encloses a surface through which the current to be measured flows.



$$I_{t_inc} = \vec{A}_{t_eq} \cdot \vec{J}_{t_inc} \quad \text{For Measurement of Distributed Current Density}$$

(a)



(b)

Figure II-4. Electrically Small Inductive Current Sensor In Free Space. (a) Norton Equivalent Circuit. (b) Inductive Current Sensor (Multiple Loops). [Baum et al., 1980].

If the inductive coupling is small, the sensor can be characterized by a mutual inductance, M , which relates the open circuit output voltage to the time derivative of the total current flowing through the surface bounded by the toroid. This output voltage is given by

$$V_o = M \partial I_t / \partial t \quad (15)$$

$$I_t = A_{eq} \bullet J_t \quad (16)$$

In all cases, these formulations are based upon the sensor being electrically small. This means that the sensor dimensions are smaller than a radian wavelength or a skin depth, as appropriate, in the medium where the fields are to be measured [Baum, 1967]. Put another way, the sensor should be electrically small so the field that is measured can be considered to be uniform in the vicinity of the sensor.

This size condition implies that the sensor size is related to the highest frequency component that is to be measured. As the sensor size increases, the available bandwidth decreases. This is important, because sensor sensitivity is proportional to the size of the sensor. Thus, we see that bandwidth and sensitivity are related. It is this decrease in bandwidth that usually constrains the available sensitivity, not physical size.

Another desirable characteristic in a sensor is the absence of any resonances, or deviations in a "flat" response, occurring in the bandwidth of interest. Resonances existing in the antenna may mask or distort the true response of the lightning waveform. One way to insure that the response of the sensor is flat across the bandwidth of interest is to make sure that it is electrically small with respect to the wavelength of the lightning frequencies to be measured. However, antennas that are small with respect to the wavelength to be received are also very inefficient and hence, insensitive. We can increase the sensitivity of the sensor by increasing its size, but we do so at the cost of adding resonances and decreasing bandwidth. Thus, in considering a single parameter, size, we see there are many tradeoffs in designing sensors for the measurement of electromagnetic field quantities.

These sensors and the equations which describe their operation are fairly simple. In reality, sensors to measure electromagnetic fields can be simple or complex depending on the frequency, sensor size and other environmental factors. Many design techniques have been developed to extend the sensor performance for making electromagnetic pulse and lightning measurements. In many cases, more bandwidth and signal may be obtained by going beyond the elementary concepts of electrically small

electric and magnetic dipoles in linear, uniform, isotropic media [Baum, 1982].

When designing aircraft lightning measurement instrumentation, care must be taken to design the system in a manner which prevents avoidable errors in the recorded data. An appreciation of how instrumentation can introduce error into the data can be gained by considering the instrumentation which was used to gather the data on airborne lightning strikes and ground simulation experiments presented in Chapter V. We will begin by considering the sensors used to measure lightning related electromagnetic field quantities.

Sensors for Lightning Measurement

A variety of different sensors have been used to make inflight and ground-based simulation measurements of lightning. Most of these sensors were originally developed for use in NEMP testing, but have found further applications in lightning testing and research. This section presents an overview of the design, specifications and operation of a few of these sensors.

D-Dot and Electric Field Sensors. When examining the many types of electric field sensors, we can divide them into two general categories: sensors that measure the

change in the electric field and sensors that measure the static (or quasi-static) electric field. The most common type of sensor used for the measurement of electric fields is a dipole antenna. Some typical small electric dipole antennas are shown in Figure II-5.

There are many difficulties in obtaining accurate electric field measurements. As mentioned previously, the open-circuit voltage produced by the electric dipole is proportional to its length and the electric field intercepted by it. At low frequencies, it is difficult to measure the open-circuit voltage from the typical electric sensor. This is due to the large (capacitive) impedance that the sensor presents to a measurement device. Also, the electrostatic field will be "static" only as long as there is no change in the position or amount of charge that causes the field. To accurately measure the static electric field, the sensor and associated components must not disturb the charge distribution in the vicinity of the sensor. Ideally, this is impossible, but in the following sensors, this condition can be closely approximated.

The D-dot sensor is used to measure the time rate-of-change of an electric field density, $\partial D/\partial t$. The sensor's response is described by the Norton equivalent circuit of Figure II-2. As can be seen from the circuit, the capacitance of this sensor should be small, because it

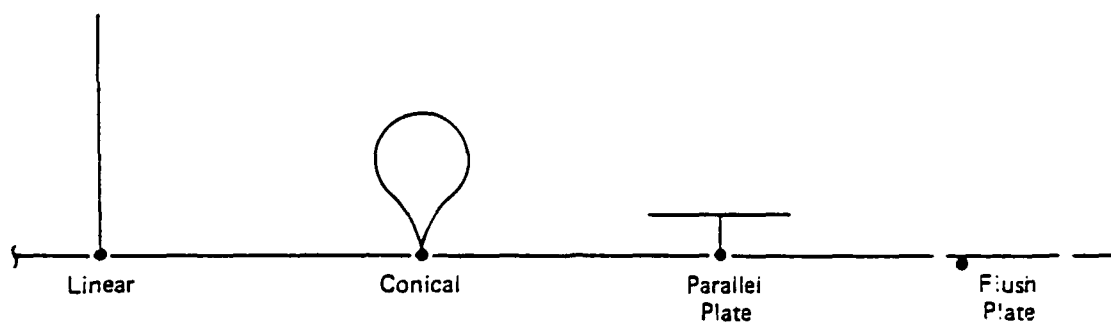


Figure II-5. Typical Dipole Sensor Configurations.
[Nanevich and Vance, 1986].

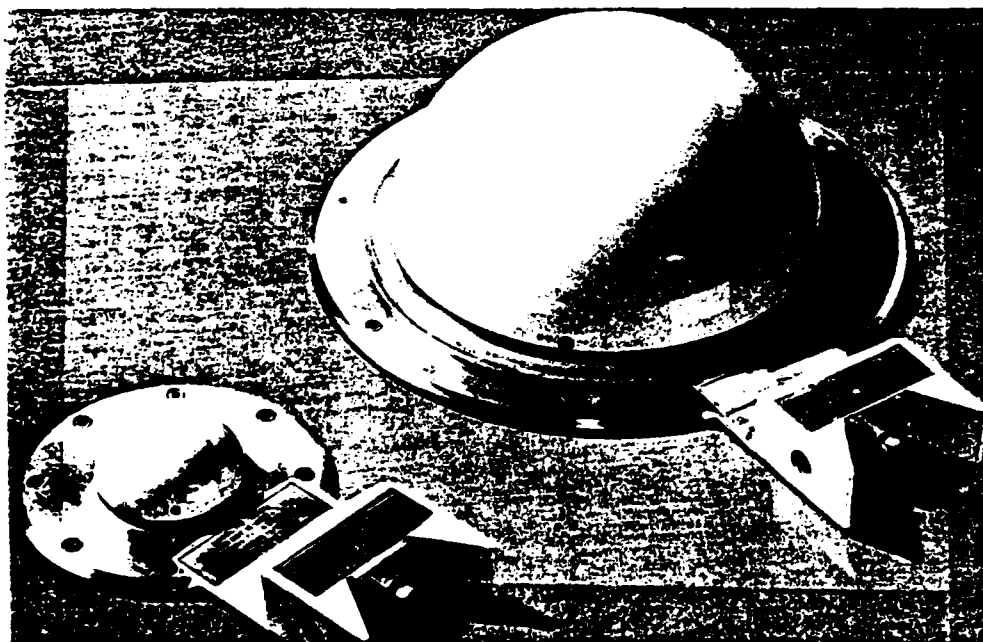


Figure II-6. Hollow Spherical Dipole (HSD) D-dot Sensor.
[EG&G, 1980]

shunts the load resistance and determines the high frequency cut-off of the basic low frequency filter type circuit.

Figure II-6 is an illustration of a sensor known as a Hollow Spherical Dipole (HSD), used to make derivative electrical field measurements. Specifications and data for this and other sensors discussed in this chapter are presented in Appendix I. This sensor's design uses the geometry of a sphere with a narrow slot around the equator. The slot is resistively loaded by the signal cables. Signal current from each hemisphere flows to the ground plate through four equally-spaced 200 Ω striplines. The striplines join at the center of the base ground plate and continue into the 50 Ω coaxial cable. These sensors are available in both free space and ground plane versions, with the ground plane version the one that is illustrated.

Figure II-7 shows the design of the Asymptotic Conical Dipole (ACD), which is also used to make free space derivative electric field measurements. The surface of this sensor is designed to correspond to an equipotential surface which, in differential form, approaches a 100 Ω cone at its base. The ACD consists of a sensor element attached to a 50 Ω semi-rigid coaxial cable that passes through the ground plane to a coaxial

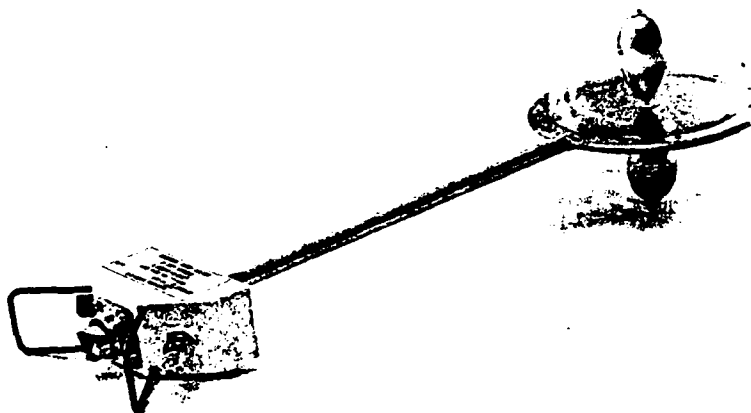


Figure II-7. Asymptotic Conical Dipole (ACD) D-dot Sensor
[EG&G, 1980].

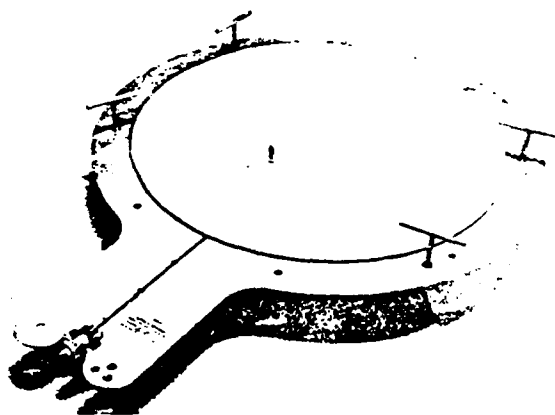


Figure II-8. Parallel Plate Dipole (PPD) E-Field Sensor
[EG&G, 1980].

connector. This sensor achieves an improved figure of merit over the HSD by being designed to lie along a particular electrostatic equipotential line. The development of the ACD geometry is described in a report by Baum [1969]

The Parallel Plate Dipole (PPD), shown in Figure II-8, is a common sensor for measuring the electric field. The PPD is designed in the form of a parallel plate capacitor. The top plate is supported above a conducting ground plane via nylon spacers. The output signal is obtained from an attenuating resistor attached to the center of the top plate in series with a 50 Ω output cable which terminates in a coaxial connector. If the resistor's stray capacitance is compensated for, the frequency domain response of this sensor is given by

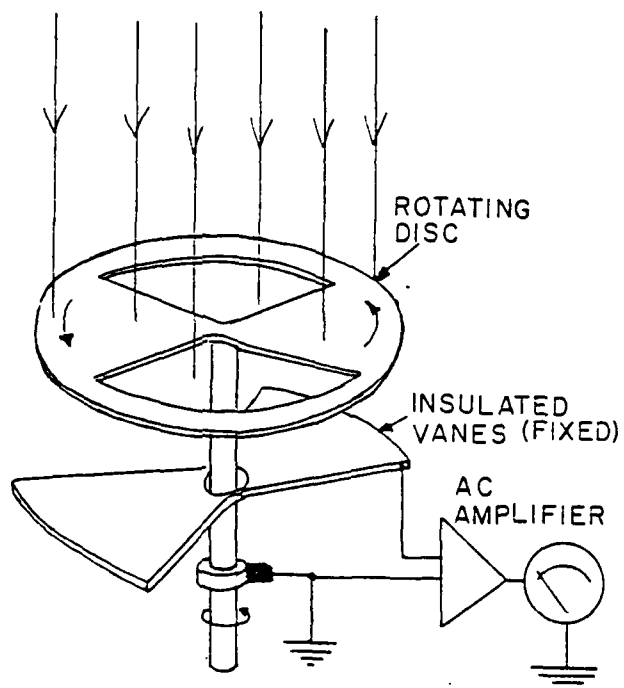
$$V_{oc}(s) = -E_{inc}(s) \bullet l_{eq} \frac{Z_c}{Z_c + R} \frac{sC(Z_c + R)}{sC(Z_c + R) + 1} \quad (17)$$

where l_{eq} = equivalent height (plate separation)
 R = attenuating resistor
 Z_c = output cable impedance

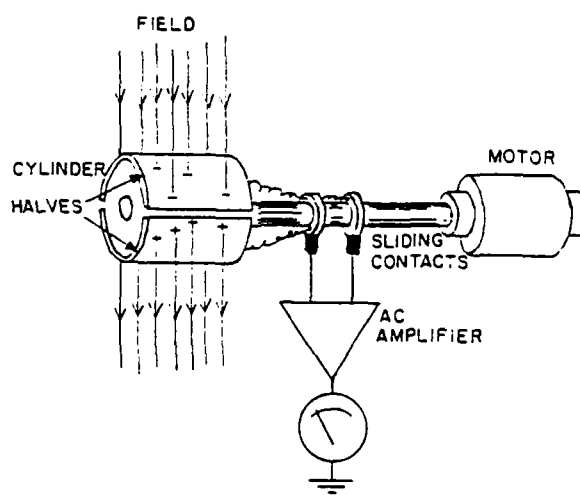
The attenuating resistor will determine both the sensitivity and the time constant (frequency response) of this sensor.

To measure quasi-static or very slowly changing electric fields, field mills are often used. One form of these sensors is a flat plate dipole sensor with a rotating vane for the top plate. By rotating the top plate, the equivalent area of the sensor is varied and minor changes in near static fields can be detected. Another form of this sensor consists of a split cylinder that rotates in the electric field to be measured. Figure II-9 shows both of these sensors. When using the results obtained from field mills, one must remember that the field measured consists of two separate fields, the ambient electric field and the field due to charges which accumulate on the aircraft. The two fields should be separated and each field considered independently. The field mill is further discussed in the text by Chalmers [1967].

Current Sensors. Current sensors are commonly used to measure the current injected during lightning simulation tests. They are also found at the base of special booms mounted on airborne lightning research aircraft to measure the lightning channel's current due to a direct strike to the boom. There are three common types: the circular parallel mutual-inductance (CPM) sensor, the I-dot one-turn insertion unit and the common current shunt.



(a)



(b)

Figure II-9. Electric Field Mills. (a) Rotating Shutter Electric Field Mill. (b) Cylindrical Electric Field Mill. [Wahlin, 1986].

The CPM sensor (Figure II-10) measures the time derivative of the total current flowing through the aperture of the sensor. It has loop turns which are oriented to be sensitive to the Φ component of the magnetic field with respect to the measurement axis. The output voltage of the sensor is given by

$$V_o = M \, dI/dt \quad (18)$$

where the mutual inductance, M , is given by

$$M = \frac{N \mu_r \mu_o w \ln(r_2/r_1)}{2\pi} \quad (19)$$

and N = the number of turns in the loop

w = cross section width

r_1 = the inner radius of the loop

r_2 = the outer radius of the loop

To date these sensors have been designed for $M = 10^{-8}$ H with a $\mu_r=1$ and diameter between 0.1 and 2 meters.

The I-dot ($\partial I/\partial t$) one-turn insertion unit measures the derivative of the current which passes through the center conductor of a coaxial cable. The basic sensor is shown in Figure II-11. This sensor's operation is basically the same as that of the CPM sensor.

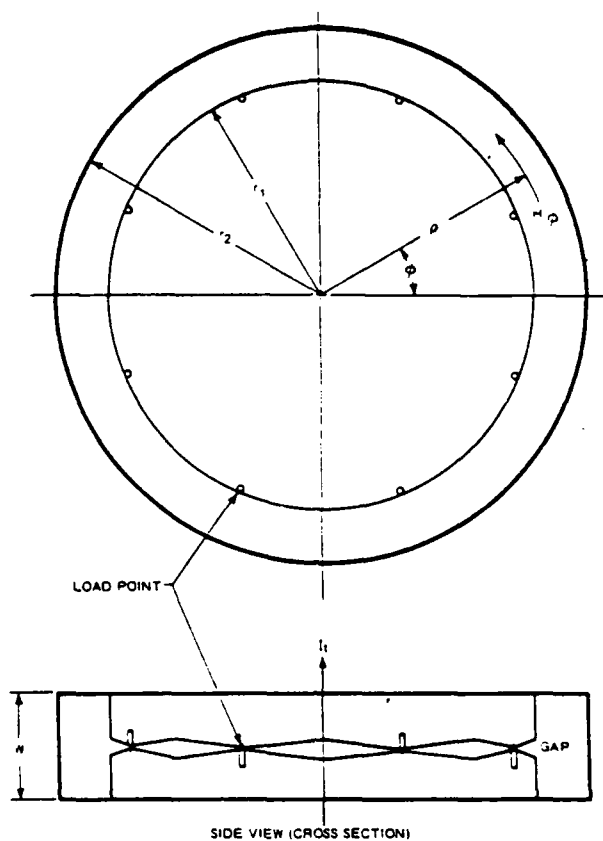


Figure II-10. Typical Circular Parallel Mutual-Inductance (CPM) Sensor Geometry. [Baum et al., 1980]

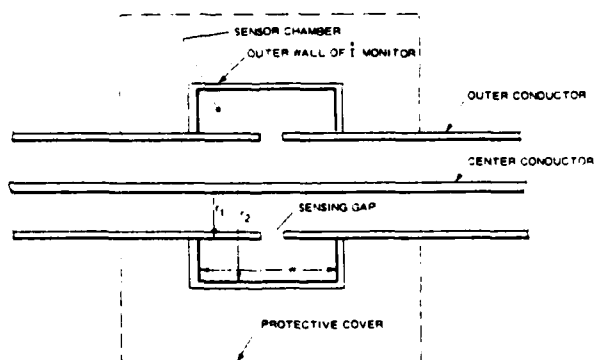


Figure II-11. I-dot One-turn Insertion Unit Current Sensor [Baum et al., 1978].

The current shunt measures currents directly and is depicted schematically in Figure II-12. The total current, I_T , is related to the voltage across the shunt resistance, V_S , by the familiar current divider relationship

$$I_T = V_S [R_S R_2 / (R_S + R_2)] \quad (20)$$

Magnetic Field Sensors. Magnetic field sensors are commonly used to measure the skin current distributions of the actual or simulated lightning currents as they are distributed over the aircraft or test object during an airborne strike or ground simulation tests.

The Multi-gap Loop (MGL) series of B-dot ($\partial B / \partial t$) sensors are used to make high frequency magnetic field measurements. The layout of the MGL sensor is shown in Figure II-13. The MGL is built as a right-handed cylinder which is printed and etched to provide the gaps and the 200 Ω striplines depicted in this figure. The sensor is divided into 4 quadrants with 2 opposing quadrants connected to form the differential output. By using opposing quadrants, the electric field effects are minimized.

The Cylindrical Moebius Loop (CML) sensor is a loop structure with signal cables wired in a Moebius

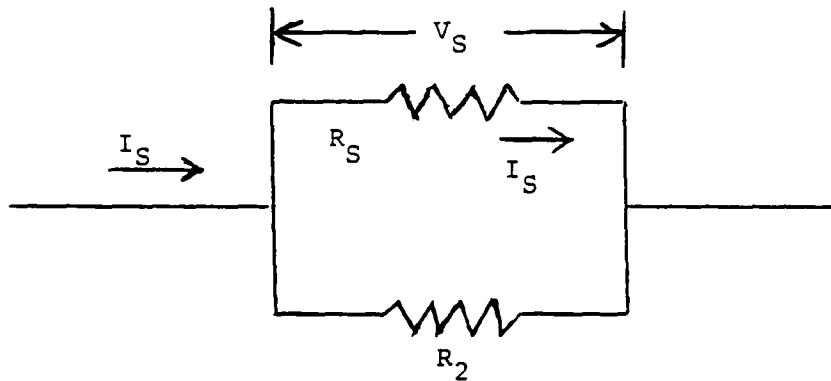


Figure II-12. Current Shunt For Measurement of Current.

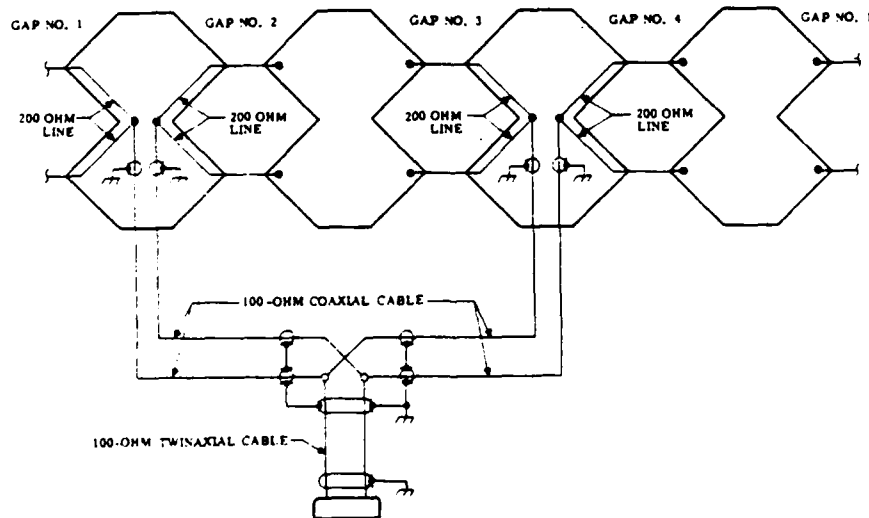


Figure II-13. Distribution of Signals in a Multi-Gap Loop (MGL) B-dot Sensor [Baum et al., 1978].

configuration to measure magnetic fields. This sensor is shown in Figure II-14. The Moebius configuration in this figure greatly reduces common mode noise currents found in simple loop type sensors. The sensor is simply a two-turn loop sensor connected to a coaxial connector. At frequencies where the magnetic field does not penetrate the shield of the gap-loading cables, the sensor acts as a single-turn cylindrical loop with a resistive gap load formed by the terminating cable's impedance.

If the response of the magnetic field sensor is predominantly due to the current flowing onto the structure upon which the sensor is mounted, rather than due to externally generated fields, the magnetic field measurement may be directly related to the skin current distribution. For example, for a cylinder with current flowing in the axial direction, the skin current distribution, J_s , on the surface is directly proportional to the magnetic field, H .

Sensors are designed for use in canonical environments such as flat, infinite half-planes or in configurations where the fields being measured are uniform. Because this ideal situation can only be approximated in the aircraft, the measurement configuration will affect the results that can be obtained. On an aircraft the sensor's location is

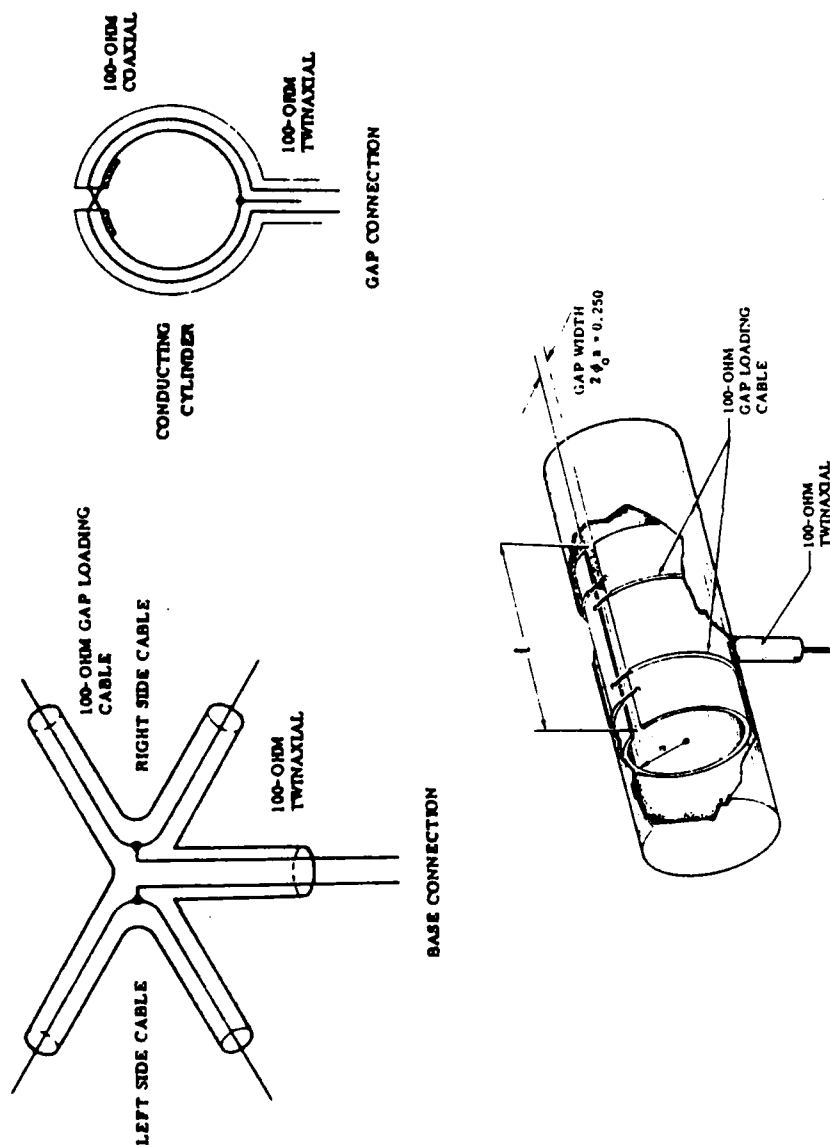


Figure II-14. Cylindrical Moebius Loop (CML) B-dot Sensor [Baum et al., 1980].

generally a compromise, with using a fairly flat surface and sufficient space beneath the fuselage to mount the sensor being the principle criteria for sensor location. The field interaction with the aircraft plays an important part in what is actually measured. One must recognize that, in general, the aircraft is also part of the sensor. Sensors should, as much as possible, be located along one of the natural symmetry planes of the aircraft, that is, perpendicular to the wings or along the plane from nose to tail. The sensor should be placed as near to the aircraft's extremities (nose, tail, wingtips) as practical.

The placement of field mills is particularly critical to the accuracy of the sensor's measurements. As Mazur, Ruhnke and Rudolph [1986] point out, "positioning sensors on or near crossing points of the lines of the aircraft's electrical symmetry (neutrality) decreases significantly the amplification of errors in the signal processing system that are transferred into errors in the ambient field estimates."

Signal Transmission Lines

Two types of signal transmission lines are commonly used to transfer the signals measured by the sensors to the signal conditioning or recording equipment. In airborne programs, triax (coax with an outer shield) is

generally used, while for ground-based simulation tests, the trend has been to use fiber optic links. The configuration effects caused by these transmission lines must be recognized, measured or otherwise accounted for in the resulting field measurements.

A coaxial cable, for example, even if perfectly matched at both ends will distort and attenuate the transmitted signal. This effect becomes particularly significant for cable lengths longer than 10 meters, such as the distance from the onboard instrumentation to a wingtip sensor. These effects, which are frequency dependent, are depicted in Figure II-15.

Fiber optic links convert the sensor's electrical signals to light signals for transmission from the aircraft or test object to the signal conditioning and recording elements, which are usually kept in shielded enclosures. This method of transmission is popular because it provides isolation between the intense electromagnetic environment caused by the lightning simulation generators and the relatively delicate electronic signal processing and recording equipment. These links require the conversion of the electrical signal to light in a fiber optic transmitter breakout box located near the sensor. Reconversion takes place at the receiver module located away from the aircraft. Fiber

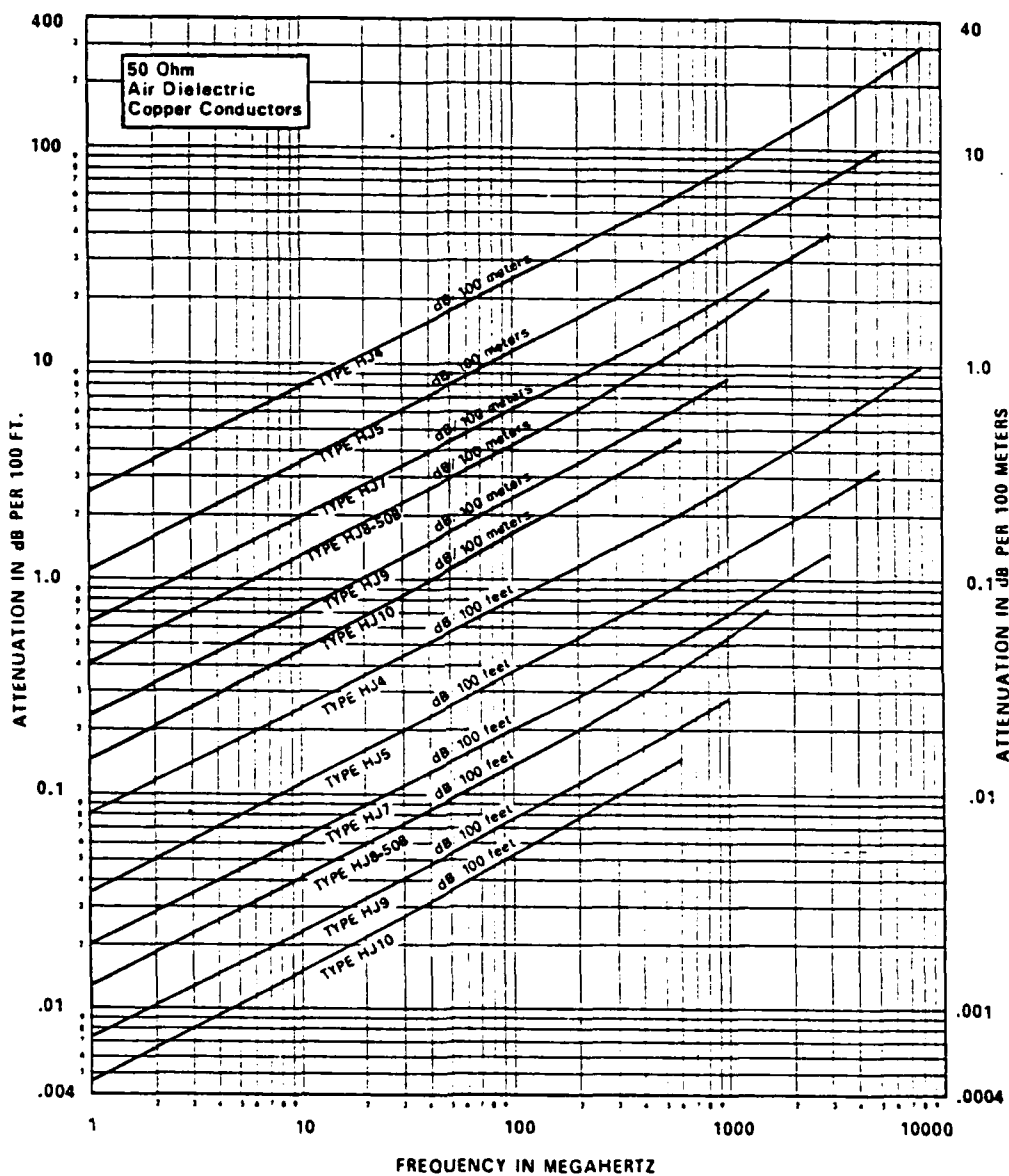


Figure II-15. Attenuation of Coaxial Cable as a Function of Frequency [Andrew Catalog 27].

optic links use simple luminescent diodes as sources and photo-detector diodes as receivers. The intensity of the signal sent down the fiber optic cable varies directly with the input signals voltage or current, depending on the design of the driving circuit.

The receiver's output is generally adjustable over a range that allows for calibration of the link using a signal generator and the recording equipment. If the tests are of long duration, frequent calibration is an important factor in preventing errors due to low battery conditions, circuit drift, etc. Network analyzers may be used to derive the frequency transfer function of the fiber optic link. An important consideration is that the link should be checked for bandwidth limitations. For most lightning work, the bandwidth of the optical fiber is much greater than that required for the lightning spectrum. However, the fiber optic transmitter and receiver must be designed to maintain a flat response over the lightning spectrum. A data sheet for a typical fiberoptic data link system is given in Appendix I. A more complete discussion of how fiber optic links function is presented in the text by Hartel [1978].

Signal Conditioning

The most common signal conditioning elements associated with lightning measurement instrumentation are attenuators, amplifiers and integrators. Attenuators are relatively simply devices, meant to reduce the level of the signal before it enters a sensor or some data transmission equipment. This helps protect sensitive electronic equipment and is also useful in expanding the dynamic range of data links and equipment. As they are passive devices, they require no power and hence no additional lines for control or power. When using attenuators, care should be taken to insure that they are not electrically overstressed. This may result in a change in their operating characteristics.

Amplifiers are useful when attempting to detect extremely small signals, or in driving signals down transmission lines. If properly designed, an amplifier can also function as an impedance matching device, serving to buffer different components in the measurement chain. The experimenter should worry not only about impedance matching, but also insure that the bandwidth of the amplifier is sufficient to prevent distortion of the transmitted signal. As the amplifier is an active device, power must be supplied to it, preferably by battery to help isolate the amplifier from external noise sources. It is also important to shield the amplifier from any

noise that might be produced by the simulator.

As many of the sensors used in electromagnetic field measurement are derivative sensors, integrators are often required to obtain the output signal in a form suitable for further processing. Integrators may be either passive or active. Factors such as bandwidth, noise rejection, impedance matching etc. also apply to selection of integrators. A useful discussion on other errors that integrators are susceptible to is given in the text by Knoepfel [1970]. Examples of integrators are presented in the data sheets in Appendix I.

Because of the proliferation of inexpensive computing equipment, software integration is becoming an acceptable alternative to hardware integration. In this case, potential problems arise if the analog-to-digital and digital-to-analog components do not have sufficient resolution, and the sampling rate is not high enough. Another way of carrying out the integration is through the use of frequency domain techniques in conjunction with the measurement of system transfer functions. This method is discussed further in Chapter IV.

Data Collection, Processing and Display

Analog records of lightning transient measurements may be accomplished by using oscilloscopes with cameras, or by recording the signal directly on an analog recorder with FM waveforms. Because of the ease in post-test analysis, this data is presently almost totally recorded with transient digitizers for time domain measurements and by discrete frequency network analyzers for frequency domain measurements.

Transient digitizers measure and record the incoming signal at a finite number of selected time intervals. The time interval between each discrete measurement must be small enough to prevent aliasing. The Nyquist criterion requires this rate be at least twice as fast as the highest frequency to be measured [Kamen, 1987]. In practice, the data is usually recorded at 5 to 10 times this rate. The digitizers used for much of the data in Chapter V are Tektronix 7612's with a maximum speed of 5 nanoseconds between discrete measurements. This allowed, in practice, measurement of signals up to 100 MHz without significant aliasing.

The gathering of lightning airborne or simulation data is a complex operation due to the signal characteristics that must be captured. The leading edge of the double-exponential or damped-sinusoidal pulse has a

fast risetime, measured in nanoseconds, while the decay period lasts for many microseconds. Because of the broad range in times that must be measured to reproduce this signal, no one analog measurement device is sufficient. Typically, the signal will be recorded on two or three digitizers or recorders, with each one using a different time-base setting. The pieces of the recorded data are then used to create a single trace by matching the appropriate segments of the signals (Figure II-16). It has been found that the difference from one time-base setting to the next should not be greater than a factor of five for achieving consistently good reconstructions of the signals [Pressley and Sower, 1986]. Therefore, 10/50/250 ns/div or 20/100/500 ns/div settings are possible choices for recording signals of 1 to 5 microsecond durations. For digital systems, this process is somewhat easier, if sufficient memory and storage capacity is available, and the digitizing rate is sufficiently high.

An Hewlett-Packard 3577A scalar network analyzer was used during this research to record the transfer functions of sensors, fiber optic links and other measurement components, as well as the aircraft circuit transfer functions. This analyzer provides a continuous wave output whose frequency is swept between two frequency limits. A finite number of measurements are made at

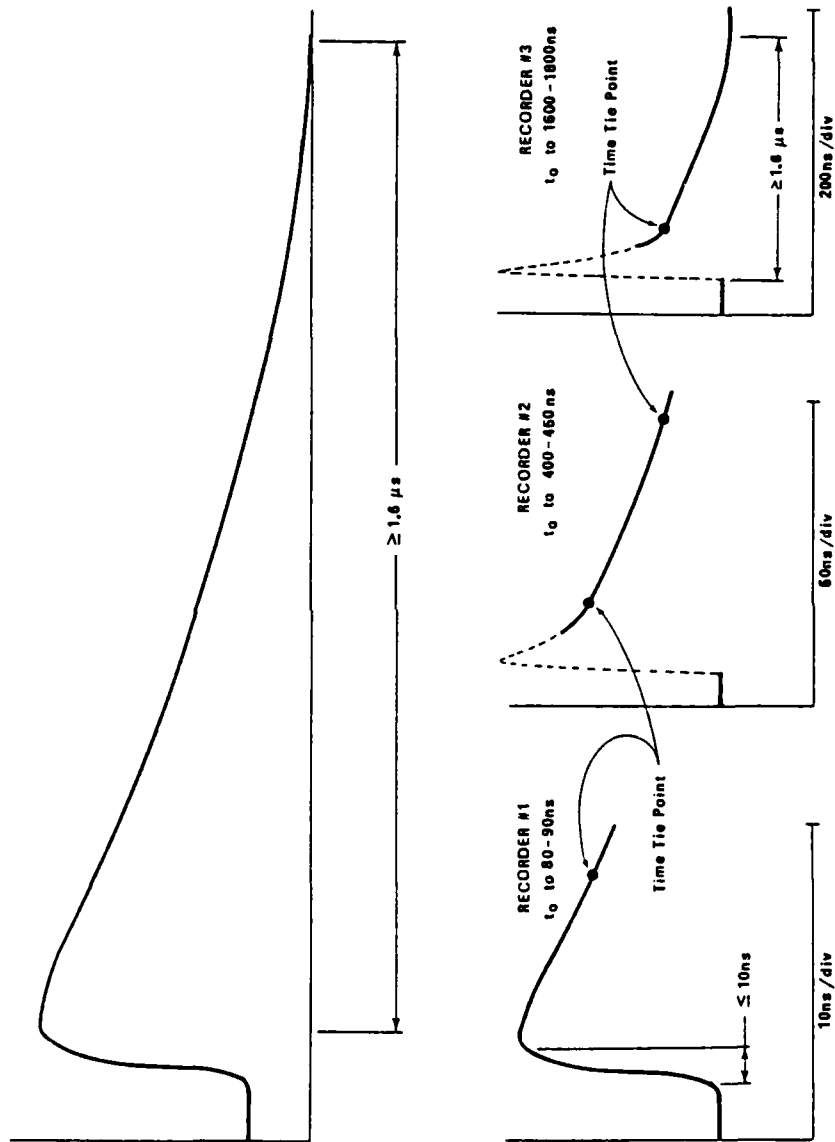


Figure II-16. Composite Waveform Derived from Three Recorders to Yield Data Spanning Several Time Bases [Pressley and Sower, 1986].

discrete frequencies within this range and are recorded digitally within the analyzer. The major concern in using this device, aside from insuring that all impedances are matched, is that measurements are made often enough to insure that a faithful reproduction of the frequency response is made.

A permanent record of the data is generally preserved on either magnetic disk or tape. Almost any type of computer may be used with the 7612's and HP3577A mentioned earlier, with the link made by either an RS-232 bus or the IEEE-488 (HPIB) bus. The use of these computers greatly eases the burden of collecting, processing and analyzing the data that results in these investigations. In addition, their data manipulation and file-handling capability makes it possible to develop graphical presentations of the results of this analysis.

The configuration effects that can be introduced into airborne or ground-based simulation measurements due to instrumentation problems can be illustrated by a contrived example of how not to set up the system.

A magnetic field with frequency content up to 100 MHz is measured by a derivative loop-type sensor which is mounted off the symmetry plane of the aircraft in a sharply diverging field, such as near the wing's edge. The

sensor's 50 Ω output is connected to a 20 meter long, 75 Ω cable, resulting in a mismatched condition and an attenuated signal. As the cable is not grounded at 2 foot intervals, it suffers from serious ground loop problems. The output of this cable is connected to a fiber optic transmitter whose battery is quickly becoming discharged, resulting in a loss of calibration. The signal is reconverted and amplified by an amplifier which only has a bandwidth of 75 MHz. The derivative signal is integrated with a large value of capacitance, that lies beyond the cutoff frequency. The signal is recorded in the time domain at a sample interval of 40 nanoseconds, giving a result that is severely aliased. Finally, the signal is recorded for future processing.

Although this is a rather extreme example of a poorly designed system, it does serve to illustrate the many factors that must be taken into consideration for system design. If these errors are not eliminated, then the results from any measurement program will be almost worthless. Fortunately, if the errors, real and potential, are recognized during the measurement system design process, they can be corrected or compensated for. As will be pointed out in the next few chapters, these are not the only errors that must be recognized and corrected.

REFERENCES - CHAPTER II

C.E. Baum, E.L. Breen, J.C. Giles, J. O'Neill and G.D. Sower, "Sensors for Electromagnetic Pulse Measurements Both Inside and Away from Nuclear Source Regions," IEEE Transactions on Antennas and Propagation, AP-26, No. 1, January 1978, pp. 22-35 and IEEE Transactions on EMC, No. 1, February 1978, pp. 22-35.

C.E. Baum, E.L. Breen, J.P. O'Neill, C.B. Moore and G.D. Sower, "Electromagnetic Sensors for General Lightning Application," Proceedings of Lightning Technology Symposium, NASA Langley, NASA Conference Publication 2128, FAA-RD-80-30, April 22-24, 1980, pp. 85-118.

C.E. Baum, "Sensors for Measurement of Intense Electromagnetic Pulses," Proceedings of 3rd IEEE International Pulsed Power Conference, Albuquerque, NM, June 1981, pp. 179-185.

C.E. Baum, E.L. Breen, F.L. Pitts, G.D. Sower and M.E. Thomas, "The Measurement of Lightning Environmental Parameters Related to Interaction with Electric Systems," IEEE Transaction on Electromagnetic Compatibility, EMC-24, No. 2, May 1982, pp. 123-137.

C.E. Baum, "Parameters for Some Electrically-Small Electromagnetic Sensors," Sensor and Simulation Note 38, Air Force Weapons Laboratory, Kirtland AFB, NM, March 1967, p 2.

C.E. Baum, "An Equivalent-Charge Method for Defining Geometries of Dipole Antennas," Sensor and Simulation Note 72, Air Force Weapons Laboratory, Kirtland AFB, NM, January 1969.

J.A. Chalmers, Atmospheric Electricity. 2nd ed. Oxford: Pergamon Press, 1967, pp. 143-145.

V. Mazur, L.H. Ruhnke, and T. Rudolph, "Effect of E-Field Mill Location on Accuracy of Electric Field Measurements with Instrumented Airplane," Proceedings of the 1986 International Aerospace and Ground Conference on Lightning and Static Electricity, Dayton, OH, June 24-26, 1986, p. 31-1.

V. Hartel, Optoelectronics, Theory and Practice. New York: McGraw-Hill Book Co., 1978.

H. Knoepfel, Pulsed High Magnetic Fields. New York: American Elsevier Publishing Co., 1970, pp. 298-301.

E. Kamen, Introduction to Signals and Systems, New York: Macmillan Publishing Co., 1987, pp. 454-460.

J.R. Pressley and G.D. Sower, "Instrumentation for Time-Domain Measurements," in Time-Domain Measurements in Electromagnetics, edited by E.K. Miller, New York: Van Nostrand Reinhold Co., 1986, pp. 189-191.

CHAPTER III

PREDICTION AND MODELING OF LIGHTNING INTERACTION
WITH AIRCRAFTOverview

There is a close relationship between the ability to predict and model the processes that occur during the interaction of lightning with an aircraft, and the ability to accurately simulate those interactions. As we create more accurate models, we are able to make more accurate predictions of the processes we are modeling. In turn, we can improve our simulations and models by comparing measured results to predicted results and adjusting the simulator or model as appropriate.

Ever since the early 1960's, when there began to be an awareness of the problems of nuclear electromagnetic pulse (NEMP) effects, researchers have examined the electromagnetic responses of aircraft that are excited by transient electromagnetic phenomena which have significant spectral content in the resonance region (2-20 MHz) of aircraft. Phenomena at these frequencies interact strongly with the aircraft, much as a tuned rf-circuit exhibits its strongest interaction with surrounding EM radiation at its resonant frequency. Many models, of varying degrees of accuracy and sophistication, have been developed over the years to model these phenomena.

Although these NEMP models have proven to be useful in describing the NEMP environment and its effects, they have been inadequate for the analysis of the lightning-aircraft interaction event. There are significant differences between lightning and NEMP, primarily in the areas of frequency content, spectral energy distribution, waveform parameters, nonlinear effects and the geometry associated with an aircraft and attached lightning channel. The result of these differences is that lightning interaction models have much more demanding requirements than NEMP models.

Recent data describing the parameters of the lightning environment show that the environment has a much larger electromagnetic field content in the aircraft resonance region than was previously thought [Perala, Rudolph and Eriksen, 1982]. Because of this, more work must be done to increase our knowledge of the interaction process and to incorporate this knowledge into more accurate models. To apply this knowledge to the prediction and modeling of what happens during that interaction, we must be able to model and simulate each part of the interaction process. The development of accurate and easily used models for each of these sub-steps is an area of active research, and requires a detailed knowledge of what happens during each step of the process.

Previously, the analysis of lightning interaction with aircraft has used low-frequency models which ignored aircraft resonances and the dynamic redistribution of charge and current on the vehicle. Also, most of this work has focused on the magnetic field, to the exclusion of the electric field. Current work in this area has begun to address these deficiencies, and models are being developed that incorporate the results of this work. Although not developed to the sophistication of the equivalent NEMP models, these lightning interaction models provide new insight to the interaction process and make it possible to refine the results obtained from current simulators.

Because of the focus of this dissertation, we will only consider those aspects of modeling and prediction that are pertinent to the correction of errors that occur in the simulation process. In the next section, we will examine the interaction process in greater detail. Following that, we will discuss the modeling of those processes. Finally, we will look at the predictions that can be obtained from those models and see how they can be applied to the correction of the simulation process.

The Lightning-Aircraft Interaction Process

Although we listed the steps involved in the lightning-aircraft interaction process and discussed them somewhat in Chapter I, let us now consider these steps in some detail, as it is the effects of these processes we will be attempting to simulate accurately. In flow diagram form, these steps are illustrated in Figure III-1, while Figure III-2 illustrates the process schematically.

The steps that occur are are:

1. The current in the lightning channel attaches to the aircraft or passes very close to the aircraft.
2. The current from the channel causes a current and charge distribution on the aircraft skin and structure.
3. The aircraft skin current and charge distribution produces magnetic and electric fields around the aircraft.
4. The electric and magnetic fields around the aircraft may then couple into the aircraft through a variety of processes.
5. Fields coupled into the aircraft can induce currents and voltages directly into electrical and electronic system in the aircraft, or onto cables and wiring which then can carry the energy to individual subsystems or components.
6. Depending on the amount of energy delivered to the subsystem or component, damage or upset may occur.

The processes in steps 1, 2 and 3 take place external to the aircraft skin, while the processes in steps 5 and 6 take place internal to the structure of the aircraft skin. Step 4 represents the coupling processes that transfer energy from the exterior to the interior of the aircraft.

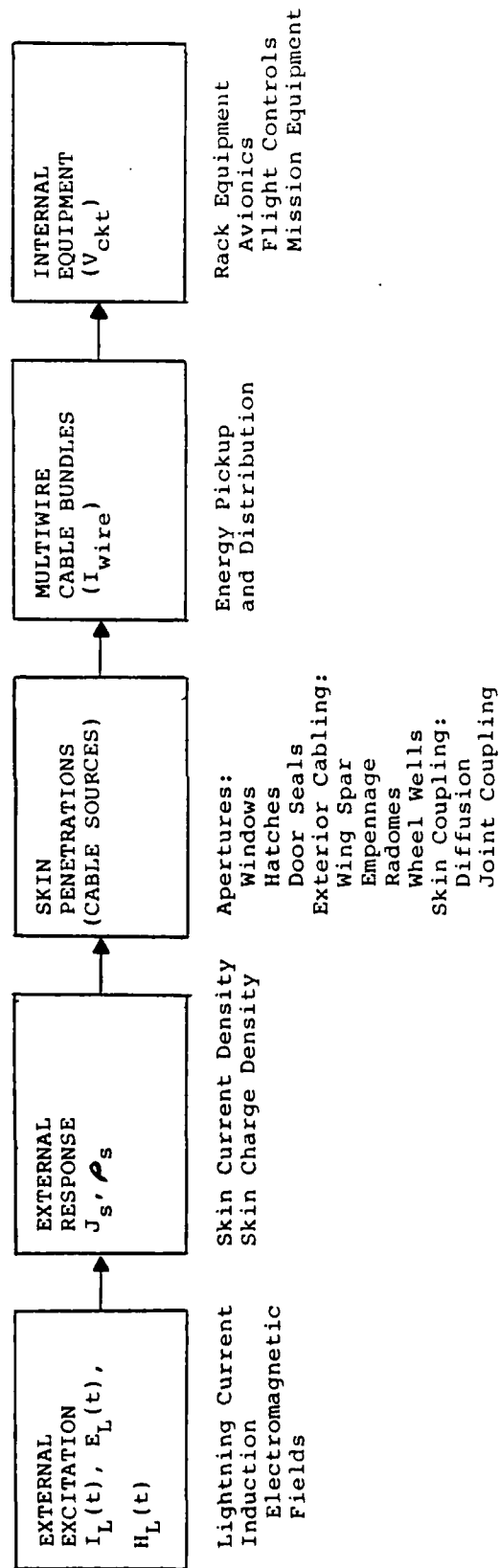


Figure III-1. Block Diagram Representation of the Lightning-Aircraft Interaction Process.
 [Corbin, 1979].

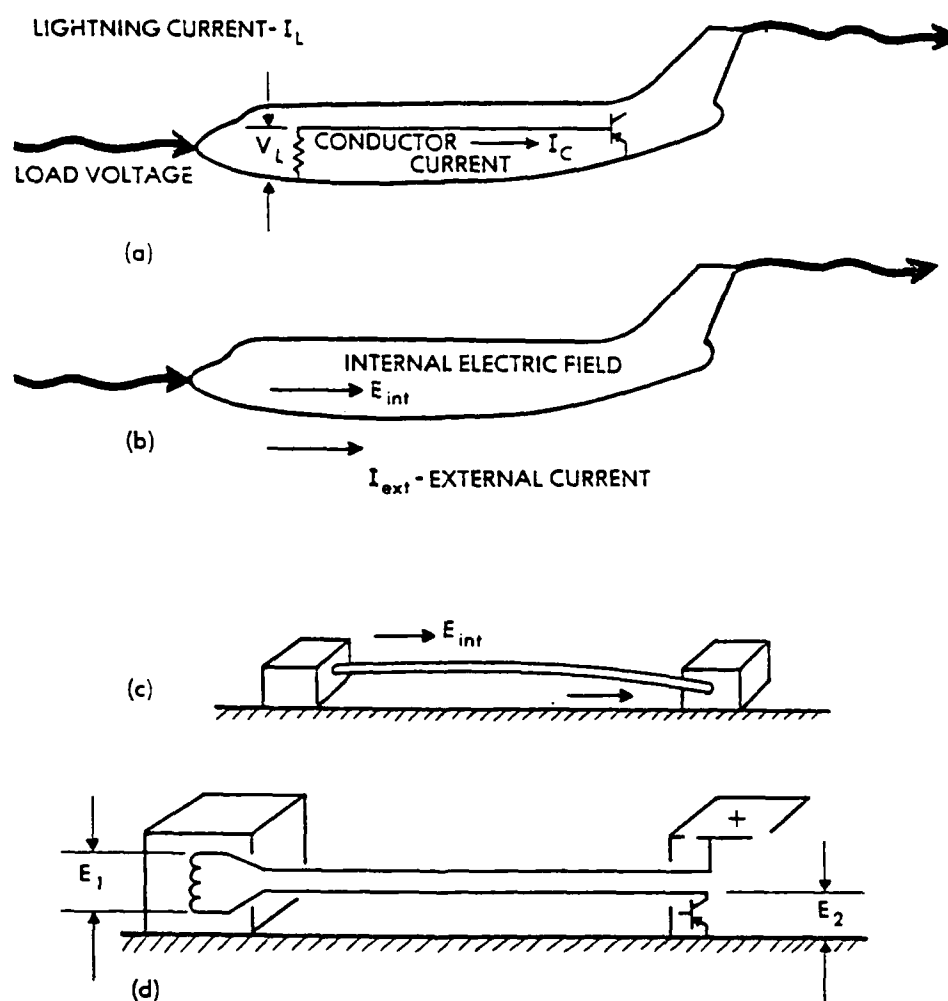


Figure III-2. The Steps in the Lightning-Aircraft Interaction Process for Indirect Effects. (a) Generation of External Currents and Charges. (b) Coupling of External Fields to the Interior. (c) Excitation of Cables Due to Internal Fields. (d) Excitation of Components by Currents Carried in Cables. [Fisher and Plumer, 1977].

Models and prediction codes in current use tend to follow these same divisions. In the next few sections, we will discuss the interaction processes occurring, based on these three divisions.

Exterior Processes. The dynamic distribution of the current and charge on the aircraft will determine how the succeeding steps of the interaction process take place. The distribution of current and charge on the aircraft's skin and structure will depend on several factors. One factor is whether the lightning channel attaches to the aircraft (direct flash), or whether the channel passes close to the aircraft (nearby flash). Another factor is the shape or geometry of the aircraft and attached structures. Finally, the type of material composing the various parts of the aircraft will affect current and charge distribution.

If the lightning channel attaches to the aircraft, then a current will flow from the entry point, through and on the structure, and out the exit point. Figure III-3, based upon work by Eriksen, Rudolph and Perala [1981], illustrates the resulting system in schematic form.

Because the aircraft and the lightning channel have different surge impedances, we can develop a first order model of this interaction using a transmission line that

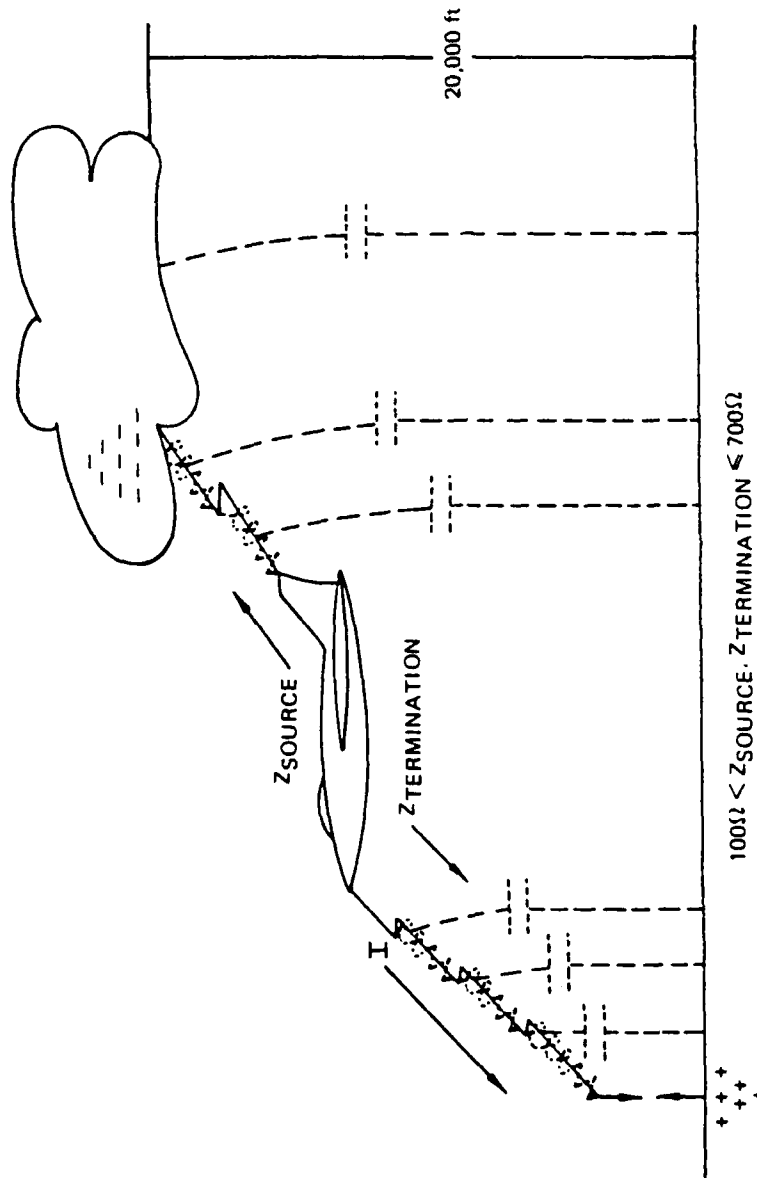
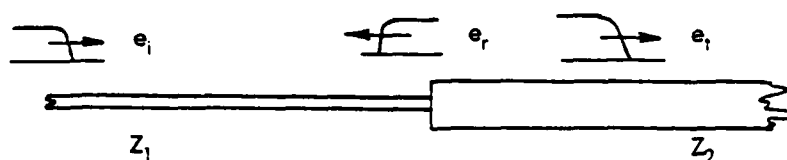


Figure III-3. Approximate Source and Termination Impedances for Inflight Lightning Strike. [Ketterling, 1987].

has a change in characteristic impedance for some distance that models the characteristic dimension of the aircraft (Figure III-4a). Because of the change in impedance at the entry and exit points, there is an impedance mismatch causing reflection, as well as transmission, of energy at the discontinuities. As seen in Figure III-4b, these reflections will travel back and forth between the discontinuities, decreasing in amplitude with each trip.

When the reflections and transmissions at each of the discontinuities are taken into account, the current waveforms at different points in the model will appear as shown in Figure III-4c. Because the lightning waveform has a fast rise time and a slower decay time, the waveform at the beginning of the low impedance section will exhibit an overshoot. The reflections will result in a current waveform on the aircraft proper which is made up of an oscillatory component superimposed over the input waveform due to the lightning channel. Finally, the current exiting the aircraft will have a slower rise time than that of the entering current.

One important point to be noted is that the faster the rise time of the input waveform, the more pronounced the oscillations on the aircraft structure. Another important point is that the period of oscillation will be dependent upon the characteristic length that the reflections



$$e_t = \alpha e_i$$

$$i_t = \gamma i_i$$

$$e_r = \beta e_i$$

$$i_r = \delta i_i$$

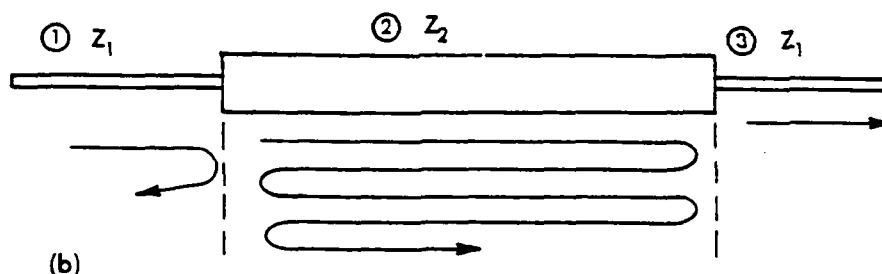
$$\alpha = \frac{2Z_2}{Z_1 + Z_2}$$

$$\gamma = \frac{2Z_1}{Z_1 + Z_2}$$

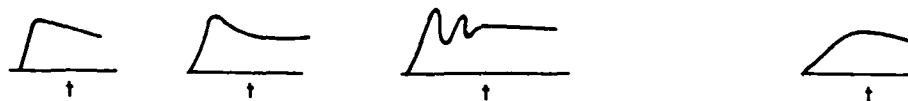
$$\beta = \frac{Z_1 - Z_2}{Z_1 + Z_2}$$

$$\delta = \frac{Z_2 - Z_1}{Z_1 + Z_2}$$

(a)



(b)



(c)

Figure III-4. Transmission Line Model of Lightning Channel and Aircraft. (a) Illustration of Mismatch at Entry Point. (b) Mismatch at Both Entry and Exit Points. (c) Waveshapes at Corresponding Points in (b). [Fisher and Plumer, 1977].

travel. For instance, if the entry point is the nose and the exit point is the tail (nose-to-tail strike) the oscillations will have a period that is characteristic of the nose-to-tail length. For a wing-to-wing strike, resonances will be set up that are multiples of the distance from wingtip to wingtip. We will examine these points in much greater detail when examining the results of simulation testing.

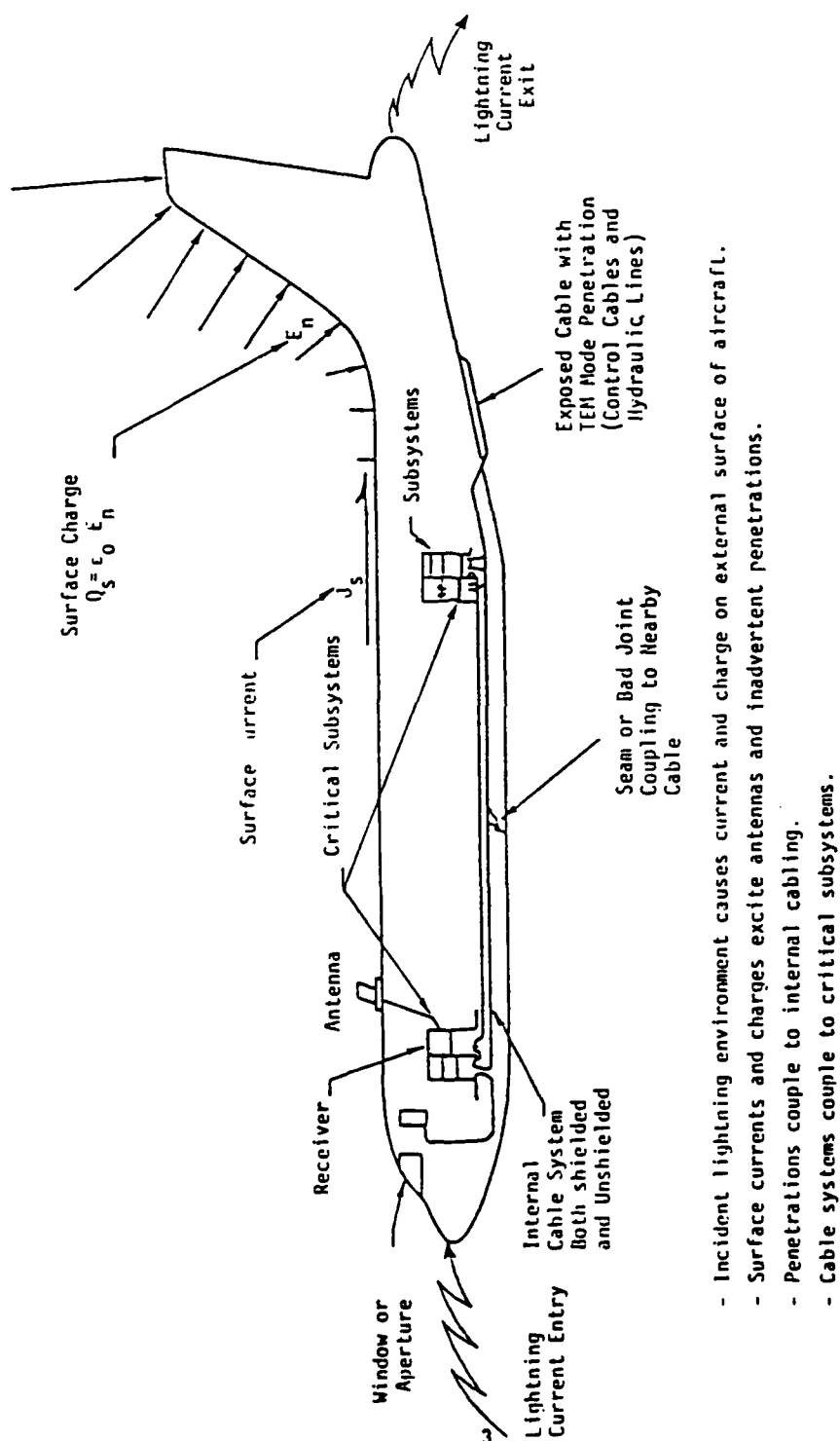
If the lightning strike does not attach to the aircraft directly, the electric field due to a nearby flash can excite the aircraft structure as though it were a dipole. In terms of Figure III-4, this represents the case where the impedance of the transmission line (channel) is infinite. In this case, there will be only reflections at the discontinuities, with no energy transmission at the entry/exit locations. There will be oscillations as before, with the only loss mechanism being that of the attenuation of the structure. The period of oscillation will be proportional to the length of the conducting path, with larger dimensions causing oscillations at lower frequencies (larger wavelengths) and with higher amplitudes.

The shape or geometry will obviously affect the current and charge distribution on the aircraft. Currents flowing on a long, cylindrical fuselage with wings at

right angles to the fuselage will produce a different electromagnetic field distribution than current flowing on a short, delta-winged aircraft. Also, the placement of apertures (canopies, entrance doors, windows, bomb bay doors, etc.) and other structures (antennas, equipment pylons, external tanks, etc.) will affect how the current flows on the vehicle. These effects are frequency dependent, as resonances will be excited when the size of these apertures and structures is on the order of the wavelength of the exciting fields.

Finally, the material of the different part of the aircraft will affect the distribution of the current and charge on the vehicle. Composite structures have a substantially different conductivity than aluminum or titanium, and the charge distribution on them will be accordingly different. Also, both metallic and composite structures will experience different coupling processes, depending on the electric and magnetic fields that will be set up around the vehicle.

Coupling Processes. The transition of energy from the exterior to the interior of the aircraft may take place by one or more electromagnetic coupling mechanisms. These mechanisms (see Figure III-5) include coupling through apertures, both deliberate (windows, canopies, etc.), and inadvertent (cracks, gaps and slots); energy



- Incident lightning environment causes current and charge on external surface of aircraft.
- Surface currents and charges excite antennas and inadvertent penetrations.
- Penetrations couple to internal cabling.
- Cable systems couple to critical subsystems.

Figure III-5. Illustration of Coupling Mechanisms. [Perala et al., 1982].

transfer by deliberate antennas and external to internal wiring (inadvertent antennas); electromagnetic field diffusion through the skin; and energy transfer by resistive or structural voltage drops in the frame and skin. Energy may be predominantly transferred by one of these mechanisms, or by a combination of several of them.

The relative importance of each of these mechanisms depends upon the type of vehicle that is being analyzed. For instance, coupling processes in composite vehicles will have a markedly different mix of mechanisms than the processes occurring in all metal vehicles. Among the other factors that will affect the way energy is transferred are such considerations as geometry of the vehicle, sizes and locations of apertures, current paths through the airframe and structures, the resistances of structural materials, and the routing of internal wires and cables. Let us briefly consider each of these coupling mechanisms, although the most common coupling mechanisms are resistive coupling and aperture coupling (Figure III-6)

The most common way for energy to enter an aircraft is by an opening in the structure of the vehicle. This opening, known as an aperture, may be either deliberate (a window) or accidental (a crack or gap). The aperture is frequently of an irregular shape and is often backed by an

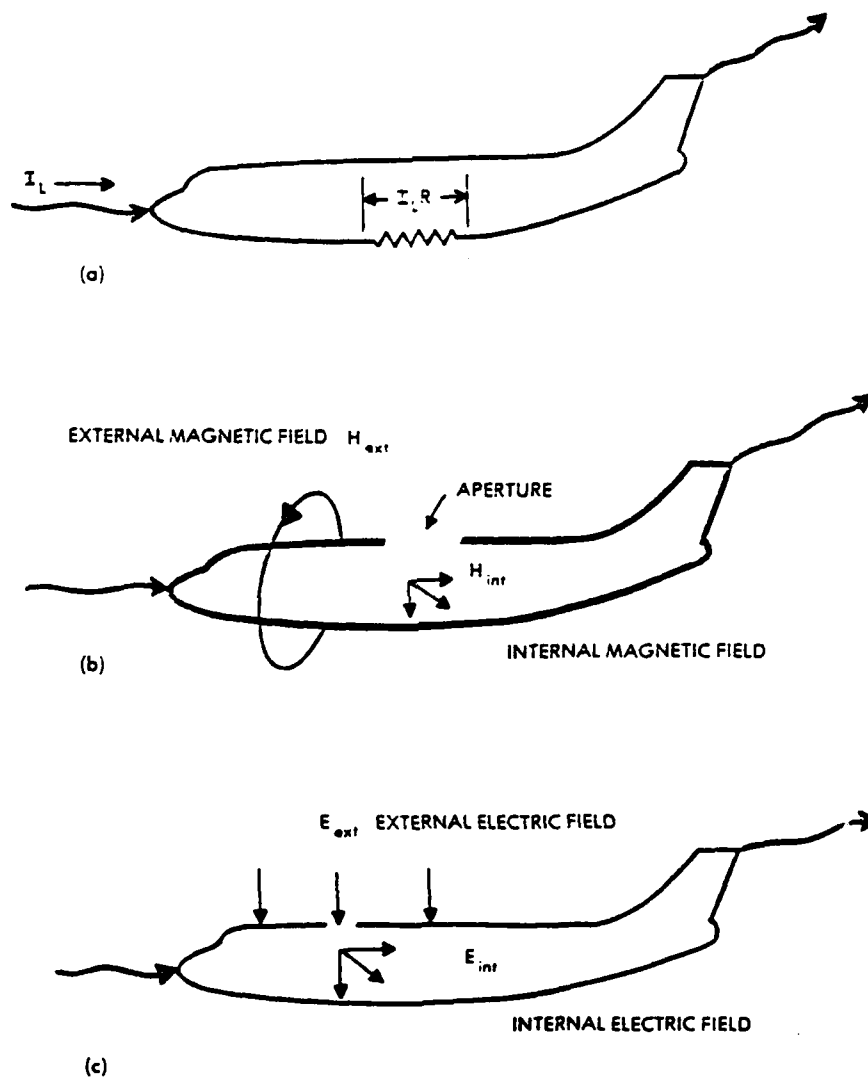


Figure III-6. Most Common Coupling Mechanisms. (a) Resistive. (b) Magnetic Fields. (c) Electric Fields. [Fisher and Plumer, 1977].

odd-shaped cavity, made of both metallic and non-metallic materials and containing multiple conductors. In addition, the aperture and cavity may be large with respect to a wavelength. Figures III-7 and III-8 illustrate the coupling of magnetic and electric fields respectively.

The coupling of electromagnetic energy into the vehicle by apertures is a complex and difficult problem, and one that is still not well understood. Because of this complexity, the actual problem is often reduced to a simpler canonical problem that can be solved. If properly chosen, these canonical problems can give a reasonable bound on what may be expected for the actual problem. The canonical problems in the literature have been divided into four classes:

- 1) apertures in a perfectly conducting, infinite plane;
- 2) apertures in perfectly conducting 2-dimensional bodies;
- 3) apertures in perfectly conducting 3-dimensional bodies;
- 4) apertures with conductors behind the opening.

There have been many solutions developed to the problem of an aperture in an infinite plane, using both frequency and time domain techniques. The solution to this problem is important, not only because it is a useful

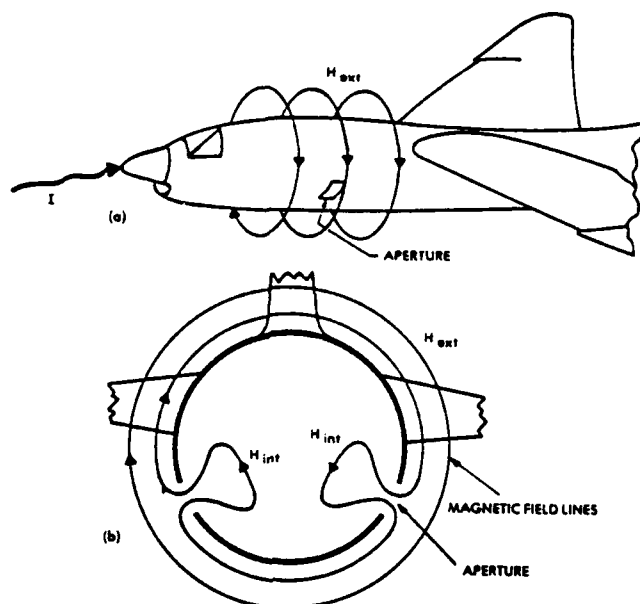


Figure III-7. Magnetic Field Coupling Through Apertures.
(a) External Field Patterns. (b) Internal Field Patterns. [Fisher and Plumer, 1977].

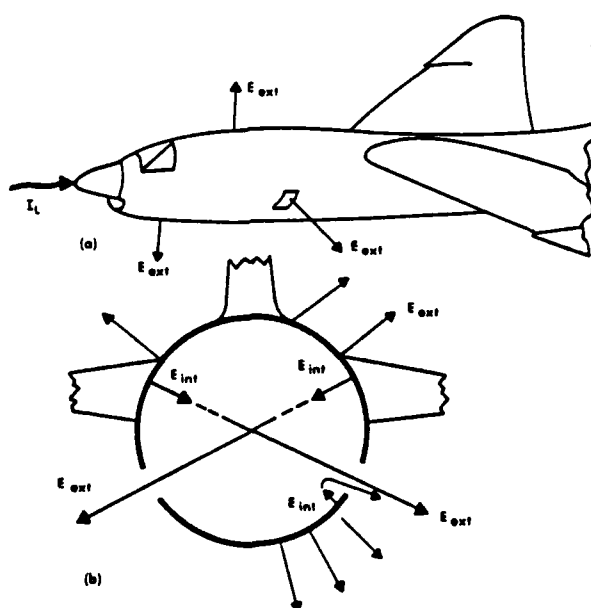


Figure III-8. Electric Field Coupling Through Apertures.
(a) External Field Patterns. (b) Internal Field Patterns. [Fisher and Plumer, 1977].

result in its own right, but also because it forms the basis for solving the other three categories of aperture problems. The most common approach is a frequency domain technique that uses a low-frequency approximation, which is limited to apertures that are small with respect to a wavelength. The approximation assumes the incident field across the aperture is uniform. This approximation is used by Babinet's equivalence principle, which says that when the field behind a screen with an opening is added to the field of a complementary structure, the sum is equal to the field when there is no screen [Balanis, 1982]. Through the use of the equivalence principle, one can calculate the aperture fields either by calculating the fields scattered from the complimentary structure [Collin, 1960] or by finding the fields radiated by an equivalent dipole (Figure III-9).

This low frequency approximation also has been used in several other approaches to develop an integral equation formulation of the aperture problem. Many integral equation techniques have been developed, in both the frequency and time domain, all requiring, except in the simplest of cases, the use of numerical techniques, such as the method of moments, for their solution. For an overview of the techniques developed for the solution of aperture problems, the article by Perala et al. [1982] lists many techniques for solving the various canonical

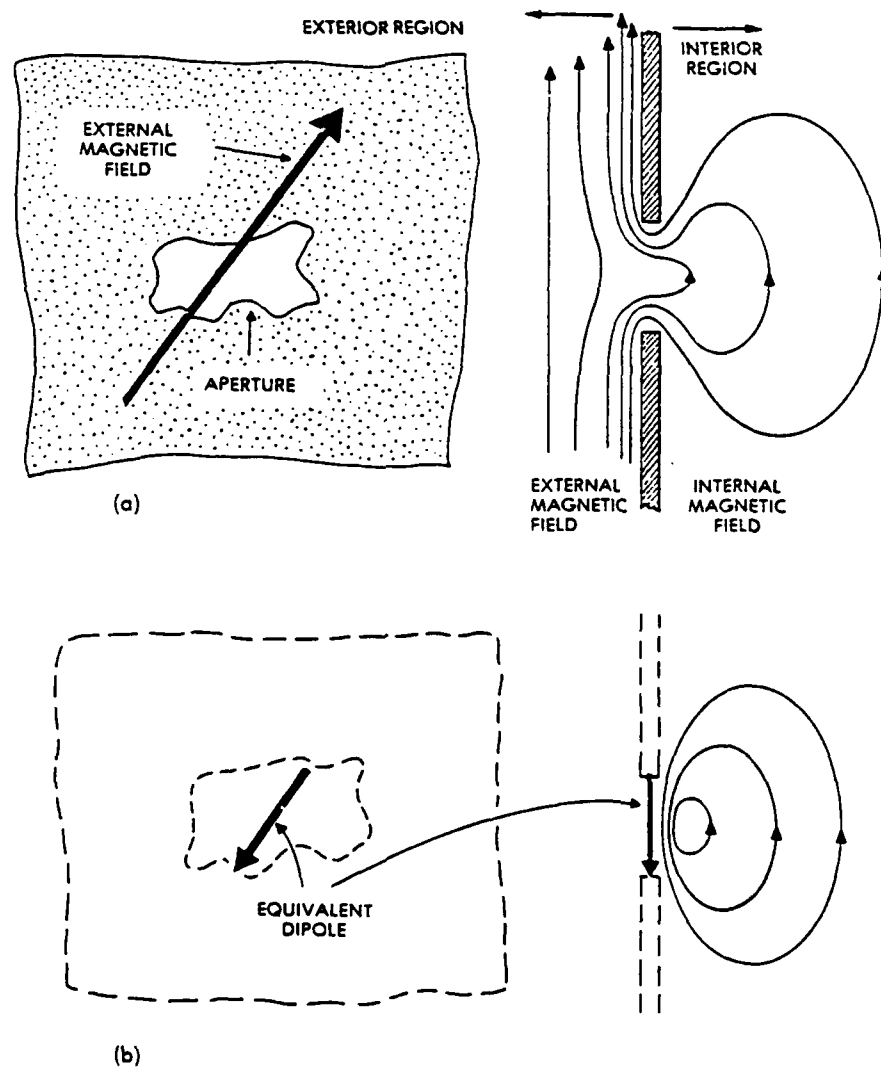


Figure III-9. The Aperture Coupling Problem. (a) Field Across an Aperture. (b) Equivalent Dipole Which Produces the Same Field. [Fisher and Plumer, 1977].

problems and gives extensive references. A more recent handbook by Lee [1986] contains a compilation of formulas for canonical coupling problems that have been developed for NEMP applications.

A solution to a special type of aperture, caused by slots and cracks, may be estimated by a simple method. This method assumes that the crack or slot can be analyzed as if it were a slot antenna. The slot antenna is the complimentary structure to the strip dipole, and the solution of the strip dipole problem indicates the solution to the slot antenna problem. Solutions to this problem are found in Balanis [1986] and Kraus [1988].

Another conduit of energy into an aircraft is by way of antennas and external wiring. Antennas and attendant transmission lines are designed to conduct energy into the vehicle and to receivers and indicators. Because of this, they are an avenue for the electromagnetic energy caused by the effects of lightning, coupling into the vehicle. Typically, this is manifested as electromagnetic noise in avionics systems. However, if antennas and transmission lines are improperly grounded, bonded and protected from lightning, large currents can flow on the cables and shields, generating electromagnetic fields which can couple the energy into unrelated electronic systems. The analysis of this type of coupling is based on the type of

antenna and the configuration it is used with. Because of the many types of antennas typically used with aircraft, including such types as monopoles, loops, blades, slots, HF wire antennas and trailing wire antennas, many types of modeling and analysis are required. A good source of information on the analysis of these problems is given by Liu, Lee and Marin [1975]. In their report, the authors analyze 16 different antennas in terms of Thevenin equivalent circuits and discuss the principles of operation of each type.

Other wiring on and in the aircraft can also act as antennas and transmission lines to bring energy into the vehicle. One example of this is the wiring used to control and power the lights located at the tips of the wings (Figure III-10) and vertical stabilizer. These components are located in attachment zones and are commonly part of attachment and exit points. Often wiring and cabling are located in the leading and trailing edges of wings. Although the wires in the leading edges are often well protected, it is very common to route wires in the trailing edge between control surfaces and the main part of the wing. This leaves the wires exposed to both current flow on the vehicle and the electromagnetic fields caused by that current flow. In addition, other metallic conductors such as fuel and hydraulic lines are routed within and on the outside of the wing and fuselage.

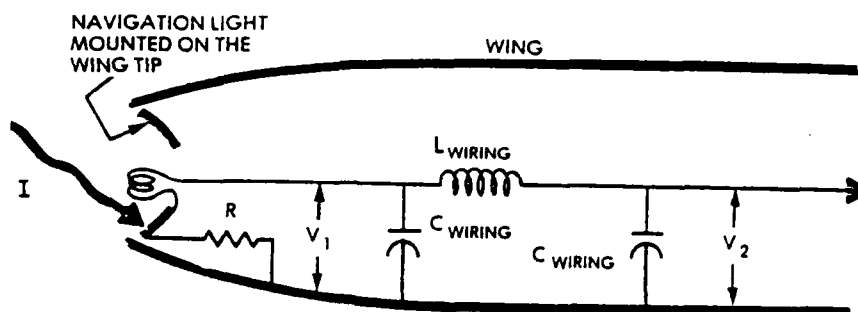


Figure III-10. Illustration of an Unintentional Antenna as a Coupling Mechanism to the Aircraft Interior. [Fisher and Plumer, 1977].

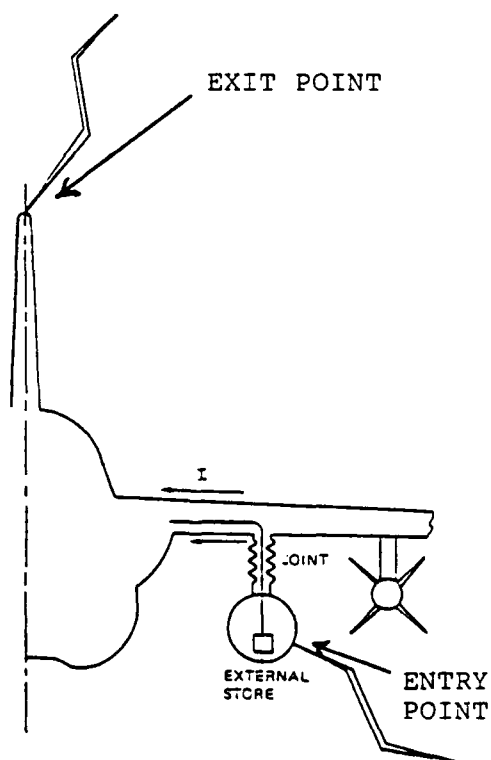


Figure III-11. Example of Joint Resistance That Concentrates Current, Resulting in High IR Voltages. [Carney and Von Bokern, 1987].

Analysis of these problems is often carried out by modeling them as wire antennas, or through the use of transmission line analysis techniques. Transmission line techniques are particularly useful, as the wiring and wing approximate a transmission line at the frequencies where the lightning spectrum contains most of its energy.

The mechanism of diffusion is based upon the direct penetration of electromagnetic fields through the skin of the aircraft. Older aircraft with highly conducting, all metal skins are very resistant to this type of coupling. However, newer aircraft containing large quantities of composites have skins, panels and structures of substantially lower conductivity. Composite vehicles are much more susceptible to this coupling mechanism, especially due to the large amount of energy in the low-frequency spectrum of the lightning return stroke.

The diffusion problem can be treated as a three-medium problem. The fields that diffuse through the conducting surface to the interior of the aircraft are due to incident electromagnetic field or surface current density on the other side of the conducting surface. Like the aperture problem, this is a well-studied problem, with exact solutions available only for a few simple canonical shapes.

Using frequency domain techniques, this problem can be reduced to finding the transfer impedance $Z_T(\omega)$, relating the external surface current density, $J_S(\omega)$, and the internal electric field, $E_{int}(\omega)$. This relationship is given by

$$Z_T(\omega) = E_{int}(\omega) / J_S(\omega)$$

The transfer impedance function is a function of geometry, interior location, shield properties and frequency. A few general observations can be made about the function, however. The transfer impedance is a monotonically decreasing function of frequency. Thus, the lower the frequency of the incident field, the easier it is for the field to penetrate. The transfer impedance decreases with increasing conductivity. For instance, the conductivity of carbon fiber composites is lower than that of metal by a factor of approximately 100, thus the transfer impedance, and hence the energy transferred, is correspondingly higher. Therefore, composites are much more susceptible to the threat posed by the low-frequency content of the lightning stroke.

A last category of coupling mechanism is the energy that is introduced into the vehicle due to energy flowing through the structure and the seams and joints of that structure. As the current flows through the structure or across these joints, it encounters a finite conductivity

which represents resistance to the flow of current. The current flowing through this resistance causes a structural voltage drop. This voltage drop will cause an electric field to be present around the structure and across the seams, joints and gaps caused by normal construction practices. In turn, this field may act as a source for any nearby wires, cables or metallic conductors.

For conventionally designed all-metal aircraft, most of the structural resistance is in the joints between structural components, not within the metal itself. As a rule of thumb, the end-to-end structural resistances of carbon fiber composite airframes have been found to be approximately 100 times greater than that of aluminum airframes of the same general size. That is, the resistance of an all-aluminum airframe will be on the order of 0.5 milliohms, while the resistance of a carbon fiber composite airframe will be approximately 50 milliohms. Thus, for the same current flowing in these two airframes, the structural voltage will be approximately 100 times larger in a composite airframe [Carney and Von Bokern, 1987].

For all composite airframes, the structural voltages are often greater in magnitude and time duration than voltages induced through apertures or by diffusion. In

addition, they are distributed through the composite structural members and skin. For example, a 200 kA lightning current flowing through a carbon fiber composite fuselage, whose end-to-end resistance is about $50 \times 10^{-3} \Omega$, would cause a nose to tail potential of 10 kV. This level is at least twice as high as the magnetically induced voltages found in wiring within the same size airframe with typical apertures caused by windshield, windows and access doors.

Neglecting fields admitted by large apertures, diffusion and structural voltage drop processes will predominate in all-composite aircraft, while magnetic field-induced voltages will predominate in an all-metal aircraft. An exception to this is circuits that pass along or across resistances concentrated in removable joints, such as pylon attachments (Figure III-11). In these specific cases, the product of concentrated current densities and higher resistances can sometimes be quite large.

Internal Processes. The internal electromagnetic environment of the aircraft is determined by the amount of energy transferred into the vehicle from the exterior by the various coupling mechanisms, and by the geometry of the internal structure of such components as wiring, control and fluid lines, etc. The problem then becomes

one of calculating the resultant voltage, current, power and energy that will appear at the connectors leading into avionics system components. This is a non-trivial problem, especially in modern aircraft avionics systems, with their ever increasing complexity.

The analysis of the internal processes and their resulting effects takes place in several steps. First, the energy that penetrates into the vehicle must couple into the internal wiring. Then the energy is propagated through the wiring toward the terminating boxes and subsystems. Finally, an assessment must be made of the upset or damage that will result from the coupled energy. The first step is analogous to the coupling processes previously discussed, except it typically happens with much smaller apertures, such as the braid used to shield cables.

The fields propagated down the lines are usually of less importance than the voltages and currents developed on them at the ends. If the cables system is short enough that transmission line effects can be neglected, the induced voltage will be proportional to

$$v_{ind} = d\phi/dt = (\mu_0 A) dH/dt$$

where v_{ind} = induced voltage (volts)
 Φ = total linking flux (webers)
 μ_0 = permeability of free space (H/m)
 A = loop area involved
 H = magnetic field intensity (A/m)

If transmission effects can not be neglected, then the problem becomes much more complicated. Aircraft wiring is grouped into harnesses or bundles, with both long and short conductors. At higher frequencies, the longer conductors will have a substantial amount of distributed capacitance and inductance. Thus, a changing magnetic field will cause an oscillatory field to appear on the wiring, the oscillation being dependent upon the exciting waveform. Even if the waveform is of a simple waveshape, the voltages in harnesses will oscillate in a complex manner.

While the maximum voltage may be difficult to predict, the amplitude of the envelope can be approximated by the above equation. The frequency of the superimposed oscillations will be inversely proportional to the conductor length. Conductors tend to oscillate as quarter-wave dipoles. However, this generalization sometimes does not apply, as the conductor will interact with the other conductors near it. Usually there will be one dominant frequency with several higher frequencies

superimposed. The only reliable relationship is that longer cables will tend to oscillate at lower frequencies. Measurements of induced voltages in fighter aircraft have indicated characteristic frequencies ranging from 1 to 10 MHz.

Because of the complexity of the wiring harnesses and other conductors inside an aircraft, the calculation of the exact voltages and currents on the wiring is difficult, often not practical, and usually not needed. Rather, such formulations and relationships as the ones discussed above are used to bound the problem and determine the amounts of hardening needed to minimize damage effects. For more accurate results, the methods derived from the study of multiconductor transmission lines can be used.

The purpose of calculating the voltage, current, power and energy delivered to connector pins is to make an assessment of the potential for system upset or damage. Upset is a temporary condition which causes the system or part to cease working for a short term. As upset is a temporary phenomenon, it usually can be corrected by a system restart, a power-off/power-on sequence or by building error correcting redundancy into the system. Rarely are analog systems upset, although they may be upset by system components becoming saturated or by large

transient signals overwhelming the analog data.

Unless sufficiently protected, digital systems are very susceptible to upset because of their low voltage levels for logic switching, and wide bandwidths. This is especially true in newer systems using very high speed integrated circuits (VHSIC) and monolithic microwave integrated circuits (MMIC) which operate at low voltage levels and high clock speeds. For instance, a new MMIC amplifier delivers more than 28 dB of gain from 50 MHz to 4 GHz. Yet the gain is adjusted by a voltage that is varied from only -0.8 to -1.7 VDC [Pengelly and Ezzeddine, 1988]. Digital flight-control systems may interpret a lightning-induced transient as an erroneous control signal, causing the positioning of control surfaces improperly. As an example of an analogous situation, at least 5 of 29 crashes of the Army's Black Hawk helicopter are suspected of being due to RFI problems adversely affecting the electronics and flight-control system [Eckert, 1988].

Damage occurs when enough energy is delivered to a component to cause permanent failure. This usually requires repair or replacement of the damaged component. As this often can only be done on the ground, damage is a considerably more serious problem for airborne aircraft. The devices most susceptible to damage are solid state

semiconductor devices which operate at low voltage levels. The most common failure mechanism is the overheating of semiconductor device junctions due to reverse biasing caused by transients and can occur with as little as 10 microjoules of energy delivered to the junction. As energy levels increase, other parts become susceptible to damage due to other damage mechanisms. Figure III-12 illustrates the comparative susceptibility of common devices that are found on modern aircraft.

Each step of the interaction process has its own complexities. When attempting to simulate these processes, a knowledge of what is to be expected as various parameters are changed is invaluable. In the next few sections, we will examine the models and codes used to predict what happens during these processes.

Modeling of the Interaction Process

One of the purposes of modeling the lightning interaction process is to provide a check on our knowledge of the processes involved. The creation of an accurate model is essential for the researcher to be able to predict what will happen as parameters are changed during the process. This prediction ability will be essential during the development of accurate ground-based lightning simulations. In addition, the development of accurate

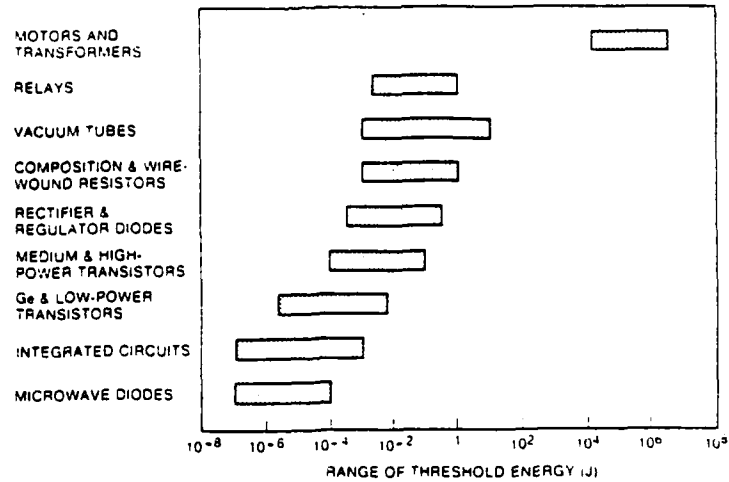


Figure III-12. Comparative Susceptibility of Common Devices to Energy Deposition. [Bell Laboratory, 1975].

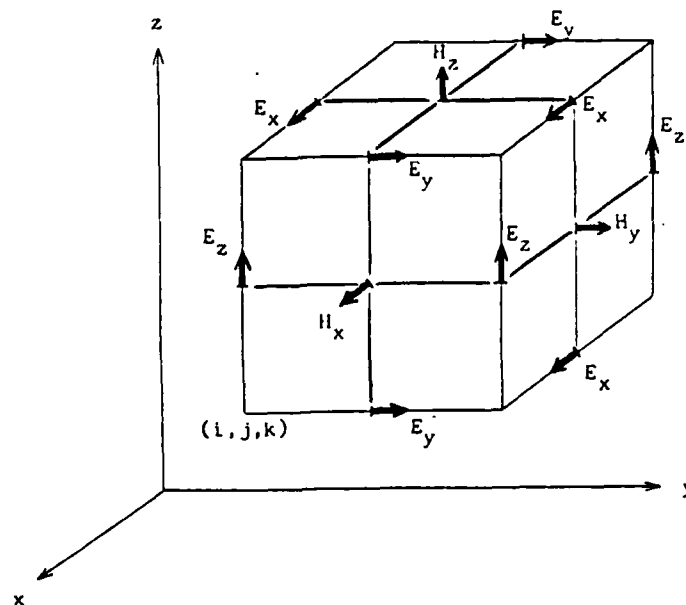


Figure III-13. Field Component Positions About the Unit Cell of the FD-TD Lattice. [Taflove, 1980].

prediction models holds the potential of further improving the validity of current simulation techniques. The purpose of the following sections is to review the current state of models for the major parts of the lightning interaction process. For instance, while early models for lightning interaction neglected airframe resonances and the dynamic distribution of current and charge on the aircraft, more sophisticated models have been developed which incorporate these and other factors.

Models have been developed for the attachment and distribution of energy on the aircraft skin, the external to internal coupling process and the coupling and propagation of energy inside the vehicle. Although these processes have been presented as independent from each other and are often analyzed and solved that way, from a strict theoretical viewpoint they are not independent. The main reason these process can be solved separately is the mutual coupling between them is weak. As an example, the presence of internal wiring is assumed not to significantly affect the distribution of fields and charges on the exterior of the aircraft. One notable exception to this is the case when an aircraft has a large aperture whose presence significantly alters the external to internal coupling process. In this case the aperture must be included in the analysis and accounted for. Since the bulk of the spectral content is located in the low

frequency range of 1-100 kHz, corresponding to wavelengths between 300 km and 3 km, the approximation of weak coupling between external and internal processes is usually valid.

In the following sections, the various methods of modeling and predicting the different interaction process will be reviewed. Models for both external and internal processes will be examined. Rather than assessing each of the many models or codes that have been developed for portions of the lightning interaction process, the major computational categories that the models fall into will be covered. For each method, the mathematical foundation will be discussed. The utility of the approach will be assessed and pertinent references will be given. For a more in-depth examination of these methods, the reports by Eriksen, Rudolph and Perala [1981] and Carney and Von Bokern [1987] should be consulted.

Models for Prediction of External Interaction Processes

The models that are used for the external interaction processes tend to fall into several categories. These categories include: (1) methods based on the solution of differential equations; (2) methods based on the solution of integral (or integro-differential) equations; (3) hybrid methods based on a combination of the above

methods; and (4) several other methods based on other approaches. Another useful approach to classifying these methods is by whether the problem is solved in the time domain or the frequency domain. This section will discuss several of the most common approaches to solving the external interaction problem. Because of the rapid changes occurring in code implementations, specific codes will not be discussed, except to give an indication of relative capability of the different approaches.

No matter what classification scheme is used to differentiate the different methods, in each case, the method must solve Maxwell's equations for the physical system being described. Therefore, they are actually equivalent methods, differing only in the physical or numerical approximations employed. For instance, if nonlinearities due to corona and streamer formation and/or attachment are left out of the physical description, then that model will be invalid in describing the impact of those processes, unless it is known a priori that they are negligible. Thus, the utility or applicability of these models to a given situation will depend upon the implementation of the model, be it an analytical solution using paper and pencil or a numerical solution using the computer.

The general problem to be solved is finding the surface current and charge densities on the outer surface of the vehicle. This requires the solution of Maxwell's equations for the total electric and magnetic fields at the surface of the vehicle due to any incident fields, while utilizing the boundary conditions that must be met at the surface of the vehicle. By manipulating Maxwell's equations, we can cast them into several forms suitable for solution, either analytically or numerically. Typically, an analytical solution is possible only with a simple, symmetric geometry and straightforward boundary conditions. Because of this, the forms of Maxwell's equations most often used are those that can be cast into an arrangement suitable for numerical work on the computer. We will now consider several forms of Maxwell's equations and see how they lead to different formulations.

As mentioned in Chapter II, the differential form of Maxwell's equations is given by:

$$\nabla \times \mathbf{E} = -\mu (\partial \mathbf{H} / \partial t) \quad (1)$$

$$\nabla \times \mathbf{H} = \epsilon (\partial \mathbf{E} / \partial t) + \mathbf{J} \quad (2)$$

$$\nabla \cdot \mathbf{E} = \rho / \epsilon \quad (3)$$

$$\nabla \cdot \mu \mathbf{H} = 0 \quad (4)$$

where field quantities have been used exclusively. The source current density, \mathbf{J} , and the source charge density,

ρ , are related by the continuity equation:

$$\nabla \cdot \mathbf{J} + \partial \rho / \partial t = 0 \quad (5)$$

There are several alternate approaches to solving these equations. Equation (4) is satisfied if \mathbf{H} is represented as the curl of some vector. Thus, we can define the vector potential \mathbf{A} by the expression

$$\mu \mathbf{H} = \nabla \times \mathbf{A} \quad (6)$$

Substituting (6) into (1) yields

$$\nabla \times (\mathbf{E} + \partial \mathbf{A} / \partial t) = 0 \quad (7)$$

Equation (7) is satisfied if the quantity $(\mathbf{E} + \partial \mathbf{A} / \partial t)$ is represented by the gradient of some scalar. Setting $(\mathbf{E} + \partial \mathbf{A} / \partial t)$ equal to $-\nabla \Phi$ defines the scalar potential. Thus the electric field strength may be expressed as

$$\mathbf{E} = -\nabla \Phi - \partial \mathbf{A} / \partial t \quad (8)$$

The expressions for \mathbf{B} and \mathbf{E} in equations (6) and (8) satisfy two of Maxwell's equations, (2) and (4). The other two expressions can be used to derive differential equations for the potential functions. If we substitute (6) and (8) into (2), we obtain

$$(1/\mu) \nabla \times \nabla \times \mathbf{A} = -\epsilon \nabla (\partial \Phi / \partial t) - \epsilon (\partial^2 \mathbf{A} / \partial t^2) + \mathbf{J} \quad (9)$$

Using the vector identity, $\nabla \times \nabla \times \mathbf{A} = \nabla \nabla \cdot \mathbf{A} - \nabla^2 \mathbf{A}$, we can write equation (9) as

$$\nabla^2 \mathbf{A} - \mu \epsilon (\partial^2 \mathbf{A} / \partial t^2) = -\mu \mathbf{J} + \mu \epsilon \nabla (\partial \Phi / \partial t) + \nabla \nabla \cdot \mathbf{A} \quad (10)$$

This is one of the needed equations. The other equation is obtained by substituting (8) into (3), yielding

$$\nabla^2 \Phi + \nabla \cdot \partial \mathbf{A} / \partial t = -\rho / \epsilon \quad (11)$$

Equations (10) and (11) are complicated by the fact that they are coupled equations. That is, the unknowns (potentials) \mathbf{A} and Φ appear in both equations. Further complicating the situation is the fact that equations (10) and (11) do not yield unique solutions for the potentials. This is a result of the Helmholtz theorem, which states that any vector field due to a finite source is specified uniquely if both the curl and divergence of the field are specified. Although the curl of \mathbf{A} is given in equation (6), the divergence is not. Also, when (8) was defined, it was done arbitrarily. In examining equations (10) and (11), we see that if the divergence of \mathbf{A} is set equal to $-\mu \epsilon (\partial \Phi / \partial t)$, these equations will decouple. In addition, they reduce to the standard wave equations with source terms:

$$\nabla^2 \mathbf{A} - \mu \epsilon (\partial^2 \mathbf{A} / \partial t^2) = -\mu \mathbf{J} \quad (12)$$

$$\nabla^2 \Phi - \mu \epsilon (\partial^2 \Phi / \partial t^2) = -\rho / \epsilon \quad (13)$$

The choice of divergence specification chosen above,

$$\nabla \cdot \mathbf{A} = -\mu\epsilon (\partial\Phi/\partial t) \quad (14)$$

is known as the Lorentz gauge condition. Although other gauge conditions are possible, such as the Coulomb gauge, it can be shown [Stratton, 1941] that if the solutions for \mathbf{A} and Φ are to represent retarded potentials, (14) must be satisfied, which will occur if equation (5) holds true.

The direct solution to the time-dependent wave equations is somewhat involved. Using the results presented in Jackson [1975], the solution to equations (12) and (13) is given by

$$\mathbf{A}(\mathbf{r}, t) = \frac{\mu}{4\pi} \int_V \frac{\mathbf{J}(\mathbf{r}', \tau)}{R} dV' \quad (15)$$

$$\Phi(\mathbf{r}, t) = \frac{1}{4\pi\epsilon} \int_V \frac{\rho(\mathbf{r}', \tau)}{R} dV' \quad (16)$$

where $\tau = t - (R/v)$

$$R = |\mathbf{R}| = |\mathbf{r} - \mathbf{r}'|$$

\mathbf{r} = vector from the origin to the field observation point

\mathbf{r}' = vector from the origin to the source point

v = velocity of wave propagation in the medium

Notice that in these expressions a time delay of (R/v) seconds has been introduced, so the potentials have been delayed or retarded by this amount. It is for this reason

that they are known as retarded potentials. In general, (16) does not need to be evaluated, as E may be obtained from the solution of (2). The usual procedure is to obtain H from A by the use of (6) and then to obtain E from H by taking its curl and integrating with respect to time. Note that $J = 0$ in (2) when the field is evaluated external to the region where the source currents are located.

The formulation of the electromagnetic problem to be solved is given as follows. Suppose an electromagnetic field, $E_i(r,t)$ and $H_i(r,t)$, is incident upon a scatterer with surface S . Assume that the fields near S and the currents and charges on S are initially zero. When the incident fields reach the scatterer S , they will induce surface currents J_s and surface charges ρ on the surface S which will flow for some time. These currents and charges, in turn, will cause fields around the surface. These scattered fields, $E_s(r,t)$ and $H_s(r,t)$, will sum with the incident fields to produce the total fields, $E_T(r,t)$ and $H_T(r,t)$. For the problem of lightning interaction with an aircraft, the incident fields are those caused by a nearby strike, or the fields resulting from an attached arc channel.

For the general scattering problem, the incident fields, the scattered fields produced by the induced

currents and charges, and the total fields are related by the expression:

$$E_T(r,t) = E_i(r,t) + E_s(r,t) \quad (17)$$

$$H_T(r,t) = H_i(r,t) + H_s(r,t) \quad (18)$$

For a perfect conductor, the problem of finding the surface currents and charges is equivalent to finding the magnetic and electric fields on the surface of the conductor. This comes from using the relationships

$$J_s(r_s,t) = \hat{n} \times H_T(r_s,t) \quad (19)$$

$$\rho(r_s,t) = \epsilon \hat{n} \cdot E_T(r_s,t) \quad (20)$$

where r_s is on the surface S , and \hat{n} is the unit vector normal to the surface S .

Using the retarded time solutions for the potentials, it is possible to derive integral expressions for the scattered fields due to the unknown surface currents and charges on the vehicle. Substituting (15) into (6), and (15) and (16) into (8) yields

$$H_s(r,t) = \frac{\mu}{4\pi} \int_V \left[\left\| \frac{J(r',\tau)}{R^2} + \frac{\partial J}{Rv \partial \tau} \right\| \times \frac{R}{R} \right] dV' \quad (21)$$

$$\mathbf{E}_S(\mathbf{r}, t) = \frac{1}{4\pi\epsilon} \int_V \left[\left\| \frac{\partial \rho}{Rv\partial\tau} + \frac{\rho(\mathbf{r}', \tau)}{R^2} \right\| \nabla R + \frac{\mu\epsilon\partial\mathbf{J}}{R\partial\tau} \right] dV' \quad (22)$$

If the fields are on the surface of a perfect conductor, with surface area A , equations (21) and (22) reduce to

$$\mathbf{H}_S(\mathbf{r}, t) = \frac{\mu}{4\pi} \int_A \left[\left\| \frac{\mathbf{J}(\mathbf{r}', \tau)}{R^2} + \frac{\partial\mathbf{J}_S}{Rv\partial\tau} \right\| \times \frac{\mathbf{R}}{R} \right] dA' \quad (23)$$

$$\mathbf{E}_S(\mathbf{r}, t) = \frac{1}{4\pi\epsilon} \int_A \left[\left\| \frac{\partial \rho}{Rv\partial\tau} + \frac{\rho(\mathbf{r}', \tau)}{R^2} \right\| \nabla R + \frac{\mu\epsilon\partial\mathbf{J}_S}{R\partial\tau} \right] dA' \quad (24)$$

Using equations (23) and (24), we can derive two integral equations which can be used to find the unknown surface currents. First, we will use the expression for the electric field in equation (24). The tangential component of the total electric field must equal zero at the surface of a perfect conductor. Thus, we have the expressions:

$$0 \quad \hat{\mathbf{n}} \times \mathbf{E}_T = \hat{\mathbf{n}} \times (\mathbf{E}_i + \mathbf{E}_S)$$

$$\text{or,} \quad \hat{\mathbf{n}} \times \mathbf{E}_i = -\hat{\mathbf{n}} \times \mathbf{E}_S \quad (25)$$

Substituting the expression for the scattered electric field, (24), into (25) yields:

$$\begin{aligned} \mathbf{n} \times \mathbf{E}_i(\mathbf{r}, t) = & \frac{\mathbf{n}}{4\pi} \int_A \left[\frac{\mu}{R} \frac{\partial \mathbf{J}_s(\mathbf{r}', \tau)}{\partial \tau} \right. \\ & \left. + \left\| \frac{\partial \rho(\mathbf{r}', \tau)}{\epsilon v \partial \tau} + \frac{\rho(\mathbf{r}', \tau)}{\epsilon R} \right\| \frac{R}{R^2} \right] dA' \quad (26) \end{aligned}$$

Equation (26), an integral equation in the related unknowns, $\mathbf{J}_s(\mathbf{r}', \tau)$ and $\rho(\mathbf{r}', \tau)$, is known as the electric field integral equation (EFIE), and is the time-domain form of the equation.

A second integral equation can be developed from the magnetic field expression for the scattered field in (23). The surface current on a conductor is related to the tangential component of the total magnetic field at the surface. Thus,

$$\mathbf{J}_s(\mathbf{r}', t) = \hat{\mathbf{n}} \times \mathbf{H}_T = \hat{\mathbf{n}} \times (\mathbf{H}_i + \mathbf{H}_s) \quad (27)$$

Using the expression for the scattered magnetic field given in (23) and following the development of Mittra [1976], it can be shown that the surface current is given by

$$\begin{aligned} \mathbf{J}_s(\mathbf{r}', t) = & 2\hat{\mathbf{n}} \times \mathbf{H}_i + \\ & \frac{\hat{\mathbf{n}}}{2\pi} \times \int_A \left[\left\| \frac{\partial \mathbf{J}_s(\mathbf{r}', \tau)}{R v \partial \tau} + \frac{\mathbf{J}_s(\mathbf{r}', \tau)}{R^2} \right\| \times \frac{R}{R} \right] dA' \quad (28) \end{aligned}$$

Equation (28) is known as the magnetic field integral equation (MFIE) in the time-domain form.

These two integral equations, (26) and (28) are used as the basis for many of the numerical models used for the computation of the currents and charges on a vehicle. There are also frequency-domain versions of the EFIE and the MFIE. Miller [1972] has found that the time domain approach is more efficient for wire structures, while the frequency domain approach is more efficient for surface structures. There are some advantages in using one formulation over the other, depending on the structure to be modeled and the accuracy required.

Generally speaking, the MFIE formulation is not well suited to treating wire-like structures or flat surfaces as the equation becomes unstable for electrically thin structures. However, if the EFIE is used with wire grid structures, care must be taken if the wire grid is intended to model a closed volume, as artificial resonances may be created. For solid surfaces, the MFIE is less singular than the EFIE, and thus preferable, as less sophisticated expansion functions may be used to represent the unknown current.

Because many of the methods used to model aircraft-lightning interaction are based on integral equations, it

is useful to briefly review the solution technique known as the Method of Moments (MoM). The development here follows the presentation used by Harrington [1968]. Consider an integral equation of the form

$$V(x) = \int_a^b K(x, x') J(x') dx \quad (29)$$

where $V(x)$ is a known function, $K(x, x')$ is the kernel of the equation and $J(x')$ is unknown. Let $J(x')$ be a surface current density. The integral in (29) is a linear operator, and the equation can be written in operator notation as

$$V(x) = \underline{L} J(x') \quad (30)$$

where \underline{L} is an operator, its domain being a function like J and its range a function like V . The function J can be expanded in a series of known functions, called basis or expansion functions, denoted by $J_n(x)$, such that

$$J(x) = \sum_{n=1}^N I_n J_n(x) \quad (31)$$

The I_n are unknown constants that are to be determined. Substituting (31) into (30) yields

$$V(x) = \sum_{n=1}^N I_n \underline{L} J_n(x) \quad (32)$$

An inner product between two functions w and V can be defined as

$$\langle w, V \rangle = \int_{l_1}^{l_2} w(x') V(x') dx' \quad (33)$$

It is possible to construct a system of linear equations from the original algebraic equations by multiplying (32) by $w_m(x')$ and integrating both sides from l_1 to l_2 , or

$$\int_{l_1}^{l_2} w_m(x') V(x') dx' = I_n \int_{l_1}^{l_2} w_m(x') \underline{L}(x') J_n(x) dx' \quad (34)$$

The functions $w_m(x')$, known as weighting or testing functions, are in the range of the operator \underline{L} . We can define a matrix element Z_{mn} and a vector element V_m by the expressions

$$V_m = \int_{l_1}^{l_2} w_m(x') V(x') dx' \quad (35)$$

$$Z_{mn} = \int_{l_1}^{l_2} w_m(x') \underline{L}(x') J_n(x') dx' \quad (36)$$

Casting the results of equations (35) and (36) into matrix form, we can write (34) as

$$[V_m] = [Z_{mn}] [I_n] \quad m, n = 1, 2, \dots, N \quad (37)$$

where the V and Z matrices contain known elements, defined by (35) and (36), and the constants I_n are to be found.

There will be N unknown I 's, one for each $J_n(x')$. Thus, we can find a solution for I_n by choosing at least N weighting functions. However, the uniqueness of the solution will be dependent upon the properties of matrix Z_{mn} . To find the unknown I_n matrix, we carry out the inversion operation occurring with the matrix equation

$$[I_n] = [Z_{mn}]^{-1} [V_m] \quad (38)$$

The existence of a solution will depend upon the existence of the matrix inverse of Z_{mn} . If $[Z_{mn}]^{-1}$ does not exist, then the solution is undefined.

A common choice of testing functions is the Dirac delta function

$$w_m(x) = \delta(x - x_m) \quad (39)$$

This testing function requires that the linear equation only has to hold at the set of points $\{x_m : m = 1, 2, \dots, N\}$. If this is the case, this method is known as point matching or collocation. If the testing function and the basis function are the same, the method is known as Galerkin's method, and is equivalent to a Rayleigh-Ritz variational method. Other common choices of basis functions include constants and sinusoidal functions.

Although the MOM approach to the solution of integral equations is very powerful, it has several disadvantages.

First, the usefulness of the technique is dependent upon the ability to solve equation (38). As previously mentioned, if the inverse of the impedance matrix does not exist, then there is no solution. Second, finding the inverse of the impedance matrix is expensive in terms of computer time and storage space as the problem size (number of unknown field components) grows. For a problem that has N unknowns, the storage space is proportional to N^2 and the execution time is proportional from N^2 to N^3 [Miller and Poggio, 1978]. Although newer techniques have been developed which do not require quite as much storage capacity and execution time, there is still a practical limit to the size of a structure that can be handled by the method of moments. Currently that limit is a structure ranging from 5 to 8 wavelengths in size. At high frequencies, this severely limits the size of structure that can be considered.

There are many implementations of the MFIE and EFIE solutions to EM interactions with bodies. In addition, there are other integral equation representations that have been used to determine the fields due to EM interaction with bodies. The interested reader is referred to Mittra [1976], Miller & Poggio [1978] and Eriksen, Rudolph & Perala [1981] for information on specific formulations, their implementation in prediction codes and their relative advantages and disadvantages.

While integral equation methods are well-developed, there are other powerful methods for solving the coupling problem. Another approach to finding the surface currents and charges is to start with Maxwell's curl equations, which are

$$\nabla \times \mathbf{E} = -\mu (\partial \mathbf{H} / \partial t) \quad (1)$$

$$\nabla \times \mathbf{H} = \epsilon (\partial \mathbf{E} / \partial t) + \mathbf{J} \quad (2)$$

Equations (1) and (2), are used to develop a solution approach known as the finite difference (FD) formulation. Although this approach can be carried out both in the time and frequency domain, we will concentrate on the finite difference time-domain (FDTD) formulation. The goal of this method is to model the propagation and interaction of an electromagnetic wave in a region of space (the problem space) containing an object that is to be studied. This method is different from the integral equation methods in that it analyzes the interaction of the incident wave with a portion of the structure at a given instant in time, instead of solving the entire problem at once.

Yee [1966] first suggested the FDTD formulation for solving Maxwell's two curl equations (1) and (2), saying that the derivatives in these equations could be expressed as differences of the field values between neighboring positions, both temporally and spatially. These difference equations yield the values of the field at a

given location in time and space if the values at all positions in the problem space are known at an earlier time. A detailed development of the three dimensional version of the FDTD code is given in a thesis by Williford [1985].

Conceptually, the solution of an electromagnetic interaction problem by the FDTD technique is straightforward. First, the problem space is gridded into a lattice of cells. The gridding procedure involves placing the components of the electric (E) and magnetic (H) fields around a unit cell (Figure III-13) and evaluating the field components at alternate half-time steps. By alternating between the E and H fields, a central difference expression can be developed for both the space and time derivatives that maintains a higher degree of accuracy than either a forward or backward difference formulation. The problem solution proceeds by time-stepping throughout the problem space, repeatedly solving the finite difference form of the two curl equations. In this fashion, the incident wave is tracked through the problem space as it intercepts and interacts with the structure in the problem space.

This solution technique has several advantage. First, no special formulation of the problem is necessary if the structure is composed of a mixture of conducting,

dielectric, magnetic, composite or other types of materials. This is because the finite difference equations are based on Maxwell's two curl equations, and the boundary conditions that must be met during the transition from one medium to another are incorporated naturally. Second, if changes in the structure are required to accomodate changes in material composition, the modifications in the program are minimal, as only the material constants need be adjusted. Finally, this method is particularly well suited for computer implementation with minimum storage and run time requirements. The storage and execution time for the FDTD approach increases linearly as the number of unknowns, N , instead of N^2 , as with the method of moments. Also, this method is easily modified to use the recent advances in parallel processing and vectorizing computers.

Yee [1966] first developed the FDTD algorithm as a method to compute the waveforms of pulses scattered from infinitely long, rectangular cross section, conducting cylinders. Other early work with this method included its use by Taylor, Lam and Shumpert [1969] for investigations of electromagnetic-pulse interactions in time-varying inhomogeneous media, by Merewether [1971] for studies of metallic bodies of revolution and by Holland [1977] for EMP coupling and scattering studies.

One of the earliest applications of the FDTD technique to lightning was the work by Rymes [1981], used to analyze data from direct lightning strikes to a NOAA C-130 aircraft. This code was later modified and used by Hebert and Sanchez-Castro [1987] to analyze the data from an inflight measurement using a CV-580 and by Williford [1985] to model an F-16 and explore the validity of different boundary conditions in the FDTD formulation. Williford, Jost and Hebert [1986] found that the FDTD technique with absorbing boundary conditions at the problem space boundary produced better results than the "hard" or reflective boundary conditions originally used by Yee, but at a cost of longer run times.

Based upon the work of these researchers, and others, the FDTD technique is an extremely useful one for the analysis of lightning's interaction with vehicles. As previously mentioned, these codes are extremely powerful and easily adapted to a variety of materials on the body under test. Another advantage is that nonlinearities and time-varying quantities can be represented in the problem space grid, if the needed equations can be written at the appropriate location. Also, they are easily adapted to parallel processing and multi-processor systems.

However, the FDTD method has some disadvantages also. The proper gridding of the vehicle may require a

significant amount of effort. Also, changes in the physical geometry often requires the regridding of the entire aircraft. Because of the storage requirements to run the model, most systems can only handle grids on the order of $30 \times 30 \times 30$. Although vehicles as large as a B-52 have been run under these constraints, the resolution of the cells is necessarily reduced. For instance, Figures III-14 and III-15 [Holland et al., 1979] show a B-52 model in a $30 \times 30 \times 30$ grid and a $50 \times 43 \times 59$ grid, respectively. It is easy to see that the finer grid can deliver better results. In general, for an $M \times N \times P$ dimensional grid, there will have to be at least a $6 \times M \times N \times P$ dimensional matrix to store the field components. Normally, increasing the fineness of the mesh will improve the resolution, but at an increased cost in run time and core storage space. In addition, the user may run into the point where increased accuracy due to a finer grid is offset by increased round-off error due to the larger number of calculations. Also, there is a limit on the number of time steps that can be used, as truncation and round-off errors accumulate as the iterations increase. Many of these disadvantages can be offset by newer machines having larger core memory sizes or multiple processors. The use of FDTD techniques should remain a good choice for many applications.

Still another approach to modeling the electromagnetic behavior of a physical system is to use an

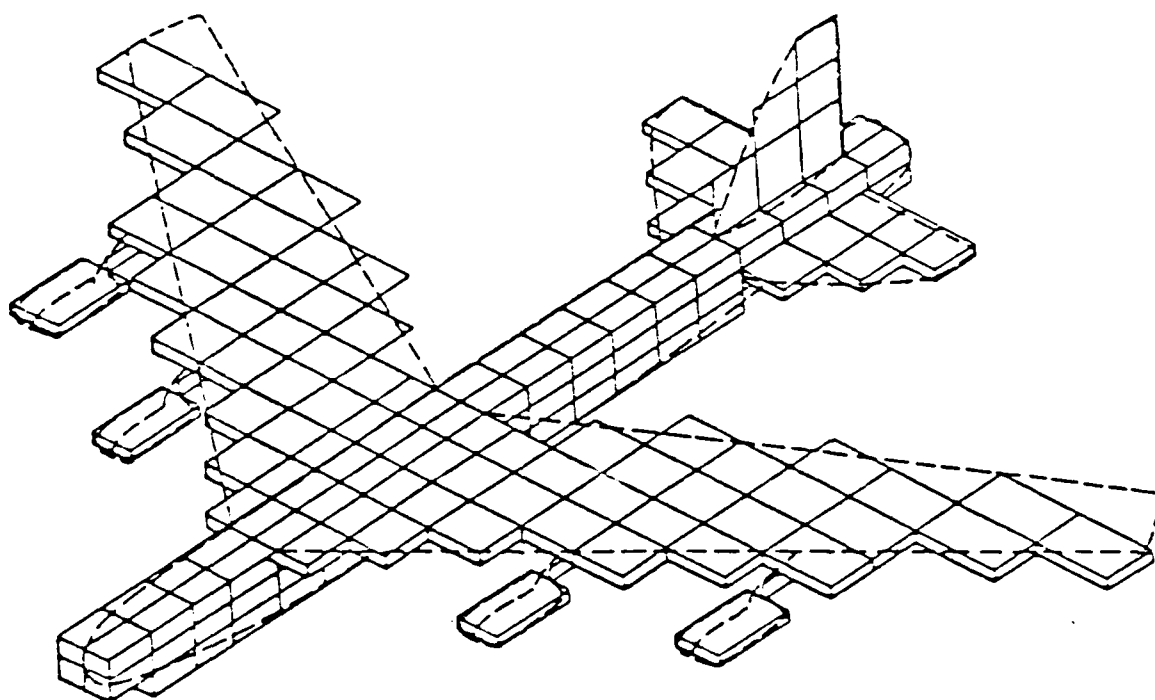


Figure III-14. A B-52 Model in a 30x30x30 THREDE Grid.
[Holland et al., 1979].

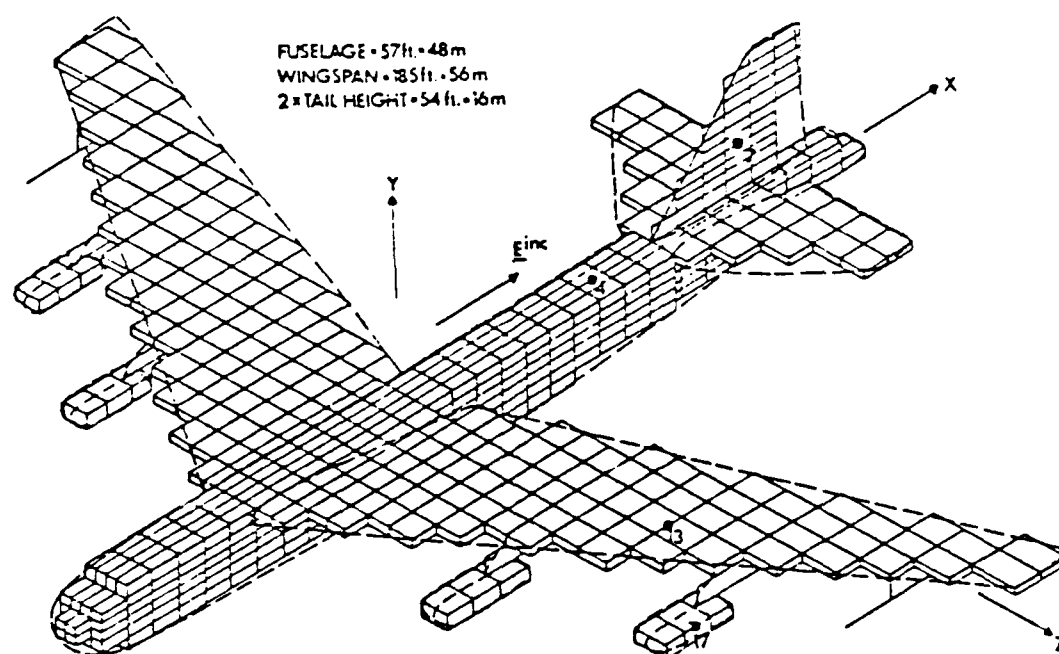


Figure III-15. A B-52 Model in a 50x43x59 THREDE Grid.
[Holland et al., 1979].

equivalent circuit network whose lumped elements represent the distributed properties of the structure. The lumped parameter network (LPN) method is one such approach to modeling the electromagnetic behavior of a system. With this method, the structure is modeled with lumped resistors, capacitors and inductors, as well as the sources needed to match any initial conditions on the structure. These models have been used for many years to model the distributed parameters of transmission lines, but have only been recently applied to the modeling of lightning interaction with aircraft.

These models are not directly derived from Maxwell's equations, but instead, are based upon the skill, experience, insight and intuition of the individual developing the model. The degree with which the model approximates what happens in the real system is dependent upon the ability of the modeler to consider all the parameters and the degree of complexity of the model. The creation of a more complex model generally results in more accurate results, but at a cost of increased calculations. Once the model is created, the system is solved by using any one of several computer codes used to analyze circuit problems. Some of the more common programs include ECAP, SPICE, SCEPTRE, CIRCUS and others.

Electromagnetic interactions with systems that have been analyzed by this method include the System Generated EMP (SGEMP) excitation of the FLTSATCOM satellite, modeled in Figure III-16 [Mangan and Perala, 1975] and the coupling of lightning to the Solid Rocket Boosters of the Space Shuttle, shown partially modeled in Figure III-17, [Perala and Robb, 1977]. A report by Fisher [1978] gives extensive information on developing LPN models, and reports on the application of this method to analyzing indirect effects of lightning on aircraft.

The methods reviewed here are not the only means whereby the external interaction problem may be analyzed. Many other methods and variations on these methods have been developed. This section should give the reader the impression that the method of analysis chosen is dependent upon the accuracy required, the computer resources available and the time available to create and analyze the model. In the next section, we will briefly review some of the methods and models for coupling the exterior environment into the aircraft.

Models for Prediction of Coupling Processes

The coupling of energy from the exterior to the interior of the aircraft can occur by several processes, but the most common avenue of energy entry is by apertures

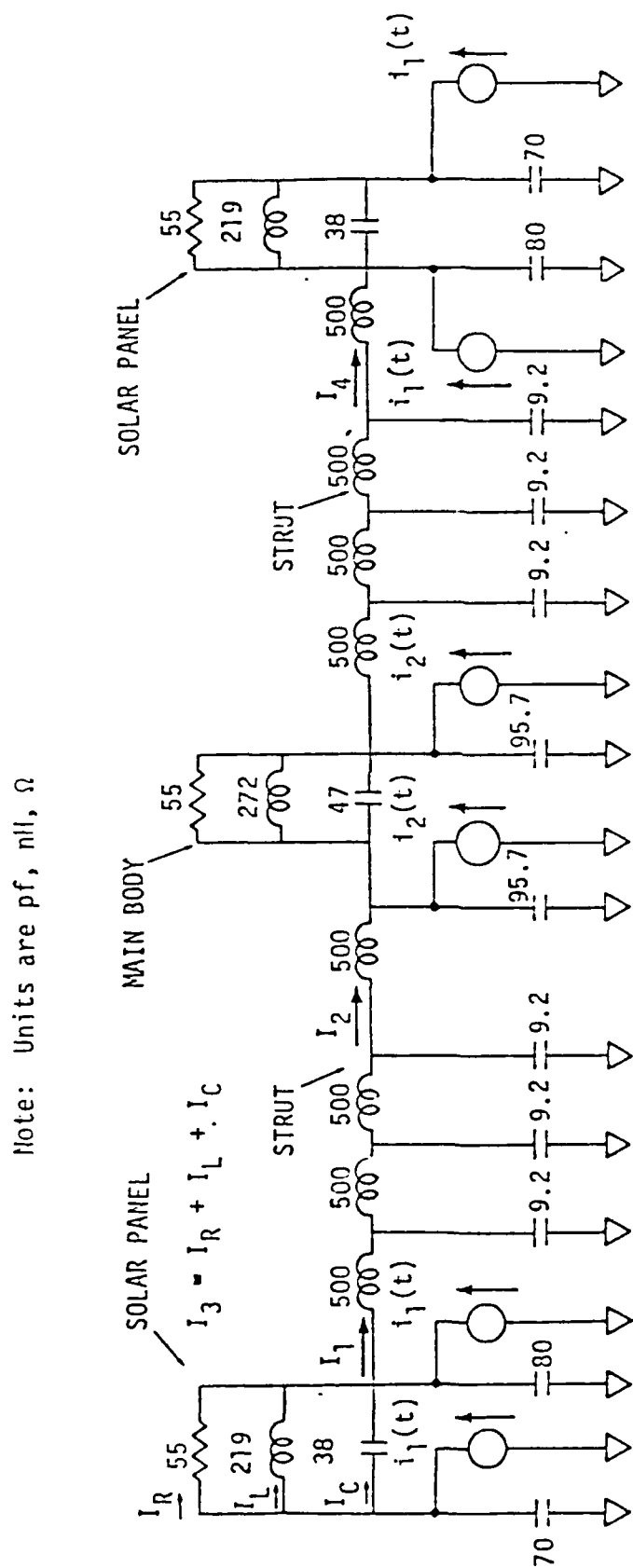


Figure III-16. Lumped Parameter Network Model Used for SGEMP Study of a FLTSATCOM Satellite. [Mangan and Perala, 1975].

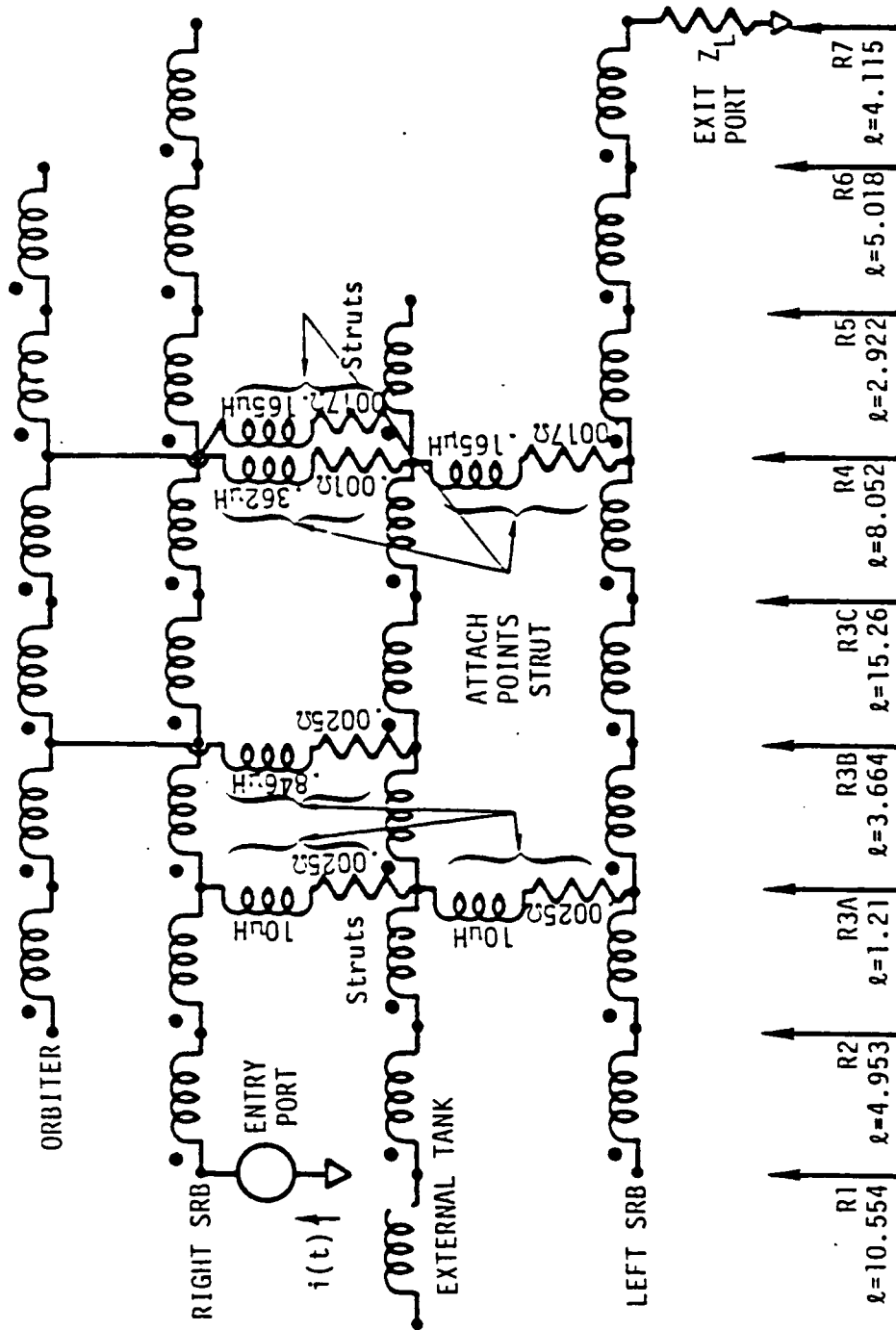


Figure III-17. Partial Circuit Model Representation for Composite Space Shuttle Vehicle Lightning Test. [Perala and Robb, 1977].

or openings in the aircraft. The apertures in an aircraft are usually complex from an electromagnetic perspective. They are often of odd shapes, backed by irregular shaped cavities that contain multiple conductors (wiring, hydraulic and fuel lines, and control cables), and are often large compared to the wavelength of the excitation source. Because of these many factors, the coupling problem is one of the most difficult to accurately model in the lightning-aircraft interaction process.

To make the analysis of the coupling problem more tractable, idealized representations of the actual problem are used. The problem is broken up into pieces that fit one of the canonical forms discussed earlier. Although exact solutions can not be found for the problem, reasonable bounds on what can be expected can be determined. Typically, the information desired from an analysis of the coupling from exterior to interior includes:

1. Total energy transmitted through the aperture.
2. The electric and magnetic fields developed inside the aperture and backing cavity.
3. The transient current and voltage developed on conductors due to the coupled energy.
4. Energy dissipated in the conductors or in the loads terminating the conductors within the interior of the vehicle.

The electromagnetic field penetration through a single aperture has been extensively studied by many individuals in connection with the threat of NEMP. Typical of these studies is one done by Taylor [1973]. Building on work by Bethe [1944], Taylor modeled the aperture with a combination of radiating electric and magnetic dipoles, or equivalent sources, whose dipole moments are proportional to the tangential electric and magnetic fields of the incident wave.

Bethe based his equivalent dipole derivation on a quasi-static approximation of the field distribution in the aperture. This approximation assumes the fields in the aperture are those that would exist if the aperture was placed within static electric and magnetic fields. For this assumption to hold, the dimensions of the aperture must be small with respect to the wavelength of the incident wave. One result of this quasi-static approximation is that the time characteristics of the internal field will be the same as the external field.

Taylor found that the pulses would penetrate the apertures with essentially no distortion and that the fields of the aperture were mostly local. He also found the field configuration was approximately that due to perpendicular, static electric and magnetic dipoles, except for cases very near resonant conditions of the

interior cavity. Although Taylor's work was done with small apertures, he stated that the results were valid and had application in other situations. The key results were:

1. The field penetrating a small aperture, less than 0.1λ , is approximated by static, crossed electric and magnetic dipoles, except for frequencies within 10% of resonance. If the internal cavity has a low Q , less than 10, then this restriction does not apply.
2. The magnetic dipole moment of the equivalent source distribution lies in the plane of the aperture and the electric dipole moment is perpendicular to the aperture.
3. The cartesian coordinates of the magnetic dipole moment are directly proportional to the corresponding components of the surface current density that would exist at the position of the aperture if it were electrically shorted.
4. The magnitude of the electric dipole moment is directly proportional to the surface charge density that would exist at the position of the aperture if it were electrically shorted.

Although this method is quite a simplification of the aperture problem, it has many useful applications.

Building upon this work, O'Neil [1986] modeled a mesh screen as an array of elliptical apertures and was able to determine an upper bound on the magnetic field penetrating the screen. Other approaches to the aperture problem have been used. Senior [1976] used the Singularity Expansion Method (SEM) that has been proposed and developed by Baum [1976, 1978]. Umashankar and Baum [1978] developed coupled integro-differential equations for the complex

coupled boundary value problem of the transient characterization of arbitrarily shaped bodies behind an aperture perforated conducting screen. An excellent tutorial article on EM penetration through apertures in conducting surfaces is given by Butler, Rahmat-Samii and Mittra [1978]. Although this work was oriented toward EMP problems, the information is applicable to the lightning coupling problem if the differences in waveform, amplitudes and frequency content are corrected for. The article contains an extensive set of references and reviews most of the approaches that had been taken to that point in time.

For more accurate results that are computationally tractable, some of the methods previously discussed are useful. One method, the FDTD approach, promises excellent accuracy, at an increase in the amount of computer resources required for the computation. Kunz and Hudson [1986] validated the FDTD approach for interior coupling responses and found the agreements between prediction and measurement very good. Kunz, Hudson and Breakall [1986] used the FDTD approach to measure shielding effectiveness and account for the interior response of a highly resonant cylinder.

In terms of other coupling mechanisms, varied approaches are available for modeling and predicting how

the field will couple into the interior of the vehicle. The FDTD approach is useful for the analysis of composite structures, because the varying conductivity of different portions of the vehicle can be easily handled. For slot and gap problems, the methods used to analyze slot antennas are pertinent. Arvas and Sarkar [1987] use a method of moments approach to study dielectric-filled slots in a conducting shell. Most of the analytical and computational methods previously discussed are available for use. Generally, the researcher has several choices for the development of models for coupling phenomenon. The final choice will depend upon the accuracy required, level of detail needed, and computational resources available.

Models for Prediction of Internal Interaction Processes

When examining the internal interaction process in an aircraft, the problem can be considered to be equivalent to an examination of the electromagnetic susceptibility of the vehicle to interference. Therefore, the large amount of literature that has been developed to address electromagnetic compatibility (EMC) problems is pertinent to these problems and processes. Physically, once energy is coupled into the interior of the vehicle, the energy then couples into surrounding cables and equipment. Because of the large number of cables and wiring in an

aircraft, the emphasis of this section is on field to cable coupling.

One approach is to study the response of a wire or cable to an electromagnetic field propagating through an aperture. This is the approach of Butler and Umashankar [1976], who investigated the excitation of a wire behind an aperture-perforated, conducting screen. They formulated integro-differential equations for the electromagnetic coupling to the wire behind the aperture, and solved those equations using the method of moments. Another study of this type was carried out by Seidel, Dudley and Butler [1977], who conducted an investigation of a wire excited through an aperture within a rectangular cavity. They formulated an integral equation in the frequency domain using imaged dipole moments to approximate the aperture, and then solved the problem numerically using the Method of Moments. Besides these more traditional approaches based upon integral equation methods, other approaches have been used.

Because of the great flexibility of the FDTD approach, many researchers are working on extending this method to the interior problem. Kunz and Hudson [1986] used the FDTD approach to measure the coupling of electromagnetic fields onto cables within a cylinder possessing an aperture. They found that it yielded

accurate results with reasonable computational times. Additional work with this method should yield the ability to model many of the nonlinear effects that make the coupling problem difficult.

Although the modeling of cable bundles and conductors by the lumped parameter network (LPN) method would seem to be a natural way to proceed, there are several problems that must be overcome. The biggest concern in using the LPN method is the determination of the number of sections that must be used to accurately model a section of the transmission line. Accurate modeling at high frequencies requires a large number of sections. As the number of sections increases, the processing time and the error due to round-off increases. Recently, Colvin [1985] has determined an efficient way to overcome this problem for two-conductor lines, even when a large number of sections is required. However, since this method is not applicable to multiconductor lines, there is still difficulty in using this approach with realistic problems.

There are two commonly used methods for modeling the internal conductors and cables that are formed into bundles within the aircraft. These methods are the multiconductor model and the bulk cable model. Multiconductor modeling requires the specification of capacitance and inductance matrices for multiconductor

bundles. The voltage and current for individual wires is found by using these matrices and solving the transmission line equations of the bundle in matrix form. This method is explained in greater detail in a series of reports by Paul [1976].

Although multiconductor transmission line theory is advanced enough to carry out an analysis of the energy coupled into aircraft wiring bundles, it is not practical to do so. The central problem is specification of how the cable bundles are configured in an actual aircraft. This data is not always available from aircraft drawings and is not practical to obtain by physical inspection. For many aircraft, the construction of the bundles is done as piecework and the layout of individual wires in the bundle is variable. The geometry and arrangement of the bundle will change as a function of the position, making modeling a difficult task. Finally, knowledge of the parameters for one vehicle would not necessarily be valid for another vehicle of the same type because of the design and manufacturing variability between aircraft of the same type.

Because of these problems, the bulk cable model has been developed. In this approach, the entire bundle is treated as a single conductor. Then one-conductor transmission line models can be used to obtain the total

current and average voltage on this conductor. The bulk response can then be used to estimate the response of a single wire in the bundle. For worst case analysis, each wire can be assumed to carry the total current and voltage. Another way to determine individual wire response is to separate a single wire from the bundle and solve for its response by treating the rest of the bundle as the excitation source.

At the present time, the generation of codes that may be used to make predictions based upon these models is as much of an art as it is a science. Most of the codes currently available are integral equation formulations based upon Maxwell's equations, and solved through moment method techniques. Other approaches that have been used include Geometrical Theory of Diffraction (GTD) codes, hybrid GTD and MOM codes, FD codes, both in the time and frequency domain, finite element method (FEM) codes and other codes specialized for specific configurations, materials or excitation sources. For an overview of many of these codes, the article by Bevensee et al. [1978] lists many of the available codes for EMP interaction and coupling. Many of these codes, with modification, have been successfully used to predict the results using the lightning threat instead of EMP excitation. Eriksen, Rudolph and Perala [1981] also discuss the tradeoffs between different approaches to codes to implement these

coupling and interaction solutions.

This chapter has provided a general overview of the modeling and prediction process for the aircraft-lightning interaction problem. The purpose of this chapter was to give an appreciation of the complexity of the physical processes to be modeled. Because of the difficulty in developing accurate prediction models and validating them, simulation processes are often employed to indicate how an aircraft will respond when the lightning threat interacts with the vehicle. These simulations, in turn, make it possible to create more accurate models with enhanced prediction capability. By using both modeling and simulation jointly, a more accurate picture of what happens to the aircraft during the actual airborne lightning interaction event can be developed. In the next chapter, the simulation process will be described, as well as the errors that can corrupt the results obtained.

REFERENCES - CHAPTER III

R.A. Perala, T. Rudolph and F. Eriksen, "Electromagnetic Interaction of Lightning with Aircraft," IEEE Transaction on Electromagnetic Compatibility, EMC-24, No. 2, May 1982, pp. 173-203.

F. Eriksen, T. Rudolph and R. Perala, "Atmospheric Electricity Hazards Analytical Model Development and Application, Vol. III: Electromagnetic Coupling Modeling of the Lightning/Aircraft Interaction Event," by Electro Magnetic Applications, Inc. Air Force Wright Aeronautical Laboratory Technical Report, AFWAL-TR-81-3084, Volume III, Wright-Patterson AFB, OH, August 1981.

C.A. Balanis, Antenna Theory: Analysis and Design. New York: Harper & Row, 1982, pp. 496-501.

R.E. Collin, Field Theory of Guided Waves. New York: McGraw-Hill Book Co., 1960, pp. 29-34.

K.S.H. Lee, ed., EMP Interaction: Principles, Techniques and Reference Data. New York: Hemisphere Press, 1986.

J.D. Kraus, Antennas, 2nd ed. New York: McGraw-Hill Book Co., 1988.

T.K. Liu, K.S.H. Lee and L. Marin, "Broadband Responses of Deliberate Aircraft Antennas, Part I," Interaction Notes, Note 228, Air Force Weapons Laboratory, Kirtland AFB, NM, May 1975.

R.L. Carney and G.J. Von Bokern, Final Report, Atmospheric Electricity Hazards Protection Program, Part V. Design Guide for Air Vehicles, by Boeing Military Airplane Company. Air Force Wright Aeronautical Laboratory Technical Report, AFWAL-TR-87-3025, Part IV, Wright-Patterson AFB, OH, June 1987, pp. 13-14.

R. Pengelly and A. Ezzeddine, "GaAs MMIC Module Tunes High Gain from 50 MHz to 4 GHz," Microwaves & RF, Vol. 27, No. 4, April 1988, pp. 163-165.

J. Eckert, "RFI and the Black Hawks," EMC Technology & Interference Control News, Vol. 7, No. 1, January-February 1988, p. 7.

J.A. Stratton, Electromagnetic Theory. New York: McGraw-Hill Book Co., 1941, p. 429.

J.D. Jackson, Classical Electrodynamics. 2nd ed. New York: John Wiley & Sons, 1975, pp. 223-226.

R. Mittra, "Integral Equation Methods for Transient Scattering," in Topics in Applied Physics, Vol. 10: Transient Electromagnetic Fields, Berlin, Germany: Springer-Verlag, 1976, Chapter 2.

E.K. Miller, "Some Computational Aspects of Transient Electromagnetics," Lawrence Livermore Laboratory, Report UCRL-51276, 1972. Also, Interaction Note 143, Air Force Weapons Laboratory, Kirtland AFB, NM, 19 September 1972.

R.F. Harrington, Field Computation by Moment Methods. New York: MacMillan, 1968.

E.K. Miller and A.J. Poggio, "Moment Method Techniques in Electromagnetics from an Applications Viewpoint," in Electromagnetic Scattering, edited by P.L.E. Uslenghi, New York: Academic Press, 1978, Chapter 9.

K.S. Yee, "Numerical Solution of Initial Boundary Value Problems Involving Maxwell's Equation in Isotropic Media," IEEE Transactions on Antennas and Propagation, AP-14, May 1966, pp. 302-307.

C.F. Williford, "Comparison of Absorption and Radiation Boundary Conditions Using a Time-Domain Three-Dimensional Finite Difference Electromagnetic Computer Code," Masters Thesis, AFIT/GE/ENG/85D-53, School of Engineering, Air Force Institute of Technology (AU), Wright-Patterson AFB, OH, December 1985.

C.D. Taylor, D.H. Lam and T.H. Shumpert, "Electromagnetic Pulse Scattering in Time-Varying Inhomogeneous Media," IEEE Transactions on Antennas and Propagation, Vol. AP-17, September 1969, pp. 585-589.

D.E. Merewether, "Transient Currents Induced on a Metallic Body of Revolution by an Electromagnetic Pulse," IEEE Transactions on Electromagnetic Compatibility, Vol. EMC-13, May 1971, pp. 41-44.

R. Holland, "THREDE: A Free-Field EMP Coupling and Scattering Code," IEEE Transactions on Nuclear Science, Vol. NS-24, December 1977, pp. 2416-2421.

M.D. Rymes, T3DFD User's Manual: Final Technical Report, August 1979--June 1981. Prepared for Air Force Flight Dynamics Laboratory, Wright-Patterson AFB, OH. Contract number F33615-79-C-3412, by Electro Magnetic Applications, Inc., (EMA-81-R-24), Denver, CO, April 1981.

J.L. Hebert and C. Sanchez-Castro, Implementation of a Three-Dimensional Finite Difference Electromagnetic Code for Analysis of Lightning Interaction with a FAA CV-580 Aircraft," Air Force Wright Aeronautical Laboratory Technical Report, AFWAL-TR-86-3008, Wright-Patterson AFB, OH, May 1987.

C. Williford, R.J. Jost and J.L. Hebert, "Comparison of Absorption and Radiation Boundary Conditions in 3DFD Code," Proceedings of 1986 International Aerospace and Ground Conference on Lightning and Static Electricity, Dayton, OH, June 24-26, 1986, pp. 44-1--44-10.

D.L. Mangan and R.A. Perala, "SGEMP Low-Level Simulation of the FLTSATCOM," Mission Research Corp., AMRC-R-49, August, 1975.

R.A. Perala and J.D. Robb, "The Experimental Verification of Circuit Modeling Techniques Used to Determine Lightning Current Distribution as Applied to the NASA Space Shuttle Vehicle," Proceedings of the 1977 IEEE International Symposium on Electromagnetic Compatibility, Seattle, WA, August 2-4, 1977, pp. 278-281.

F.A. Fisher, "Analysis and Calculations of Lightning Interactions with Aircraft Electrical Circuits," by General Electric Company, Air Force Wright Aeronautical Laboratory Technical Report, AFFDL-TR-78-106, Wright-Patterson AFB, OH, August 1978.

C.D. Taylor, "Electromagnetic Pulse Penetration Through Small Apertures," IEEE Transactions on Electromagnetic Compatibility, Vol. EMC-15, February 1973, pp. 17-26.

H.A. Bethe, "Theory of Diffraction by Small Holes," The Physical Review, Vol. 66, October 1944, pp. 163-182.

J.L. O'Neil, "Analysis of Lightning Induced Magnetic Field Penetration Through Protective Metal Screens Using an Equivalent Dipole Moment Representation of an Array of Elliptic Apertures," Masters Thesis, AFIT/GE/ENG/86D-30, School of Engineering, Air Force Institute of Technology (AU), Wright-Patterson AFB, OH, December 1986.

T.B.A. Senior, "Electromagnetic Field Penetration into a Cylindrical Cavity," IEEE Transactions on Electromagnetic Compatibility, Vol. EMC-18, May 1976, pp. 71-73.

C.E. Baum, "The Singularity Expansion Method," in Topics in Applied Physics, Vol. 10: Transient Electromagnetic Fields, edited by L.B. Felsen. Berlin, Germany: Springer-Verlag, 1976, Chapter 3.

C.E. Baum, "Toward an Engineering Theory of Electromagnetic Scattering: The Singularity and Eigenmode Expansion Methods," in Electromagnetic Scattering, edited by P.L.E. Uslenghi, New York: Academic Press, 1978, Chapter 15.

K.R. Umashankar and C.E. Baum, "Transient Electromagnetic Characterization of Arbitrary Conducting Bodies Through an Aperture-Perforated Conducting Screen," Interaction Note 343, Air Force Weapons Laboratory, Kirtland AFB, NM, March 1978.

C.M. Butler, Y. Rahmat-Samii and R. Mittra, "Electromagnetic Penetration Through Apertures in Conducting Surfaces," IEEE Transactions on Antennas and Propagation, Vol. AP-26, January 1978, pp. 82-93.

K.S. Kunz and H.G. Hudson, "Experimental Validation of Time-Domain Three-Dimensional Finite-Difference Techniques for Predicting Interior Coupling Responses," IEEE Transactions on Electromagnetic Compatibility, Vol. EMC-28, February 1986, pp. 30-37.

K.S. Kunz, H.G. Hudson and J.K. Breakall "A Shielding-Effectiveness Characterization for Highly Resonant Structures Applicable to System Design," IEEE Transactions on Electromagnetic Compatibility, Vol. EMC-28, February 1986, pp. 18-29.

E. Arvas and T.K. Sarkar, "TM Transmission Through Dielectric-Filled Slots in a Conducting Cylindrical Shell of Arbitrary Cross Section," IEEE Transactions on Electromagnetic Compatibility, Vol. EMC-29, May 1987, pp. 150-156.

C.M. Butler and K.R. Umashankar, "Electromagnetic Excitation of a Wire through an Aperture-Perforated, Conducting Screen," IEEE Transactions on Antennas and Propagation, Vol. AP-24, July 1976, pp.456-462.

D.B. Seidel, D.G. Dudley and C.M. Butler, "Aperture Excitation of a Wire in a Rectangular Cavity," Interaction Note 345, Air Force Weapons Laboratory, Kirtland AFB, NM, June 1977.

D.H. Colvin, "Computationally Efficient Method of Calculations Involving Lumped-Parameter Transmission-Line Models," IEEE Transactions on Electromagnetic Compatibility, Vol. EMC-27, February 1985, pp. 41-43.

C.R. Paul, "Applications of Multiconductor Transmission Line Theory to the Prediction of Cable Coupling, Vol. I, Multiconductor Transmission Line Theory," Rome Air Development Center Technical Report, RADC-TR-76-101, Vol. I, Griffiss AFB, NY, April 1976.

C.R. Paul, "Frequency Response of Multiconductor Transmission Lines Illuminated by an Electromagnetic Field," IEEE Transactions on Electromagnetic Compatibility, Vol. EMC-18, November, 1976, pp. 183-190.

R.M. Bevensee, J.N. Brittingham, F.J. Deadrick, T.H. Lehman, E.K. Miller, A.J. Poggio, "Computer Codes for EMP Interaction and Coupling," IEEE Transactions on Antennas and Propagation, Vol. AP-26, January 1978, pp.156-165.

CHAPTER IV

LIGHTNING SIMULATION AND CONFIGURATION EFFECTS

Overview

In this chapter, we will examine the purposes of simulating the lightning-aircraft interaction event, what should be simulated in the lightning-aircraft interaction event and how those simulations may be carried out. Several of the techniques currently used for the simulation of lightning's effects on systems will be discussed. In our discussion, we will concentrate on indirect effects simulation because the results of indirect effects testing are more sensitive to configuration effects. We will examine the interaction between the simulation system, the measurement system and the device under test, and see how those interactions can affect the results that are obtained. We will identify errors that may be introduced into the results of testing due to these configurations effects. Finally, we will discuss ways of eliminating many of these errors.

One way to verify our knowledge of what happens in the lightning-aircraft interaction process is to simulate the process under investigation and to compare the results of this simulation with known results. These results may be obtained from theoretical solutions of the interaction problem, such as canonical solutions, or from actual

measurements taken of the interaction process. The accuracy of this simulation will determine how closely we can validate the models developed through theoretical considerations. It will also give us insight into the accuracy of our measurement system when used to measure the actual event. Thus, a valid simulation is useful in advancing the knowledge and understanding of a process.

Simulation of the Lightning-Aircraft Interaction Event

When simulating any physical event, the first step is to decide what is to be simulated. This decision, in turn, is dependent upon the reason the simulation is to be carried out. One reason might be to try to reproduce the actual processes occurring during an event. This can lead to a deeper understanding of the physics of the processes making up the event. Another motivation might be to reproduce the effects of the event. This helps us understand how the event interacts with different environments and the effect that process has on its environment and vice versa.

When considering the lightning-aircraft interaction event, there are many reasons to carry out simulations. One reason might be characterization to investigate the physics of the processes occurring during the event. Another reason might be to advance the state-of-the-art concerning the technology associated with lightning

measurement or warning systems. Still another reason is to verify that a lightning protection scheme for an aircraft is effective. Finally, if a protection scheme is known to be good initially, how can the protection scheme be validated if the aircraft undergoes maintenance or modification.

Each of these simulation scenarios may require a different type of simulation technique. The approach used will depend on the results desired. In attempting to simulate the effects of lightning on an aircraft, we could attempt to reproduce a lightning flash interacting with an aircraft. To simulate the physics of the lightning event, we require a detailed knowledge of those physical processes occurring during the lightning-aircraft interaction event. If our knowledge of the processes is detailed enough, and we can reproduce those processes, then we should be able to reproduce the same effects that the actual lightning flash would. In essence, we are proceeding from cause to effect.

Another approach to simulating the effects of lightning on an aircraft might proceed from cataloging all the effects that the lightning event caused. Then we need to find techniques that cause the same effects that lightning does. Here, our focus is on the effects themselves, not what causes those effects. In this

approach, we go backwards from effect to cause.

The previous paragraphs might be considered ad hoc approaches to consideration of the lightning-aircraft interaction process. Whatever approach is used, there must be a reason why the simulation is done. One of the most common reasons for lightning simulation is to determine the vulnerability of an aircraft and its complex electronic systems to the potential damage and interference caused by a direct or nearby lightning strike. Simulations are required to determine the vulnerability of the aircraft to the lightning event because, as Baum [1980] states, the total aircraft system is too complex to completely understand its electromagnetic response to the lightning event from first-principles. It is this complexity which defies closed form, analytical verification of lightning protection schemes. Baum goes on to say that:

"In general the system complexity and possibility (or even probability) that there are important signal paths which are not even identified (even implicitly) in the formal statement of the system design (blueprints, etc), makes a reliance on first-principle analysis usually untenable for system vulnerability assessment."

We will consider this to be the reason we utilize lightning simulation to investigate the lightning-aircraft interaction event. The objective of our lightning simulation is to determine whether the system under consideration will be safe and/or fulfill mission

requirements in the presence of the lightning threat. User requirements dictate the amount of protection required. The first requirement is always safety of flight. The aircraft should always be able to return to a base following a lightning strike. Components and subsystems that are required for safe flight might be termed safety critical. Assuming that the aircraft is adequately protected from a safety standpoint, the aircraft should be able to carry out its mission after suffering a lightning strike. This requires that there be no failure of system components or electronics that have been defined to be mission critical. These are components or subsystems that will keep the mission from being carried out if they fail. Some components are required not only for safety, but also for mission fulfillment. For instance, complete failure of the engine control system is not only a safety hazard, but will also cause an abort of the mission, thus the engine control system would be considered to be safety critical as well as mission critical.

Not only do we wish to determine the vulnerability of mission critical components, we need to know, to a high degree of confidence, if there will be any failures in those components under investigation. This is an important point when considering the type of threat to which the components in question are subjected. As

lightning is a threat that is statistical in nature, there is an inherent amount of uncertainty in the actual process. When simulating the lightning-aircraft event, it is very critical that all possible errors be identified, and eliminated if possible. This is crucial to narrowing the uncertainty level, thereby increasing the confidence in the results obtained through simulation. Safety of flight considerations require that this uncertainty be minimized.

This reduction in uncertainty is very important to both the system designer and the end user. Because the goal is to design and build a system that safely and economically meets mission requirements, system vulnerabilities must be identified and compensated for. In terms of lightning protection, compensation consists of hardening the system against the effects of the electromagnetic interaction of the lightning with the aircraft. This hardening may take the form of additional shielding, re-design of electronic subsystems with less vulnerable components, re-routing of cables and control wires, elimination of unnecessary apertures, etc.

This hardening process is expensive, not only in terms of initial extra cost, but in other costs over the lifetime of the aircraft. The sum of these costs is called the life cycle cost of the system and includes the

developmental cost, acquisition cost, the cost of ownership and operation and the cost of final disposition. Every pound of weight added for lightning protection adds to the cost of operation and represents a cost in terms of decreased fuel efficiency, limiting operational range, space unavailable for equipment or cargo, or some combination of these. In addition, there is an increased cost of ownership for the maintenance cost that extends over the lifetime of the aircraft. Lightning protection must be verified at regular intervals, and the more protection incorporated, the greater the costs incorporated in protection verification and surveillance. Thus, there is a natural desire to incorporate only that protection required, consistent with safety and reliability requirements established by the end user.

Given that there is sufficient motivation to carry out the simulation process, it is now appropriate to examine the simulation process itself. Just as the effects of lightning on aircraft are divided into direct and indirect effects, we usually design a simulator and associated measurement configuration to simulate either direct effects or indirect effects. Because of the many differences between the causes of these effects, and how they affect the aircraft and its systems, they are addressed separately in the standards and procedures covering lightning testing.

Lightning Simulation Waveforms

It is very important to realize that the goal of practical lightning simulation is not to reproduce the entire natural lightning event. Rather, we are trying to simulate or reproduce the significant direct and indirect effects of lightning on aircraft. The use of the term practical is chosen to indicate that we are emphasizing the lightning qualification of commercial and military aircraft, not the research activities. The decision to take this approach to lightning simulation has a direct bearing on the design of the simulator and related measurement configuration. Because we are interested in lightning's effects, we need to find appropriate waveforms which produce those same effects in bodies under test. We see that this approach is reflected in the test standard for lightning qualification of military aircraft.

The criteria for military lightning simulation testing is documented in MIL-STD-1757A, which presents the waveforms to be used in lightning simulation tests and for the qualification of lightning protection for military aircraft. The waveforms and components, depicted in Figures IV-1 through IV-3, are idealized and are generally used for analytical review of the lightning-aircraft simulation event. Thus, they need not be reproduced exactly for actual simulation tests. Instead, the requirement is that the numerical parameters defining the

waveform be met.

For qualification testing, there are three voltage waveforms, A, B, and D which represent the electric fields associated with a lightning strike. Voltage waveforms A and D, shown in Figures IV-1 and IV-2 respectively, are used to test for possible dielectric puncture and other potential attachment points. Voltage waveform B is used to test for streamers, while voltage waveform C is used for scale model testing of attachment points.

For qualification testing, there are four current components, A, B, C, and D, that are used to determine direct effects. Components A, B, C, and D each simulate a different part of the lightning flash and are shown in Figure IV-3. They are applied individually or, less commonly, as a composite of two or more components together in one test. Current waveform E, also shown in Figure IV-3, is intended to be used in the determination of indirect effects.

Instead of using waveforms that reproduce those measured during actual lightning strikes, these idealized waveforms have been selected to represent the severe threat. These idealized waveforms are related to the severe threat discussed in Chapter I and were chosen because of analytical constraints. An actual lightning

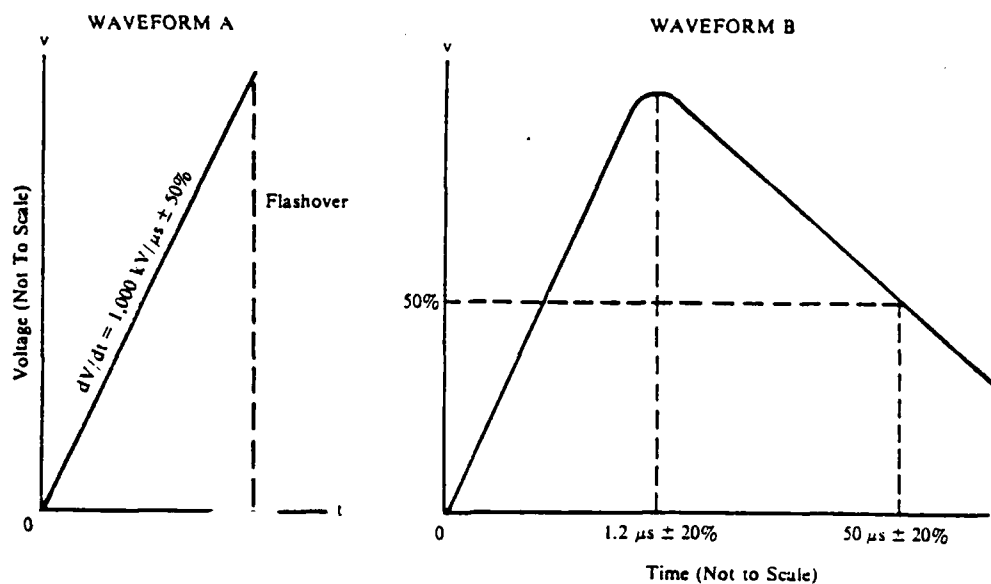


Figure IV-1. Voltage Waveforms A and B. [MIL-STD-1757A, 1983].

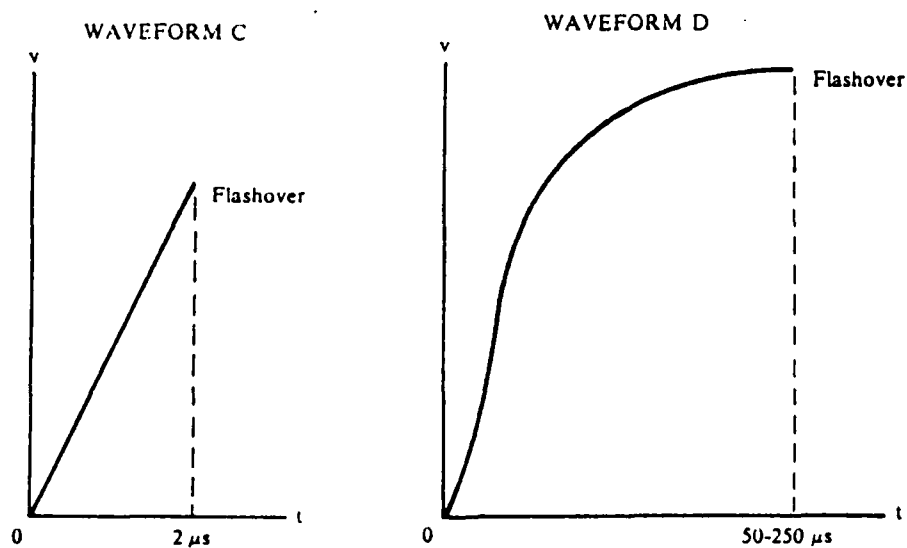
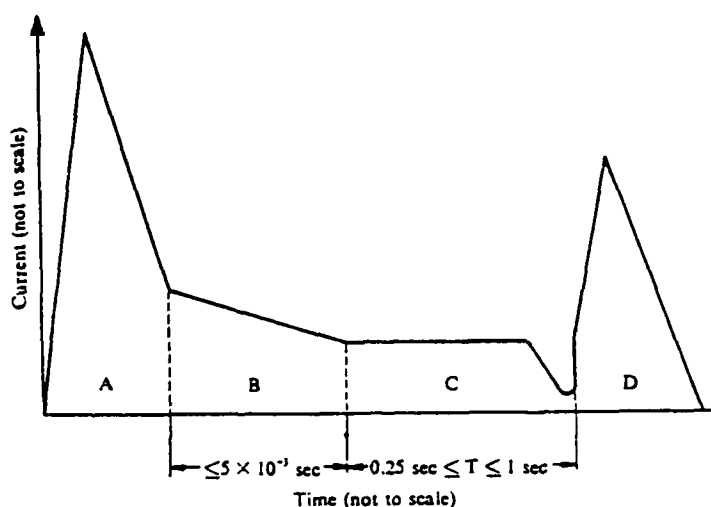


Figure IV-2. Voltage Waveforms C and D. [MIL-STD-1757A, 1983].



COMPONENT A (Initial Stroke)
 Peak amplitude = $200\text{kA} \pm 10\%$
 Action integral = $2 \times 10^6 \text{A}^2 \cdot \text{s} \pm 20\%$
 Time duration $\leq 500 \mu\text{s}$

COMPONENT C (Continuing Current)
 Charge transfer = $200 \text{ Coulombs} \pm 20\%$
 Amplitude = $200\text{--}800\text{A}$

COMPONENT B (Intermediate Current)
 Maximum charge transfer = 10 Coulombs
 Average amplitude = $2\text{kA} \pm 10\%$

COMPONENT D (Restrike)
 Peak amplitude = $100\text{kA} \pm 10\%$
 Action integral = $0.25 \times 10^6 \text{A}^2 \cdot \text{s} \pm 20\%$
 Time duration $\leq 500 \mu\text{s}$

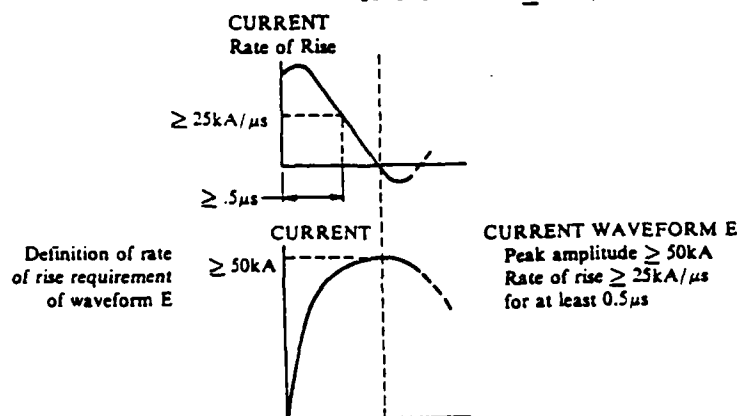


Figure IV-3. Current Waveforms. [MIL-STD-1757A, 1983].

strike creates extremely complicated waveforms which are not easily reduced to an exact analytical model which can be incorporated into prediction codes. These waveforms have the advantage that they are easily incorporated into analysis schemes. Unfortunately, they are often difficult to apply to full scale vehicles in a test program.

It would be extremely expensive to construct and operate a simulator capable of delivering both the high voltages and currents that comprise the severe threat. However, according to a report issued by a subcommittee of the Society of Automotive Engineers [SAE, 1978], "With a few exceptions, it is not necessary to simulate high-voltage and high-current characteristics together." Thus, simulators can be designed which concentrate on a subset of the waveforms used in testing. Because of the physical difficulty in generating the idealized threat waveforms, other waveforms are often used for the actual testing of full scale vehicles. However, these alternate waveforms must have the property that test results derived from them can be extrapolated, scaled or transformed to those which would be obtained from the idealized waveforms. In this fashion, the chain from measured results of testing to actual measured lightning threat is linked.

There are many approaches to developing alternate waveforms. For instance the actual, idealized waveforms

could be used, but with a smaller amplitude. The greatest advantage of this approach is that the results of this testing can be scaled to threat levels simply by multiplying the results by a scalar constant. However, this requires linearity over the range of scaling. While this is usually a valid assumption, and often gives conservative results, the larger the scale factor, the greater the chance that the assumption of linearity does not hold. In addition, certain processes due to mechanisms such as corona streamers and arcing are inherently nonlinear and will not scale linearly. For this reason, test levels should be as high as possible, balancing such factors as cost, safety, measurement accuracy, etc.

A second approach would involve the use of the double exponential waveform. This waveform, pictured in Figure IV-4, has the advantage that it is similar to the lightning channel return stroke current waveform and closely represents the portion of the exterior lightning response that couples to the interior of the aircraft by aperture coupling, structural IR voltages and diffusion. The internal current waveforms due to aperture coupling and structural IR voltages generally follow the exterior current waveforms. Waveforms from diffusion typically have slower rise times and longer duration times than the waveforms of the exterior current. This is more

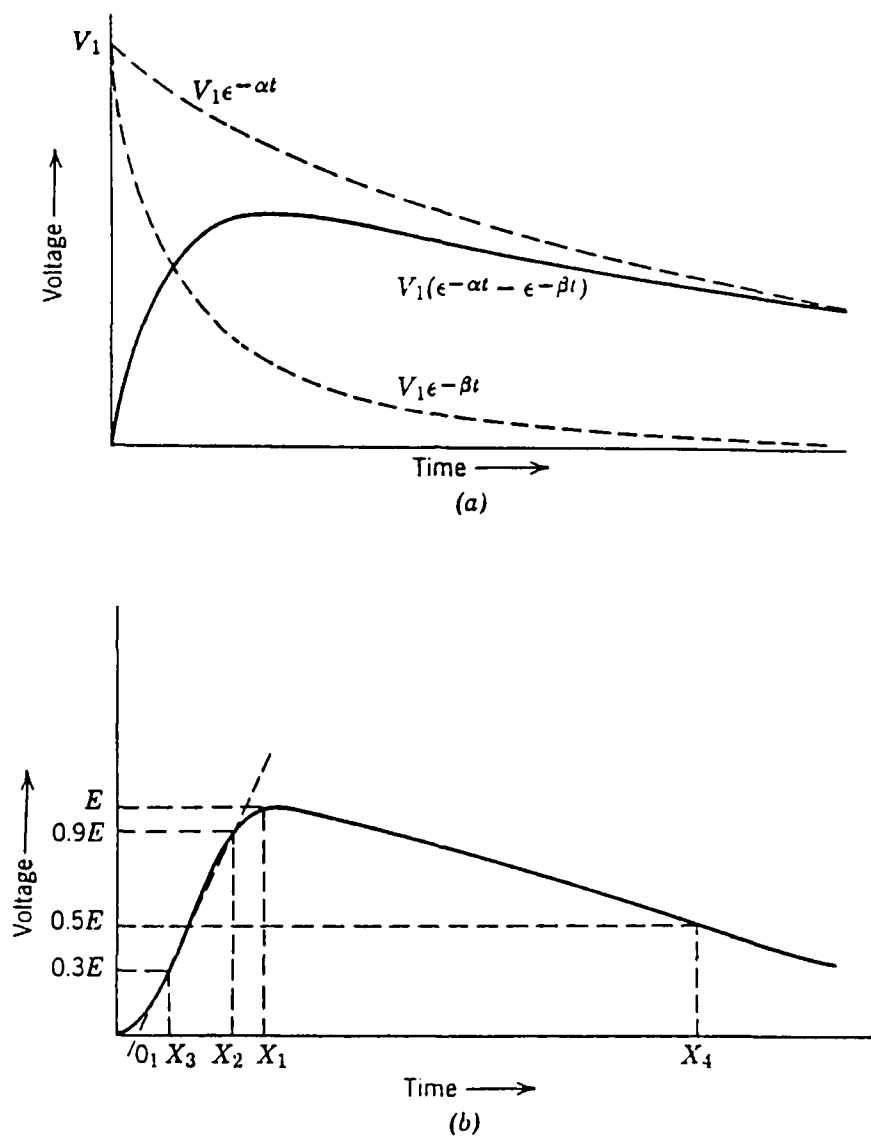


Figure IV-4. Typical Double-Exponential Voltage Waveforms.
 (a) Ideal Double-Exponential Waveform.
 (b) Typical Waveform Actually Generated by Impulse Generator. [Greenwood, 1971]

noticeable with the more conductive materials associated with composite structures and less so with metallic structures.

A third approach is to use a damped sinusoid generator with large values of i and di/dt . This waveform is advantageous because it is much less expensive to build a generator for this waveform than one for the double exponential waveform, especially at high levels. While large peak currents and a large di/dt can be obtained, it is at the cost of working with a bipolar waveform, instead of the unipolar waveform created by the double exponential. A typical waveform is shown in Figure IV-5. By choosing the frequency of the sinusoid, we can concentrate on the effects of aperture coupling (higher frequencies) or study simultaneously aperture coupling, diffusion and current redistribution effects.

A final approach is the use of a network analyzer system in a method known as swept frequency continuous wave (SFCW) approach. This system is used to obtain the complex (magnitude and phase) frequency dependent transfer function between the source waveform and aircraft cable responses. By the use of Fourier analysis techniques, this frequency domain transfer function can be related back to the time domain response of the idealized waveform. As in the first approach, the low level signals

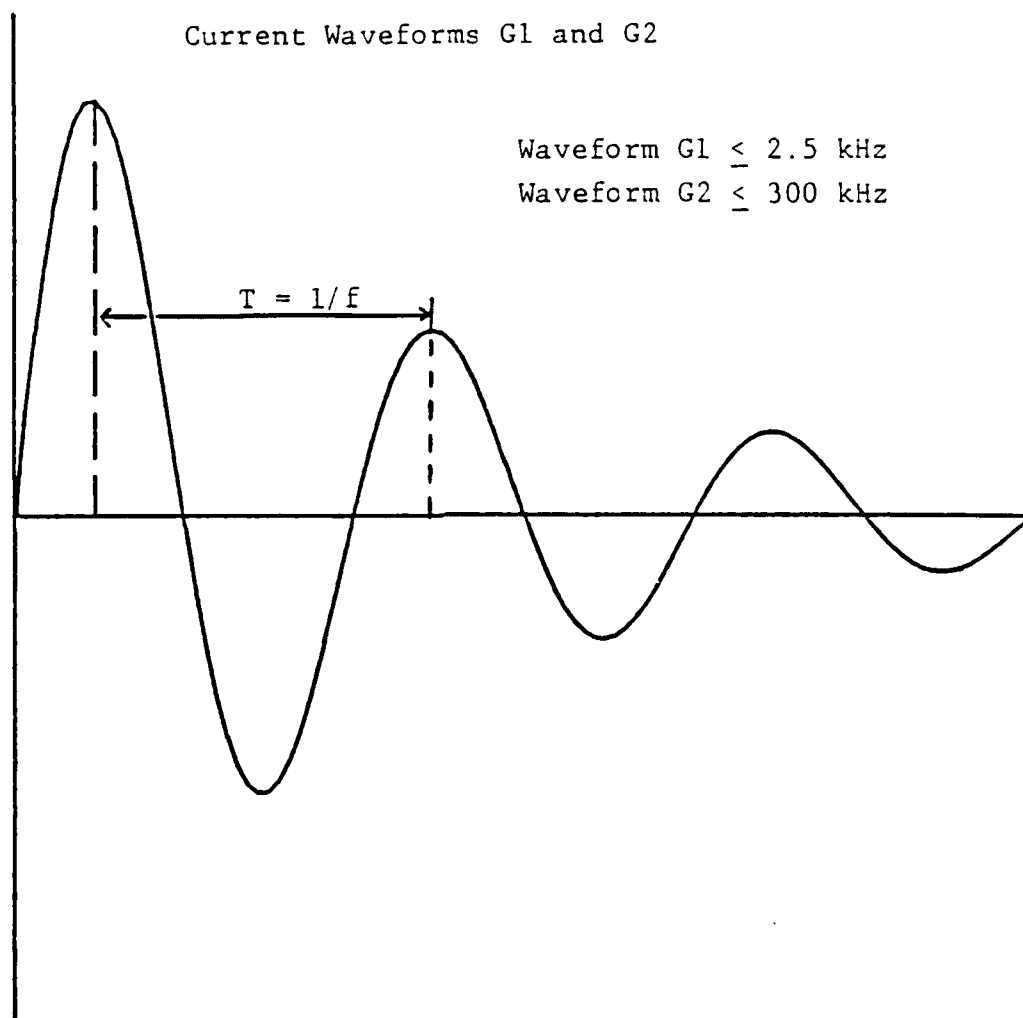


Figure IV-5. Damped Sinusoidal Test Current Waveform.
[SAE, 1987].

are scaled up to threat levels, so the comments concerning linearity previously made also apply to this method.

Although this method is much more complex than the first method, it has the advantage of the much larger dynamic range of a continuous wave system over a pulsed systems (> 120 dB vs. 25-45 dB). In addition, today's modern network analyzers can be highly automated, and under computer control, the entire process from measurement to data analysis can be performed automatically.

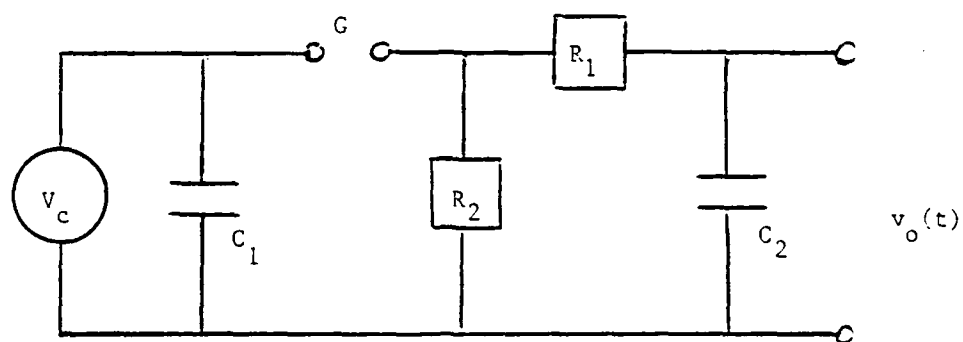
Although these are not the only possible approaches to testing waveforms, they are among the most commonly used. Other sources of information concerning simulation waveforms include publications by the FAA [1983], Rasch [1984] and the SAE [1987]. In addition to MIL-STD-1757A, DOD-STD-1795, "Lightning Protection of Aerospace Vehicles and Hardware," also has information applicable to lightning testing waveforms.

Simulator Design

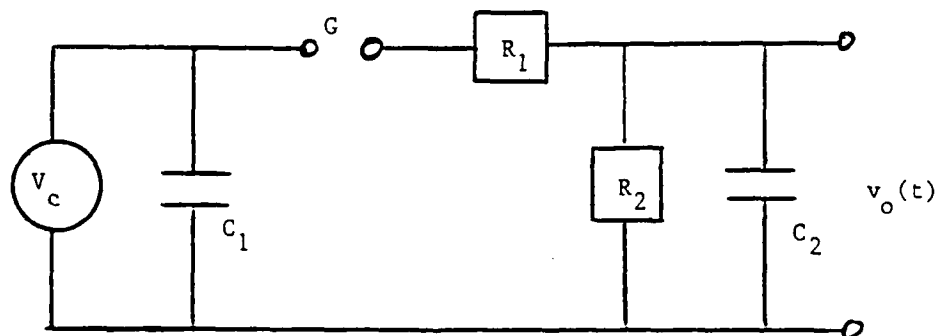
Once a testing waveform is chosen, then an appropriate generator, waveshaping network and return path must be designed to create a simulator. Although there are significant differences between simulators designed for direct and indirect effects, the basic components are the same. A lightning simulator designed to produce high voltages or currents can be broken down into the following

sections: (1) an energy source, (2) components for the control and switching of stored energy, (3) a waveshaping network, and (4) the return path. Even though this division has been made, it should be realized that there is some overlap between the different divisions due to interaction. For instance, although some components can be specifically identified with the wave shaping network, it is clear that the energy source, item to be tested and the return path will all affect the waveform produced by the simulator.

Single-stage Impulse Generators. To understand the design of commonly used simulators for high voltage and high current testing, we will first look at a single-stage generator, then we will examine a multi-stage Marx generator. The circuit of a simple single-stage impulse generator is presented in Figure IV-6. As can be seen, a generator for voltage tests will be represented by lumped parameters for its distributed resistance and capacitance. Operation of both of these circuits is relatively simple and with a small amount of analysis, we will show that these configurations yield the double-exponential waveform presented in Figure IV-4. The following analysis is for the case of high voltage tests. For high current tests, the load is generally represented by an inductance, varying from 4 microhenries to 20 microhenries, instead of a capacitor. The same type of analysis can be used, but



(a)



(b)

Figure IV-6. Simplified Single-Stage Impulse Generators.

instead of an RC circuit, an RLC circuit must be analyzed.

Capacitor C_1 is the main storage medium of the energy used to break down spark gap G. The spark gap acts as a voltage-limiting, voltage-sensitive switch whose time to voltage breakdown is very short in comparison to the "front" time, or rise time of the waveform. Resistors R_1 and R_2 are used to control the shape of the output waveform. C_2 represents the capacitance of the entire load. That is, the capacitance of the device to be tested, plus the capacitance of any measurement devices, any capacitance used to control output variations if the test object is changed, etc. It should be noted that the maximum stored energy of the storage capacitor C_1 is given by

$$W = 1/2 C_1 (V_c)^2 \quad (1)$$

As capacitor C_1 is always much larger than C_2 , this value determines the main cost of the generator.

Conceptually, the operation of the generator is simple. Capacitor C_1 is charged from a high voltage DC source, V_c , until the spark gap G breaks down. After the gap breakdown occurs, the voltage V_c is applied to the series combination of R_1 and C_2 . The smaller the time constant ($R_1 C_2$), the faster the voltage $v(t)$ will approach its peak value. Thus, we may suspect that the parameter β is dependent upon ($R_1 C_2$). At the same time that the

combination of R_1 and C_2 is charging up, the combination of C_1 and C_2 is discharging through R_2 , but at a slower rate. Thus, the exponential decay of the tail of the impulse wave, controlled by the parameter α , is determined by the time constant ($C_1 R_2$) or $C_1(R_1 + R_2)$, depending on whether the circuit in Figure IV-6 (a) or (b) is used, respectively. In practice, the circuit of Figure IV-6 (a) is preferred to (b). This is because in circuit (b), the resistors R_1 and R_2 form a voltage divider which lowers the efficiency of the circuit. We will define the voltage efficiency, η , of the circuit as

$$\eta = V_p / V_c \quad (2)$$

where V_p is the peak value of the output voltage and V_c is the maximum charging voltage applied to capacitor C_1 before gap breakdown.

To carry out an analysis of the generator, and determine what the generator output is, we will use Laplace transform techniques. For our first order analysis, we have assumed that there is no inductance in the circuit. This is generally a good approximation, as inductance in the actual circuit is minimized to prevent a delay in the front of the waveform. As we are mainly interested in the output waveform of the generator, we will also neglect the load impedance of the test object in this analysis, although it should be factored in when analyzing the entire circuit, as it will affect the final

result.

Resistors R_1 , R_2 , and capacitance C_2 comprise the main components of the wave-shaping network of the generator, in conjunction with the charging capacitor C_1 . For our analysis, let us use transformed circuit IV-7. To simulate the boundary conditions, we will use the fact that for $t \leq 0$, C_1 has a voltage of V_c across it, and for $t > 0$, C_1 is connected to the rest of the waveshaping network. The transformed output voltage, $V_o(s)$, is given by

$$V_o(s) = \frac{V_c}{s} \frac{Z_2}{Z_1 + Z_2} \quad (3)$$

where

$$Z_1 = R_1 + 1/sC_1 \quad (4)$$

$$Z_2 = \frac{(R_2)(1/sC_2)}{R_2 + 1/sC_2} \quad (5)$$

Substituting the expressions for Z_1 and Z_2 into (3) and simplifying the expression for $V_o(s)$ yields Equation (6):

$$\begin{aligned} V_o(s) &= \frac{V_c}{s} \frac{[R_2 / (sR_2C_2 + 1)]}{R_1 + [1 / (sC_1)] + [R_2 / (sR_2C_2 + 1)]} \\ &= \frac{V_c}{R_1C_2} \left\{ \frac{1}{s^2 + \left[\frac{R_1C_1 + R_2C_2 + R_2C_1}{R_1R_2C_1C_2} \right] s + (R_1R_2C_1C_2)} \right\} \quad (6) \end{aligned}$$

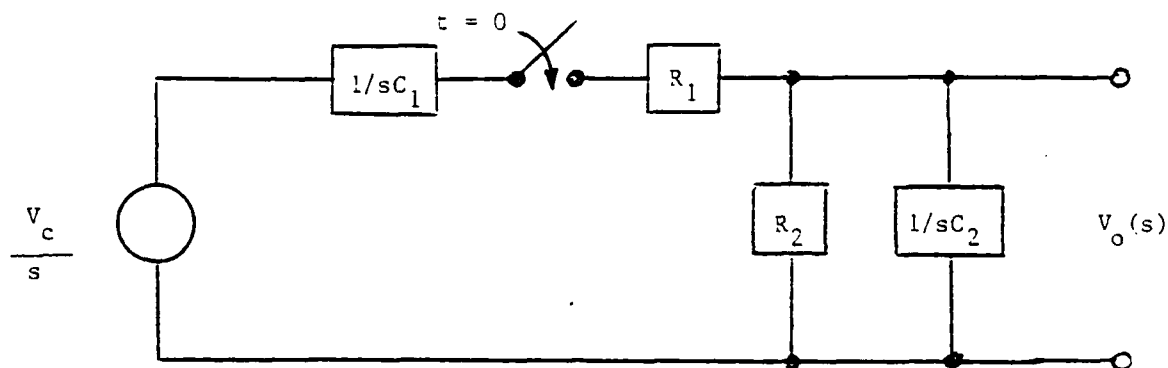


Figure IV-7. Transformed Generator Circuit for Laplace Analysis.

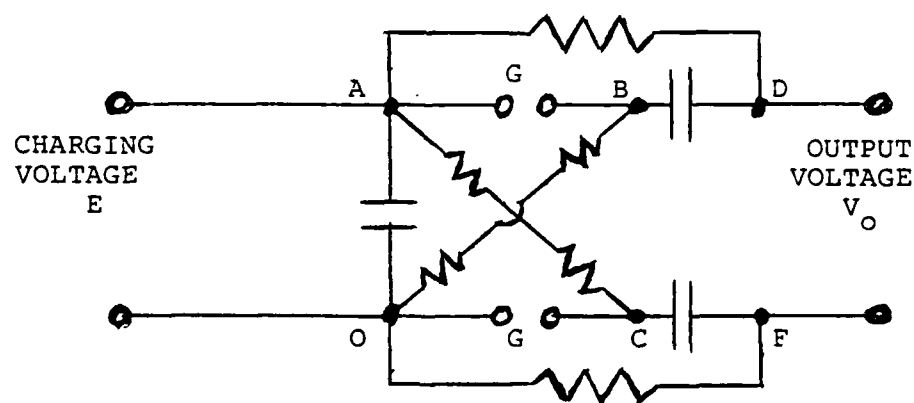
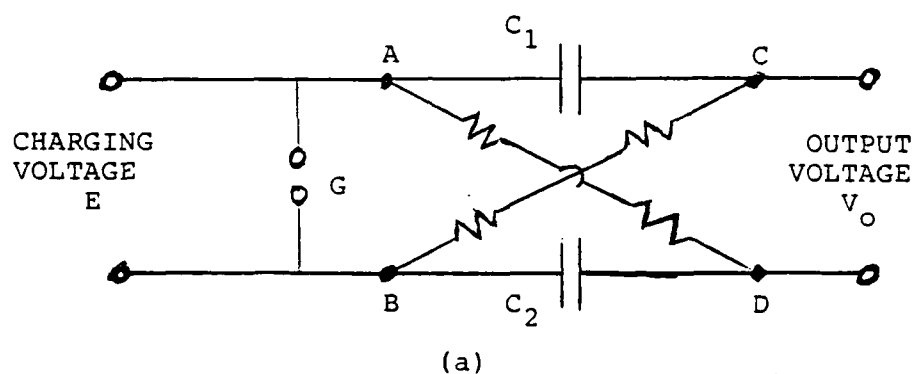


Figure IV-8. Marx's Original Voltage Multiplication Circuits.
 (a) Voltage Doubler. (b) Voltage Tripler.
 [Edwards et al., 1951].

We can re-write (6) in the form

$$= \frac{V_c}{R_1 C_2} \left\{ \frac{1}{s^2 + as + b} \right\} \quad (7)$$

where

$$a = \frac{R_1 C_1 + R_2 C_2 + R_2 C_1}{R_1 R_2 C_1 C_2}$$

$$b = \frac{1}{R_1 R_2 C_1 C_2}$$

Solving the quadratic expression in (7) for its roots yields:

$$s = \frac{a}{2} \mp \sqrt{\left(\frac{a}{2}\right)^2 - b} \quad (8)$$

If we re-write the roots of (8) in terms of our original quantities, we have:

$$\begin{aligned} \beta &= \frac{1}{2} \left\| \frac{R_1 C_1 + R_2 C_2 + R_2 C_1}{R_1 R_2 C_1 C_2} \right. \\ &+ \left\{ \left[\frac{R_1 C_1 + R_2 C_2 + R_2 C_1}{R_1 R_2 C_1 C_2} \right]^2 - \frac{4}{(R_1 R_2 C_1 C_2)} \right\}^{1/2} \left\| \quad (9) \end{aligned}$$

$$\alpha = \frac{1}{2} \left\| \frac{R_1 C_1 + R_2 C_2 + R_2 C_1}{R_1 R_2 C_1 C_2} \right.$$

$$\left. - \left\{ \left[\frac{R_1 C_1 + R_2 C_2 + R_2 C_1}{R_1 R_2 C_1 C_2} \right]^2 - \frac{4}{(R_1 R_2 C_1 C_2)} \right\}^{1/2} \right\| \quad (10)$$

since we have chosen the root $\beta > \alpha$, our output voltage is positive and (7) becomes:

$$V_O(s) = \frac{V_C}{R_1 C_2} \left[\frac{1}{\beta - \alpha} \right] \left[\frac{1}{s + \alpha} - \frac{1}{s + \beta} \right] \quad (11)$$

Taking the inverse Laplace transform of (11) yields:

$$V_O(t) = \frac{V_C}{R_1 C_2} \left[\frac{1}{\beta - \alpha} \right] \left[\exp(-\alpha t) - \exp(-\beta t) \right] \quad (12)$$

If we perform the same type of analysis with the circuit in Figure IV-6(a), we will obtain a result which has the same form as (7) except the constant a has the value

$$a = \frac{R_1 C_2 + R_2 C_2 + R_2 C_1}{R_1 R_2 C_1 C_2}$$

where the first term in the numerator becomes $R_1 C_2$ instead of $R_1 C_1$. Thus, the output voltage of the generator of Figure IV-6(a) has the same form as Equation (12) with the parameters α and β having the values

$$\beta = \frac{1}{2} \left\| \frac{R_1 C_2 + R_2 C_2 + R_2 C_1}{R_1 R_2 C_1 C_2} + \left\{ \left[\frac{R_1 C_2 + R_2 C_2 + R_2 C_1}{R_1 R_2 C_1 C_2} \right]^2 - \frac{4}{(R_1 R_2 C_1 C_2)} \right\}^{1/2} \right\| \quad (13)$$

$$\alpha = \frac{1}{2} \left\| \frac{R_1 C_2 + R_2 C_2 + R_2 C_1}{R_1 R_2 C_1 C_2} - \left\{ \left[\frac{R_1 C_2 + R_2 C_2 + R_2 C_1}{R_1 R_2 C_1 C_2} \right]^2 - \frac{4}{(R_1 R_2 C_1 C_2)} \right\}^{1/2} \right\| \quad (14)$$

In either case, the generator output is a wave that has the form of a constant times the difference of two exponentials. As resistor R_2 is always much larger than R_1 , and capacitor C_1 is much larger than C_2 , we can find approximate expressions for β and α and show that

$$\beta \approx 1/(R_1 C_2)$$

that is, the rise time of the wave is dependent upon R_1 , and

$$\alpha \approx 1/(R_2 C_1)$$

or the decay (tail) time is dependent upon R_2 .

A similar result is obtained for a high current generator in which the load is often characterized as an inductance with values between 4 microhenries and 20 microhenries. This load inductance is dependent upon the

size and length of the aircraft and the type of return path. For an inductive load, the equivalent RLC circuit causes the parameters β and α to become $\beta = R/L$ and $\alpha = 1/RC$.

A single-stage generator is limited to an output of approximately one megavolt due to practical reasons. First, the peak output voltage of the generator is limited by the maximum charging voltage, V_c , of the DC supply. Typically, this is limited to a value of 200-250 kV. Spherical electrodes are employed as they provide a field distribution which is approximately uniform. The sphere size is normally chosen so the spacing to withstand the maximum charging voltage does not exceed its diameter. However, as the voltage on the charging capacitor increases, a larger sphere gap diameter is required to prevent an excessively inhomogeneous field distribution between the gap spheres. Although flat electrodes could also provide the uniform field, corona problems become significant at the corners and edges. In addition, there is difficulty in suppressing corona discharges from the structure and leads during the charging period. Finally, a single charging-capacitor circuit requires an extra-high voltage capacitor, which tends to be heavy, large and expensive. To avoid these problems, impulses of high amplitude are generated through the use of a generator consisting of several single-stage units cascaded to form

a multi-stage generator.

Multi-stage Marx generators. Marx's original patent [1923] is the first known published description of the method of achieving high voltage impulses by charging capacitors in parallel, through resistors of a high ohmic value, and then discharging the capacitors in series through a spark gap arrangement. Figure IV-8 is a schematic representation of Marx's original voltage-doubling and voltage-tripling circuits. Both of these circuits suffer from the problem that the full charging voltage is applied across the load points. In the case of the voltage-doubler of Figure IV-8(a), the voltage E is applied across points C and D. When the spark-gap breaks down, an impulse of magnitude E is superimposed across the load so that the output voltage suddenly rises from E to $2E$ and then decays back to E . A similar situation occurs in the circuit of Figure IV-8(b).

Figure IV-9 shows a modern multi-stage Marx generator system. This arrangement corrects the problems inherent in Marx's original patent and eliminates the need for any part of the generator circuit to carry more than a fraction of the full generator voltage. This generator can be separated into a charging representation (Figure IV-10(a)) and a discharge representation (Figure IV-10(b)). Operation of this generator is straight forward.

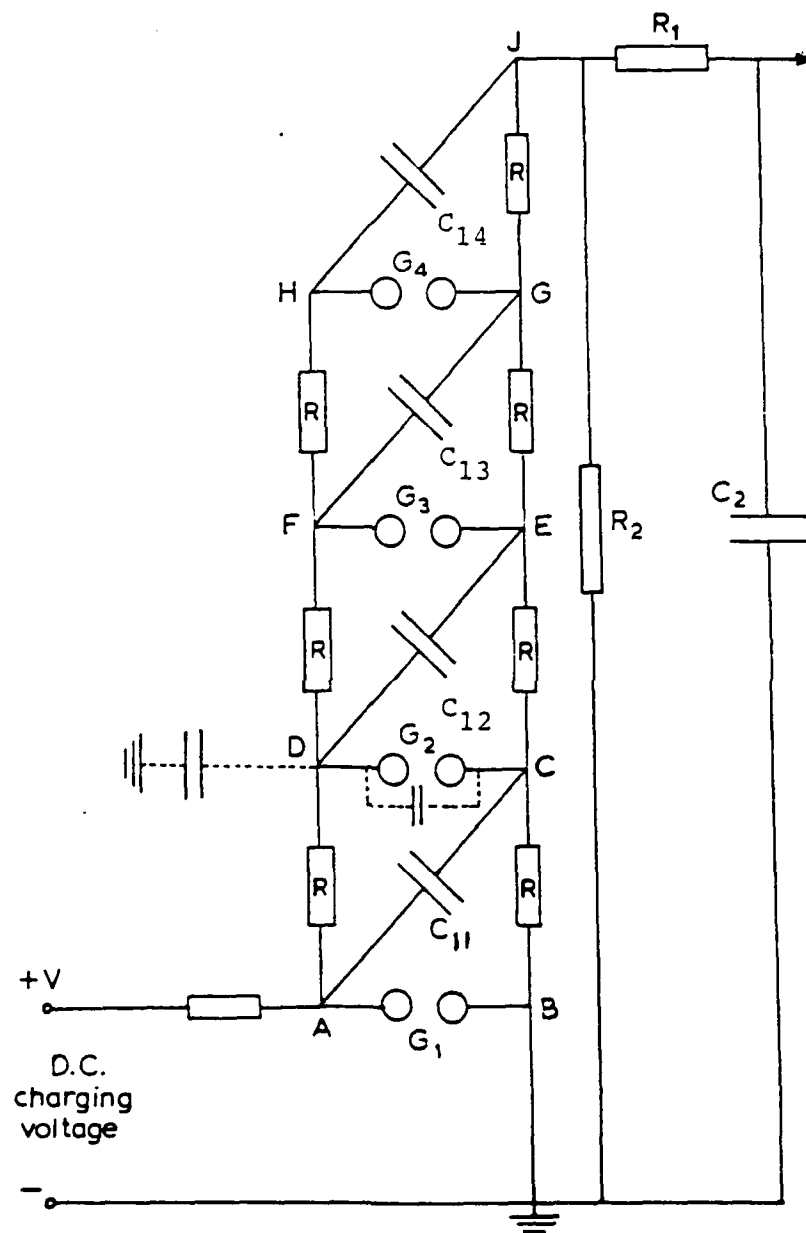


Figure IV-9. Basic Circuit of a Four-Stage Impulse Generator.
[After Gallagher and Pearmain, 1983].

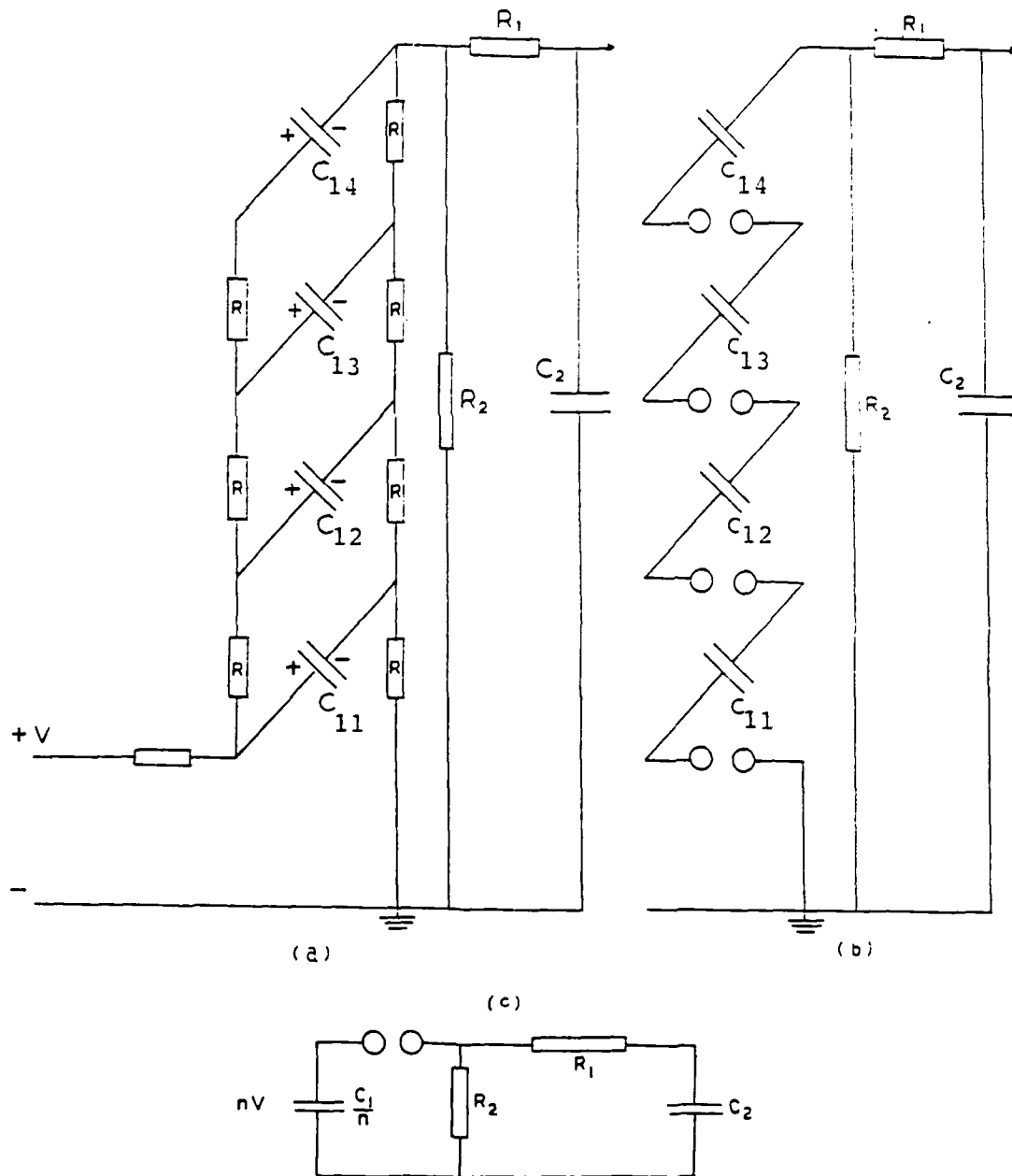


Figure IV-10. Circuits of a Four-Stage Impulse Generator.
 (a) Charging Phase. (b) Discharging Phase.
 (c) Equivalent Circuit While Discharging.
 [After Gallagher and Pearmain, 1983].

A high voltage DC source is used to charge the source capacitors C_{11} to C_{14} through the charging resistors R . These typically have a value ranging from 10 k Ω to 100 k Ω . The resistors controlling the rise time and decay time are R_1 and R_2 , respectively, while the load capacitance is represented by the capacitor C_2 .

When the capacitors C_{11} to C_{14} are charged to the charging voltage V_c , the charging current no longer flows and the generator reaches the situation depicted in Figure IV-10(a). Generator discharge begins when spark gap G_1 breaks down. Immediately the spark gaps separating capacitors C_{11} through C_{14} are overvoltaged by the combined voltages of the capacitors already linked in series and they begin to successively flash over through the remaining spark gaps. Because the charging resistors have such a large value, they are considered to be open circuits during the discharge process, and the discharging generator can be represented by Figure IV-10(b). Ideally, the full voltage of each of the capacitors is summed up and applied to the load through the waveshaping resistors R_1 and R_2 .

When spark gap G_1 (Figure IV-9) breaks down, the sequence of events in the discharge process proceeds as follows:

- (a) The potential of point A changes from the charging voltage V_c to zero, or goes through a change of $-V_c$.
- (b) Because of the charge on C_{11} , the potential at point C must "instantly" change from zero to $-V_c$, causing a potential difference of $2V_c$ to appear across spark gap G_2 .
- (c) Because of the potential difference across spark gap G_2 , it breaks down, causing the potential difference at point D and the left-hand plate of C_{12} to change by $-2V_c$.
- (d) This causes point E to change from zero to $-2V_c$, placing a voltage of $3V_c$ across spark gap G_3 , causing it to break down also.

This sequence continues until point J is at a potential of $-4V_c$ with respect to the ground. After all the stages have broken down, the generator can be represented by the equivalent circuit shown in Figure IV-10(c). At this point the Marx bank is commonly referred to as being "erected". Although the preceding analysis does not put any limits on the operation of the generator, certain practical considerations do come into play.

The peak output voltage of an n-stage Marx generator has a theoretical value of the maximum charging voltage V_c times the number of stages, n. Practically, the maximum output voltage will be somewhat lower due to the resistance and inductance of the generator, return path, test circuits and load.

It has been shown by Edwards, Husbands and Perry [1951] that the gap capacitance and stray capacitance (shown in dotted lines in Figure IV-9) can prevent the spark gaps from firing due to an alteration of the field distribution across the gap. For consistent operation, the first spark gap is usually set to break down at a voltage slightly below the second gap. Also, the load capacitance normally is much greater than the stray capacitances, assisting the transient phenomena necessary for the proper breakdown of all gaps.

A detailed discussion of the history and design of high-voltage impulse generators is given by Edwards et al., [1951]. Additional information on the design of multi-stage Marx generators is given in Gallagher and Pearmain [1983] and Kuffel and Zaengl [1984]. Greenwood [1971] discusses the design of generators for impulse testing of components commonly used in the electric power industry, while Clifford, Crouch and Schulte [1982] review information on impulse generators for aircraft testing.

Although we have only taken a cursory look at the the generator and waveshaping portions of a simulator, this is sufficient to understand the part they play in the simulation process. Another major part of a simulator is the return path to be used with the generator and wave shaping network. Because the return path can strongly

affect the validity of the simulation, it will be examined separately in the next section.

Return Paths. If an airplane in flight (free space) is struck by lightning, the vehicle becomes part of the lightning channel that conducts the current to the ground. The electrical circuit that is formed by the cloud (source), channel (conductor) and earth (ground) can be extremely large and the return paths for the lightning current are often ill-defined. Typically, the lightning current return path for the portion of the channel containing the aircraft is far enough removed from the vehicle (often measured in kilometers) that it has no effect on the vehicle.

However, when the lightning-aircraft interaction event is simulated on the ground, major differences exist. First, the vehicle is no longer in free space. The aircraft is on the ground, typically inside of a building, and the electromagnetic environment varies greatly from that in the atmosphere. The surrounding environment consists of media (structural steel, concrete, moist soil, etc.) which have a relatively high conductivity compared to the atmosphere. Second, the test currents generated in the simulator will be returned to the generator by conductors of aluminum or copper. Because of practical limitations in the circuit, these return conductors must

be relatively close to the aircraft.

The return path not only enables a complete circuit to be made, but is usually constructed in such a fashion as to generate as uniform an electromagnetic field around the object under test as is physically and economically possible. While this has the advantage of creating a system that is more easily analyzed, it also has the potential of giving invalid results if improperly done. Since an aircraft in flight is in free space, a considerable distance from any return path or ground plane, the ideal simulator will attempt to reproduce this situation. The success with which this simulation of free space is achieved will weigh heavily upon the validity of the simulation. Because the type and form of the return path will influence the success of the simulation, its design should be carefully considered.

EMP simulators have been constructed and used for many years and the types of configurations employed for this purpose have been adapted to lightning simulation. Several different EMP simulator configurations are illustrated in an overview article by Baum [1978], showing different styles of return paths. Many different configurations of conductive structures have been used for return paths. For our purposes, the different types of return paths used for lightning simulators can be broken

down into ground plane (or flat plate) return paths and coaxial return paths.

Ground plane return paths, as the name indicates, consist of a large conductive structure which acts as a ground plane beneath the object under test. A typical example of this is illustrated in Figure IV-11, where a ground plane constructed of wire mesh is in place under a CV-580 aircraft. A less common configuration, resembles that of a parallel plate EMP simulator (Figure IV-12). Because of the uniformity of the field within the structure, this type of simulator finds its greatest use in the calibration of sensors for the measurement of lightning level voltages and currents.

Coaxial return paths are arranged in such a fashion that the object under test becomes the center of a coaxial configuration, with the return path taking the place of the shield or outer conductor. The actual implementation of the coaxial arrangement can take many forms. A true coaxial arrangement is shown in Figure IV-13, where a coaxial return path made of wire mesh is in place around a cylindrical test object. Another coaxial type of configuration is employed to encircle the fuselage of a CV-580 aircraft (Figure IV-14). Still another approach is to approximate the field distribution due to a coaxial arrangement, as the flat plate configuration shown in

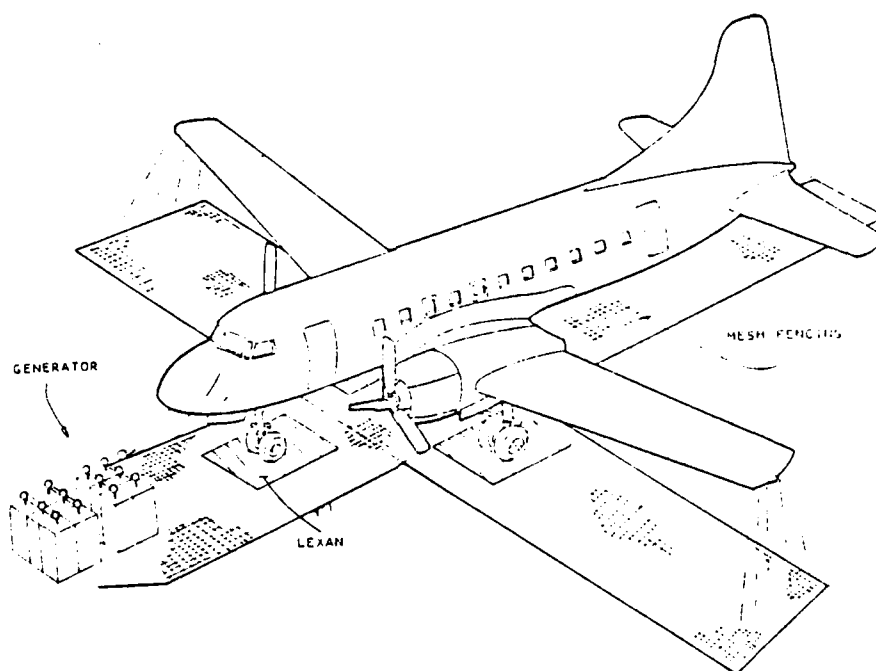


Figure IV-11. Illustration of the Four Microfarad, 200 Kilovolt Generator with Flat Ground Plane Return Path. [Hebert et al., 1986].

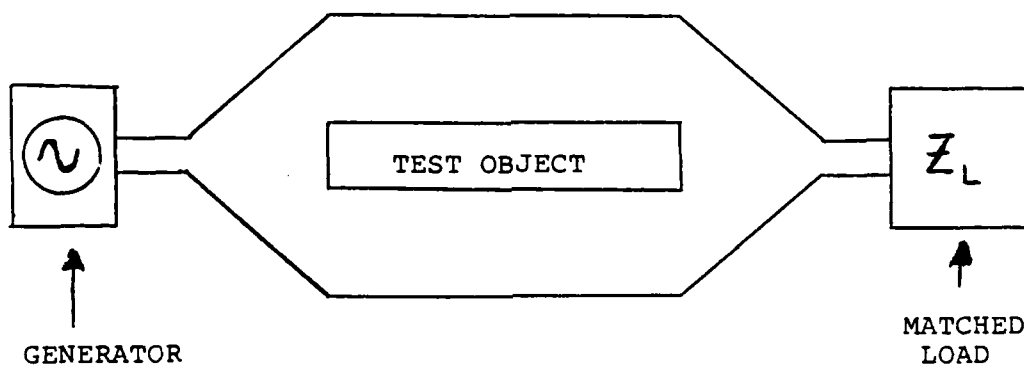


Figure IV-12. Side View of a Flat Plate EMP Simulator.

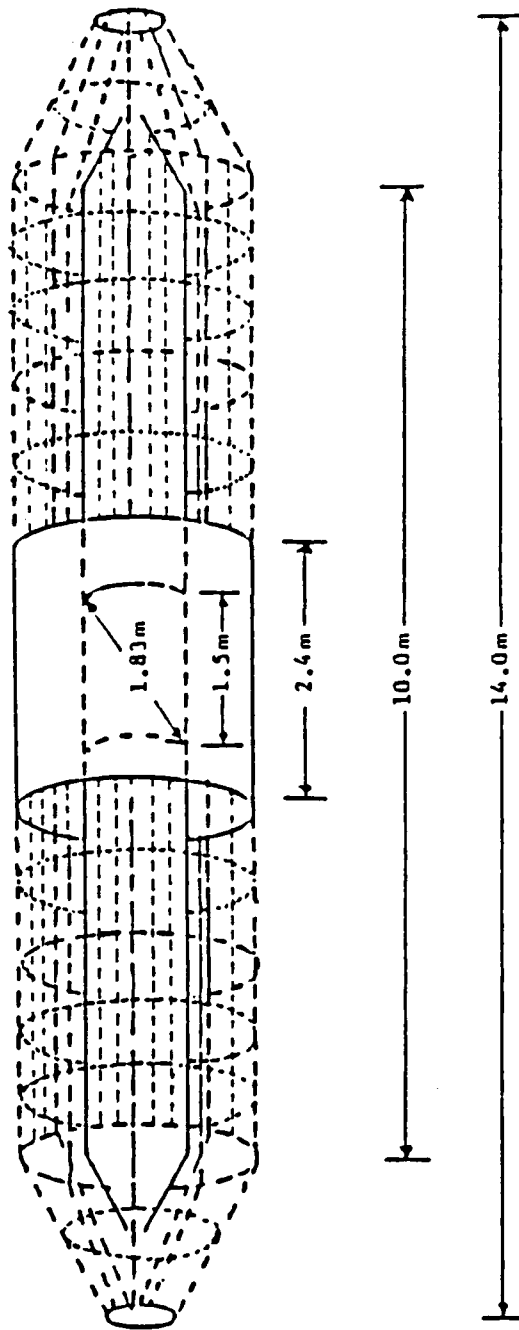


Figure IV-13. Coaxial Return Path Around the AFIT Lightning Test Object.



Figure IV-14. Coaxial Retrun Path Around a CV-580 Aircraft.
[Hebert et al., 1986].

Figure IV-15 attempts to do. Although this is not a true coaxial configuration, if carefully done the field distribution has many of the same attributes.

A quasi-coaxial or conformal approach can be considered one in which the return path attempts to take a coaxial form, while closely following the contours of the object under test. Not only does Figure IV-15 fall into this category, other examples of this approach are shown in Figure IV-16, where a UH-60A helicopter is the test object, and Figure IV-17, where the test object is an F-14 fighter aircraft.

When determining the type of return path to use, two major factors must be considered. In addition, many variations are possible when designing a specific type of return path. The first factor that should be considered is the purpose of the return path. As stated by Little, Hanson and Burrows [1979], the return path should be constructed in such a fashion that "... the current flow patterns for both fast-changing and slow pulses is the same as it would be in a natural in-flight strike." As an example of what results when this concept is not followed, Figure IV-18 illustrates the change in the field distribution around an aircraft when a ground plane return path is brought near the fuselage. The field distribution caused by the incorrectly placed return path is very

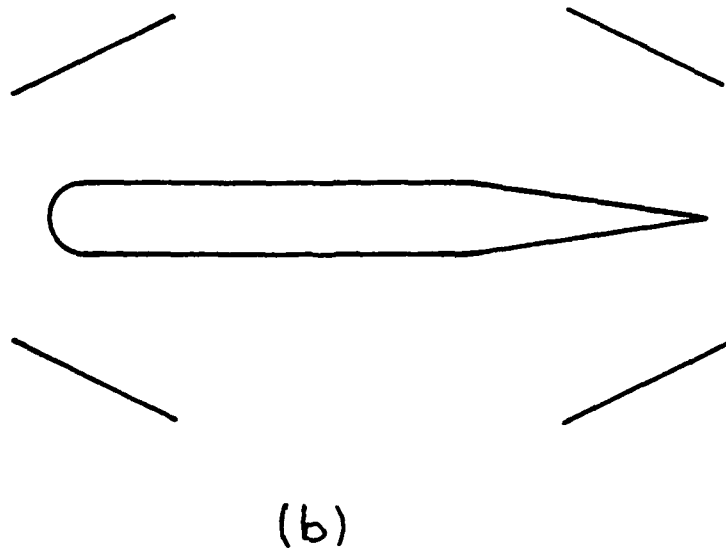
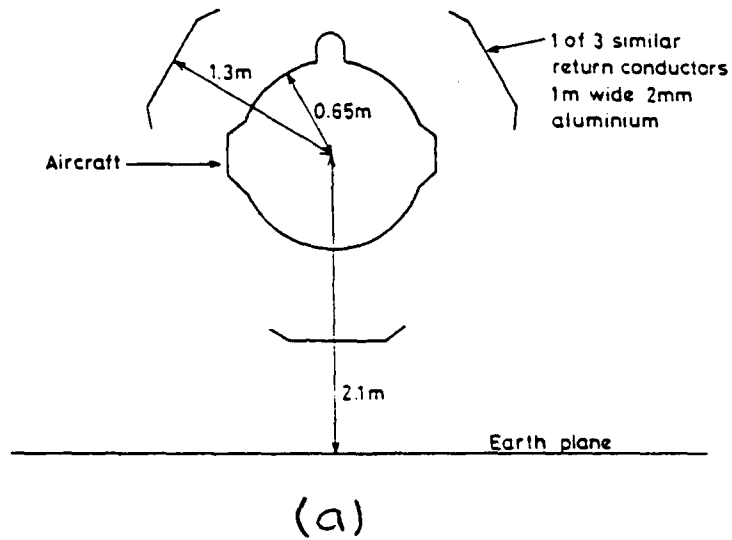


Figure IV-15. Quasi-Coaxial Return Path Systems. (a) Three Conductor System Around Fuselage. (b) Four Conductor for Wing Test. [Little et al., 1979].

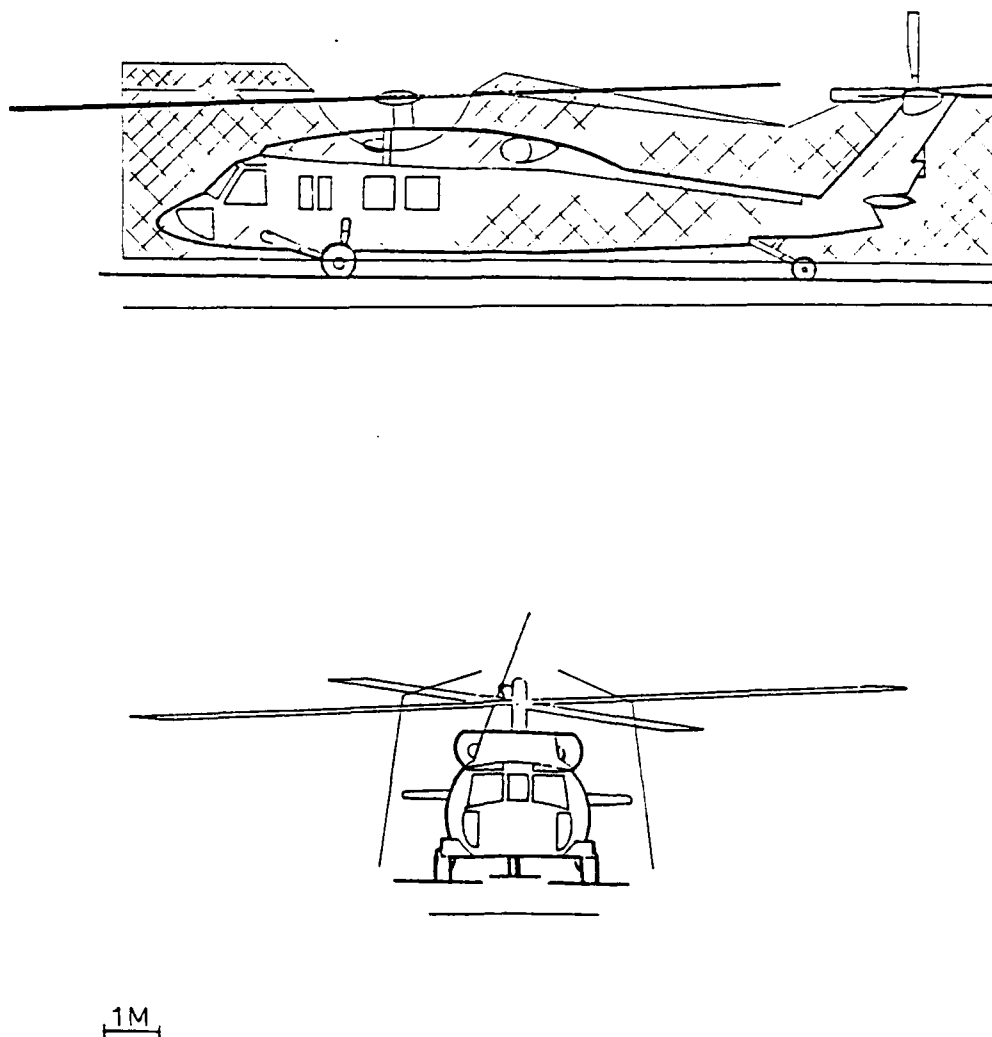


Figure IV-16. Coaxial/Conformal Return Path Around a UH-60A Helicopter. (a) Side View. (b) Front View. [Hebert, 1985].

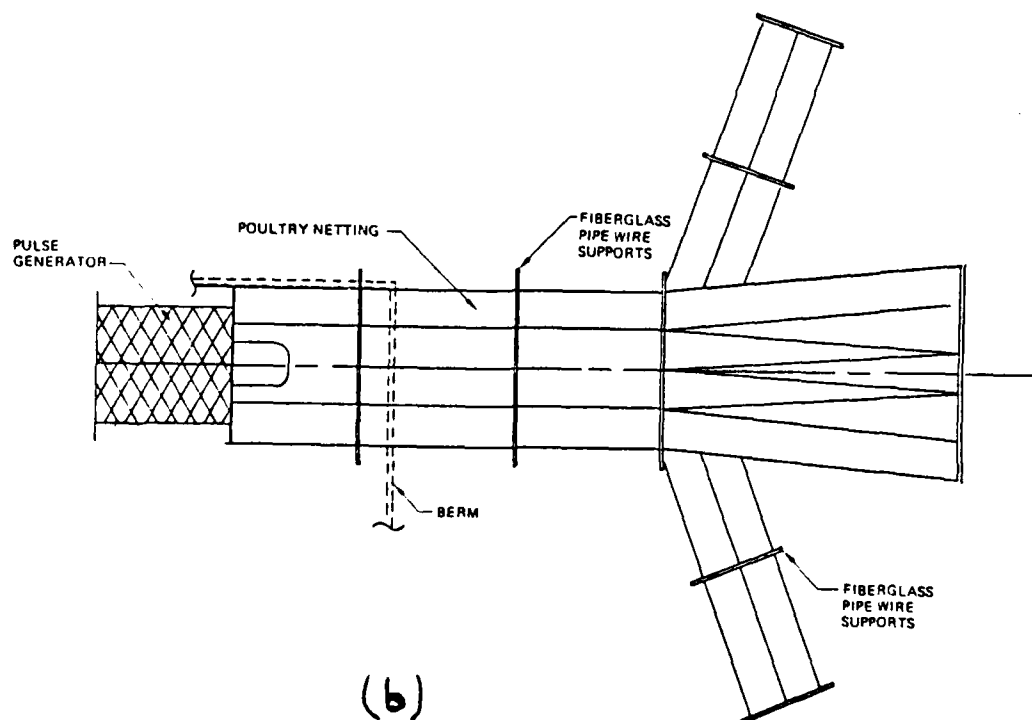
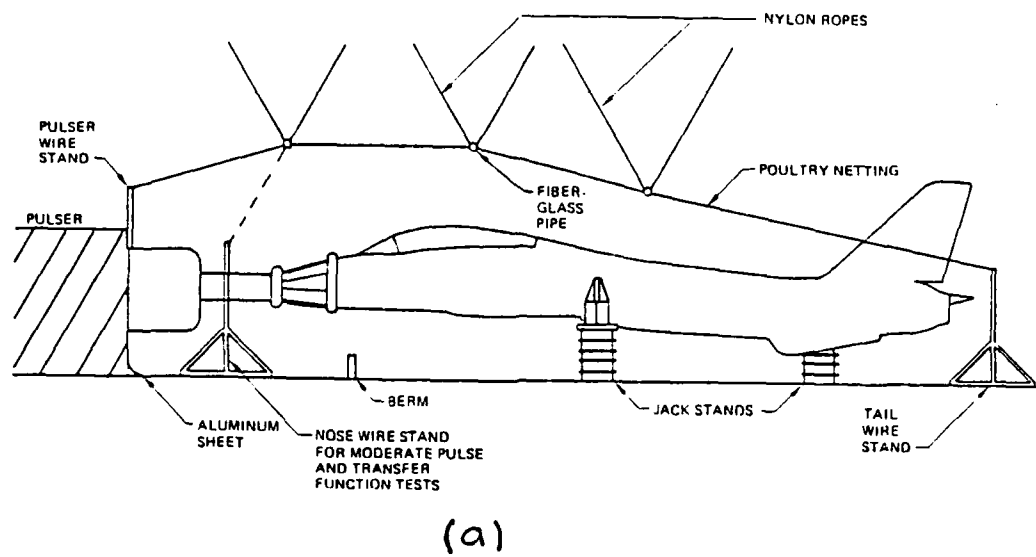


Figure IV-17. F-14A Return Path Arrangements. (a) Side View. (b) Top View. [Walén and Simpson, 1987].

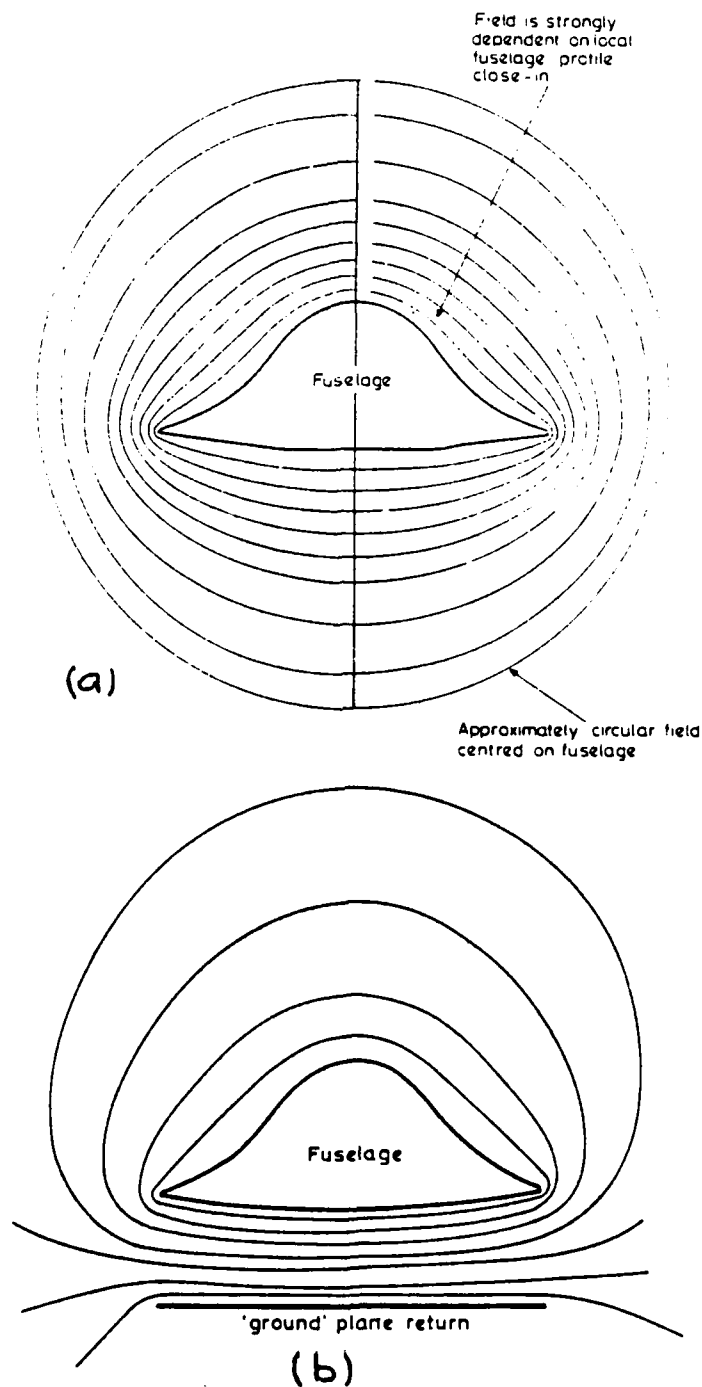


Figure IV-18. Effect of Return Path on Field Distribution Around Test Vehicle. (a) Free Space Field Distribution. (b) Distortion of Field Distribution Due to Close Spaced, Single Return Path. [Little et al., 1979].

evident and will generate excessively high aperture and diffusion flux voltages on the lower panels of the vehicle, while the voltages on the top panels will be lower than expected.

A second factor to consider is that the return path conducts current back to the generator. From this perspective, the return path also affects the waveshaping network because of the load that it presents in association with the test object. According to Little et al., [1979], a low inductance (approximately 1 microhenry) return path will simplify and reduce the cost of a full threat test.

The effect of the return path on the generator and wave shaping network is an important consideration, because many different materials in various forms have been employed for the construction of return paths. These materials have typically been aluminum, copper or steel, and have normally taken the form of thin wires, wire mesh of varying degrees of coarseness and sheets of varying widths. A choice of a possible material type and form represents a tradeoff between inductance and capacitance values affecting the total system response and the physical factors of weight, strength and ease of construction of the return path.

When the first measurements of lightning induced voltages were made with simulated lightning currents [Lloyd, Plumer and Walko, 1971], the experimenters used a single conductor, aluminum foil return path laid on the floor beneath the right-hand wing of the F-89J aircraft, the subject of the experiments. In later tests on an entire F-89J aircraft two return paths were used [Walko, 1974], and on an F-8 aircraft, multiple aluminum foil conductors were used under and around the vehicle [Plumer, Fisher and Walko, 1975]. It was felt that these arrangements would better approximate the current distributions on the fuselage due to in-flight conditions, but no tests were conducted to verify this assumption. Also, the distributed nature of the transmission system formed by the aircraft and the return path was not taken into consideration.

More recently, investigators such as Little et al., [1979], and Crouch and Plumer [1980] have begun to consider the distributed nature of the transmission system formed by the test object and the return path system. In an attempt to generate a field distribution around the test object that reproduces the one which would be found in the free space configuration, they have gone to a coaxial return path configuration. While these improvements in return conductor positioning have improved the current distribution, and thus, the magnetic field

distributions around the test objects, they have also affected the electric field around the vehicle due to increased distributed capacitance of the aircraft [Crouch and Plumer, 1980].

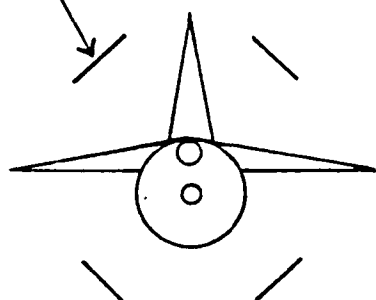
If a true coaxial arrangement could be constructed using the test object and the return path, then the application of the test current would create a traveling wave within the simulator, between the test object and the return path. If the simulator is properly terminated in the characteristic impedance of the coaxial system, there will be no reflections back toward the generator. Also, a solid, conducting return path would minimize possibility of interaction between the test set up and surrounding objects. Therefore, a properly terminated, solid conductor, coaxial return path would be the optimal measurement configuration, in terms of eliminating spurious reflections within the simulator and interactions between the simulator and surrounding objects.

Unfortunately, it is usually not possible to build an actual, coaxial system, due to the complexity of the test object. Often an approximation to a coaxial return path is all that can be achieved, within the bounds of experimental time and money. In addition, the return path is often constructed of wire mesh to minimize the weight of the return path and to increase the flexibility of the

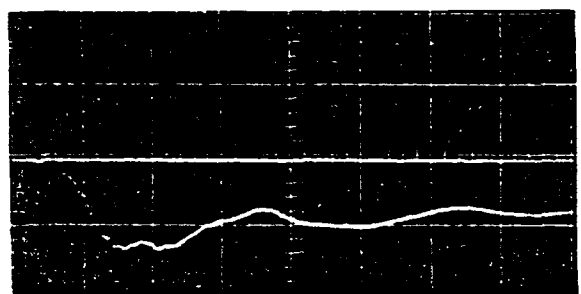
experimental set up. Thus, it is extremely difficult to avoid the introduction of errors into the measurement. In a series of experiments on an F-8 aircraft, Crouch and Plumer [1980] investigated several of these issues. They were able to verify the interaction between the return conductors and the electrical system of the building within which the tests were conducted. In employing a quasi-coaxial return conductor arrangement, they also were able to show the effects of unbalanced conductors. Figure IV-19 shows the result of eliminating the upper two conductors while keeping the bottom two. A discernible difference results in the measured induced voltages.

The connecting wires from the generator to the return path, the return path to the load, the generator to the test object and the test object to the terminating load can also have a dramatic effect on the propagation of the fields on and around the aircraft. These connections must be designed to avoid abrupt geometrical changes that may result in considerable mismatches in the characteristic impedance between portions of the total system. The task of designing a connecting configuration which takes the energy from a concentrated point, the output of the generator, to an often quite large coaxial transmission line is quite challenging. Normally this connection should be made using a conical arrangement so the change is gradual rather than abrupt. Even this arrangement is a

Return Conductors (4)



F-8



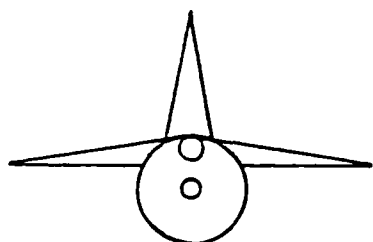
2V

712

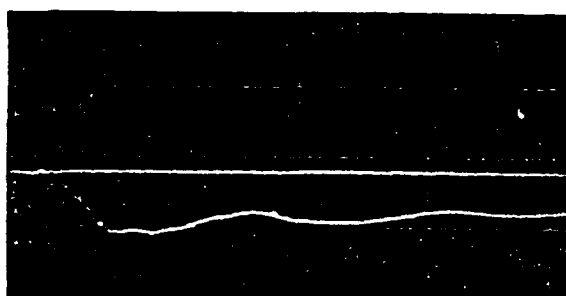
0.5 μ s

(a)

F-8



Return Conductors (2)



2V

713

0.5 μ s

(b)

Figure IV-19. Comparison of Induced Voltages Due to Various Conductor Arrangements. (a) Balanced Arrangement. (b) Unbalanced Arrangement. [Crouch and Plumer, 1980].

compromise because the added wire length used to form the cone adds distributed inductance which further limits the magnitude of the peak currents the generator can produce.

All these factors must be considered in the design of a valid return path for the total measurement configuration. In the next section, we will see how the generator, wave shaping network and return path come together into a simulator to be used for simulation testing. Also, we will briefly discuss some of the techniques used to simulate the effects of the lightning threat. In our discussion, we will concentrate on indirect effects simulation because the results of indirect effects testing are more sensitive to configuration effects.

Simulation Test Techniques

As previously stated, the purpose of the simulation must be decided before a simulation test technique can be selected. Although there are many reasons to employ the various simulation techniques available, we will focus our discussion on the qualification of aircraft in terms of hardening for lightning protection. When discussing lightning protection we must cover the two major categories of effects - direct effects and indirect effects. Different simulation techniques may be used for each of these categories. To be complete, techniques for

direct effects testing will be briefly discussed, then the remainder of the section will focus on indirect effects testing.

It should be pointed out that there are standards to be followed when certifying that an aircraft meets the needed levels of lightning protection. Among the many standards and specifications that are used, the following standards are used heavily by the Department of Defense:

MIL-STD-461B: Electromagnetic Emission and Susceptibility Requirements for the Control of Electromagnetic Interference,
1 April 1980.

MIL-STD-462: Measurement of Electromagnetic Interference Characteristics, 31 July 1967.

MIL-STD-1757A: Lightning Qualification Test Technique for Aerospace Vehicles and Hardware,
20 July 1983.

DOD-STD-1795 (USAF): Lightning Protection of Aerospace Vehicles and Hardware,
30 May 1986.

MIL-B-5087B(ASG): Military Specification for Bonding, Electrical and Lightning Protection for Aerospace Systems,
30 July 1954.

FAA-AC-20-53A: Protection of Airplane Fuel Systems Against Fuel Vapor Ignition Due to Lightning, October 1984.

SAE-AE4L-87-3: Recommended Draft Advisory Circular - Protection of Aircraft Electrical / Electronic Systems Against the Indirect Effects of Lightning,
4 February 1987.

Each of these standards and specifications has sections which address issues relevant to the testing of aerospace vehicles for the direct and indirect effects of lightning, and should be consulted when an actual test plan is to be produced. The impact of these standards will be briefly examined when the lightning simulation test techniques are covered in the next few sections.

Simulation Test Techniques for Direct Effects Testing

Because most of the direct effects due to a lightning strike to an aircraft can cause significant physical damage to the vehicle, few organizations are willing to subject a flyable aircraft to direct effects testing. The risk of damage or loss is too great at full threat levels. A complicating factor is that the damage done during a reduced level test does not scale linearly. Therefore, direct effects testing is almost always done on components and coupons (small sections or pieces of a structural panel) at full threat level.

The most common test of direct effects concerns the protection of the fuel system against ignition or explosions due to arcing and sparking in the fuel distribution and storage system. Because of the potentially catastrophic loss that can occur due to inadvertent fuel ignition, much attention has been given to the protection and testing of the fuel system and its

components. MIL-STD-1757A and FAA advisory circular AC-20-53A contain extensive testing procedures to insure that systems are adequately protected.

Another type of direct effects test is one to determine where lightning may attach to the vehicle, the areas known as strike zones. This test will also help determine the probability of puncture for dielectric structures and any other paths the current may take in flowing on the vehicle. Although the standard specifies the use of full scale structures, a common way to do preliminary attachment studies is with scale models. In this case the generator can be scaled down in voltage and the testing requirements are more easily met.

Other tests done to verify direct effects protection include tests for damage to structures such as probes, booms, antennas, lights, landing gear, etc. and the effects of coronas and streamers which can affect fuel vent and dump outlets, radomes, antennas, canopies and other components exposed to the atmospheric electric fields. MIL-STD-1757A contains testing procedures to determine the direct effects of lightning for each of these categories. For each type of test, the standard specifies the generic apparatus to be used, the test setup, types of waveforms to be used, test procedure, and data to be collected.

Simulation Test Techniques for Indirect Effects Testing

Because of the complexity of the lightning-aircraft interaction event, it is necessary to use ground-based lightning simulation and testing to assess the effects of lightning on aircraft. As with direct effects testing, there are standards for the testing of aerospace vehicles for their susceptibility to indirect effects. These standards and procedures are contained within the same documents previously mentioned. When using any of the methods we will examine, the experimenter must insure that the appropriate procedures are followed. While there are many ways to simulate the indirect effects of lightning on an aircraft, we will concentrate on three techniques: Current Injection, Shock Excitation and Swept Frequency Continuous Wave (SFCW). These three techniques are the most widely used currently and each has advantages and disadvantages.

Current Injection Technique. The current injection technique, also known as the current pulse or lightning transient analysis (LTA) technique was originally developed by the General Electric High Voltage Laboratory [Walko, 1974]. This technique is done by injecting a current pulse -- low-level, moderate-level or full threat-level -- through the structure of the object under test. In this technique, a current generator, typically a large bank of capacitors, and wave shaping network are connected

directly to the device under test at the predetermined entry point, and the current return path is then hard-wired from the exit point back to the generator (Figure IV-20).

The test configuration can be modeled as a simple series RLC circuit, with the test object in the circuit. The inductance of the configuration is assumed to be determined by the current return path and the test object, while the resistance and capacitance of the system are determined by the wave shaping network and current generator respectively. The parameters of the configuration are chosen such that a unipolar, double exponential, impulse current waveform. The equations describing the injected current waveform are given by [Walko, 1980]:

$$i(t) = \left[\frac{V_c}{2kL} \right] \left[e^{(k-a)t} - e^{-(k-a)t} \right]$$

$$a = R/2L$$

$$k = (a^2 - 1/LC)^{1/2}$$

where

$i(t)$ = time-varying current (amperes)

V_c = Capacitor Voltage (Volts)

L = Circuit Inductance (Henries)

R = Circuit Resistance (Ohms)

C = Circuit Capacitance (Farads)

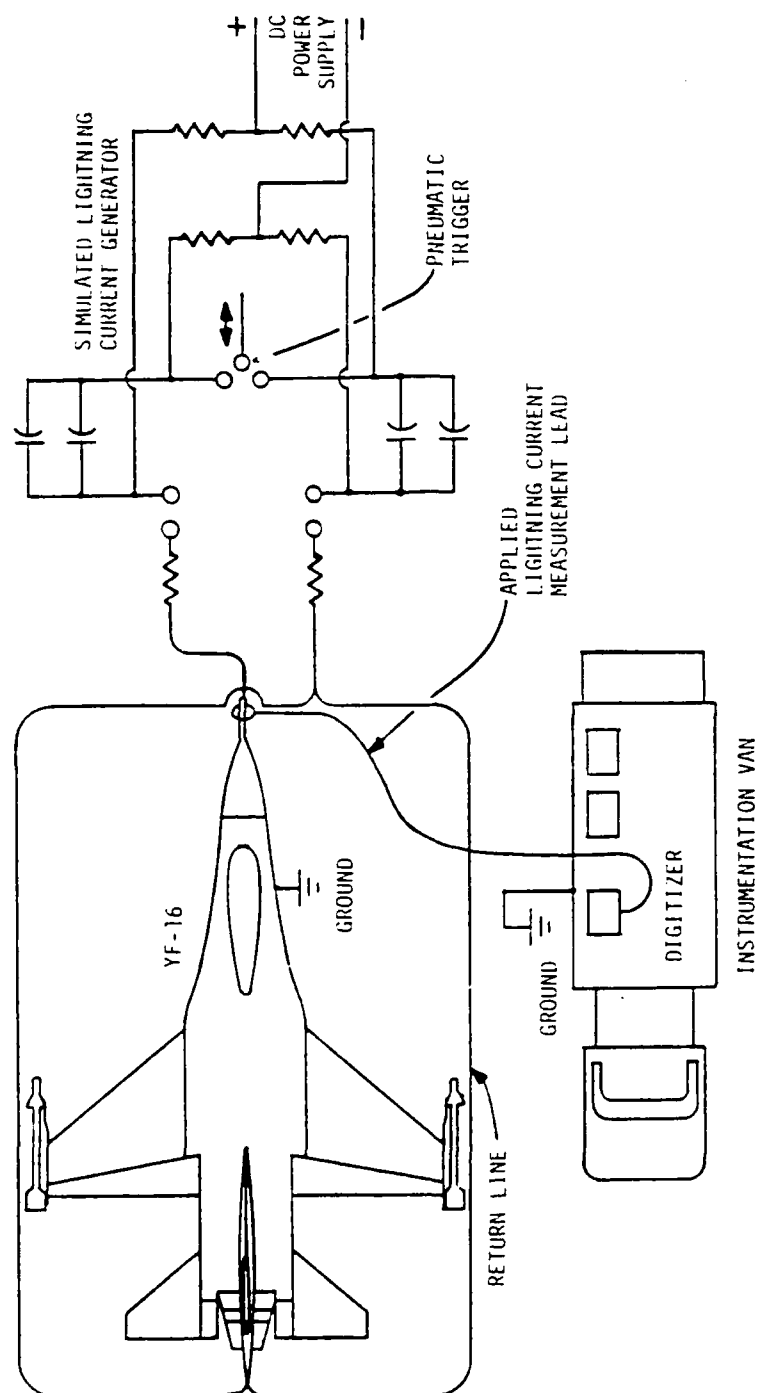


Figure IV-20. Lightning Simulation Test Configuration Used for Current Injection Technique. [Walko and Schneider, 1980].

To find the required circuit component values of the test setup, numerical techniques are used to optimize the test configuration. Using the Kirchhoff voltage equation for equivalent circuit of the test configuration, we obtain the following series RLC equation at time $t = 0^+$:

$$V_c = (1/C) \int i(t)dt + R[i(t)] + L[di(t)/dt]$$

whose time derivative is given as

$$0 = (1/C)[i(t)] + R[di(t)/dt] + L[d^2i(t)/dt^2]$$

From this time derivative equation, a discrete state-space approximation can be made. The peak current is then numerically optimized as a function of R, L and C.

Normally the current injection technique is used with a low or moderate threat-level current waveform and the resulting induced transients are linearly extrapolated to determine those expected from the full threat, typically due to a current peak of 200 kA. The resistively coupled transients are extrapolated from the peak current, while the inductively coupled transients are extrapolated from the current time rate-of-change. The current injection technique assumes that linear extrapolation of the induced transients is valid if the injected current waveform is identically scaled to the full threat level lightning waveform [Butters et al., 1981].

From analytical and experimental investigations, McCormick, Maxwell and Finch [1978] reported on the validity of the current injection test technique. Using the time and frequency domain inputs derived from lightning simulation test data, they concluded that the current injection technique is a valid method for assessing the susceptibility and vulnerability of aircraft to lightning's effects and hazards. They also concluded that the linearity of the current injection configuration is a valid and justified assumption, and that linear extrapolation to the full threat lightning level is an appropriate analysis [McCormick et al., 1978].

Shock Excitation Technique. The shock-excitation technique, developed by the McDonnell Aircraft Company differs from the current injection technique in that the test object is electrically isolated from the generator and ground by spark gaps [Robb, 1981]. By the incorporation of these input and output spark gaps, the shock-excitation test produces both charging and discharging transients. An example of the setup employed by McDonnell Aircraft Company is shown in Figure IV-21.

A high voltage Marx generator is used to provide the voltage and current excitation to the object under test, and to break down the air in the spark gaps isolating the test object from the generator and ground. The arc

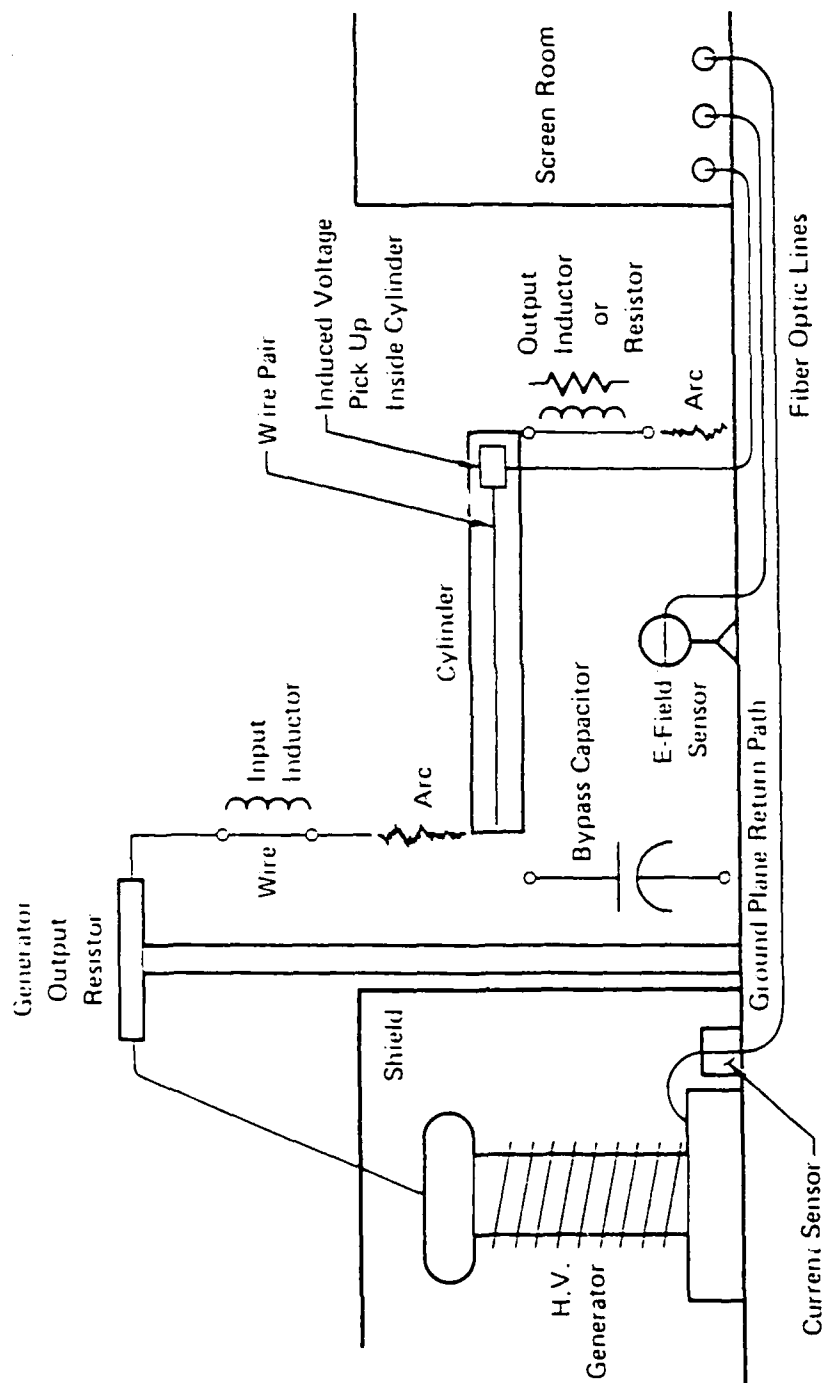


Figure IV-21. Shock-Excitation Test Setup Used at McDonnell Aircraft Company. [Butters et al., 1981].

breakdown of air between small spherical electrodes occurs at approximately 10 kilovolts per centimeter. Thus, an air gap of 1 meter will breakdown when the potential difference across it approaches one million volts. By adjusting the length of the input and output spark gaps, the voltage potential on the test object can be varied. Because of the probability that breakdown between the test object and return path will occur at high voltages, the return path used is normally a ground plane type instead of a coaxial type.

The sequence of events in this process proceeds as follows. First, the discharging Marx generator produces a rapidly changing E-field between the input electrode and the test body. After a few microseconds, an arc will be established in the spark gap which will produce a rapid charging of the test body. The second spark gap will then break down, completing the path from generator to ground, and the test body will rapidly discharge. Finally, with the completion of this circuit, a high current will flow from the generator through the body to ground.

According to Clifford and Zeisel [1979], this test simulates three separate coupling conditions related to lightning-aircraft interaction processes. These conditions are those caused by (1) nearby lightning, (2) stepped-leader attachment and (3) return stroke discharge.

These conditions are simulated by (a) fields from the rapidly changing E-field, (b) the charging of the test body and (c) the discharging of the test body, respectively.

A first order approximation to the voltages and currents on the test body during the charging process can be found by modeling the system as a series RLC circuit. Solving for the current in the circuit, we find that it is given by

$$i(t) = (V_0/\omega L) e^{-\alpha t} \sin(\omega t)$$

while the voltage on the test body is given by

$$v(t) = (1/C_t) \int_0^t i(t) dt$$

where

V_0 = Generator voltage

C_t = Capacitance of test body

R = Series resistance

L = Total inductance

α = $R/2L$

ω = Frequency of oscillation (rad/sec)

Taking the first derivatives of the above quantities, we obtain

$$\frac{di(t)}{dt} = \left[\frac{V_o}{\omega L} \right] e^{-\alpha t} [\omega \cos(\omega t) - \alpha \sin(\omega t)]$$

$$dV_o(t)/dt = i(t)/C_t$$

The values used in a typical set-up result in very rapid discharges, yielding very high dE/dt 's, often approaching values of 10^{12} V/m/sec. With these high field values, the electric field becomes a significant coupling mechanism, and may more accurately simulate some of the other effects caused by nearby or an actual lightning strike. This test set-up also simulates the nonlinearities of the attachment process, such as attendant corona effects and streamers (filaments of current discharging into space) due to the high electric fields.

Swept Frequency Continuous Wave. The swept frequency continuous wave (SFCW) technique is based upon the use of RF excitation of the vehicle to determine the basic RF transfer function which can then be analyzed by Fourier transform techniques to provide the transient response [Robb, 1981]. This technique originated by Young and Piszker [1978], has been used extensively by Boeing Aircraft Company and the Air Force to investigate the vulnerability and susceptibility of aircraft. An example of the SFCW test setup instrumentation used by Young and Piszker is shown in Figure IV-22.

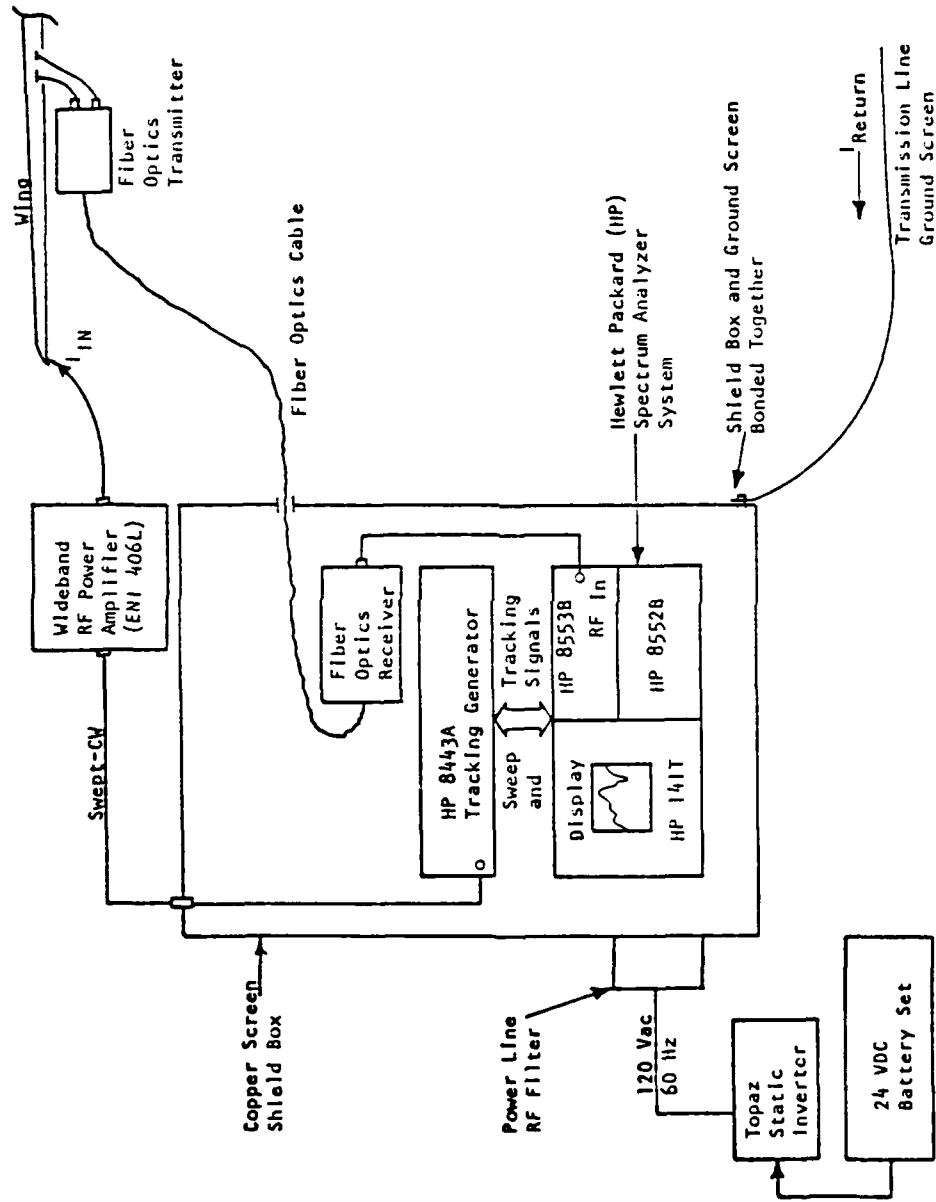


Figure IV-22. Block Diagram of the Swept Frequency Continuous Wave Instrumentation System. [Young and Piszker, 1978].

SFCW testing produces amplitude versus frequency data for transfer functions. Test data consists of digitized frequency responses, which are recorded on magnetic tape or disk for further computer processing. During the processing of the data, calibration and scaling factors for the test equipment are computed, and the data collected is corrected. Finally, the data undergoes an inverse FFT and the current and voltage waveforms are plotted.

There are many benefits in using this method of testing. The use of the low-level SFCW techniques eliminates the cost of custom designed and constructed high-level current and voltage generators, by substituting readily available, relatively inexpensive off-the-shelf test equipment. Although early test arrangements used the equipment typified by Figure IV-22, newer test setups are much easier to use because of the increasing sophistication of available equipment. The instrumentation system depicted in Figure IV-23 uses a scalar network analyzer, such as the Hewlett-Packard 3577A, to provide source, display and data capture capabilities in one compact unit. The resultant total system, shown in Figure IV-24, is very reliable, simple to use and capable of rapid collection of experimental data. Because the SFCW system operates with low voltages and currents, high voltage isolation and standoff equipment is

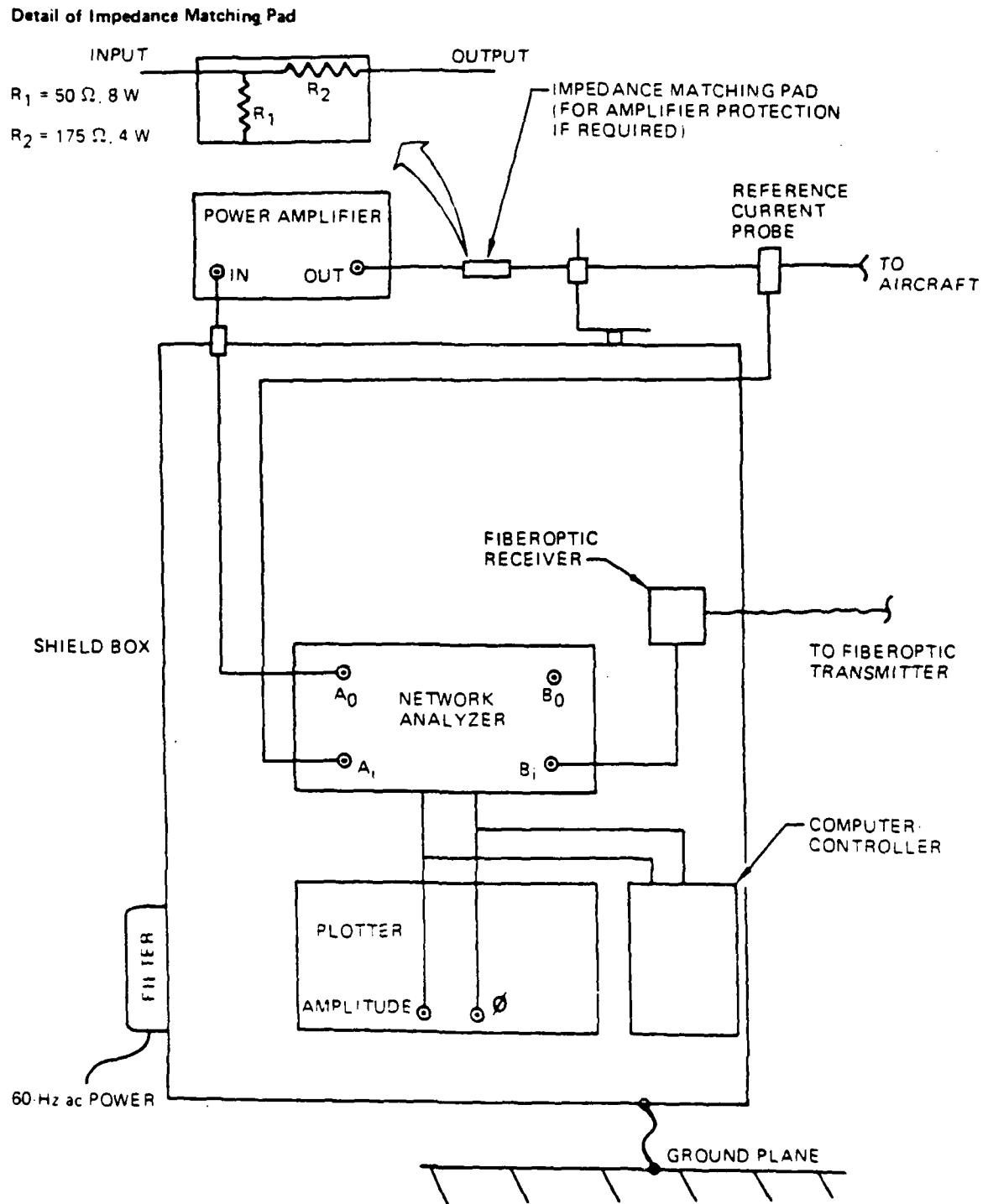


Figure IV-23. Swept Frequency Continuous Wave Instrumentation System Setup. [Ketterling, 1987].

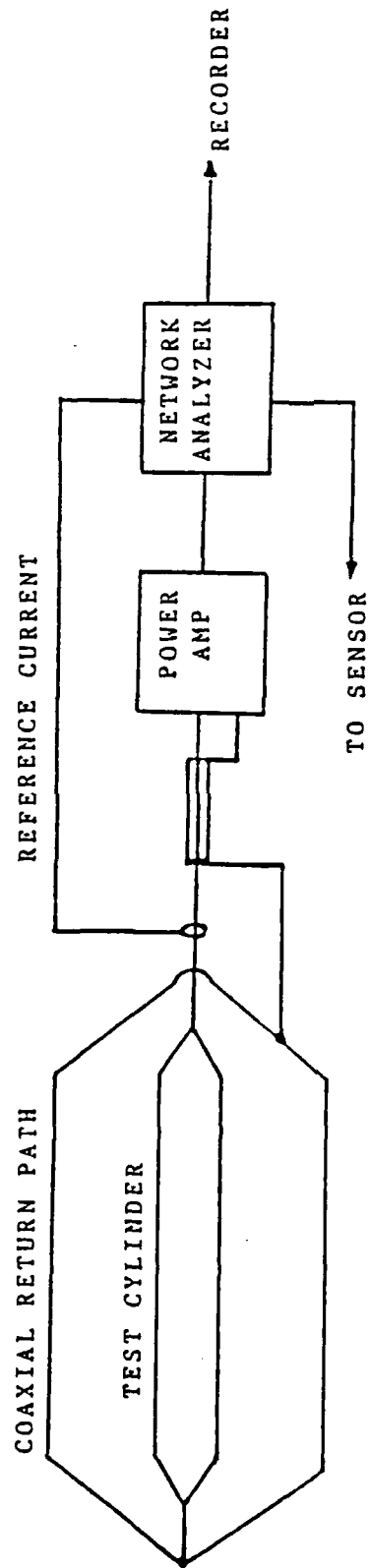


Figure IV-24. AFIT Swept Frequency Continuous Wave Test Setup.

not needed, and the safety hazards to personnel conducting the test are minimized.

There are some disadvantages to using this method. These include: (1) low drive levels do not cause arcing to occur and may not adequately simulate other nonlinear effects; (2) post-processing of data is needed to obtain time domain waveforms; (3) accurate measurements at low frequencies (less than 1 kHz) are difficult to make because of low signal-to-noise ratio due to limitations of instrumentation and extraneous signals such as power line harmonics; (4) contact resistances may be high because of small excitation currents.

Predicted voltages and currents that use low-level SFCW measurements have been compared to time domain results and found to be conservative for metal aircraft [Ketterling, 1987]. In this context, the term conservative is used to mean that a method predicts a greater threat than would actually exist. Thus, if a vehicle is protected to a level indicated by a conservative result, there is an additional safety margin built in. Although there is a large base of experimental data to support the results obtained from metal aircraft, a comparable database does not yet exist for composite aircraft. Also, the coupling measured on composite vehicles will be different than for metal aircraft, since

composites provide less shielding, and voltage drops on cables and structures will be larger at low frequencies. Thus, much work remains to be done for the characterization of composites using this technique.

These are only a few of the ways that lightning simulation is carried out. As a working premise, we will assume that what we are trying to simulate is the effects of the airborne lightning-aircraft interaction event, and we will further specialize this to indirect effects. One type of information we often want to obtain is measurements of the field and current distributions surrounding and on the aircraft. From this information we try to predict the coupling into the aircraft and assess the vulnerability of the aircraft. Knowing what information is desired, we can then catalog the types of errors that could affect our measurement. In the next section, we will see how the total configuration affects the accuracy and validity of the measured data from the simulation. Also, we will discuss methods to correct for these configuration effects.

Configuration Effects

Regardless of the purpose or approach we use in simulating some physical process, the accuracy of the simulation will determine the accuracy of the results.

Thus, we should identify and eliminate every possible source of experimental error in our simulations. For the simulation of the interaction of lightning with an aircraft, the possible sources of error will fall into several categories. Error is introduced by a failure to recreate the lightning-aircraft interaction environment and the non-ideal characteristics of simulation system. If we consider the simulation process, then our errors may be caused by any combination of the experimenter, the environment, the simulator or the measurement system.

One source of errors in the system can be attributed to "operator errors." These are errors such as choosing the wrong values for waveshaping networks, selection of incorrect ranges on measurement instrumentation, the programming of invalid algorithms for the processing of collected data, etc. Although these errors can greatly affect the validity of the results, they can be corrected for relatively easily, once they are recognized. Another source of errors is due to the failure of equipment in a "properly designed" simulation experiment. For instance, if a fiber optic link malfunctions during a measurement run, then the data collected will be in error, even though it was properly working earlier. The consideration and elimination of errors caused by the experimenter is not within the scope of this dissertation, as these errors are dependent upon the knowledge and skill of the

experimenter.

This dissertation is concerned with the impact of errors or effects caused by the physical configuration used in the simulation, and the remainder of this section will focus on these effects. These effects, which we call configuration effects, are all effects which occur during lightning simulation tests which would not be present during the airborne lightning-aircraft interaction event. This includes the effects of the simulation generator, hook-ups, measurement system and break out boxes inside the aircraft, return paths, environmental noise and other facility effects which cause the electromagnetic field distributions on and in the aircraft to differ from those produced by the airborne lightning interaction event.

Errors caused by the environment include variation introduced by such factors as temperature, humidity, dust, spurious electromagnetic noise from surrounding sources, etc. These errors can be minimized by the careful choice of experimental location, and by controlling the variations in the environment. If experiments must be carried out in less than ideal conditions, such as on a flight line, then careful attention must be given to recording the experimental conditions. In this way, it is possible that anomalous results may be correlated to environmental factors. No further consideration will be

given to these errors, other than to indicate their contribution to invalid results.

Although this may seem to be somewhat of an arbitrary division, it can be argued that those errors introduced by configuration effects represent a fundamental limitation on the validity and accuracy of the simulation. It is important to realize that there is a difference between the validity of the simulation and the accuracy of the simulation. Often much attention is paid to increasing the accuracy, while less emphasis is placed on insuring that the simulation is a valid one. There is little utility in achieving an additional 5 dB of accuracy in measuring the electric field, if the field measured does not represent the field that is actually present during the interaction event.

Many individuals have previously noticed the effects of the measurement configuration on the results obtained. Butters and Clifford [1977] noted during a study of lightning induced transients that the fast initial transient could be affected by varying the configuration parameters, but concluded that the changes had no major effect on the magnitude or frequency range of the induced transient.

Investigations by Lee, Butters and Lauber [1979] noted that the orientation of the aperture with respect to the ground plane had a significant effect on the measured induced transients and this has implications on the validity of the measurements if generator placement and ground return paths are arbitrarily chosen and changed during the course of the measurement.

Lenz, Clifford and Butters [1980] conducted a study of system resonances with different types of simulation excitation modes: with a cylinder hard wired to the generator, with the cylinder connected to ground through long arcs and with the cylinder excited by radiated E-fields. They showed that the resonances of the different modes were affected by the test object (cylinder) and return path configuration and they observed that the system resonances of the cylinder were only seen when the cylinder was irradiated by the EM pulse.

Walko and Hebert [1985] report on two series of tests conducted on the FAA CV-580 aircraft. In June 1984, the authors made measurements on the CV-580 aircraft using an impulse generator delivering both 200 kV oscillatory and unipolar pulses. The measurement system used a ground plane arrangement consisting of wire mesh under the fuselage and wings, while the aircraft was isolated from ground by Lexan sheets. In October of 1984, the tests

were repeated, with two significant changes. In addition to the generator used earlier, a fast rise time generator achieving sub-microsecond rise times and delivering 40 kA pulses was used. Also, the return path configuration was changed to a coaxial structure. In discussing their results, the authors noted that for a wing-to-wing configuration with the wire mesh return path the measured fields exceeded the calculated field by 52% to 78%. However, when a coaxial return path was used the measured values were between 92% and 98% of the calculated values. In this case, we see a substantial influence on the measured results, depending on the configuration.

In a follow up paper, Hebert, Reazer, Schneider, Risley and Serrano [1986] again noted that the choice of lightning simulation generators and return paths had a pronounced effect on the current levels and distributions experienced on the aircraft as evidenced by the transfer functions resulting from each configuration tested.

Work by Melander [1984] on the characterization of the lightning threat using parameter measurements made on instrumented towers noted that the effect of the tower could have an impact on the characteristics of lightning arc measurements and should be corrected for. Rustan and Axup [1984] also reported on tower derived lightning measurements that clearly indicated that the effects of

the tower on the measured values was significant.

The most comprehensive work to date has been the assessment of lightning simulation test techniques carried out by Butters, Clifford, Murphy and Zeisel [1981]. While making an assessment of the current pulse and shock-excitation lightning simulation test techniques on a simple cylindrical structure they noted that the aperture location, cylinder dissipation, cylinder characteristic impedance and cylinder length were important parameters affecting the measured results.

It should be noted that in each of these cases, the work was not done primarily to study the effect of the configuration on the lightning simulation process. However, each experimenter noted that the configuration was important to the final results. In the case of the work by Melander and Rustan & Axup, the effects of the measurement tower were potentially very significant in determining accurate parameters for lightning characterization.

After considering the preceding, we see that there is great potential for error caused by the simulation configuration being reflected in our measured data. The errors introduced by the simulation configuration can be attributed primarily to the simulator and the measurement system, and their interactions with the test object.

After cataloging many of these errors and discussing their causes, ways to eliminate or correct these errors will be presented.

Errors that may be introduced by the measurement system are the same as those caused by any instrumentation system. When considering the measurement system, we will include sensors, data transmission paths (fiber optic and coaxial cables) and data acquisition equipment. First, the instrumentation used may generate or pickup electrical noise which can corrupt the data collected. This problem can be minimized or eliminated by careful attention to proper grounding and shielding. Techniques, such as those presented in the text by Morrison [1986], are well known and have been developed to correct for these problems. One factor unique to these simulations is the large voltages and currents used. These present unique challenges when isolating equipment. Because of their inherent noise resistance and isolation properties, fiber optic data transmission lines are often used.

Another error source is due to the use of non-ideal sensors. The perfect sensor does not perturb or alter the quantity being measured. Since the sensors we use are not perfect, we must compensate for these errors. One of the causes of these errors is the finite bandwidth that the sensor has. To minimize the effects of this limitation,

it is important to use sensors that have sufficient bandwidth. In addition, the fiber optic data transmission lines must also be checked for bandwidth limitations. Another parameter of importance is the sensor's characteristic impedance. The impedance must match that of the transmission system, to maximize the signal that is returned to the data acquisition system. This is particularly important in view of the potentially high noise levels that may exist in the system.

If improperly designed, the simulator itself is potentially the largest contributor to error. Each major portion of the simulator - generator, waveshaping network and return path - has a major influence on the accuracy and validity of the results that can be obtained. The generator not only serves as an excitation source, it has the potential of being a source of large amounts of noise. For this reason, remedial measures such as shielded rooms for instrumentation, fiber optic signal transmission lines and electromagnetic shields between generator and sensors are employed. Also, the generator unavoidably becomes part of the total circuit that affects the responses measured on and within the test object. Thus, the generator has substantial interaction with the test object.

The waveshaping network affects the measured data in several ways. The waveshaping network's purpose is to modify the output of the generator so the waveform will cause the same effects to the test object that a real lightning strike would. At the same time, the waveshaping network must act as a matching device between generator and test body. Also, the matching network must not load the test object. The problem is we are employing lumped elements to approximate the distributed parameters of the lightning channel. It is extremely difficult to choose a reasonable set of lumped elements that can successfully fulfill all of these requirements simultaneously.

Mismatches between the test object and the generator will show up as reflections that may not be physically present in the actual airborne lightning strike event. In turn, these spurious reflections will affect the current and charge distributions on the skin of the aircraft, altering the electromagnetic coupling processes into the aircraft.

Finally, the return path of the simulator will play a key role in the validity of the simulation. This is because the return path significantly affects and alters the field distribution around the aircraft. In the air, there is no return path in the immediate vicinity of the vehicle. On the ground, though, some type of return path around the test object is required, not only to complete the electrical circuit, but to modify the fields around

the test object so they are the same as would be experienced in the free space environment. Although this is the ideal that is aimed for, it is very difficult, if not impossible to obtain. For instance, the coaxial configuration is often employed to yield uniform fields. However, there are difficulties in employing this technique at threat level voltages and currents when arc attachment is desired, as there can be problems with arcing between test object and return path. In addition, a true coaxial structure resulting in the desired fields can not be built around very complex objects.

All of these errors, taken together, make up the configuration effects that influence the data collected. Without some method of correcting for these effects, the simulation will not achieve the objective of being a valid representation of the airborne lightning strike event. Rather, these configuration effects will perturb the interaction process and mask what is actually happening. One way to correct for these effects is to use an approach that is similar to the one used to correct the transfer functions of the measured data for the non-ideal effects of the sensors. Simply stated, the use of frequency domain techniques, as well as accurate prediction and modeling techniques, provides the needed tools to correct the results currently obtained from ground based lightning simulations.

Frequency domain techniques are a powerful and flexible way to analyze and compare, in terms of transfer functions, the adequacy of generator/return path combinations in simulating the airborne event. Through the use of these techniques, many of the effects of generators, return paths, the sensors, measurement system and other perturbing influences can be removed from the data taken during simulation testing. In addition, frequency domain techniques have many other uses which have not been fully exploited. They also provide a powerful diagnostic tool in analyzing the response of the test object to the effects of the measurement system.

Frequency domain techniques were employed in this research as follows. First, the frequency domain transfer functions of the total test configuration are measured and recorded from DC to the configuration's (or instrumentation's) upper frequency limit using a Hewlett-Packard 3577A scalar network analyzer. The network analyzer produces a swept frequency continuous wave output and measures the response of the configuration. By dividing the configuration's output responses to the input at discrete frequencies a transfer function of the configuration is produced. The time domain waveforms are transformed into the frequency domain using the Fast Fourier Transform (FFT).

The next step in using frequency domain techniques for diagnostics is to remove the effects of the measurement system from the measured data responses. The frequency domain transfer functions of the sensors and fiber optics links are measured and recorded from DC to the components' upper frequency limit using the network analyzer. By dividing the component's output responses to the input at discrete frequencies a transfer function for the component is produced. The time domain waveforms are transformed into the frequency domain by Fast Fourier transforms. The transform is corrected by dividing out the transfer function of the measuring components leaving a more accurate representation of the source which produced the sensor's measured response. This corrected Fourier transform is inverse transformed back into the time domain to produce a time domain signal. All time domain signals are corrected in this manner. An interesting side benefit of this procedure is that responses measured by derivative field sensors are automatically integrated to display the source excitation which caused the sensor's output. This results in a transfer function that represents more accurately represents the test configuration, by eliminating some of the measurement system errors.

The transform of the configuration can then be modified by dividing out the transfer function of the

portion of the configuration to be removed, leaving a less complicated transfer function representation of the portion of the configuration under study. Finally, the modified Fourier transform can be inverse transformed back into the time domain to produce a time domain signal. All time domain signals can be modified in this manner, separating out the various pieces of the configuration from each other. In the next chapter, results obtained by employing these techniques will be reported.

REFERENCES - CHAPTER IV

C.E. Baum, "Simulation of Electromagnetic Aspects of Lightning" Proceedings of Lightning Technology Symposium, NASA Conference Publication 2128, FAA-RD-80-30, NASA Langley, Hampton, VA, April 22-24, 1980, pp. 283-284.

Military Standard, "Lightning Qualification Test Techniques for Aerospace Vehicles and Hardware," MIL-STD-1757A, 1983.

Society of Automotive Engineers, "Lightning Test Waveforms and Techniques for Aerospace Vehicles and Hardening," Report of the SAE Committee AE4L, June 20, 1978.

Federal Aviation Administration, "Protection of Aircraft Fuel Systems Against Fuel Vapor Ignition Due to Lightning," FAA Advisory Circular AC 20-53A, 1983.

N. Rasch, "User's Manual for AC-20-53A Protection of Aircraft Fuel Systems Against Fuel Vapor Ignition Due to Lightning," U.S. Dept. of Transportation, Report No. DOT/FAA/CT-83/3, October 1984.

Society of Automotive Engineers, "Recommended Draft Advisory Circular, Protection of Aircraft Electrical/Electronic Systems Against the Indirect Effects of Lightning," Report of the SAE Committee AE4L, Report AE4L-87-3, February 4, 1987.

Department of Defense Standard, "Lightning Protection of Aerospace Vehicles and Hardware," DOD-STD-1795 (USAF), 30 May 1986.

E. Marx, Deutsches Reichspatent, No. 455933, 1923.

F.S. Edwards, A.S. Husbands and F.R. Perry, "The Development and Design of High-Voltage Impulse Generators," Proceedings of the IEE, Vol. 98, Part I, No. 111, May 1951, pp. 155-180.

T.J. Gallagher and A.J. Pearmain, High Voltage - Measurement, Testing and Design, (Chichester, England: John Wiley & Sons, 1983), pp. 103-116.

E. Kuffel and W.S. Zaengl, High Voltage Engineering - Fundamentals. (Oxford: Pergamon Press, 1984), pp. 53-85.

A. Greenwood, Electrical Transients in Power Systems. (New York: John Wiley & Sons, 1971), pp. 509-519.

D.W. Clifford, K.E. Crouch and E.H. Schulte, "Lightning Simulation and Testing," IEEE Transaction on Electromagnetic Compatibility, EMC-24, No. 2, May 1982, pp.209-224.

C.E. Baum, "EMP Simulators for Various Types of Nuclear EMP Environments: An Interim Categorization," IEEE Transactions on Antennas and Propagation, AP-26, No. 1, January 1978, pp. 35-53.

P.F. Little, A.W. Hanson and B.J.C. Burrows, "Test Techniques for Simulating Lightning Strikes to Carbon (Graphite) Fibre Composite Structures," Federal Aviation Administration - Florida Institute of Technology Workshop on Grounding and Lightning Technology, FAA Report No. FAA-RD-79-6, Melbourne, FL, March 6-8, 1979, pp. 121-126.

K.J. Lloyd, J.A. Plumer and L.C. Walko, "Measurements and Analysis of Lightning-Induced Voltages in Aircraft Electrical Circuits," by General Electric. National Aeronautics and Space Administration, Contractor Report NASA CR-1744, February 1971.

L.C. Walko, "A Test Technique for Measuring Lightning-Induced Voltages on Aircraft Electrical Circuits," by General Electric. National Aeronautics and Space Administration, Contractor Report NASA CR-2348, February 1974.

J.A. Plumer, , F.A. Fisher and L.C. Walko, "Lightning Effects on the NASA F-8 Digital-Fly-By-Wire Airplane," by General Electric. National Aeronautics and Space Administration, Contractor Report NASA CR-2524, March 1975.

K.E. Crouch and J.A. Plumer, "Improved Test Methods for Determining Lightning-Induced Voltages in Aircraft," by Lightning Technologies, Inc., National Aeronautics and Space Administration, Contractor Report NASA CR-3329, September, 1980.

L.C. Walko and J.G. Schneider, "Full Scale Lightning Test Technique," Proceedings of Lightning Technology Symposium, NASA Conference Publication 2128, FAA-RD-80-30, NASA Langley, Hampton, VA, April 22-24, 1980, pp. 449-458.

W.G. Butters, D.W. Clifford, K.P. Murphy and K.S. Zeisel, "Assessment of Lightning Simulation Test Techniques," by McDonnell Aircraft Company. Air Force Wright Aeronautical Laboratories Technical Report, AFWAL-TR-81-3075, Part 1, Wright-Patterson AFB, OH, October 1981, p. 3.

W. McCormick, K.J. Maxwell and R. Finch, "Analytical and Experimental Validation of the Lightning Transient Analysis Technique," by Technology Incorporated. Air Force Flight Dynamics Laboratory Technical Report, AFFDL-TR-78-47, Wright-Patterson AFB, OH, March 1978, p. 142.

J. Robb, "Atmospheric Electricity Hazards Analytical Model Development and Application, Vol. II: Simulation of the Lightning/Aircraft Interaction Event," by Lightning and Transients Research Institute. Air Force Wright Aeronautical Laboratory Technical Report, AFWAL-TR-81-3084, Volume II, Wright-Patterson AFB, OH, August 1981, p. 23.

D.W. Clifford and K.S. Zeisel, "Evaluation of Lightning-Induced Transients in Aircraft Using High-Voltage Shock Excitation Techniques," Proceedings of the 1979 IEEE International Symposium on Electromagnetic Compatibility, San Diego, CA, October 9-11, 1979, p. 160.

D.E. Young and L.D. Piszker, "The Use of CW Test and Analysis Techniques in Lightning Vulnerability Assessment of Aircraft Systems," Federal Aviation Administration - Georgia Institute of Technology Workshop on Grounding and Lightning Protection, FAA Report No. FAA-RD-78-83, Atlanta, GA, May 2-4, 1978.

G. Ketterling, Final Report, Atmospheric Electricity Hazards Protection Program, Part V. Qualification and Surveillance Test and Analysis Procedures, by Boeing Military Airplane Company. Air Force Wright Aeronautical Laboratory Technical Report, AFWAL-TR-87-3025, Part V, Wright-Patterson AFB, OH, June 1987, p. 3-13.

W.G. Butters and D.W. Clifford, "Lightning Induced Electrical Transient Testing on Aircraft Wiring System," Proceedings of the 1977 IEEE International Symposium on Electromagnetic Compatibility, Seattle, WA, 2-4 August, 1977, pp. 237-241.

J.E. Lee, W.G. Butters and R.J. Lauber, "Laboratory Simulation of Near-by Lightning Induced Electrical Transients," FAA Report No. FAA-RD-79-6, Federal Aviation Administration - Florida Institute of Technology Workshop on Grounding and Lightning Technology, Melbourne, FL, March 6-8, 1979, pp. 287-303.

J.E. Lenz, D.W. Clifford and W.G. Butters, "Experimental Resolution of System Resonances Produced by Simulated Lightning Excitation," Proceedings of Lightning Technology Symposium, NASA Conference Publication 2128, FAA-RD-80-30, NASA Langley, Hampton, VA, April 22-24, 1980, pp. 21-37.

L.C. Walko and J.L. Hebert, "Lightning Simulation Tests on FAA CV-580 Lightning Research Aircraft," Proceedings of the 10th International Aerospace and Ground Conference on Lightning and Static Electricity, Paris, France, 10-13 June 1985, pp. 137-147.

J.L. Hebert, J.S. Reazer, J.G. Schneider, M.D. Risley, and A.V. Serrano, "Current Levels and Distributions on an Aircraft During Ground Simulation Tests and In-Flight Lightning Attachments," Proceedings of 1986 International Aerospace and Ground Conference on Lightning and Static Electricity, Dayton, OH, June 24-26, 1986, pp.19-1--19-21.

B.G. Melander, "Effects of Tower Characteristics on Lightning Arc Measurements," Proceedings of 1984 International Aerospace and Ground Conference on Lightning and Static Electricity, Orlando, FL, June 26-28, 1984.

P. Rustan and P. Axup, "Analysis of Lightning Current Measurements," Proceedings of 1984 International Aerospace and Ground Conference on Lightning and Static Electricity, Orlando, FL, June 26-28, 1984.

R. Morrison, Grounding and Shielding Techniques in Instrumentation. New York: John Wiley & Sons, 1986.

CHAPTER V

GROUND LIGHTNING SIMULATION TEST RESULTS

Overview

This chapter will describe the various tests that were performed or used for this research effort. Data recorded during actual lightning strikes to a specially instrumented CV-580 aircraft is presented. This CV-580 data is important because it provides a common baseline with which to compare the validity and accuracy of several simulation techniques. Next, data obtained during a series of current injection tests is described. These tests report the results of injecting threat level currents into various test objects. Data obtained during Swept Frequency Continuous Wave (SFCW) tests follows. These tests have the advantage of requiring minimal equipment for system excitation and of being safe to perform. Finally, data for tests using the shock-excitation technique is presented. These tests were developed to simulate other aspects of lightning interaction with aircraft which are not normally produced by the current injection method above. The data from each of these ground simulation test techniques is analyzed and compared with the airborne lightning strikes. The results are presented in terms of how configuration effects cause the ground-based simulation measurements to differ from the airborne case.

CV-580 Airborne Test Program

General. This section provides a considerable expansion of the type of work presented by Hebert et al. [1986]. During 1984 and 1985, a specially instrumented CV-580 aircraft supplied by the Federal Aviation Administration and instrumented by AFWAL's Atmospheric Electricity Hazards Group was flown in and near active Florida thunderstorms. The aircraft measured and recorded the electromagnetic fields and current distributions resulting from 50 direct lightning strikes. This program collected much useful data which can be used as a baseline to determine if ground based lightning simulations are accurately representing what happens during the airborne strike. In particular the measured lightning strike data from this program allows the isolation of simulation configuration effects which are present in ground simulation tests, but absent during the airborne lightning strike.

Before and after the 1984 summer thunderstorm flights and prior to the 1985 summer program, the CV-580 was subjected to extensive lightning simulation tests described in a later section of this chapter. These tests provide the unique opportunity to compare ground based simulation results with the actual airborne aircraft-lightning interaction event, allowing a check of the validity and

accuracy of ground lightning simulations tests and a measure of how much the generator, return paths, connections, etc., can perturb the data collected during ground tests.

Test Objective. The objective of the CV-580 research program was to measure the electromagnetic interaction of the aircraft with lightning strikes and to characterize the significant parameters of lightning which contribute to this interaction.

Test Set-up and Configuration. The CV-580 airborne lightning strike data presents the best possible baseline, because there is only minimal external configuration to influence the electromagnetic measurements. The aircraft differs slightly from its usual flight configuration, due to the presence of sensors installed on the aircraft skin. In addition, any sensor signal transmission lines added to the aircraft's normal circuitry slightly perturb the process of electromagnetic fields coupling into the aircraft. However, these sensors and circuits were designed to minimize and account for these effects such that this data provides a fair representation of the day to day situation faced by operational aircraft.

Generator and Measurement System. The "source generator" for this series of tests was natural lightning

at various altitudes and locations which struck the CV-580 in Florida during the summers of 1984 and 1985. Lightning currents were measured at the base of booms equipped with current shunts (ILW and IRW) which were installed at the wing tips in 1984 and 1985 and the tail (ITB) and top of the rear vertical stabilizer (IVS) in 1985. The shunts were oriented to produce a negative polarity waveform when conventional current flowed onto the aircraft. The skin current distributions on the fuselage and wings were measured by four EG&G Multi-gap Loop (MGL) derivative magnetic field sensors (J_S). These sensors were located under each wing between the engine and the fuselage ($J_{S\text{RW}}$ and $J_{S\text{LW}}$), one on the top forward fuselage ($J_{S\text{FF}}$) and one on the top aft fuselage ($J_{S\text{AF}}$). These sensors were oriented to produce a negative output when currents pass from nose to tail or from right wing to left wing. Electric fields were measured by three EG&G Flush Plate Dipole (FPD) displacement current (J_N) derivative electric field sensors. These sensors were located under each wing tip ($J_{N\text{RW}}$ and $J_{N\text{LW}}$) and one on the left side of the vertical stabilizer ($J_{N\text{VS}}$). In addition, video cameras were used to visually record the entry and exit locations during lightning attachments. The location of the field sensors on the aircraft is shown in Figure V-1.

The outputs of the field sensors were recorded in the

following ways:

1. Shunts - The signal was split in two, with one input sent to a Tektronix 7612 digitizer and the other sent to a 9-track analog tape recorder.

2. Magnetic field sensors - Signal split in two, with one sent to a Tektronix 7612 digitizer and the other integrated and sent to a 9-track analog tape recorder.

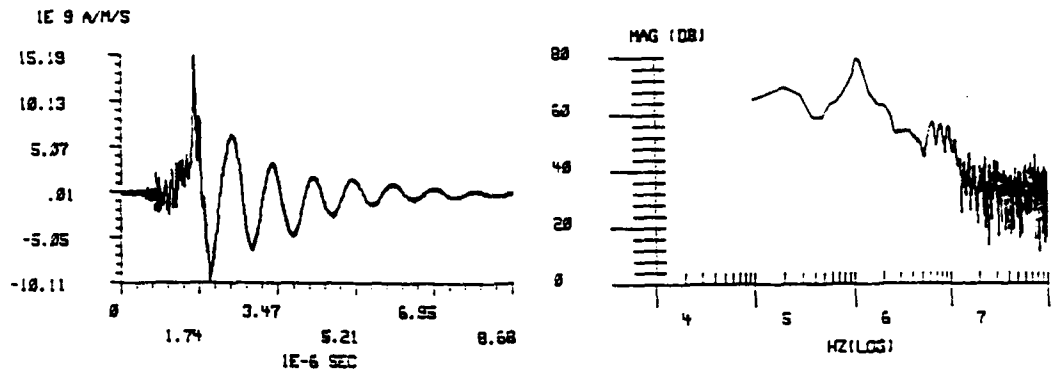
3. Electric field sensors - Signal split in two, with one sent to a Tektronix 7612 digitizer and the other integrated and sent to a 9-track analog tape recorder.

Airborne Data Processing. Frequency domain analysis techniques were used to process the airborne data to analyze the results of the airborne experiments and to allow comparison of this data with the results obtained from other studies and the ground simulation tests described in this chapter.

The first step in this frequency domain analysis was to remove the effects of the measurement system from the measured data responses. The frequency domain transfer functions of the aircraft's derivative magnetic field sensors, the ground input current transformer sensor and fiber optics links are measured and recorded from DC to

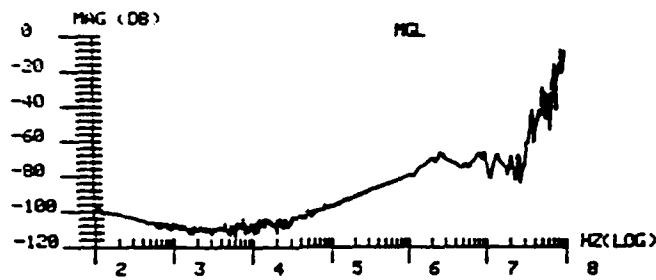
the component's upper frequency limit (generally 100 MHz) using a Hewlett-Packard 3577A network analyzer. The network analyzer produces a swept frequency continuous wave output and measures the responses of the components. By dividing the component's output responses to those of the input at discrete frequencies, a transfer function for the component is produced. The time domain waveforms are transformed into the frequency domain by Fast Fourier transforms (FFT). The transform is corrected by dividing out the transfer function of the measurement components, leaving a more accurate representation of the source which produced the sensor's measured response. This corrected Fourier transform is inverse transformed back into the time domain to produce a time domain signal. All time domain signals are corrected in this manner. An interesting side benefit of this procedure is that responses measured by derivative field sensors are automatically integrated to display the source excitation which caused the sensor's output.

This procedure is illustrated in Figure V-2 for a multi-gap loop magnetic field sensor mounted on an aircraft [Hebert et al., 1986]. Figure V-2a shows the original time derivative waveform and V-2b its Fast Fourier transform as recorded during a ground test with a fast rise time generator. Figure V-2c shows the transfer function of the multi-gap loop sensor as measured using



A.
Time Domain Derivative Waveform from Multi-Gap
Loop Sensor on Aircraft

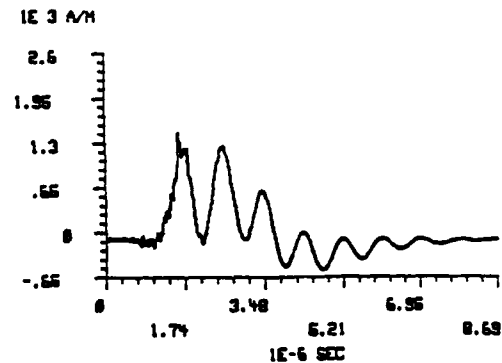
B.
Log-Log Polar Plot of Fast Fourier Transform
of (A)



C.
Frequency Response of Multi-Gap Loop Sensor from 100 Hz to 100 MHz



D.
Log Log Polar Plot of Corrected Fast Fourier
Transform of (A)



E.
Inverse Transform of (D) to Produce Integrated,
Corrected Multi-Gap Loop Sensor Output

Figure V-2. Illustration of the Techniques Used to Correct Sensor Data for Nonlinearity in the Measurement System. [Hebert et al., 1986].

the Hewlett-Packard 3577A network analyzer. Figure V-2d shows the corrected Fourier transform which results when the original transform is divided by the transfer function of the sensor and Figure V-2e presents the resulting inverse transformed time domain signal which provides a fairly accurate measurement of the excitations currents which caused the sensor's response. This benefit can best be appreciated by those who have experience with the software integration of time derivative digital sensor data. This process eliminates common problems with zero reference values and with integration error drift. The procedure is also more accurate as software integration assumes that the sensor is a perfect derivative sensor. The transfer function illustrated in Figure V-2c shows this is definitely not the case as a perfect derivative sensor would produce a transfer function which has a straight line from zero with a slope linearly related to the frequency. This type of frequency domain processing allows the sensor's effects to be removed whether the sensor response is perfect or, more commonly, is less than perfect.

The next step in a frequency domain analysis is to produce the transfer function of the aircraft at the sensor locations for the sources to be studied. These were formed using the following relationship:

$$T(\omega) = R(\omega)/S(\omega)$$

where $T(\omega)$ is the frequency domain transfer function, $R(\omega)$ is the corrected Fourier transform of the multi-gap loop sensor response, with the sensor's transfer function removed, and $S(\omega)$ is the Fourier transform of the applied current source, also with that sensor's transfer function removed. By creating the transforms of various sources, such as the defined standardized lightning threat waveform and other excitation sources, and convolving them with the aircraft's transfer function at various locations, the response of the aircraft to different types of threats and excitations can be studied and compared.

Results. Lightning Strikes - Figure V-3 shows the time domain surface current distributions measured by the J_s sensors during a lightning strike to the nose of the CV-580 which occurred on 20 August 1984. Figure V-4 shows a similar record of a strike which attached to the right wing boom on 5 September 1984. This strike data is particularly interesting because it includes the shunt measurement of the actual lightning current which attached to the aircraft. Figure V-5 shows the frequency domain transfer functions for the right wing strike at several locations formed by dividing the sensors' responses by the right wing shunt attachment current.

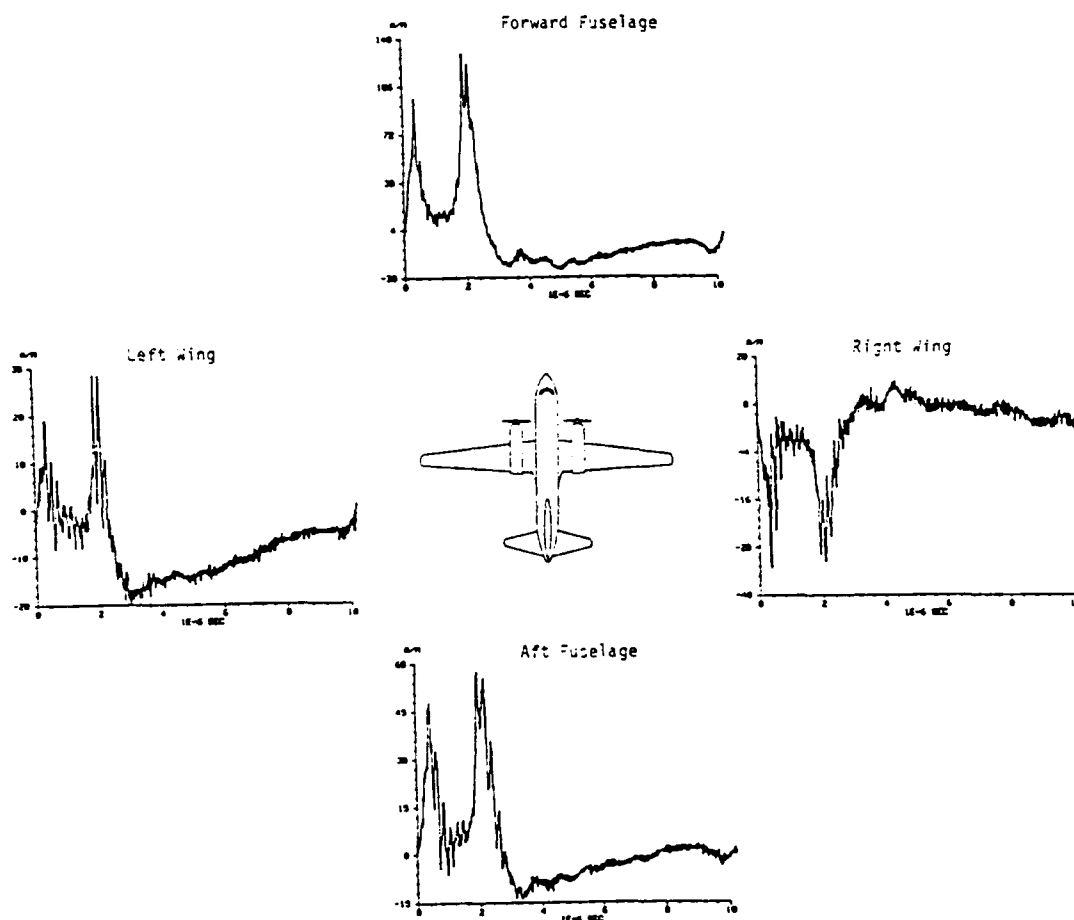


Figure V-3. Time-Domain Surface Current Waveforms Recorded by the Surface Current Sensors on the CV-580, During a Lightning Strike to the Aircraft Nose. [Hebert et al., 1986].

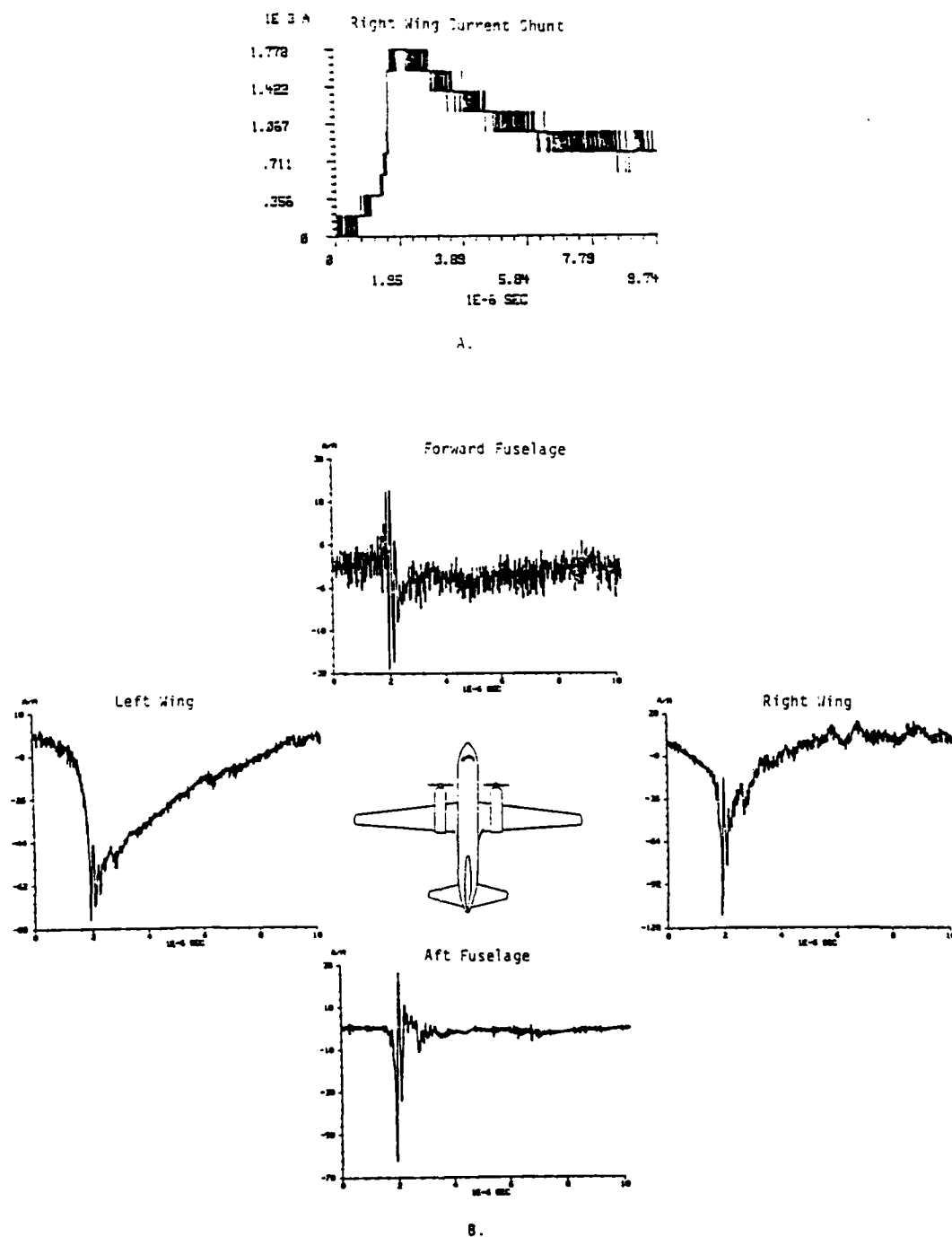


Figure V-4. Lightning Strike to the Right Wing of the CV-580.
 (A) Current Measured at the Right Wing Current Shunt
 (B) Surface Current Waveforms Recorded on CV-580.
 [Hebert et al., 1986].

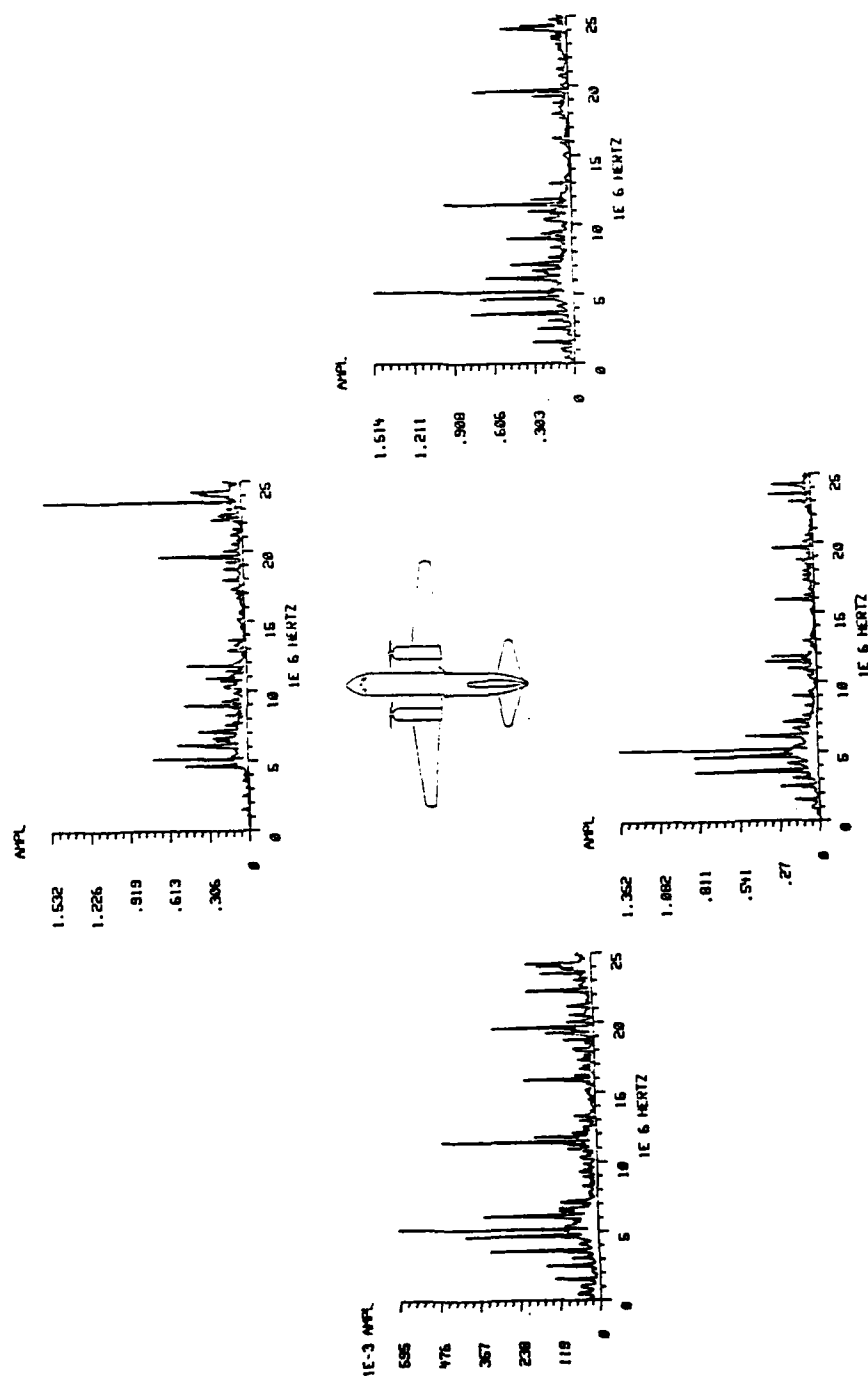


Figure V-5. Transfer Functions at the Four Surface Current Sensors from the Right Wing Lightning Strike to the CV-580. [Hebert et al., 1986].

1. Although the 20 August strike to the nose does not provide a direct measurement of the attachment current, it does show that the current which flowed onto the forward fuselage probably exited from both wing tips and the tail. The rear three sensors show a bit more resonant activity than the forward fuselage which was closest to the entry point.

2. The 5 September strike is far more interesting because the entry current was directly measured by the right wing shunt in addition to the four skin current sensors. The time delays in the propagation of the re-distributed lightning currents on the aircraft's fuselage at the sensor locations shows that the path of this strike was most probably right wing to left wing. The forward and aft sensors show considerable resonant activity. The input looks much like the threat waveform defined by the Military Standard 1757A for lightning simulation testing, but the magnitude is considerably smaller. A more detailed picture of the interaction develops when the natural resonances displayed in the frequency domain are considered.

Many of the prominent peak magnitudes in these transfer functions occur at frequencies which relate quite closely to dimensions of the aircraft. The spike at 4.7 MHz represents a half wavelength of approximately 105

feet, the distance from wing tip to wing tip. At 5 MHz or 98 feet, the frequency may correspond to the distance from the wing tip to the tip of the vertical stabilizer, the distance from the wing tip to the tip of the horizontal stabilizer or from the wing tip to the aircraft tail. Nine MHz (55 feet) corresponds to the distance from the wing tip to the fuselage and 7.2 MHz (68 feet) to the distance from the wing tip to the far engine mount. The 11-12 MHz frequencies correspond to the distance from the wing tip to the closer engine mount.

The left wing, right wing and aft upper fuselage transfer functions show peaks at 1.5, 2.5 and 3.6 MHz which are too low to correspond to direct aircraft dimensions. These frequencies correspond well, however, to frequencies which are multiples or combinations of aircraft distances. For example, 2.5 MHz is 197 feet or twice the distance from the wing tip to the tail or roughly the combined distance of wing tip to wing tip and nose to tail. The frequency of 3.6 MHz represents a distance of 137 feet, twice the distance from the wing tip to the far side of the fuselage or the combination of the distance from wing tip to tail and the distance from the wing tip to the near engine mount. The frequency of 1.5 MHz could relate to the combination of several aircraft dimensions. The transfer functions are particularly interesting to the electromagnetic analyst concerned with

lightning protection, as they clearly show that the interaction of lightning produces resonances which are more complex than those predicted simply by wing to wing or nose to tail dimensions and may closely correspond not only to direct aircraft dimensions but also to combinations of these dimensions. The data shows that the aircraft's complex geometrical shapes and lengths strongly influence the re-distribution of lightning currents on the aircraft.

Current Injection Tests

This section discusses the configuration effects measured during current injection type ground lightning simulation tests. In general, past lightning simulation tests have been conducted with only minor attention paid to the configuration effects of the generator and return paths. Return paths are usually designed with the following criteria in mind: (1) To provide a configuration which has low inductance so the rise time of the injected current from the generator (capacitor banks) may be reduced; (2) To provide electric and magnetic fields that are as uniform as possible, as this has long been considered essential to simulate the airborne case; (3) To provide sufficient spacing to avoid voltage breakdown between test object and return path; and (4) Can be constructed within the time and cost constraints of the

particular test. The above criteria often results in compromises. For instance, the trade-off between time and costs vs. field uniformity often results in the use of flat plate parallel return paths rather than coaxial type return paths.

Two recent test programs have investigated the configuration effects of ground simulation test set-ups. One of these was incidental to the test procedures being carried out by Hebert et al. on a specially instrumented CV-580 lightning research aircraft. The other test was a series of planned experiments by the author on the AFIT Lightning Test Object (LTO). The test, objectives of the test, test set-up and configuration, measurement system, measurements and results for each series using the current injection test method are discussed.

CV-580 Ground Simulation Tests

General. Hebert et al. [1986] compared the current levels and distributions recorded during in-flight lightning strikes to a specially instrumented CV-580 lightning characterization research aircraft and those resulting from ground lightning simulation tests which used four distinctly different lightning simulation test configurations. These tests and their results are

important because they afford the opportunity to compare the configuration effects of several lightning simulation test set-ups with actual in-flight lightning strike data.

Test Objective. These tests were conducted to provide a lightning susceptibility assessment of the CV-580, to allow lightning measurement and acquisition system check-out, to allow data acquisition trigger levels to be set and to perform system calibration.

Test Set-up and Configuration. Two return path configurations were used during these tests. The first return path was coaxial, placed around the aircraft's fuselage and wings at a distance of roughly 3 feet from the surface (Figure IV-14). The second return path used was a flat plate return path consisting of a wire mesh placed under the aircraft's fuselage and wings (Figure IV-11).

Generator and Measurement System. Two generators were used in these tests. One was a 4 microfarad, four stage Marx bank with a top voltage rating of 200 kilovolts. The generator is capable of high currents, but has a fairly slow rise time. This generator is known as the Pulse Simulation Unit (PSU). The second generator was a 4 Megavolt Marx bank which used a .25 nanofarad 40 stage peaking capacitor to produce very fast rise times. This

generator is known as the Fast Rise Time Generator (FRG).

Test Data Processing. The data from this test and the remaining tests to be discussed were all processed using the frequency domain techniques described in the previous section for the airborne program. Only procedures that substantially differ from the previous processing or illustrate some test peculiarity will be discussed in the following sections.

Results. (1) PSU Tests -- Figure V-6 shows the transfer functions for the left wing J_s sensor for wing to wing ground simulation tests using the PSU generator with the coaxial and flat plate return paths. Figure V-6 (Top) shows the source waveform and the resulting transfer function for a coaxial return path. Figure V-6 (Bottom) shows the same waveforms for a flat plate return path. With the exception of the spike at 5.5 MHz, neither transfer function shows evidence of the pronounced, discrete frequencies seen in the airborne data or produced by the FRG. The slower rise times in this configuration do not provide sufficient high frequency content to excite several of the natural modes of the aircraft which are evident in the airborne transfer functions and ground tests with the FRG.

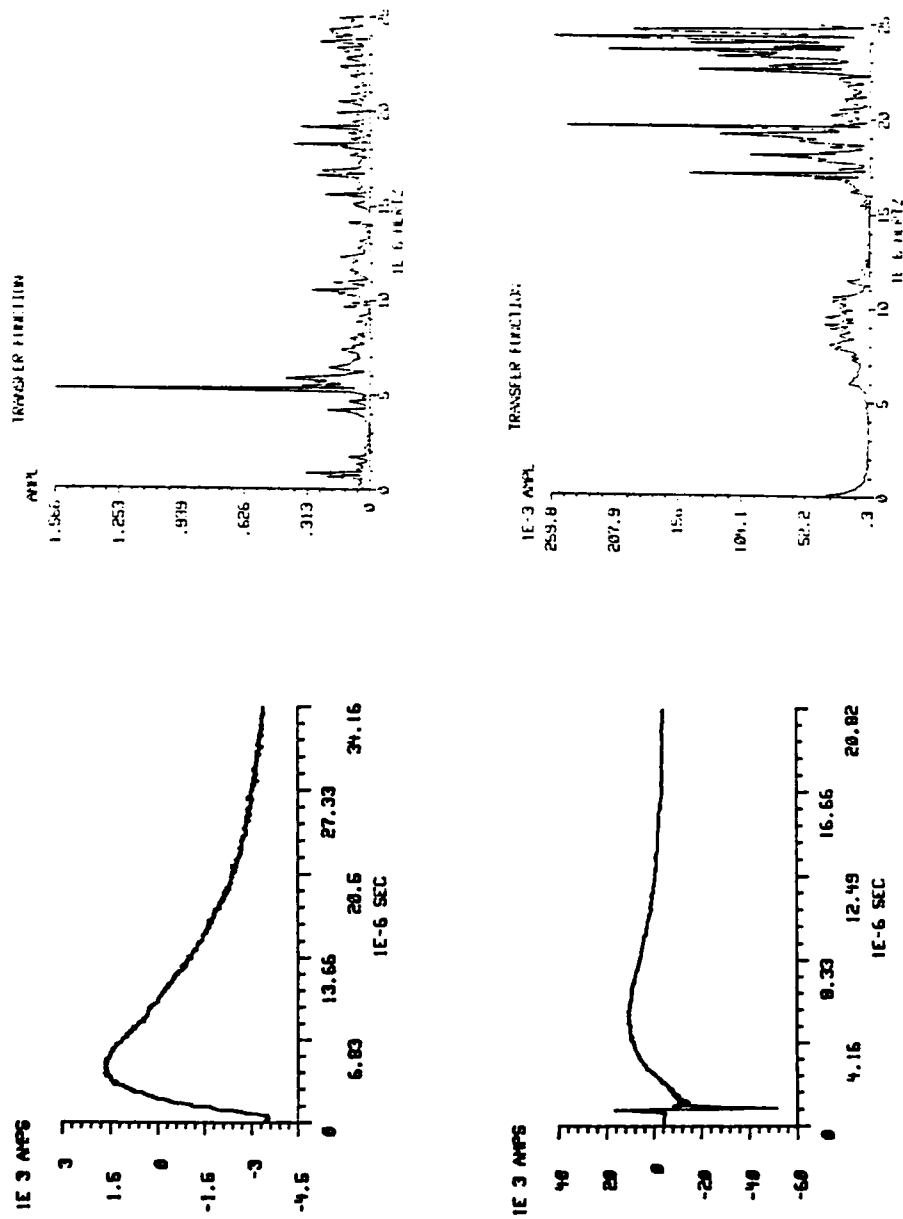


Figure V-6. Injected Current Waveforms from the Pulse Simulation Unit, and Resulting Transfer Functions at the Left Wing Current Sensor. (Top) Coaxial Return Path. (Bottom) Flat Plate Return Path. [Hebert et al., 1986].

(2) FRG Tests -- Figure V-7 shows the time domain input and response waveforms for tests using the FRG generator with a coaxial return path in the wing to wing configuration. Figure V-8 shows the same waveforms in terms of the transfer functions of the responses. Figure V-9 shows the same transfer function, but for tests with the FRG generator with the flat plat return path in the wing to wing configuration. These figures clearly show that the lightning generator and return paths (part of the configuration effects) have considerable impact on the resulting skin current distributions.

Figure V-8 shows the transfer functions at the four sensor locations for the ground test with the FRG and the coaxial return paths in the wing-to-wing configuration. The overall distribution of the transfer functions peak magnitudes corresponds well to the airborne case for the ranges of 4 to 13 MHz, 20 MHz and at 23-25 MHz. These transfer functions show additional resonances at 16-17 MHz which were not present in the airborne strike.

Figure V-9 shows the same transfer functions for the FRG with the flat plate return paths in the wing-to-wing configuration. These transfer functions have peaks at about 10 MHz which are not found in either the airborne case or with the coaxial return paths. In this configuration the transfer functions do not display as

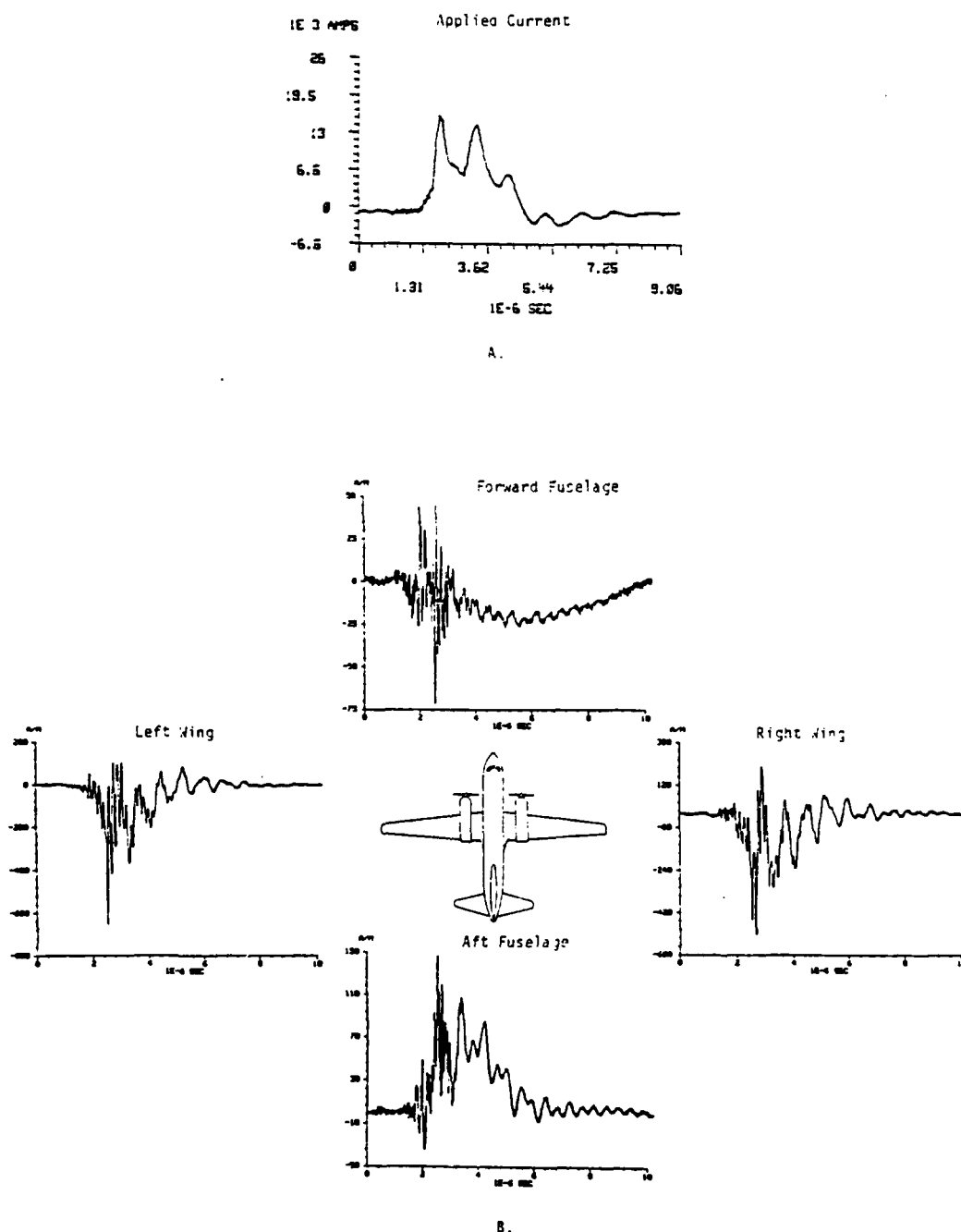


Figure V-7. Input Waveform and Response from Fast Rise Time Generator Using Coaxial Return Path. (A) Applied Current Waveform. (B) Recorded Surface Current Waveforms. [Hebert et al., 1986].

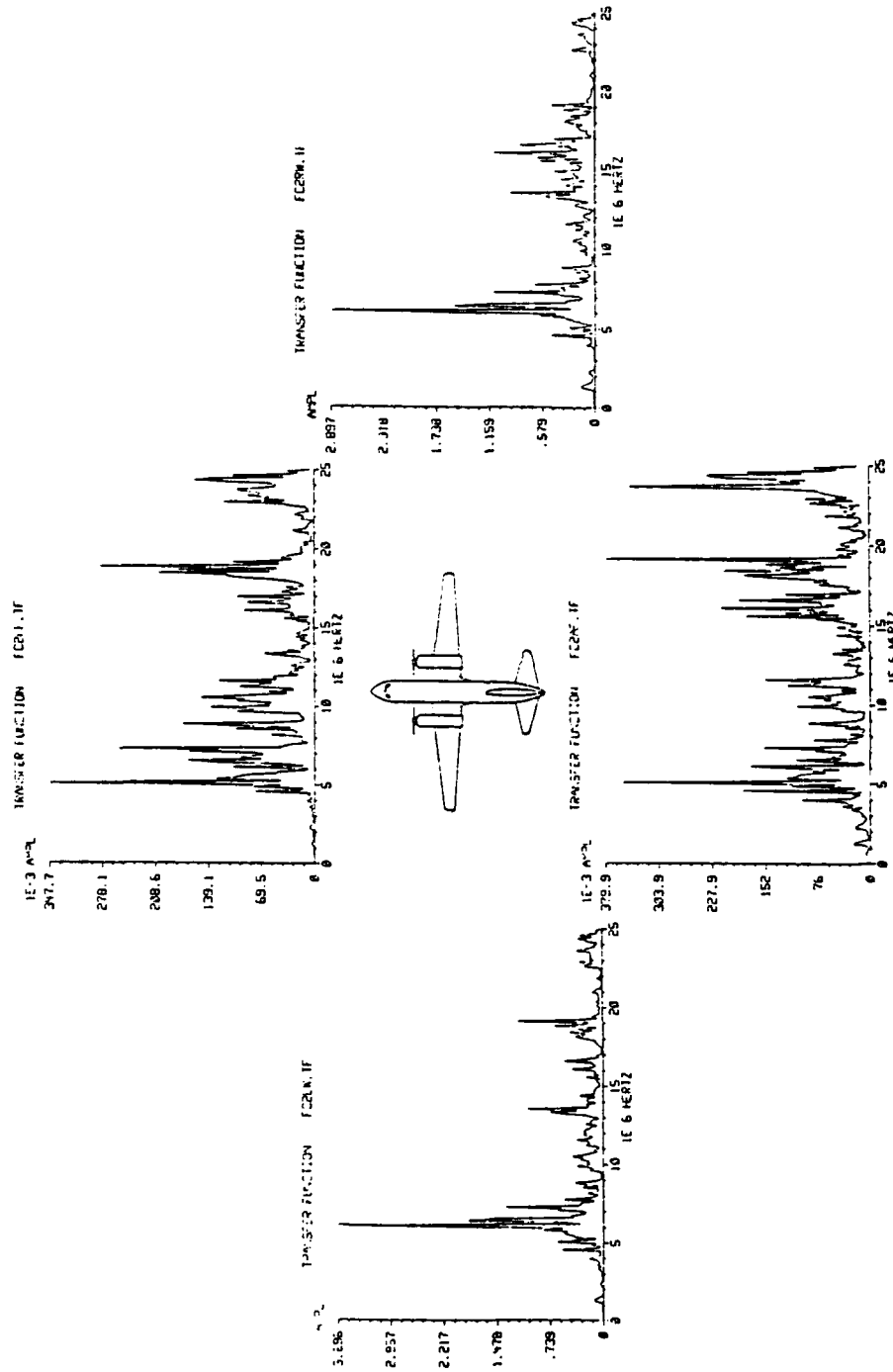


Figure V-8. Transfer Functions at the Four Surface Current Sensors. Results from the Fast Rise Time Generator and Coaxial Return Path. Simulated Wing-to-Wing Lightning Strike to CV-580. [Hebert et al., 1986].

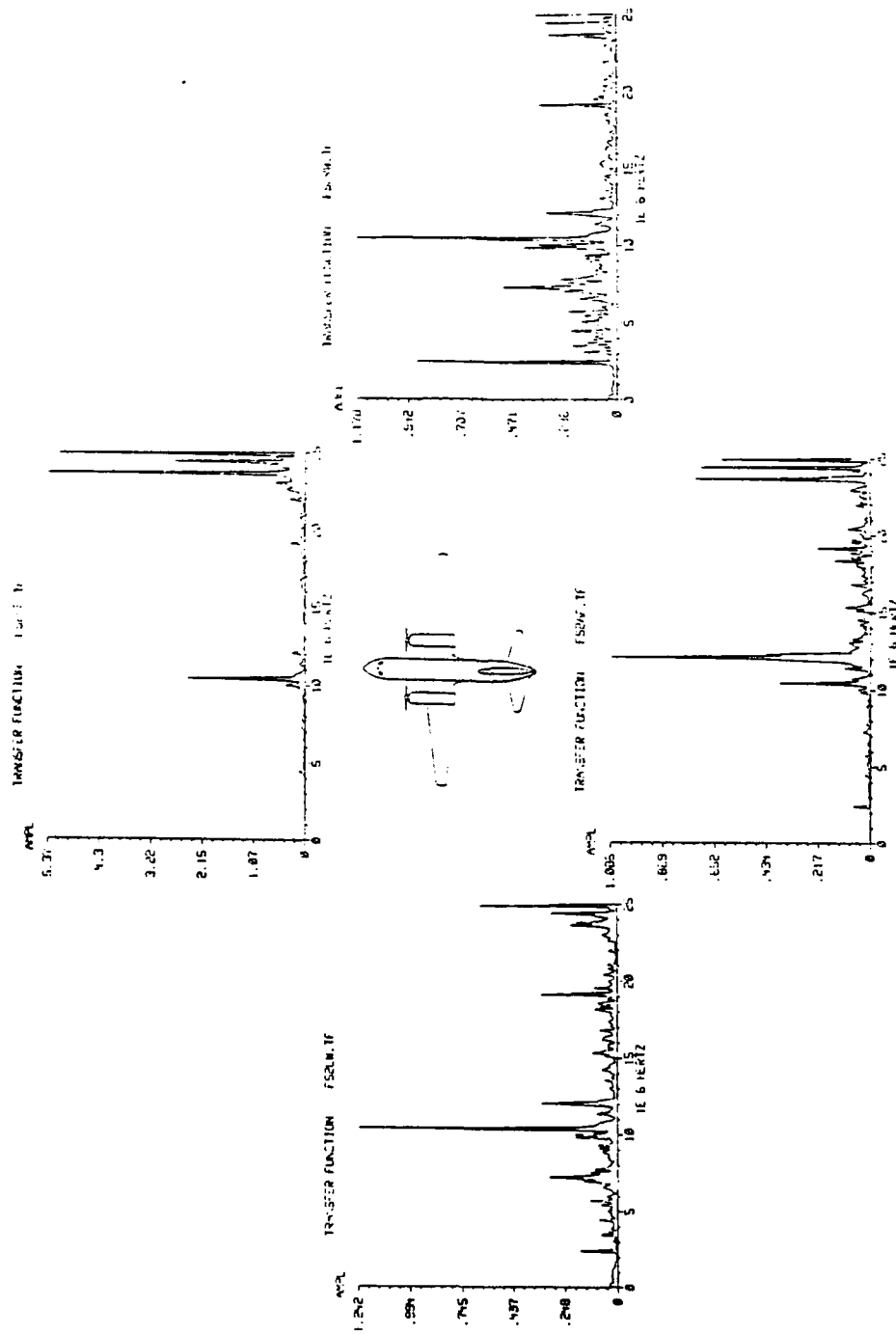


Figure V-9. Transfer Functions at the Four Surface Current Sensors. Results from the Fast Rise Time Generator and Flat Plate Return Path. Simulated Wing-to-Wing Strike to CV-580. [Hebert et al., 1986].

many peak magnitudes at frequencies below 10 MHz. Above 15 MHz, the flat plate return path provides a very faithful reproduction of the airborne measured transfer function with spikes at 19 MHz and in the 23-24 MHz range.

The airborne resonances at which energy couples to the aircraft do not correspond well to those from any of the ground tests as shown by their transfer functions. The addition of spikes not present in the airborne case or the absence of spikes in the ground case are clearly attributable to configuration effects. Simply stated, the ground simulation tests do not produce the same current distributions which were experienced by the aircraft during the airborne strikes. Of the configurations considered, the coaxial return path with the FRG does the best job overall, but clearly, a technique to minimize or remove configuration effects would enhance ground simulation results.

AFIT LTO Current Injection Tests

General. The tests performed by Hebert et al. described above were rough due to operational limitations and time constraints on testing. They did, however, give the first indications of: how much the configuration effects could influence the skin distributions on an aircraft; the fact that ground tests may not adequately

simulate the airborne event; and a method to analytically relate the ground simulation results to that which would be expected in flight needs to be developed. These results prompted the author to carry out a more carefully controlled set of lightning simulation tests to investigate these configuration effects.

The research carried out by AFIT had several objectives. The first objective was to investigate the various lightning simulation test techniques and test waveforms in terms of how well they represented the airborne lightning event. The second objective was to examine the differences between the various simulation techniques. Finally, the investigation was carried out to see how the configuration effects associated with the ground tests caused the measurements to differ from the airborne case.

Various lightning simulation test techniques were performed and evaluated on a lightning test object (LTO) developed by the Air Force Institute of Technology (AFIT) and the Air Force Wright Aeronautical Laboratories' Atmospheric Electricity Hazards Group (AFWAL/FIESL). The LTO with a coaxial return path is shown in Figure IV-13. It was designed by Captain James L. Hebert of AFWAL/FIESL and Captain Randy J. Jost of AFIT to realistically model the fuselage of an aircraft or missile and is over 10

meters long with a diameter of one meter. To test the effects of the interaction of lightning with various aircraft construction materials, the cylinder has a large aperture in which various panels may be mounted.

Test Objective. An extensive series of lightning simulation tests were carried out on the LTO during the spring and summer of 1987. Current injection, SFCW and shock excitation tests were performed on the LTO by Captain Randy J. Jost and 2Lt Rudy Braza. Jost investigated the configuration effects of various lightning simulation test techniques with different test set-ups, while Braza investigated the differences between the current injection, SFCW and shock excitation test techniques [Braza, 1987]. The objective of the current injection portion of the test program was to generate current injection test data to support an investigation of how the measurement configuration would respond to different current injection waveforms. The waveforms used would also allow a comparison of the unipolar waveform with the oscillatory waveform, and a moderate threat level waveform with a severe threat level waveform. The particular choice of waveforms was also made to gain some insight into effects of linear extrapolation from the low magnitudes at which lightning simulation tests are typically performed to the higher magnitudes of the defined threat levels. Finally, the results of the

current injection tests were correlated to other test techniques using the LTO as a simple uniform test object.

Test Set-up and Configuration. The basic test set-up of LTO and return path is shown in Figure IV-13. A coaxial return path was placed at a distance of one meter from the surface of the LTO, with an emphasis on preserving the symmetry of the structure about the long axis of the cylinder. The coaxial return path was used to create uniform, symmetrical electric and magnetic fields on the LTO. The ratio of the radius of the return path to that of the LTO was 2.3, yielding a coaxial structure with a characteristic impedance of approximately 50 ohms. All tests were performed by injecting the current pulse into one end with the current exiting at the other end. Because of the symmetry of the structure, either end was suitable for the entry or exit point.

Generator and Measurement System. The generator, shown schematic form in Figure V-10, consisted of two banks of capacitors, with each having a capacitance of eight microfarads. Each capacitor bank can be charged to 100 kV, resulting in a 200 kV potential difference capability for the current pulse generator. For the AFIT research, three different current pulse waveforms were injected into the LTO. The first type of current pulse used was a unipolar, double exponential waveform with a

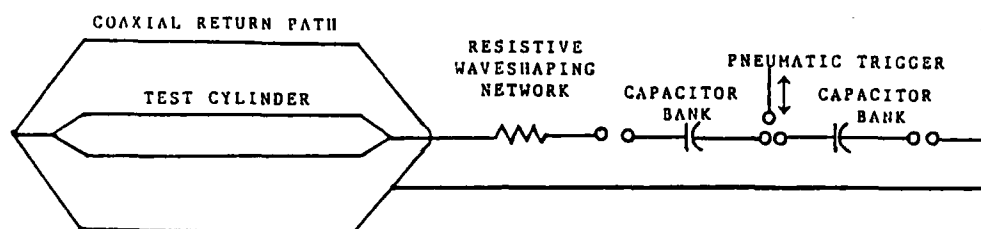


Figure V-10. Current Injection Test Setup for AFIT Current Injection Tests with LTO.

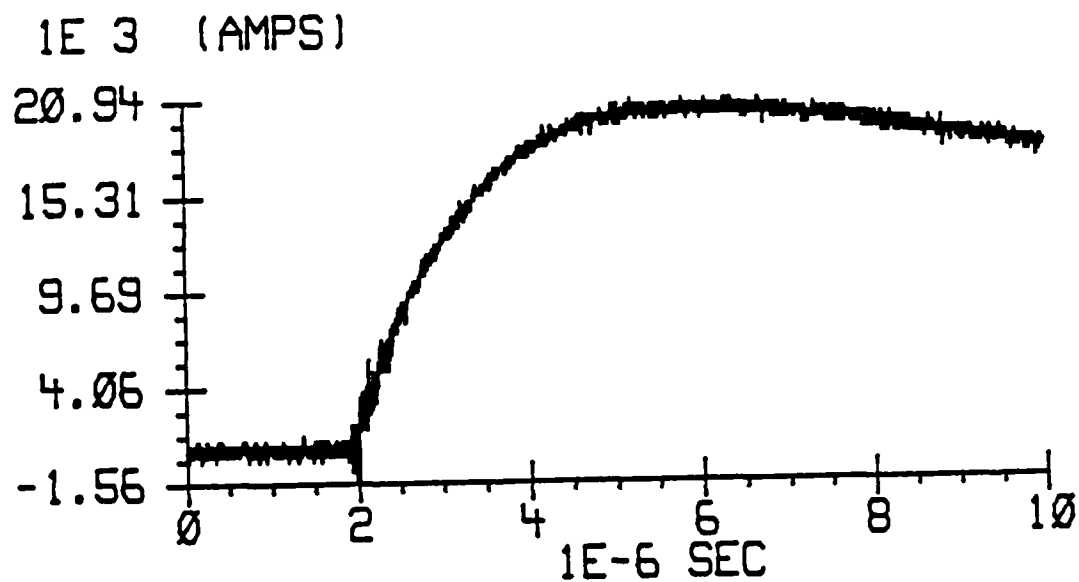
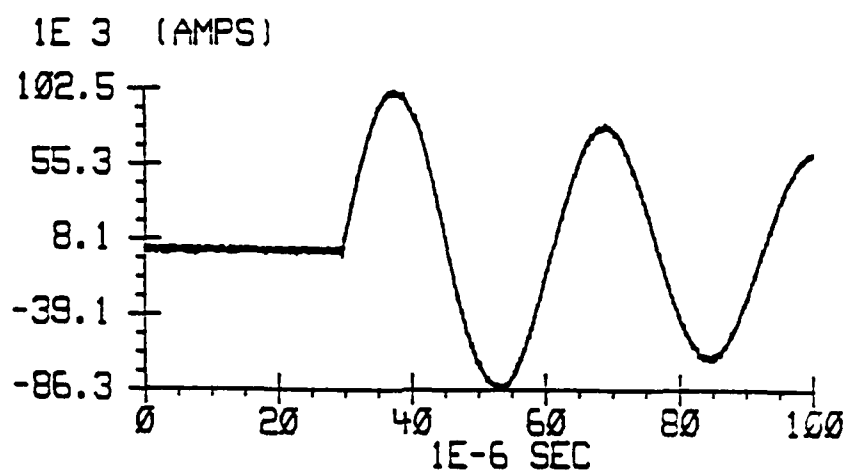


Figure V-11. Unipolar, Double-Exponential 20kA Current Waveform Used in AFIT Current Injection Tests.

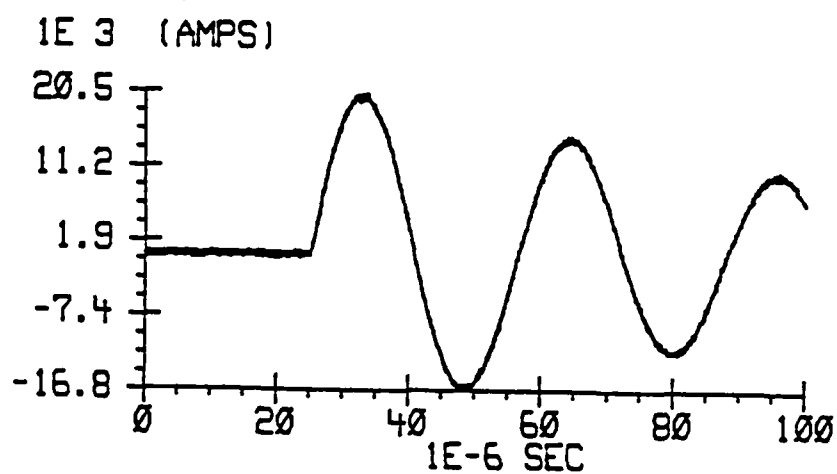
current peak of 20 kA. A typical waveform is shown in Figure V-11. This overdamped, unipolar, RLC-type of double exponential waveform was achieved by inserting a resistive network, totaling 5.5 ohms, into the test configuration between the generator output and the LTO.

The other two current pulse waveforms used were damped, oscillatory waveforms. The first oscillatory waveform had a peak value of 20 kA, to allow for comparison with the unipolar waveform. The second oscillatory waveform was meant to approximate a high-level threat waveform. To achieve the higher level of current for injection into the LTO, it was necessary to remove the waveshaping resistors from the generator. With the resistive network removed, an oscillatory current waveform with peak levels of 100 kA was achieved. Figure V-12a shows a typical 100 kA, damped, oscillatory waveform measured with a 100 microsecond window, while a typical lower level 20 kA, damped, oscillatory waveform is shown in Figure V-12b.

The current pulses were measured with a T&M current transformer located at the end opposite from where the current was injected. The current transformer represented a load of 0.005 ohms. In addition to the current measurement, external and internal field measurements around the cylinder were taken. The external magnetic



[a]

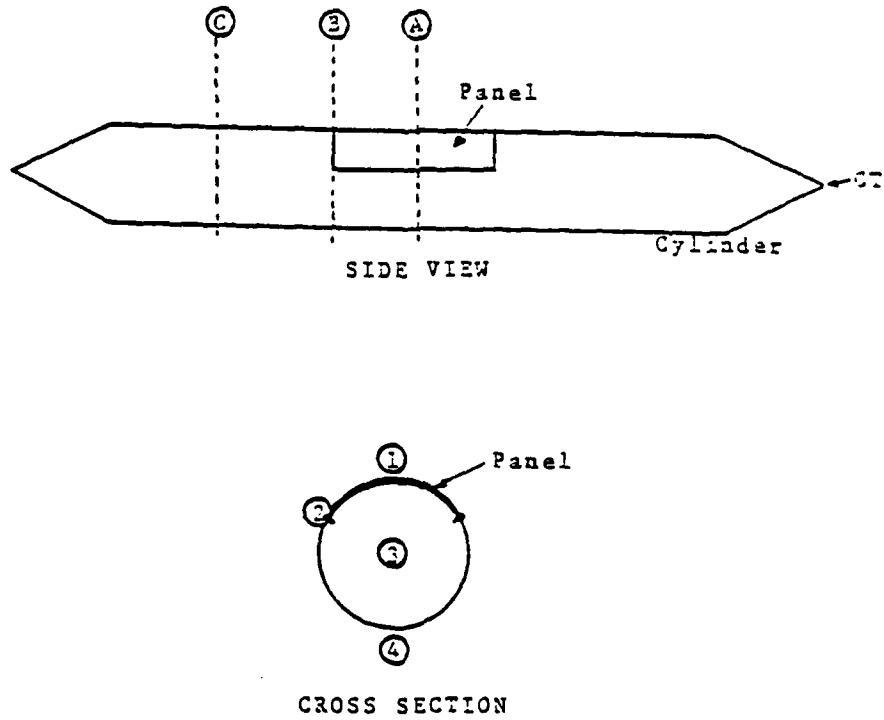


[b]

Figure V-12. Representative Oscillatory Current Waveforms.
(a) 100 kA Peak Current. (b) 20 kA Peak Current.

field measurements were made using the EG&G Cylindrical Moebius Loop (CML) B-dot sensor for the unipolar 20 kA current pulse test. For the oscillatory current waveforms, the external magnetic field measurements were made with the EG&G MGL B-dot sensor. The internal magnetic field measurements were taken with the CML B-dot sensor. External electric field measurements were made with the EG&G Asymptotic Conical Dipole (ACD) D-dot sensor, while internal electric field measurements were made with the EG&G Hollow Spherical Dipole (HSD) D-dot sensor. The specifications of the sensors used in this dissertation are given in Appendix I. The locations of the measurement sensors during the current injection tests are shown in Figure V-13.

The output of each sensor was fed into a fiber optic transmitter. After conversion of the electrical signals into optical signals, the output was sent to fiber optic receivers located in an electromagnetically shielded instrumentation room. The battery operated, pneumatically actuated fiber optic links were used to eliminate common mode interference and ground loop problems in the severe electromagnetic environment generated by the lightning simulation tests [Butters et al., 1981]. Four fiber optic channels were used, and the transmitters were shielded to reduce noise pickup. For each simulation set-up, noise checks were performed to insure that the transmitters were



<u>Sensor Locations</u>	
<u>D-dot</u>	<u>B-dot</u>
A1	A1
A2	A2
A3	A3
A4	A4
B1	B1
B2	B2
B3	B3
B4	B4
	C1
	C4

Figure V-13. Sensor Locations During Current Injection Tests.

not affected by any noise from surrounding sources of electromagnetic interference including radar, navigation and communication signals from a nearby active flight line.

After conversion back into electrical signals, the sensor responses were fed into two 2-channel Tektronix 7612D waveform digitizers. The digitizers, which were triggered by one of the sensors, were configured to read the data in 2048 samples, with a sampling interval of 5 nanoseconds. This provided a 10.24 microsecond data window with a frequency response of 100 MHz. This sampling rate was chosen to match the one used during the airborne lightning measurement program. The data from the digitizers were then read into a Digital Equipment Corporation PDP 11/34 computer and recorded on 9-track magnetic tape. The PDP 11/34 controlled the data acquisition and was used to perform data reduction. A block diagram of the data acquisition system is shown in Figure V-14.

Results. Figure V-15 shows a typical result for the overdamped, unipolar 20 kA current pulse. Shown is the input current, the external H-field and the transfer function for a sensor at location A1. For this measurement, the LTO was configured with a solid panel in the aperture. A similar set of figures is shown in Figure

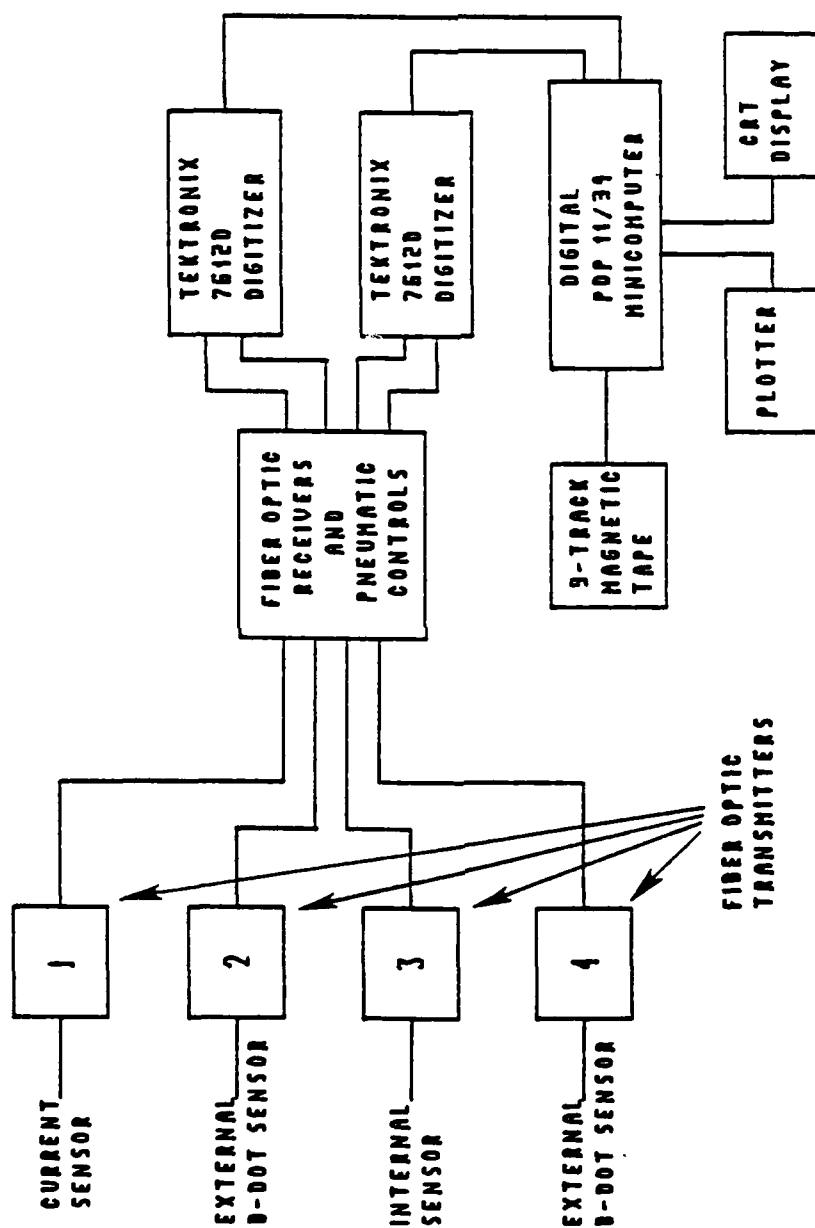


Figure V-14. Block Diagram of the Data Acquisition System Used During the AFIT Lightning Simulation Tests.

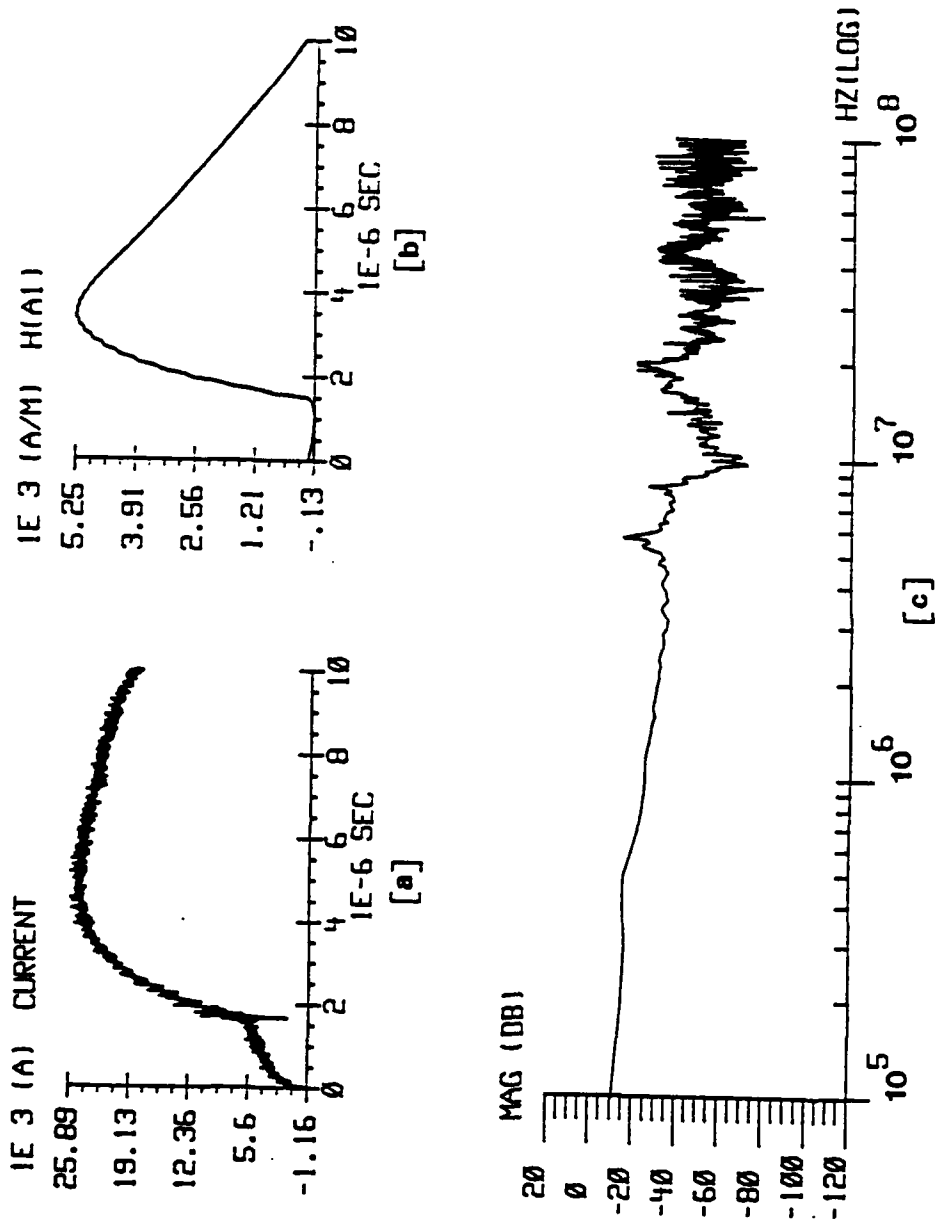


Figure V-15. 20 kA Unipolar Current Injection Data, Solid Panel.
 (a) Input Current Waveform. (b) External Magnetic Field.
 (c) Resulting Transfer Function.

V-16 for the same configuration with the E-field measured instead. In Figure V-17, the typical external H-field response at location A1 for the three waveforms used for current injection is shown. Figure V-18 shows the same results for the external E-field response.

The transfer functions of Figures V-15 and V-16 demonstrate the value of frequency domain analysis of lightning simulation data. They show frequency dependent activity not observable in the time domain current waveform. They also provides a better understanding of the interaction of the simulator and the simulator currents with the object under test. The electric and magnetic fields appear to be related by a constant, implying the system acts as if a transverse electromagnetic (TEM) wave is flowing through a two conductor structure.

This observation is also reinforced by the time domain signals depicted in Figures V-15 and V-16. Because the response follows the input waveform, we may assume that the LTO and return path set up a fairly uniform field configuration, which is to be expected for the coaxial system that is excited. Also, the external magnetic field responses of Figure V-17 follow the same waveshape of the injected current. This is due to the direct proportional relationship between the current and magnetic field on a

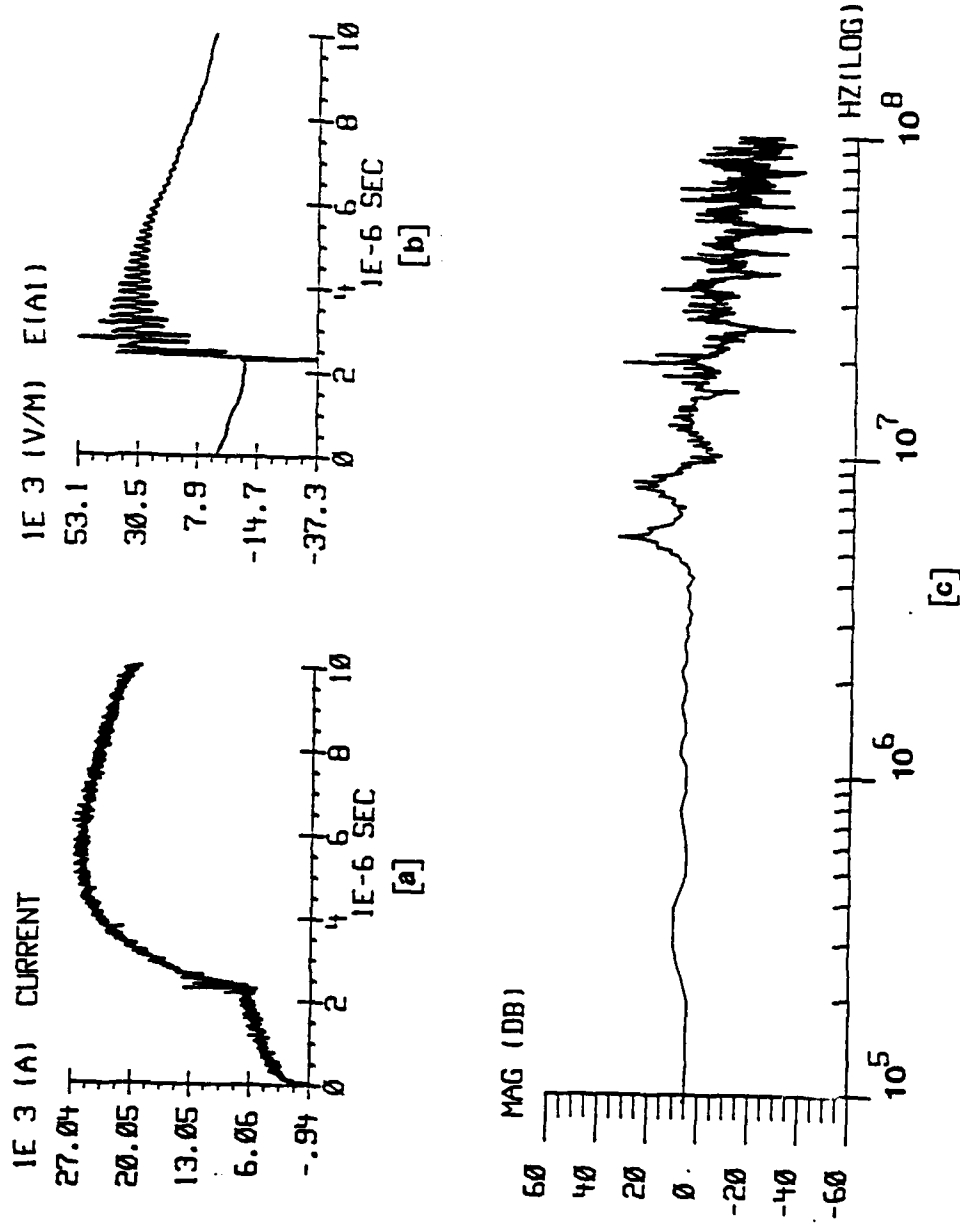


Figure V-16. 20 kA Unipolar Current Injection Data, Solid Panel.
 (a) Input Current Waveform. (b) External Electric Field.
 (c) Resulting Transfer Function.

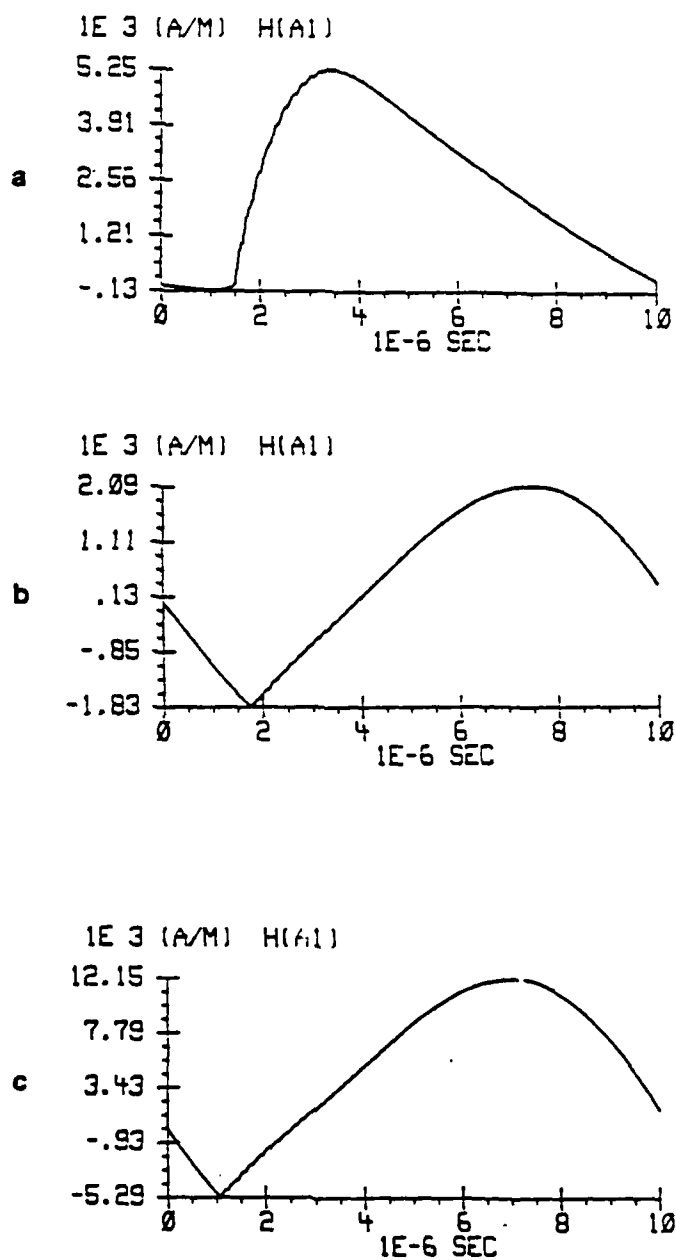


Figure V-17. External Magnetic Field Responses for Current Injection Tests, Solid Panel, Location A1. (a) 20 kA Unipolar Input. (b) 20 kA Oscillatory Input. (c) 100 kA Oscillatory Input.

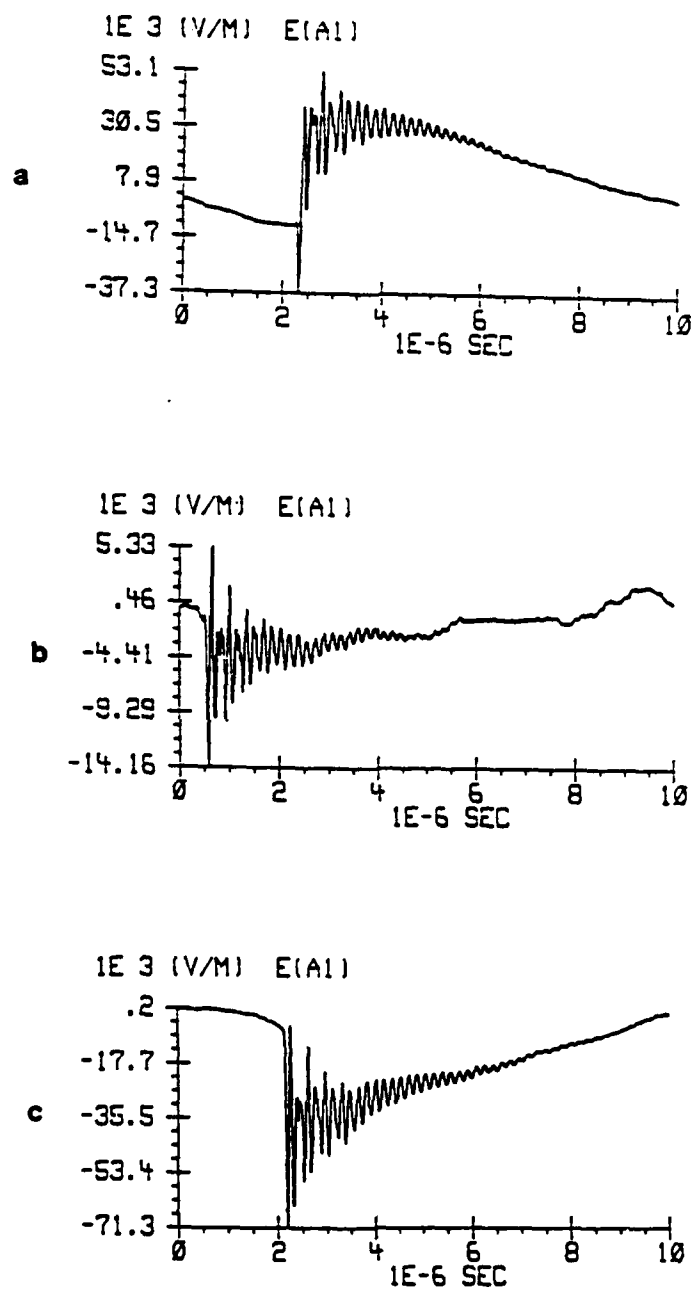


Figure V-18. External Electric Field Responses for Current Injection Tests, Solid Panel, Location A1.
 (a) 20 kA Unipolar Input. (b) 20 kA Oscillatory Input. (c) 100 kA Oscillatory Input.

cylindrical structure, best expressed as Ampere's law.

The voltage waveform in Figure V-16 and as well as those in V-17 show an interesting phenomenon. There is an initial voltage reversal in the unipolar waveform that is not displayed for the 20 kA and 100 kA oscillatory inputs. The only significant difference between these circuits is the absence or presence of the waveshaping resistors, resulting in the circuits being either underdamped or overdamped respectively. In both cases, the generator must be able to build up the voltage potential across the test object necessary to create a breakdown voltage across the gap. With no resistor, the current flows so fast, we may not see a current reversal if it happens. With the added waveshaping resistance, the process is slowed down and the reversal becomes evident.

While examining these figures, some initial observation can be made. There appears to be three distinct regions into which the test object and configuration interactions can be subdivided. These regions could be called the quasi-static region, transition region and the resonance region.

We can define the quasi-static region as that portion of the response where the configuration effects are negligible. In other words, below some characteristic

frequency the results are not dependent upon the return path, this being the major influence on the configuration effects. Because the majority of the energy is contained in the low frequency portion of the lightning spectrum, small changes in the measurement configuration will not affect the low frequency response, especially in terms of electric field coupling.

The transition region provides a bridge between the quasi-static and resonance regions. In this region the configuration effects are noticeable and the lumped circuit parameters of the generator, return path, test object, etc., dominate the response. In other words, the configuration effects can be characterized by the lumped circuit parameters of the measurement configuration.

In the resonant region, the configuration effects are dominated by the distributed parameters of the system. In this region, we would be more interested in the resonant lengths of the structures than the lumped parameters of those structures. Thus, the distributed nature of the test object and return path dominate, and traveling wave effects are important. For instance, if the return path is mesh instead of a solid conductor, there will be interaction between the measurement configuration and the surrounding environment as the frequency increases and the electric field penetrates the mesh.

In the remainder of this chapter we will use this taxonomy as a framework to characterize the interaction effects that are observed in the measured data. We will see that the results of the other experiments also show that this is a useful way to characterize the data obtained.

Swept-Frequency Continuous Wave Tests

This section describes three series of lightning simulation tests performed using the swept frequency continuous wave (SFCW) test method, and some of the results of those tests. The tests were performed on an Air Force UH-60A "Black Hawk" Rescue Helicopter, a Navy F-14A "Tomcat" Fighter, and the AFIT Lightning Test Object (LTO). The test, objectives of the test, test set-up and configuration, measurement system, measurements and results for each series using the SFCW test method are discussed.

The UH-60A Black Hawk SFCW Tests

General. These tests were performed by the Atmospheric Electricity Hazards Group, Flight Dynamics Laboratory, Air Force Wright Aeronautical Laboratories, Wright-Patterson AFB, Ohio, with Captain James L. Hebert as the principle investigator and project manager for the

tests, The tests were performed on an Air Force UH-60A "Black Hawk" rescue helicopter at the 655th Combined Aircraft Maintenance Hanger facility at Eglin AFB, Florida, during the last three weeks of October 1985.

Test Objective. The stated primary objective of these tests was to perform a limited assessment of the vulnerability of flight critical and mission critical equipment to lightning electromagnetic pulse (EMP) as baseline data for the development of helicopter lightning protection in the Atmospheric Electricity Hazards Protection Advanced Development Program (AEHP/ADP) [Hebert, 1985].

Test Set-up and Configuration. For this test, the helicopter was rolled onto Lexan and plywood pads consisting of one sheet of 3/4" plywood covered by one sheet of 1/8" Lexan to isolate the helicopter from the hanger floor. A wire mesh return path was configured around the helicopter at a distance of approximately three feet to produce an equivalent 50 ohm lumped impedance at the inputs (Figure IV-16). The helicopter was tested in two strike configurations. The entry attachment points were direct connections to either the main rotor hub or the rear rotor hub. The exit point was the two main wheels.

Generator and Measurement System. The SFCW generator and measurement system for the UH-60 test is shown in Figure V-19. The Hewlett-Packard (HP) 3577A Network Analyzer was housed inside a double-walled copper shielded enclosure. The analyzer produce a signal which was swept from 100 Hz to 100 MHz in discrete increments. The signal was amplified to approximately 25 watts and this low level signal was injected into the entry points. The input signal was monitored at the entry point by a current transformer sensor whose signal was converted to an optical signal and transmitted back to the analyzer via a fiber optic link. The resulting transient voltages and currents on the helicopter's electronic circuits were measured by a breakout box as shown in Figure V-20. This breakout box was inserted at the input connector of flight critical avionics boxes such as the Signal Data Converter and Flight Computer. The transients measured were converted to optical signals and transmitted back to the network analyzer by a second fiber optic link. The data from eight separate sweeps was averaged and then stored. This data was transmitted via an IEEE 488 data bus to a Digital Equipment Corporation (DEC) PDP 11/34 computer in a specially instrumented test van for processing and storage. A noise measurement with no signal injected was made and stored for each test point.

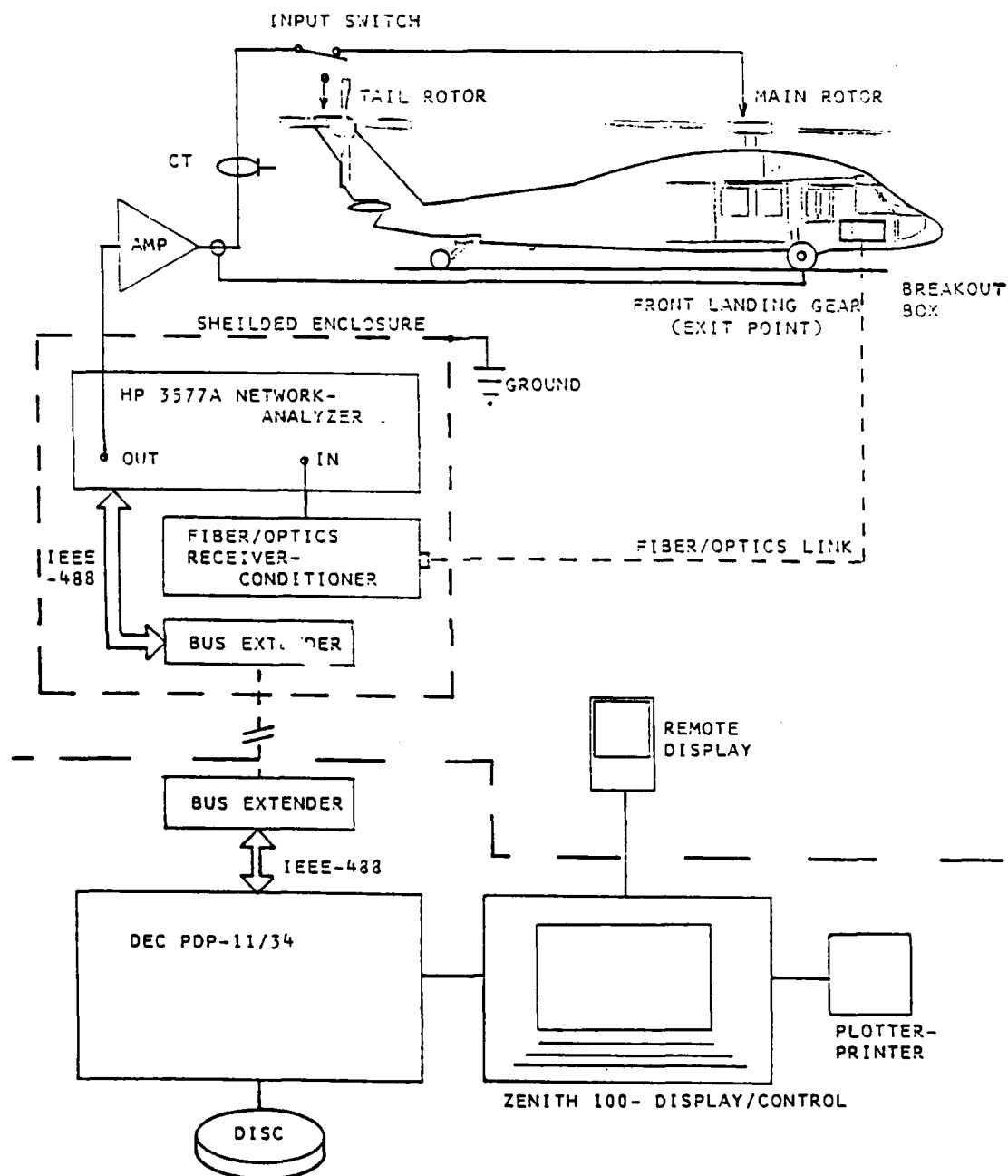


Figure V-19. Measurement System Used for the UH-60A SFCW Tests.
[Hebert, 1985].

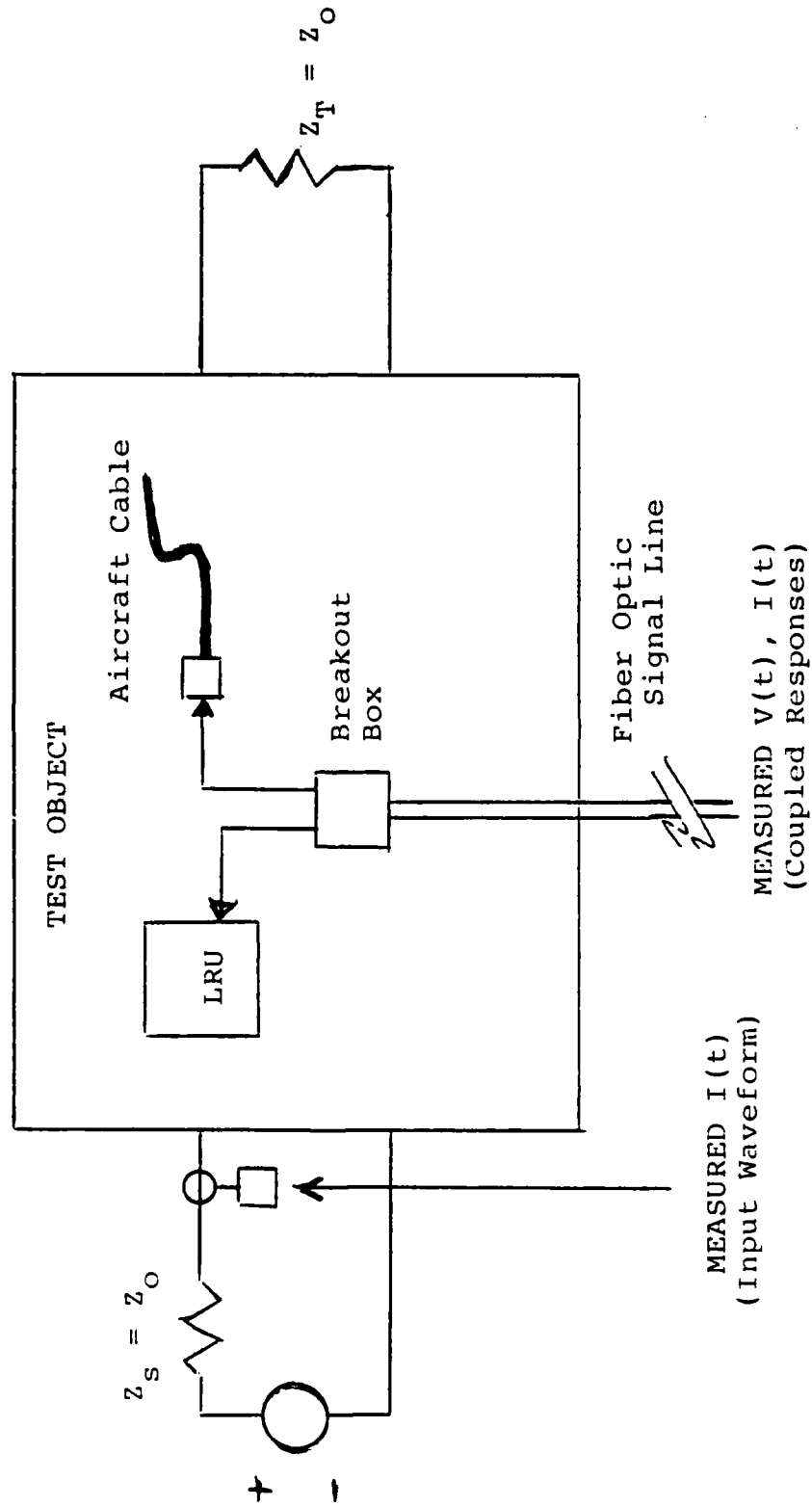


Figure V-20. Typical Measurement Setup for the UH-60A Tests.

Test Data Processing. The transfer functions of the breakout box, including the voltage probe, current probe, current transformer and the fiber optic links were measured (each measurement being the average of eight sweeps) and are presented in Figure V-21. As can be seen, each of these components has relatively flat transfer functions between 200 Hz and 50 MHz. The voltage and current breakout box has amplification as was shown by the positive 20-40 dB levels. These transfer functions are divided out of each circuit transient measurement transfer function formed by dividing the response by the input. The next stage of data processing is depicted in Figures V-22 and V-23. The signal response transfer function is compared to the noise level for each shot. That part of the transfer function where the signal exceeds the noise floor by at least 10 dB is retained for further processing. The logarithmically recorded signal is converted to linear points via simple interpolation and a boxcar filter is applied to provide data points which could be easily transformed via Discrete Fourier Transforms (DFT). The signals were measured in two ranges, from 400 Hz to 1 MHz and from 48 kHz to 100 MHz. The transfer function is inverse Fourier transformed into the time domain and then is convolved with the lightning threat defined by MIL-STD-1757 to determine the circuit's predicted response to that threat waveform. The resulting linearly extrapolated full severe threat induced

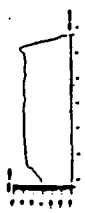

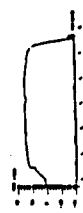

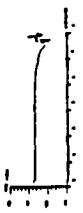
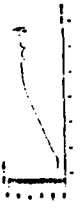
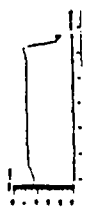
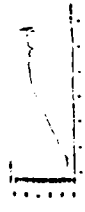
ITEM	CHARACTERISTICS	STORAGE REGISTERS	
BREAKOUT- BOX - VOLTAGE	 (BOBE)	D2 - I (S)	 APPLIED CURRENT SIGNAL (UNI)
BREAKOUT- BOX - CURRENT	 (BOBI)	(CURRENT SOURCE)	 CT
CURRENT TRANSFORMER	 (CT)	D3 - I (S) x BOBI	 I (S)
FIBER / OPTIC	 (F/O)	D4 - I (S) x BOBE	 F/O

Figure V-21. Representative Transfer Functions of Major UH-60A Measurement Components. [Hebert, 1985].

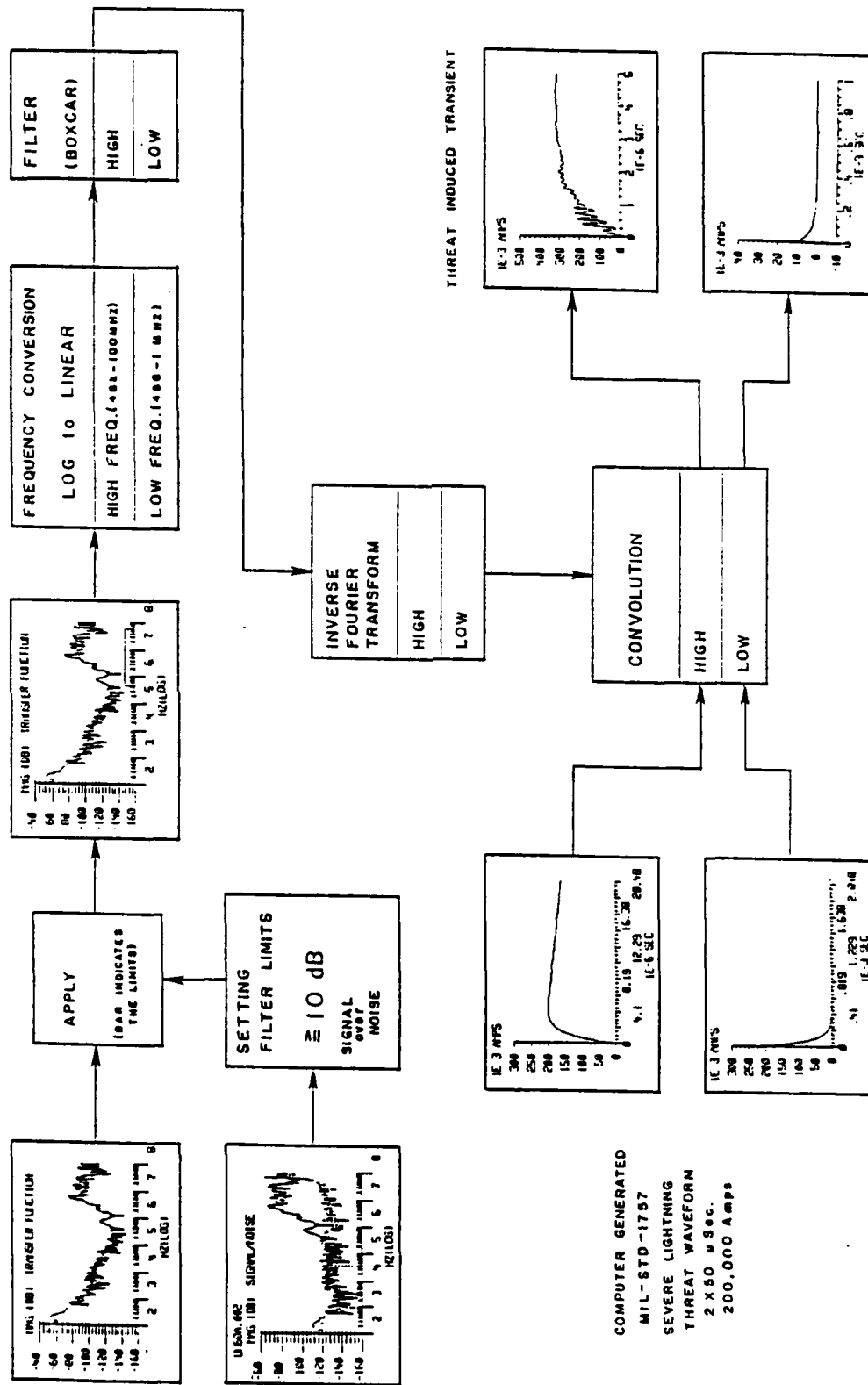


Figure V-22. Measured Transfer Functions Resulting From the Application of The Threat Waveform to the UH-60A. [Hebert, 1985].

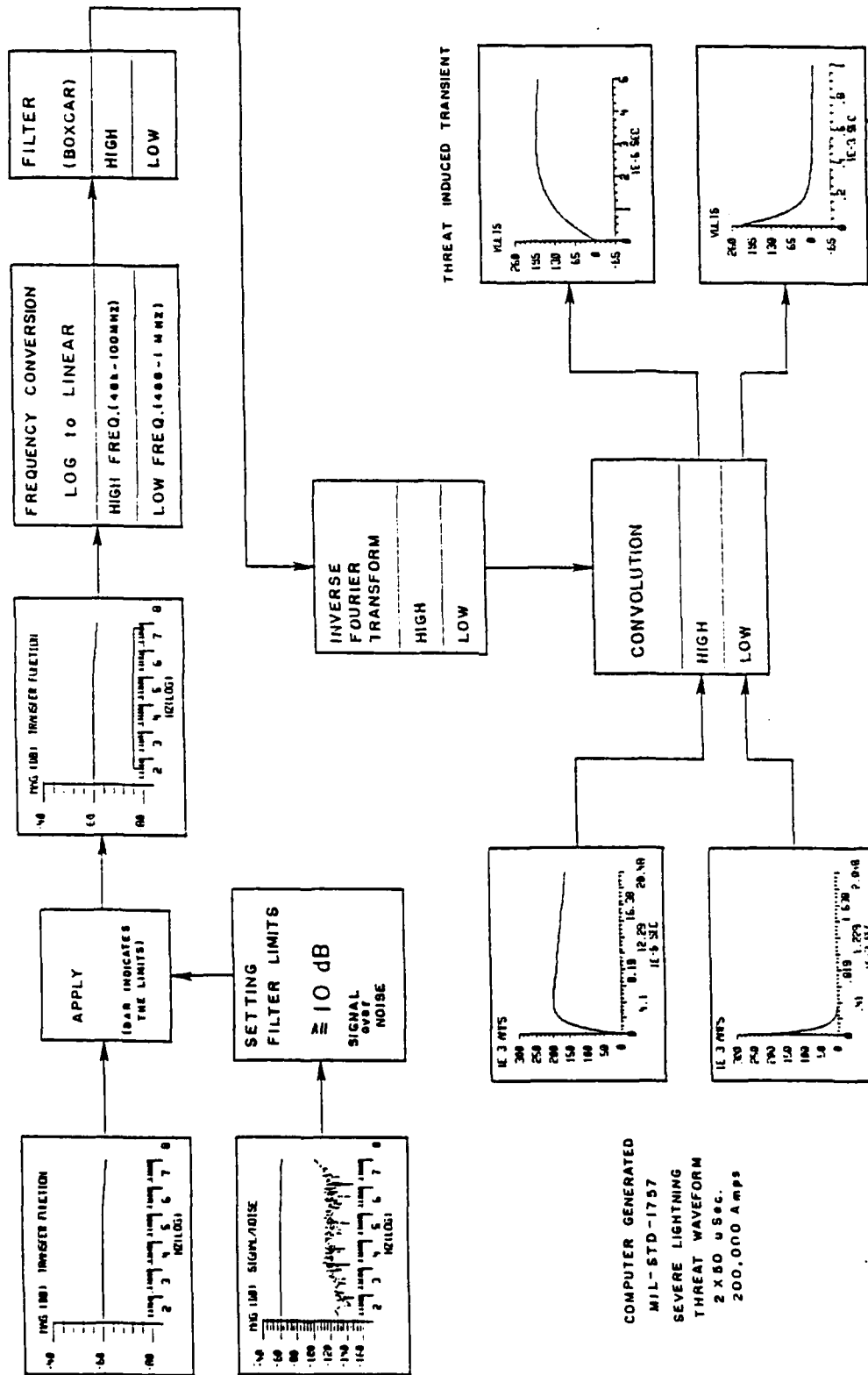


Figure V-23. Measured Transfer Functions Resulting From the Application of the Threat Waveform to Measurement System Only. [Hebert, 1985].

transients are then plotted. The data processing system was verified as shown in Figure V-23. The flat transfer function which is more than 10 dB higher than the noise level should reproduce the threat waveform and it does.

Results. The transfer functions and resulting predicted induced avionics circuit transients from the UH-60A SFCW tests display phenomena which would be expected on an aircraft with rather large apertures and long unshielded cable runs.

Figures V-24 through V-27 show actual transfer functions measured during these tests on two avionics circuits: the voltage transient on pin S of the J215 connector on the Generator Control Unit (GCU) measured with respect to signal ground; and the voltage transient on pin 52 of the J117 connector on the Caution Advisory Panel (CAP) measured with respect to the Line Replaceable Unit's (LRU's) ground [Hebert, 1987]. (Note: Most avionics "boxes" on the UH-60A and most aircraft are LRU's so they can be easily switched out on the flight line.) The transfer functions for each of these circuits is presented for two test configurations: entry at the main rotor and exit at the main landing wheels; and entry at the tail rotor and exit at the main landing wheel. These transfer functions and the resulting predicted voltage transients with respect to the defined MIL-STD-1757A

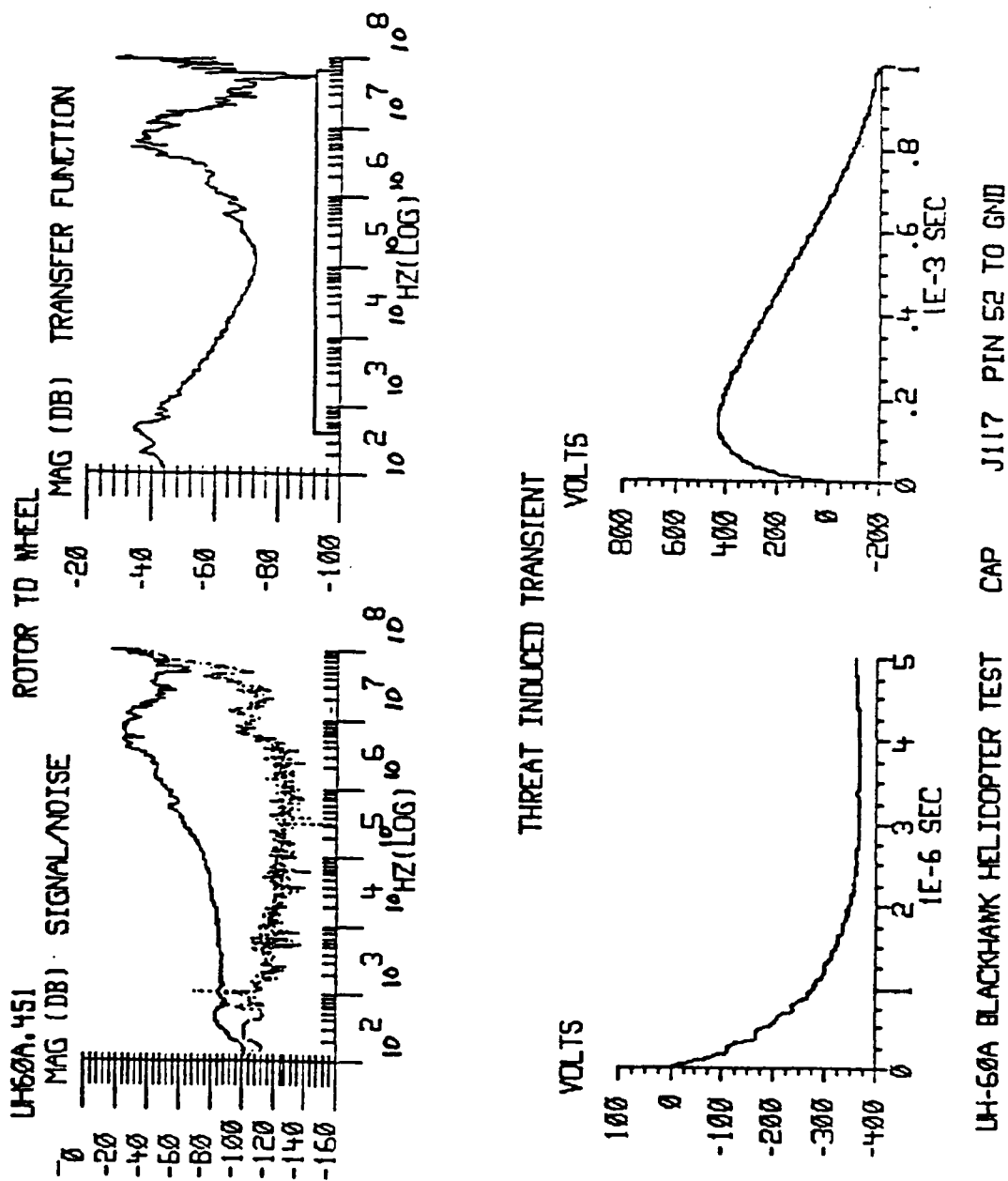
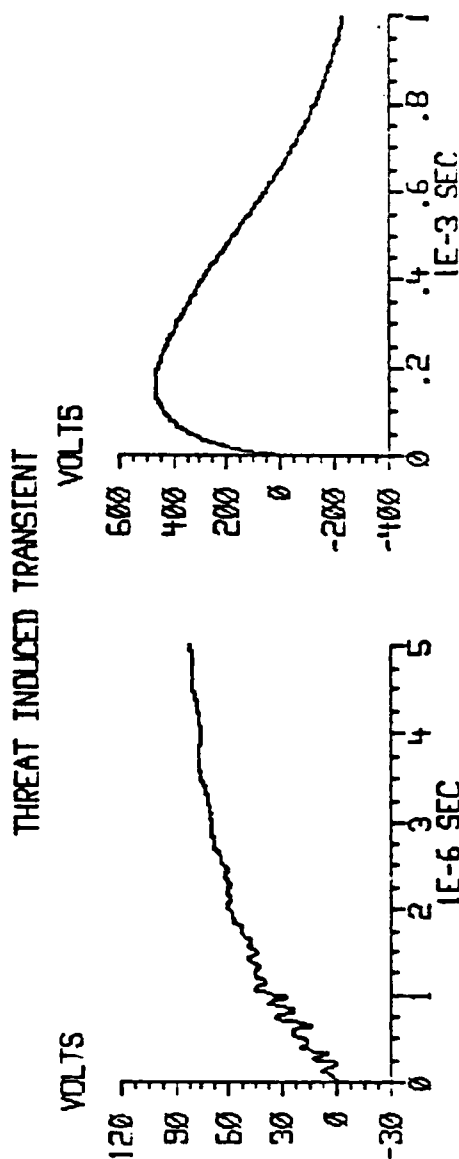
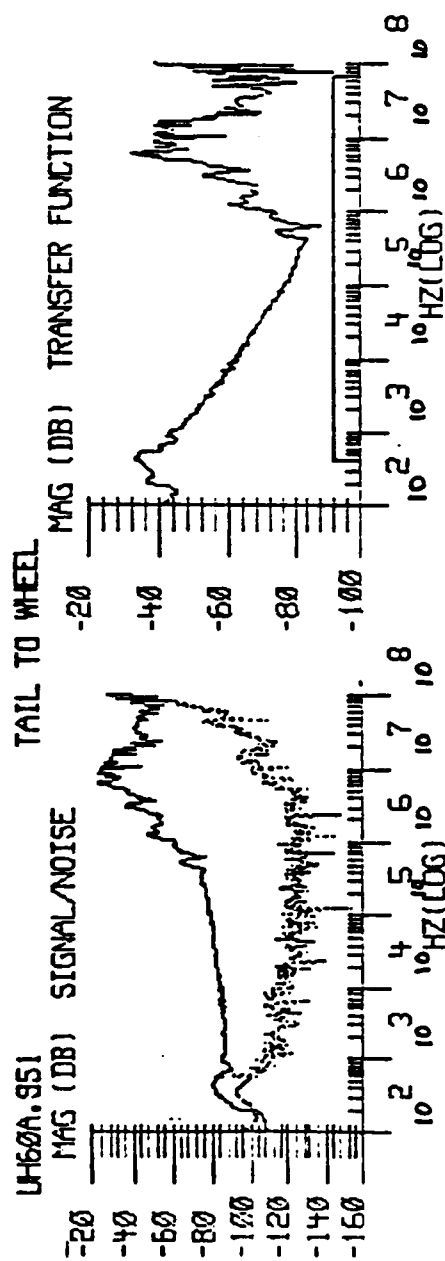
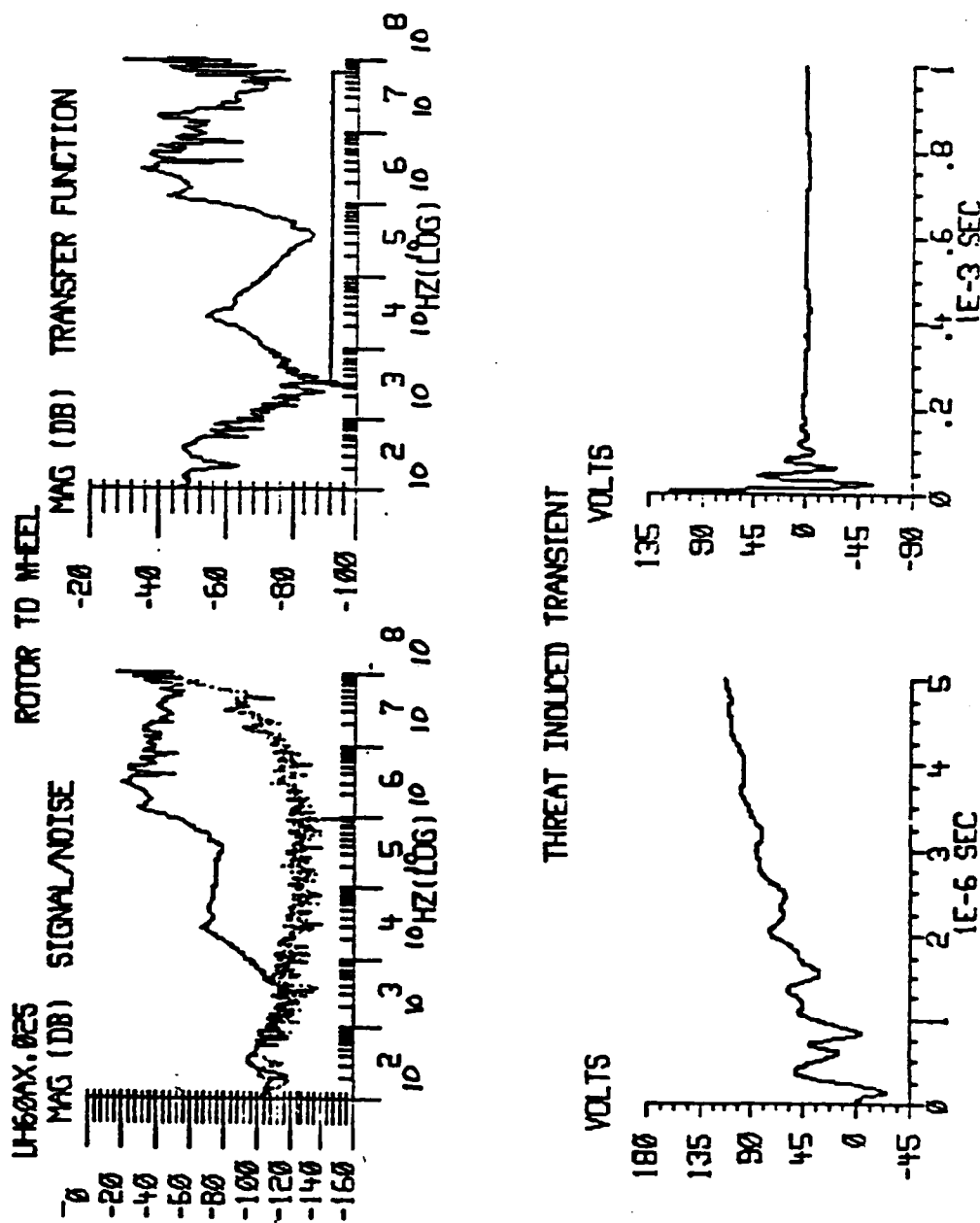


Figure V-24. Transfer Function From UH-60A SFCW Tests - Simulated Rotor-to-Wheel Strike Measured at CAP. [Hebert, 1985].



UH-60A BLACKHAWK HELICOPTER TEST CAP J117 PIN 52 TO GND

Figure V-25. Transfer Function From UH-60A SFCW Tests - Simulated Tail-to-Wheel Strike Measured at CAP. [Hebert, 1985].



UH-60A BLACK HAWK HELICOPTER TEST GCU J215 PIN 5 TO GND

Figure V-26. Transfer Function From UH-60A SFCW Tests - Simulated Rotor-to-Wheel Strike Measured at GCU. [Hebert, 1985].

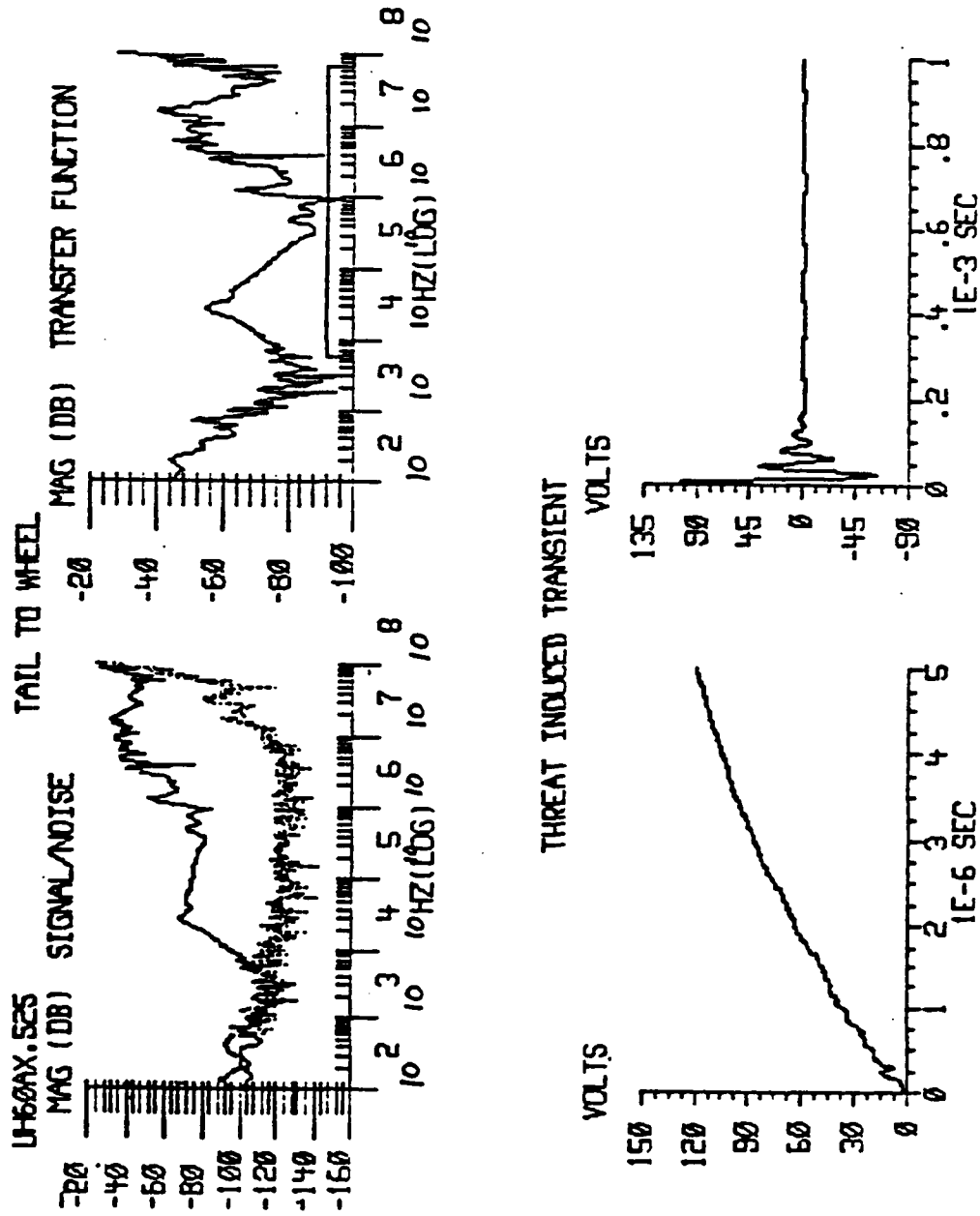


Figure V-27. Transfer Function From UH-60A SFCW Tests - Simulated Tail-to-Wheel Strike Measured at GCU. [Hebert, 1985].

threat waveform presented in Figure V-28 are discussed separately and then compared.

(1) Tests UH60A.451 and UH60A.951 show the transfer functions for pin 52 of the J117 connector on the CAP measured with respect to ground in the main rotor to main landing wheel (Figure V-24) and tail rotor to main landing wheel (Figure V-25) configuration respectively. The CAP is located on the instrument display panel of the UH-60A (co-pilot side). The CAP indicates unsafe engine conditions and/or malfunctions and various lighted indicators on this panel stay lit as long as the unsafe condition exists. Pin 52 displays the signal which monitors the oil temperature on the number two engine. The cables for this circuit run from the CAP through the helicopter along the walls to the top of the UH-60A and connects to the oil temperature sensor on the number two engine.

(a) Main rotor to wheel - In this configuration the circuit shows a relatively flat transfer function (Figure V-24) with an average magnitude at about -50 dB. There is rather significant coupling to this circuit in both the low frequency (< 1 MHz) and the high frequency (> 1 MHz) regions which might be expected because this circuit, which has little shielding, exits to the exterior of the aircraft, and is subjected to direct coupling as well as

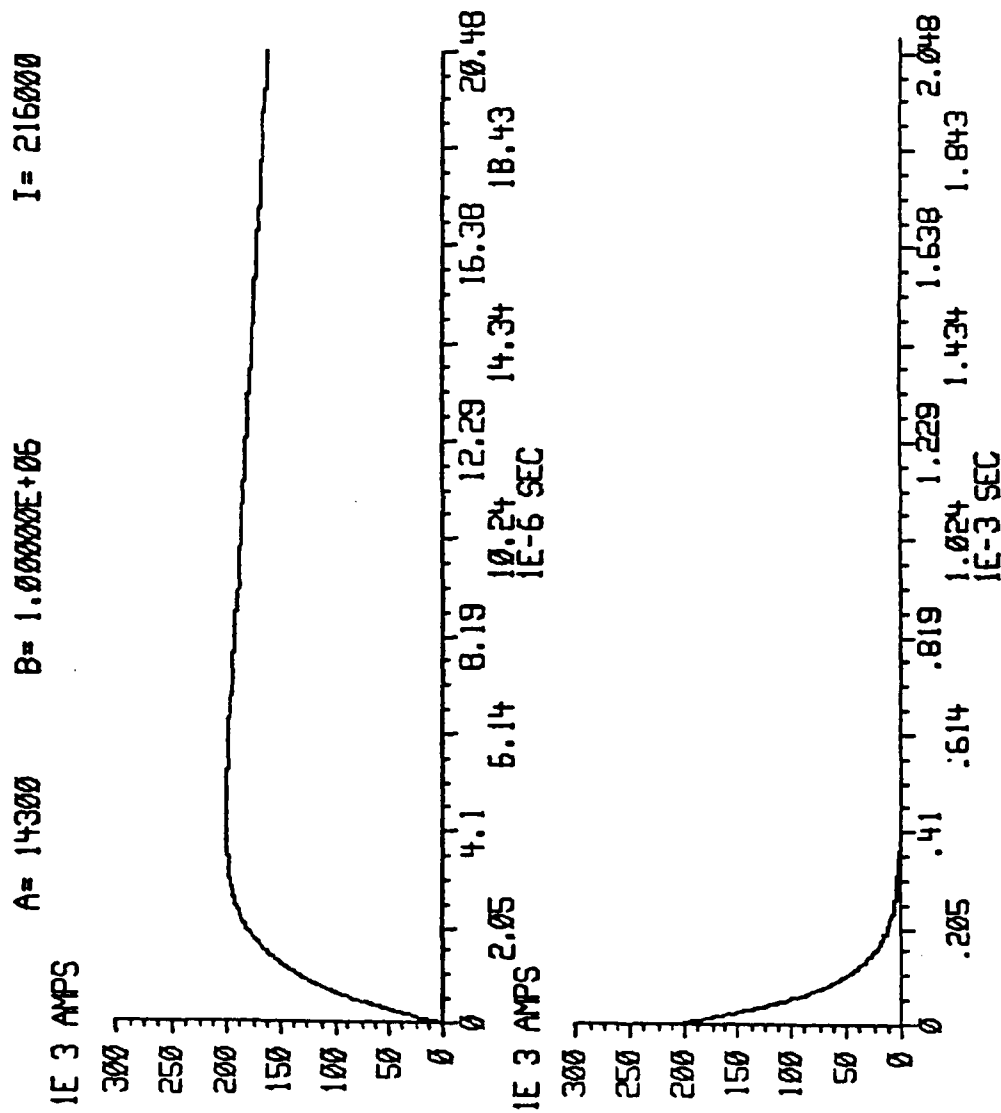


Figure V-28. Defined MIL-STD-1757A Threat Waveform Used in UH-60A SFCW Tests. [Hebert, 1985].

aperture coupling. The direct coupling follows the input closely, and appears to be related to what we would expect from the quasi-static region. Aperture coupling, however, is related to the voltage and current time derivatives (ie. dv/dt and di/dt). Therefore, this coupling is frequency dependent and is the type that would be expected to dominate in the resonance region. Thus, we see that the waveform can be broken up into three regions.

The transient that results from the input waveform is rather high (475 Volts Peak) and is a fairly good copy of the threat waveform. This was expected because of the flat transfer function. In the quasi-static and transition region and because much of the waveform's energy is concentrated in the lower frequency region, and the configuration plays a small part in the coupling process in the structure. In the resonance region, the coupling is dominated by the time derivatives and is greatly affected by the configuration.

(b) Tail rotor to wheel - The transfer function for this configuration (Figure V-25) is basically the same as in the main rotor to wheel configuration except in the range of 70 kHz to 5 MHz, where the tail rotor to wheel configuration displays less coupling than the main rotor to wheel. This is probably due to the redistribution of currents on the aircraft. This circuit is very near to

the direct path between the main rotor and wheel, allowing more direct coupling in the area of the top of the UH-60A. In the tail to wheel configuration the currents have more opportunity to redistribute on the lower portions of the fuselage. The high frequency regions of transfer function (> 5 MHz) are very similar because the resonances set up on the the helicopter due to the aircraft and return path configuration and the apertures are identical for both tests; only the entry points differ. The low frequency regions are also similar. This results in induced transients which are similar.

(2) Tests UH60AX.025 and UH60AX.525 show the transfer functions for pin S of the J215 connector on the UH-60's number one GCU. They were measured with respect to the CRU's signal ground in the main rotor to wheel and tail rotor configurations respectively. This generator control unit is located behind the sound proofing panel and is bolted to the top bulkhead over the pilots head inside the aircraft. The GCU controls the UH-60A's number one electric generator (connected to the number one engine) and provides proper power to the UH-60A. This circuit runs along the top bulkhead and exits in a relatively short cable direct to the generator.

(a) Main rotor to wheel - In this test configuration the transfer function (Figure V-26) shows distinctive

regions of frequencies where coupling is more significant than others. A significant region is centered at about 25 kHz. The transfer function drops off as the frequency increases, until about 1 MHz, where it increases to levels on the same order as were measured on the CAP circuit. This circuit shows less coupling in the lower frequency region (< 1 MHz) and more coupling at frequencies in the higher region. This suggests that this circuit experiences less direct (external) coupling than that of the CAP, but more indirect coupling at the higher frequencies (> 1 MHz) due to aperture, joint or diffusion coupling.

(b) Tail rotor to wheel - This configuration shows the same distinctive region of coupling centered at about 25 kHz, but far less coupling in the region of 1 to 4 MHz (See Figure V-27). With all configurations the same, these differences are directly attributed to the difference in the entry points, main rotor or tail rotor, and the resulting differences in the manner in which the currents redistribute on the UH-60A with respect to the circuit cables and apertures.

Since 1 MHz corresponds to a full wavelength of 300 meters, $1/2$ wavelength of 150 meters and $1/4$ wavelength of 75 meters, it is doubtful that much coupling in the region below 1 MHz is due to resonant activity. However, 10 MHz

corresponds to a full wavelength of 30 meters, $1/2$ wavelength of 15 meters and $1/4$ wavelength of 7.5 meters, and the coupling above this frequency may logically be attributed to frequency dependent resonances. In the region where direct coupling would seem to dominate, below 10 MHz, any frequencies which couple into the circuit are of particular significance because of the level of energy the threat possesses in this frequency region. The high frequency coupling displayed by all four transfer functions is of particular concern in the threat regions of electromagnetic activity due to nuclear electromagnetic pulse (NEMP), electromagnetic compatibility (EMC) and electromagnetic interference (EMI).

In all cases the configuration effects due to the differences in entry point is well displayed. Both of the circuits experienced enhanced coupling in the 1 to 4 MHz range when the circuit was near the direct path between the main rotor and wheel. Less coupling was measured when the circuits were out of the direct path between the entry and exit points (tail to wheel configuration). In the tail to wheel tests the currents had to redistribute to the top of the UH-60A, whereas in the rotor to wheel test the currents were injected near the circuit's physical location.

The UH-60A tests dramatically demonstrate the effects of the configuration in the various stages of the interaction process described in Chapter III. Not only does the generator and return path influence the re-distribution of the external fields on the helicopter, but the actual configuration of the apertures and circuit path locations also add to the complexity of the interaction process.

The Boeing F-14A SFCW Tests

General. The Boeing Aircraft Company has made extensive use of the SFCW test method in lightning simulation and qualification tests for the military and the Federal Aviation Administration (FAA). These tests have been performed on: an F-16 composite forward fuselage and an F-14A fighter aircraft as a part of the Air Force's Atmospheric Electricity Hazards Protection/Advanced Development Program (AEHP/ADP); an F-18 aircraft for the Navy/Defense Nuclear Agency (DNA) FFLASH program; and for the lightning qualification tests on the 747, 757 and 767 commercial airliners as required by the FAA. This section will only discuss tests performed on the Navy F-14 aircraft.

Test Objective. This section discusses tests performed on a Navy F-14A aircraft as part of the Air Force's AEHP/ADP and results from those tests [Whalen, 1986; Whalen and Simpson, 1987]. These tests were performed to evaluate and recommend lightning protection, design, analysis, specification and qualification test techniques.

Test Set-up and Configuration. The F-14A fighter aircraft was placed on jackstands constructed of Permalloy and Lexan sheets to position the aircraft well above the flat plate return path placed on the hanger floor. The remainder of the return path consisted of poultry netting (chicken wire) placed above the aircraft as shown in Figures IV-17a and IV-17b. This presented a parallel return path arrangement above and below the aircraft. The aircraft was tested in two configurations: nose-to-tail and nose-to-wing. The return path configuration presented a lumped drive impedance of about 12 microhenries.

Generator and Measurement System. The Boeing SFCW generator and measurement system is presented in Figure V-29. This system is very similar to that presented in the UH-60A section above, but differs by the use of two network analyzers. An HP 8505A was used to cover low frequency ranges and an HP 3570A was used to cover the higher frequency ranges, while a single analyzer was used

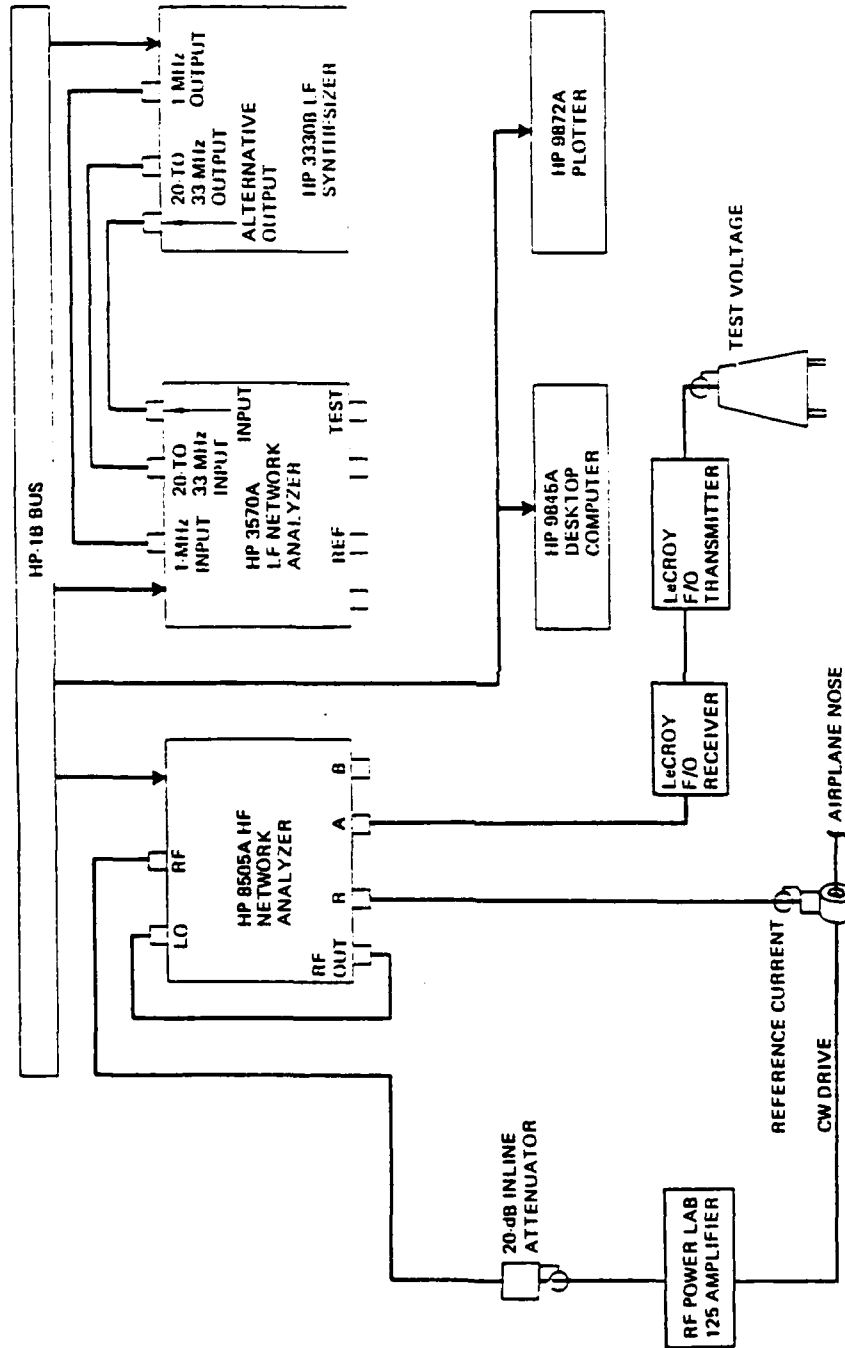


Figure V-29. Boeing Generator and Measurement System Used for the F-14A SFCW Tests. [Whalen and Simpson, 1987].

for the helicopter tests. The Boeing system uses an HP 9845A computer instead of a PDP 11/34. The test methodology and measurements to form the transfer functions are very similar. The Boeing report referenced above also presents a comparison of the predicted SFCW transient responses to a moderate and full lightning threat waveform. The moderate threat waveform (28 kA) was produced by the Boeing moderate threat level lightning simulation generator. This generator is a Marx bank with an electrical crowbar. The full threat tests were performed using the AEHP/ADP's 200 kA full threat lightning simulation generator. This generator is a Marx bank with a high energy laser crowbar and is one of the two generators in the world capable of injecting the MIL-STD-1757A 200 kA current threat waveform into a full sized aircraft. The current pulse characteristics of these generators are presented in Table V-1.

Table V-1. Current Pulse Characteristics.

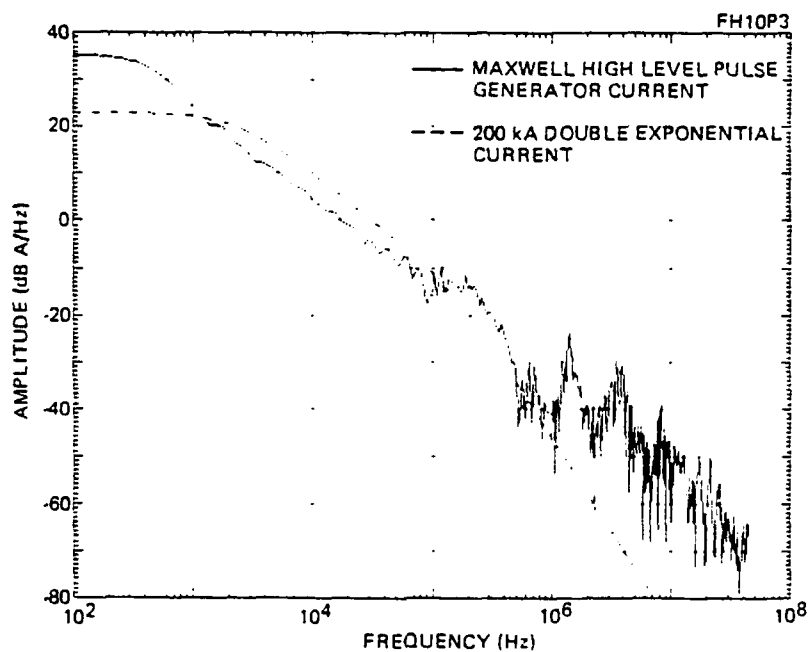
Parameter	Moderate	High
Peak Current (kA)	28	200
Rate of Rise (10%-90%) (A/sec)	3×10^{10}	1.7×10^{11}
Time to Half Value (10^{-6} sec)	80	40
Action Integral (A^2 -sec)	3.5×10^4	2.5×10^6

Test Data Processing. The transfer functions for test points on the F-14A were measured as responses

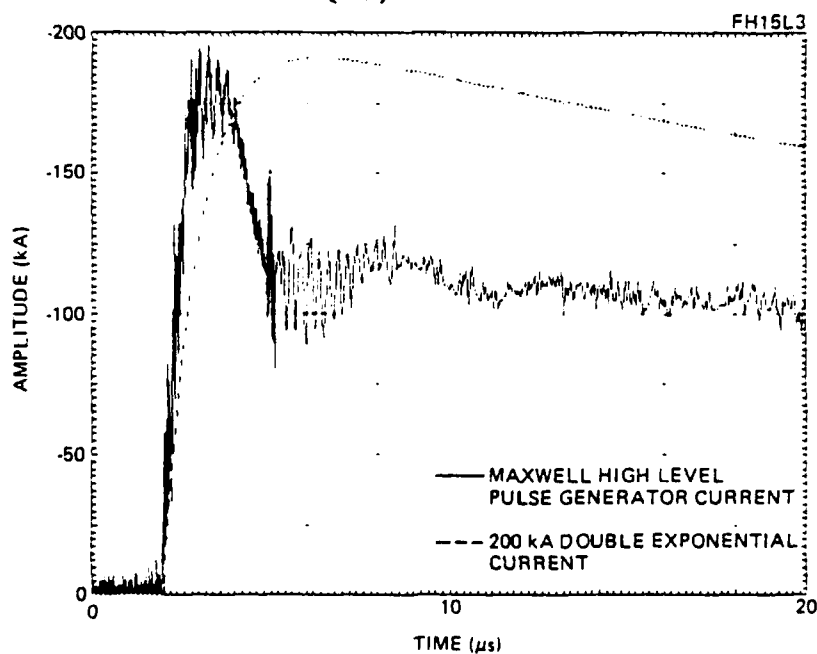
relative to the drive input current at the nose of the F-14A in a manner similar to the UH-60A data, except the transfer function was estimated in the regions below 1 kHz where there was less than 10 dB of separation between the signal and noise. This estimate was extrapolated from the trend of the magnitude and phase above 1 kHz [Whalen, 1986]. The measured responses were corrected to compensate for sensor and reference current variations through the use of a Fourier transform program.

Like the UH-60A tests, the transient responses were calculated/predicted for the severe threat level and for the moderate threat level waveform inputs. The Boeing SFCW test results are significant because in these tests the predicted SFCW transfer function extrapolated predicted responses are compared with actual impulse responses produced by injecting a moderate level 28 kA current waveform.

Results. (a) Source Waveforms. Figure V-30 shows the high level current pulse frequency spectra and waveform as it compares to the defined MIL-STD-1757A 200kA waveform. These waveforms show that although the time domain waveforms differ somewhat, the frequency characteristics are very similar in the region below 1 MHz, where the majority of the threat waveform's energy is located.



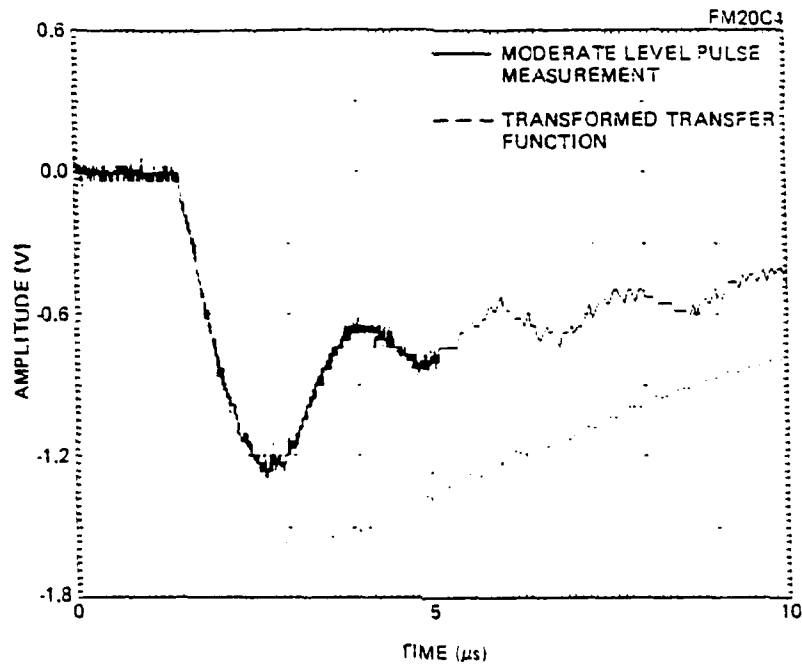
(a)



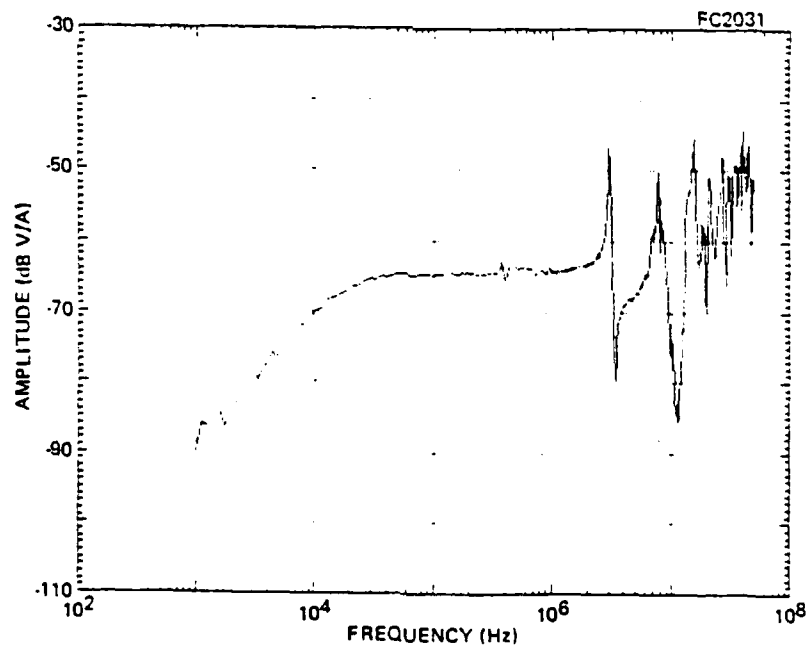
(b)

Figure V-30. Excitation source for the Boeing F-14A SFCW Tests.
 (a) High-Level Current Pulse Spectra.
 (b) High-Level Current Pulse Waveform.
 [Whalen and Simpson, 1987].

(b) Internal Field Measurements. Figure V-31 shows the results of internal field measurements made under a graphite-epoxy panel (Panel 1222-2) located over an avionics bay in the front section of the F-14A. Figure V-31a shows that the output voltage of the loop probe is proportional to the drive current. Figure V-31a also shows a comparison of the response predicted using this transfer function to that actually measured when injected by the moderate threat level signal. Figure V-31b shows the transfer function of the electric field sensor which was placed under the graphite-epoxy panel. The transfer function shows considerably better shielding is provided inside the equipment bay than was afforded by the helicopter. This is because the helicopter circuits were exposed to both direct coupling and significant aperture coupling. The graphite epoxy panel completely covers the F-14A's equipment bay, providing a shielded enclosure. There is, however, rather high coupling at distinct frequencies at 2 MHz and above. The coupling at these frequencies is probably due to aperture and slot coupling, diffusion and structural voltage drops across the graphite-epoxy panel. The actual impulse signal is lower than that which was predicted by the convolution of the moderate threat level signal with the SFCW derived transfer function.



(a)



(b)

Figure V-31. Results of Measurements Made Under a Graphite-Epoxy Panel on the F-14A. (a) Measured Field Probe Voltage. (b) Transfer Function of the Measured Field Probe Voltage. [Whalen and Simpson, 1987].

(c) Structural Voltage Measurements. Figure V-32 shows a comparison of the structural voltage drop across a graphite-epoxy panel (Panel 1222-2) over an avionics equipment bay in the front of the F-14A. Again the predicted induced voltages are higher than that which were actually measured. The predicted voltage waveform would have resulted if the transfer function was fairly flat, as it directly follows the input moderate threat waveform. The actual measurements show that the panel actually influences the skin current distribution; the higher resistivity of the panel at lower frequencies causes the currents to partially by-pass the panel and flow on the aluminum skin of the fuselage. The lower frequency components of the waveforms are not on the panel and do not induce the lower frequency responses predicted by the extrapolated transform. Thus, the graphite-epoxy panel has a low magnetic field shielding effectiveness at low frequencies, with the shielding effectiveness increasing with frequency.

(d) Figure V-33 shows the comparison for the voltage transient predicted and measured on the FCSE throttle actuator wire, a test circuit placed inside the F-14A. Although the waveforms are similar in magnitude, the phase and magnitudes at various frequencies vary significantly. The predicted waveform is fairly well-behaved showing responses at distinct frequencies. The actual measured

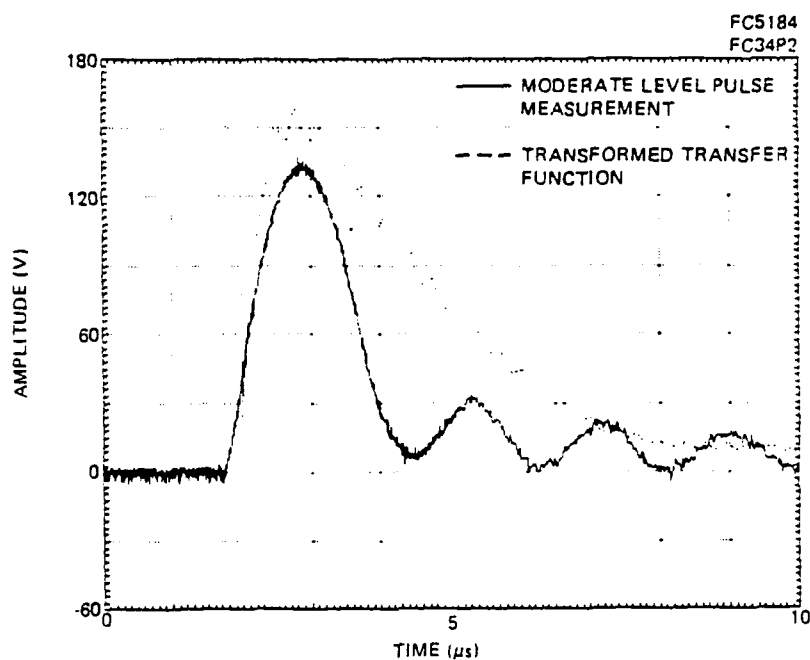


Figure V-32. Predicted Versus Measured Voltage Drop Across a Graphite-Epoxy Panel. [Whalen and Simpson, 1987].

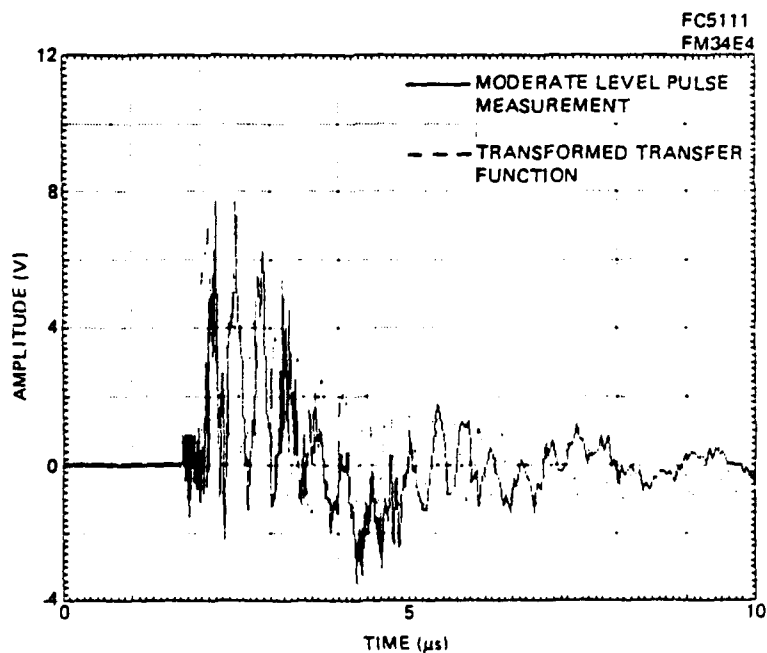


Figure V-33. Predicted Versus Measured Voltage Transient on the FCSE Throttle Actuator Wire. [Whalen and Simpson, 1987].

signal shows more non-linear activity. The coupling frequencies are somewhat higher and lower than that measured by the SFCW tests. The peak amplitudes of the measured pulse response was 3 percent higher than the transformed transfer function response peak. The oscillations at the aircraft quarter-wavelength resonance dominates the response, which indicates the high-frequency coupling to the wire [Whalen, 1986].

The Boeing report [Whalen and Simpson, 1987] relates that the results of the 28 kA pulse test response varies from 3 percent higher to 27 percent lower than the transformed transfer function responses. This leads to the important conclusion that determining predicted aircraft circuit responses to threat waveforms using low-level measured SFCW test transfer function results must be performed carefully. They may under or over estimate the level of response which will occur during a lightning strike which produces currents between 1 kA and 200 kA. In turn, the use of these results for protection design may lead to excess protection, with its long term costs to the aircraft, or to inadequate protection, with potentially catastrophic results if a severe threat strike should hit the aircraft.

AFIT LTO SFCW Tests

General. The SFCW tests performed on the LTO were done by the author as part of a comprehensive investigation into the effects of the test set-up configuration on the results of the measurements taken. These experiments were run during the summer of 1987.

Test Objective. The objectives of the SFCW tests on the LTO were: (1) to investigate different test configurations and their effects on the measured SFCW results of a simple test object, (2) to further check the validity of a linear scaling to full threat levels from the very low levels used in the SFCW technique, and (3) to correlate the results of the SFCW test method to other simulation techniques on a well-behaved test body.

Test Set-up and Configuration. The basic test configuration for most of the tests is shown in Figure V-34. A series of SFCW tests were performed using various modifications to this cylinder and coaxial return path. This series was used to investigate the interaction of the return path with the test object. Another series of SFCW tests were performed with the cylinder in various configurations above a ground plane, with no surrounding coaxial return path. Again, the object of the tests was to investigate the interaction of the test object with the

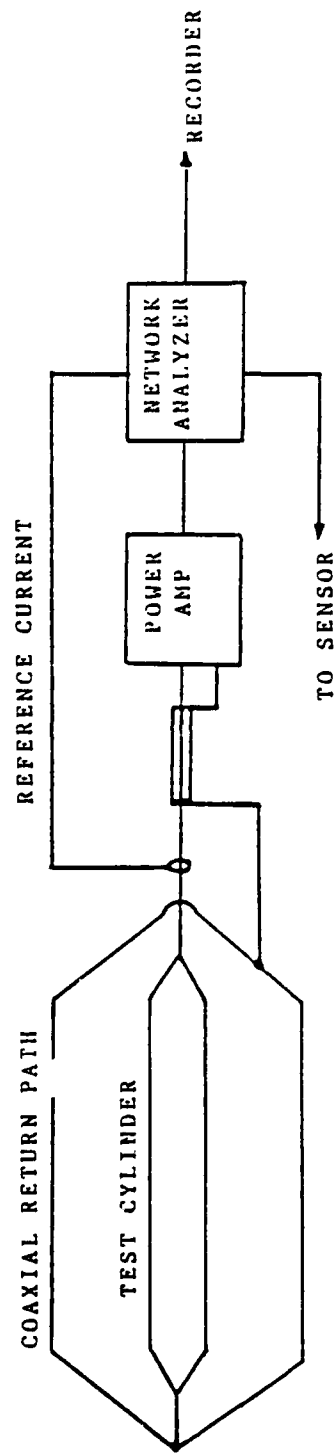


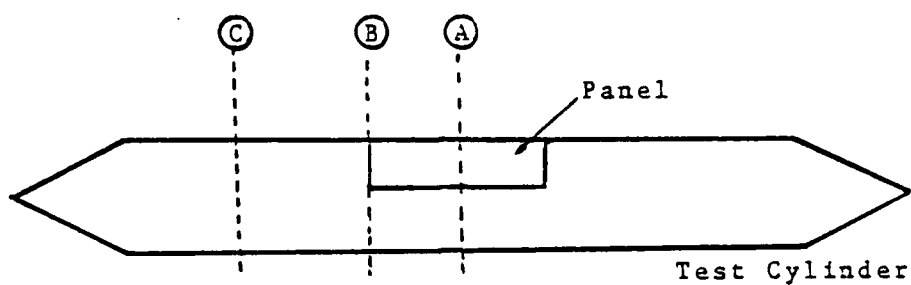
Figure V-34. Basic Test Setup Used During AFIT SFCW Tests.

measurement configuration (return path).

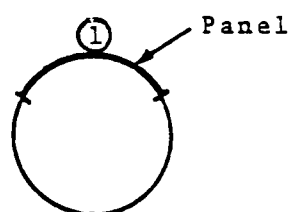
Generator and Measurement System. The SFCW system and measurement set-up used for this test was the same as that used for the UH-60A test described earlier. The block diagram of the data acquisition system is identical to Figure V-14, the system for the AFIT LTO current injection tests. The sensor locations used for the LTO SFCW tests are shown in Figure V-35.

Test Data Processing. Processing of the SFCW test data from the LTO used a refinement of the processing performed on the UH-60A data. Experience in processing the data from the helicopter showed the advantages of sweeping the frequency linearly rather than as a logarithmic progression. This greatly simplified post-test processing by eliminating the need to interpolate logarithmically measured points to linear frequency spacing.

The time domain data was post-processed to remove the effects of the sensors and fiber optics. Removing the sensor effects from derivative electric field and magnetic field measurements resulted in the integration of these measurements from $dE(t)/dt$ and $dH(t)/dt$ to $E(t)$ and $H(t)$. Current transients were measured by current transformers and current shunts and were also corrected by removing



SIDE VIEW



CROSS SECTION

B-Dot Sensor Locations

A1

B1

C1

Figure V-35. Sensor Locations Used in AFIT LTO SFCW Tests.

sensor effects. However, the current sensors did not require an integration of the data.

Results. The tests on the LTO produced some interesting results with regard to test techniques and configuration effects. Illustrations of some of the different configurations and typical results measured with the LTO will be presented in this section.

Figure V-36 shows an external SFCW magnetic field measurement on the LTO near the center of the cylinder, with the solid aluminum panel in the aperture. The two time domain waveforms were Fourier transformed, corrected for sensor effects and the response was divided by the input current to produce the transfer function. The transfer function shows that below 10 MHz the transfer function is basically the same as the static distribution, calculated as

$$H = I/2\pi R$$

Above 10 MHz, the length of the cylinder, connecting wires and generator return path lumped parameter resonant wavelengths correspond well to the resonant 1/2 and 1/4 physical geometric and electrical resonant wavelengths. Were configuration effects such as lengths and electrical characteristics not an influence, the transfer function would be flat up to 100 MHz.

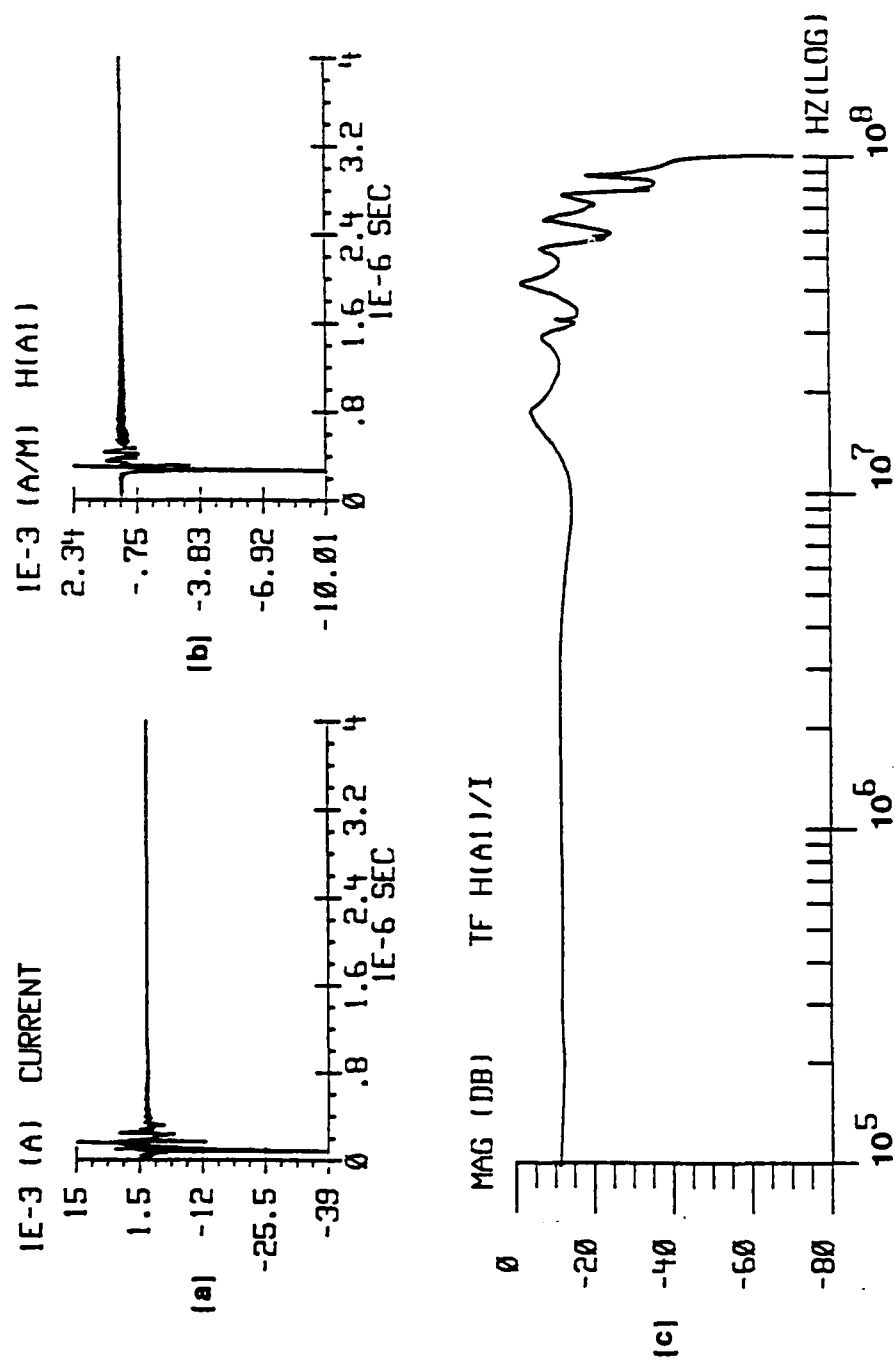
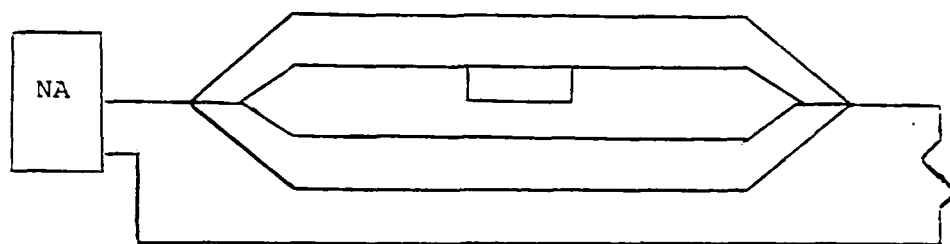


Figure V-36. SFCW Field Measurements on LTO with Solid Panel. (a) Input Current Waveform. (b) External Magnetic Field. (c) Resulting Transfer Function.

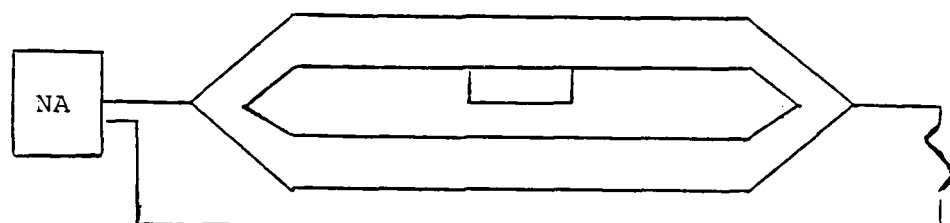
To investigate the effects of the set-up configuration, specifically the return path, on the measurements, a series of SFCW tests were carried out with the LTO and various combinations of cylinder terminations and return paths. To reduce the parameters to be considered, the LTO was configured with the solid aluminum panel. To take advantage of the symmetry of the structure, these measurements were made with the sensor located at location A1, as shown in Figure V-35. Figure V-37 shows the various combinations considered in this series of tests. Representative measurements made from the configurations depicted in Figure V-37 are depicted in Figures V-38 through V-41.

When examining the results presented in Figures V-38 through V-41, several observations can be made. When considering the return path only (Figure V-40) and the case where the cylinder is attached to the return path (Figure V-38) there is little difference in the response below 50 MHz, implying that the response falls into the quasi-static region. Above 50 MHz, the configuration effects take over. In this case, there is a very small transition region.

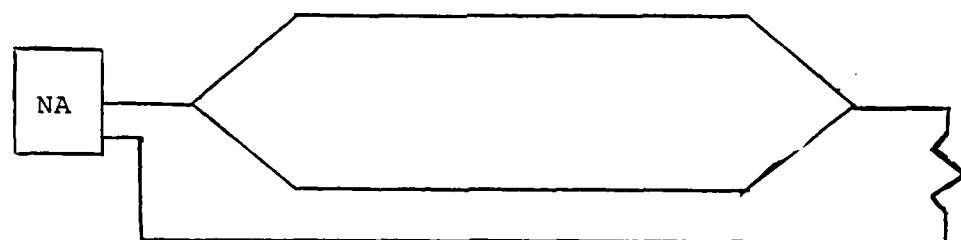
When considering the case of the return path and the cylinder floating within the return path (Figure V-39), we have results that contain significant differences. In



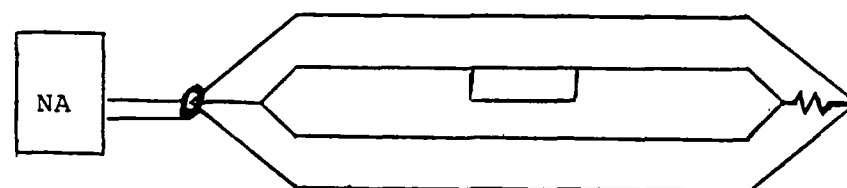
(a)



(b)



(c)



(d)

Figure V-37. Various Coaxial Return Path Configurations Used in AFIT SFCW Tests. (a) Cylinder Shorted to Return Path. (b) Cylinder Floating In Return Path. (c) Return Path With No Cylinder. (d) Cylinder Attached to Return Path With Matched Load.

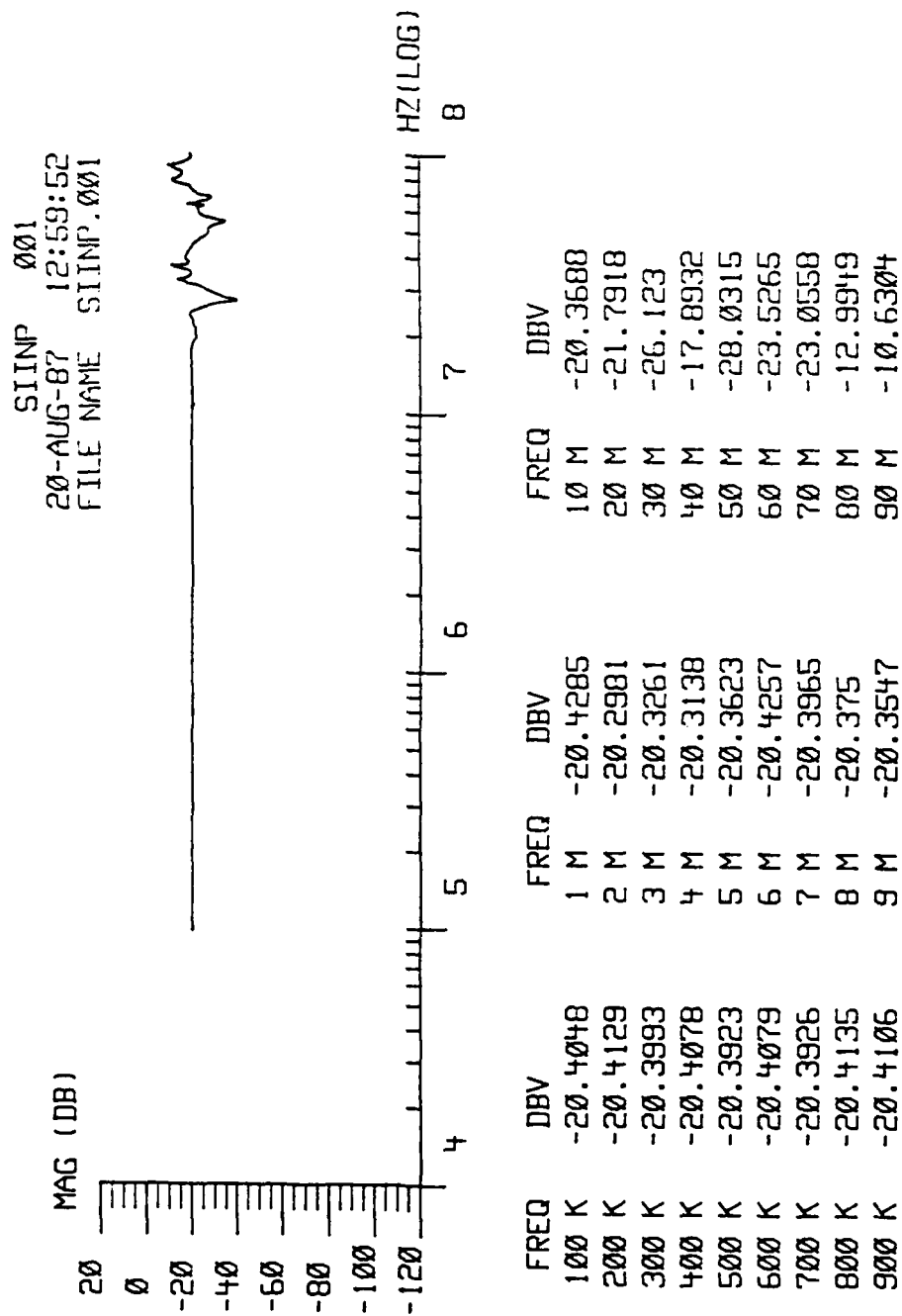


Figure V-38. SFCW Transfer Function of Magnetic Field Measured With Configuration Depicted in Figure V-37a.

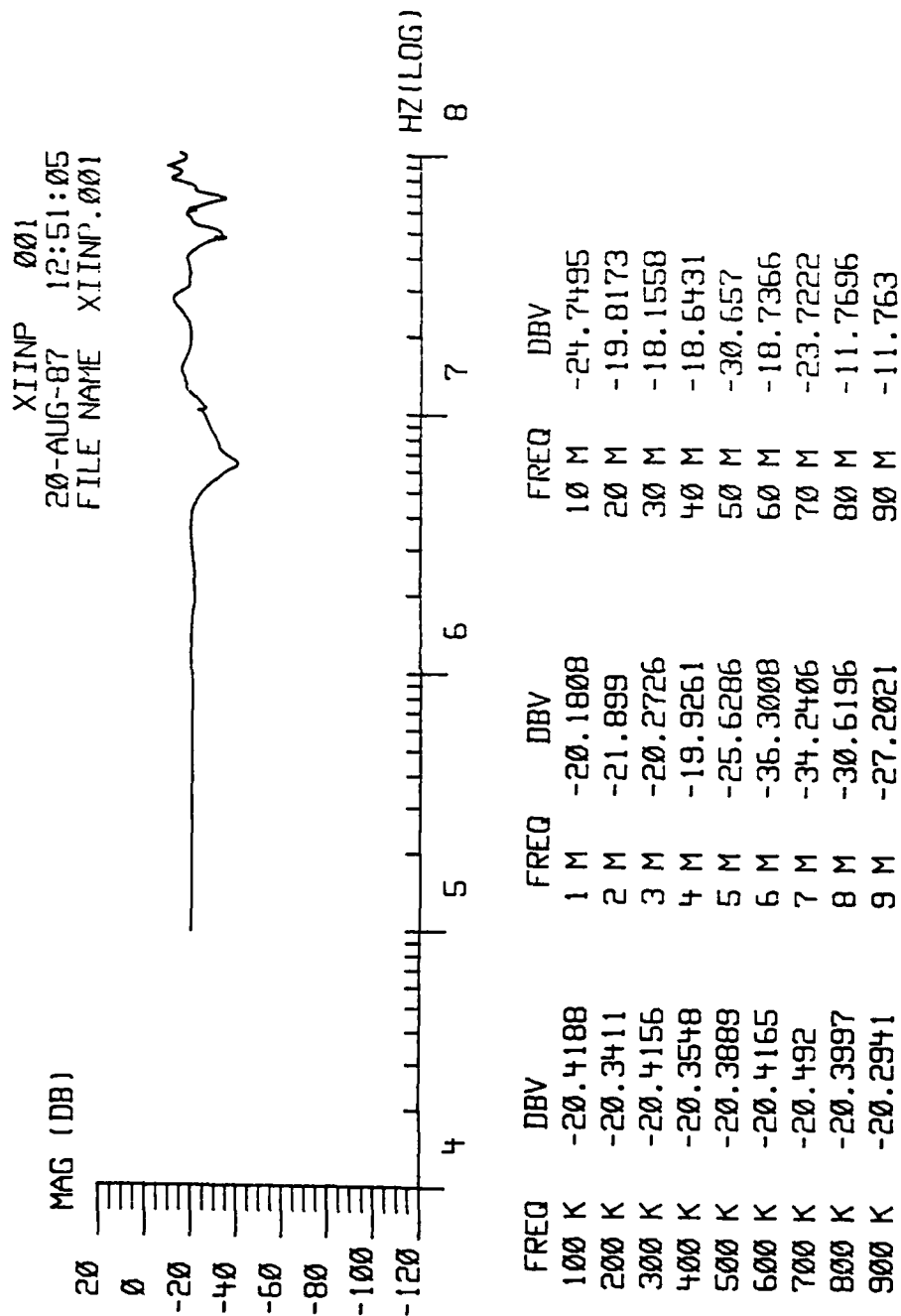


Figure V-39. SFCW Transfer Function of Magnetic Field Measured With Configuration Depicted in Figure V-37b.

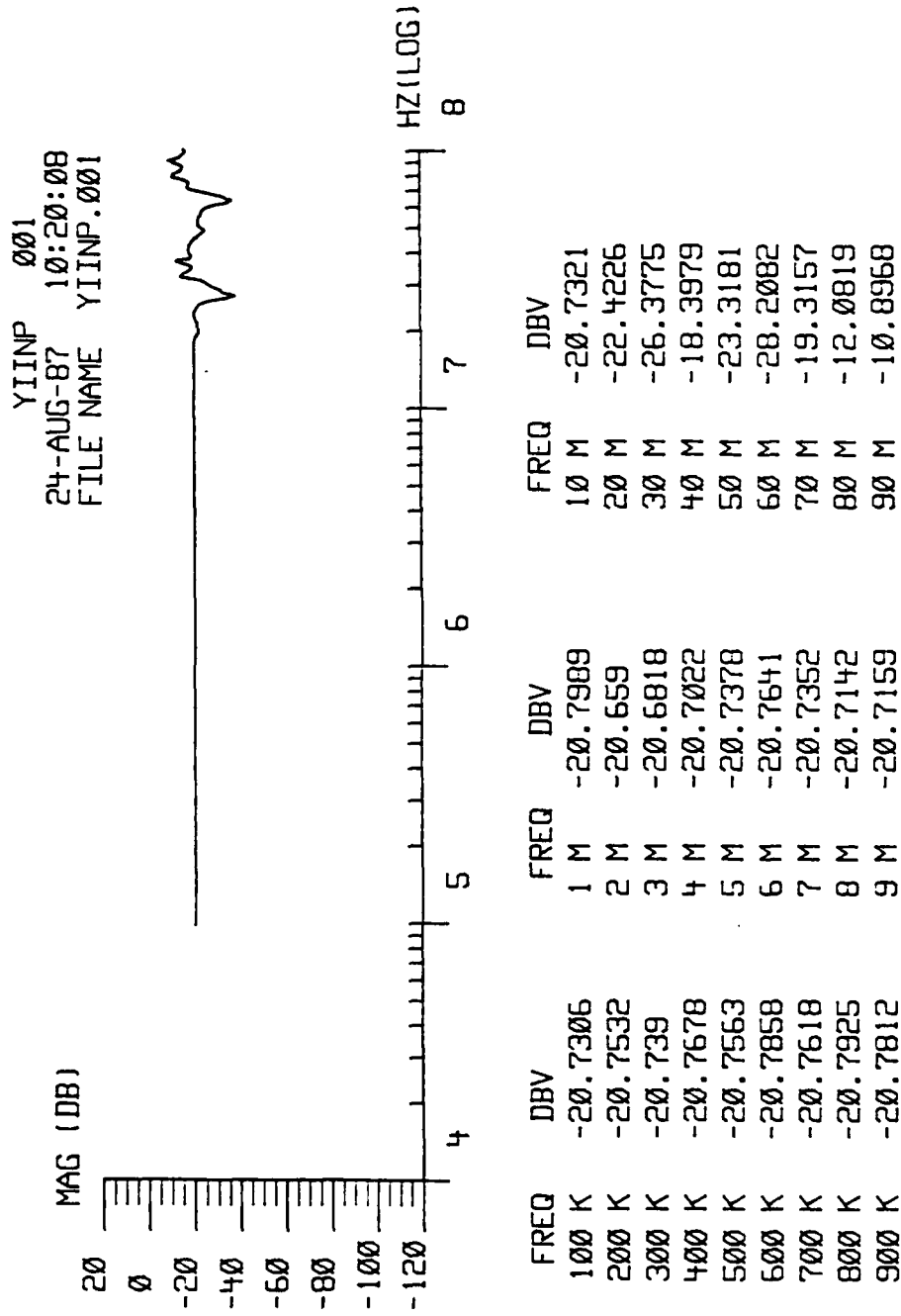


Figure V-40. SFCW Transfer Function of Magnetic Field Measured With Configuration V-37c.

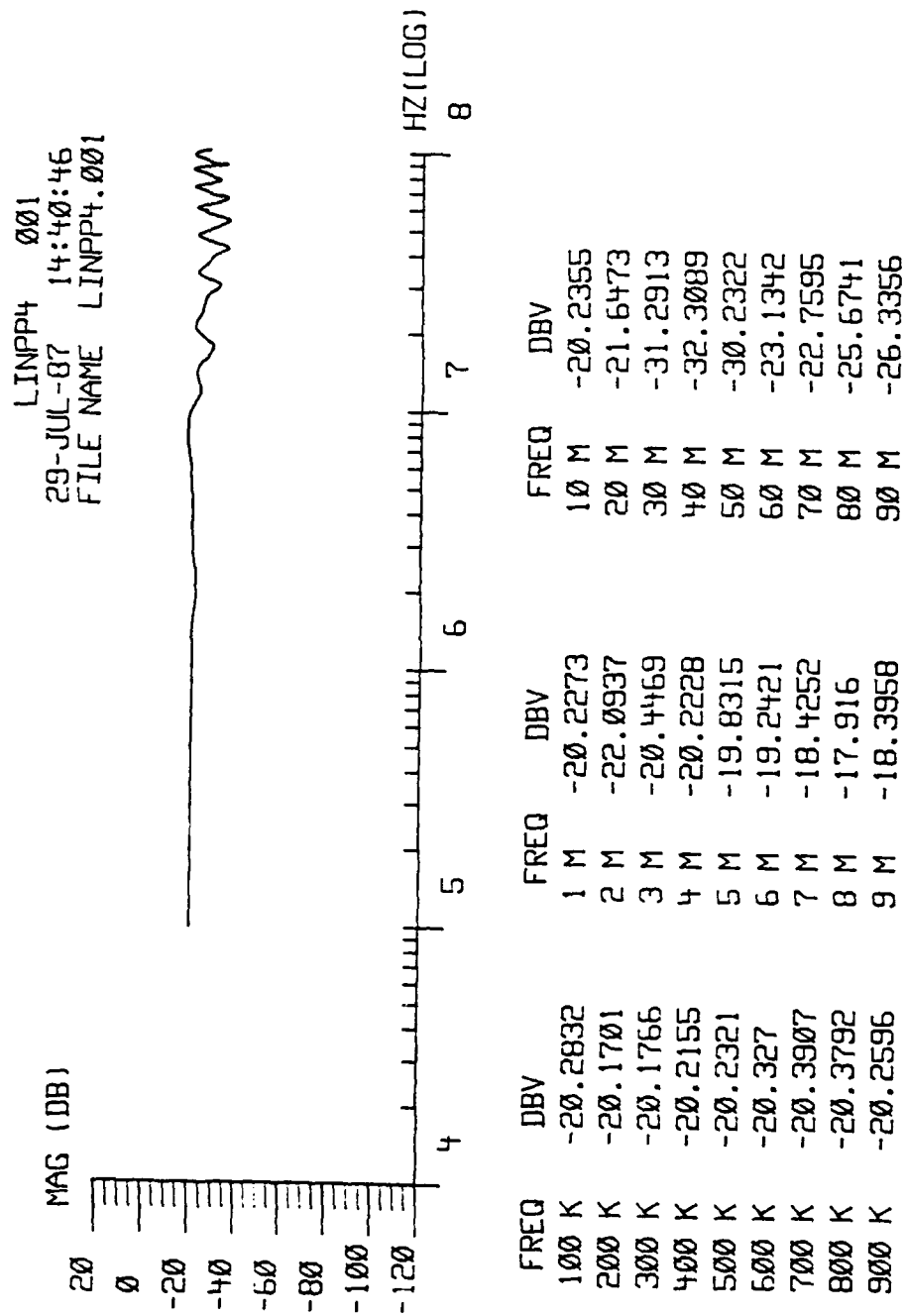


Figure V-41. SFCW Transfer Function of Magnetic Field Measured With Configuration Depicted in Figure V-37d.

this case, we have three distinct regions, one above 50 MHz, that matches the previous results, one region between 50 MHz and 3 MHz, and one below 3 MHz. Below 3 MHz, we again see the quasi-static response, while between 3 and 50 MHz, we have a transition region.

In the case of the cylinder attached to the return path with a matched load, we see that the matching resistor results in reduction in reflections at exit. This results in a transfer function that has most of its variation at the higher frequencies. This also illustrates that the use of a matching resistor to prevent reflections can strongly influence the electric and magnetic fields in the configuration.

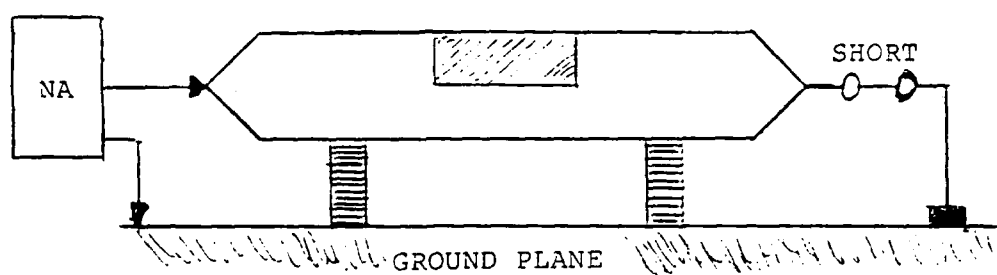
These configurations demonstrate that the quasi-static solution is present as illustrated by the flat response at lower frequencies. At higher frequencies, the return path strongly affects response of the cylinder even when cylinder is not connected. This is not unexpected, as we have a structure that can support many distinct modes at different frequencies.

To make comparisons between the SFCW data and the data obtained from the shock-excitation experiments, another series of SFCW experiments was carried out with the LTO, supported by dielectric stands, suspended above a

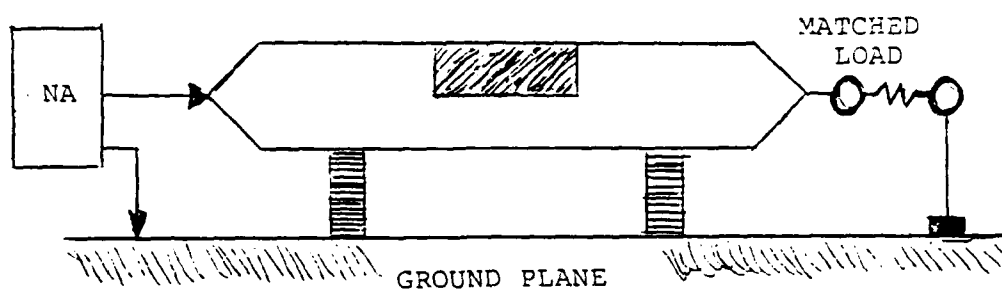
ground plane. The network analyzer was connected between the ground plane and the input end of the LTO. The other end of the LTO was then "connected" to the ground plane by either a short, open or matched load (Figure V-42). To assess the sensitivity of these effects, a solid panel, two different composite panels and no panel were placed within the aperture of the LTO. In addition, the open aperture was oriented both away from and toward the ground plane. As before, these measurements were made at sensor location A1.

Because of the large number of possible configurations, only the most pertinent results will be presented. Measurements for the solid panel, the two composite panels, and the open panel, oriented up and down are shown for each of the three terminations in Figures V-43 through V-47. In examining these results, we see that there are noticeable similarities, differences and trends between the different measurements.

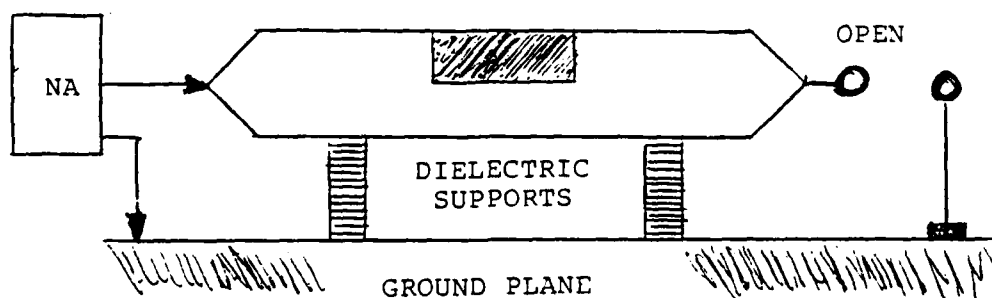
For Figure V-43, the solid aluminum panel that is used for baseline measurements, we see that there are three distinct regions. Up to approximately 3 MHz, the responses are roughly identical, matching what would be expected in the quasi-static region. From 3 MHz to approximately 50 MHz the results are those expected of the transition region and the expected large differences are



(a)

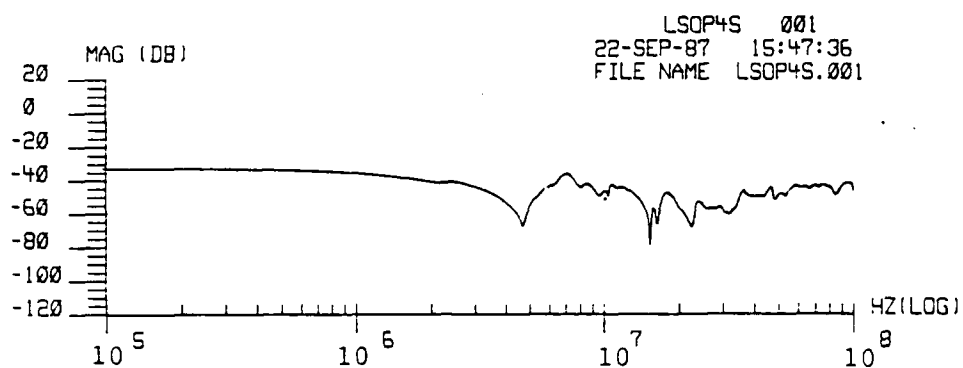


(b)

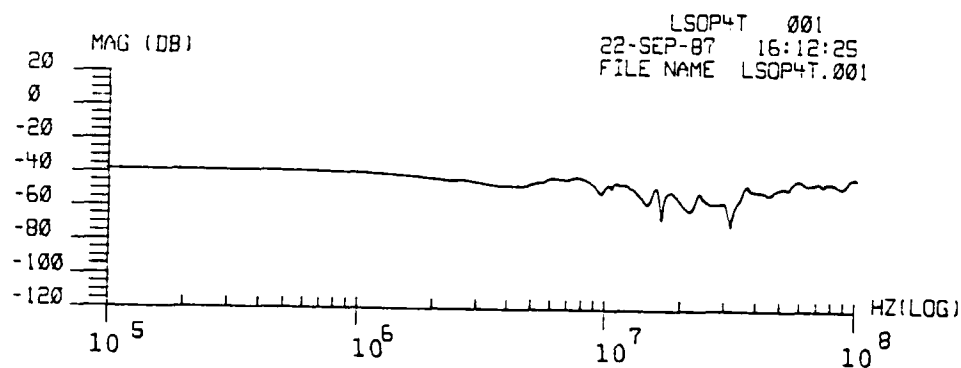


(c)

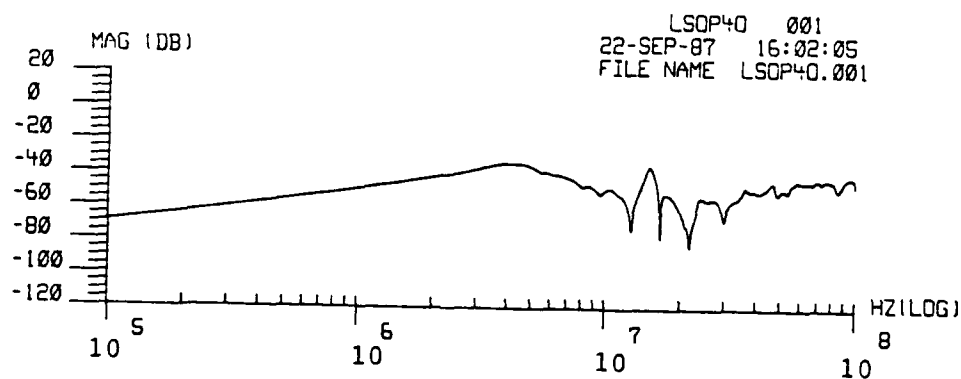
Figure V-42. Configurations Used to Make SFCW Measurements on LTO While in Shock-Excitation Configurations.
 (a) LTO Terminated to Ground Plane With a Short.
 (b) LTO Terminated With a Matched Load.
 (c) LTO Terminated With an Open.



(a)



(b)



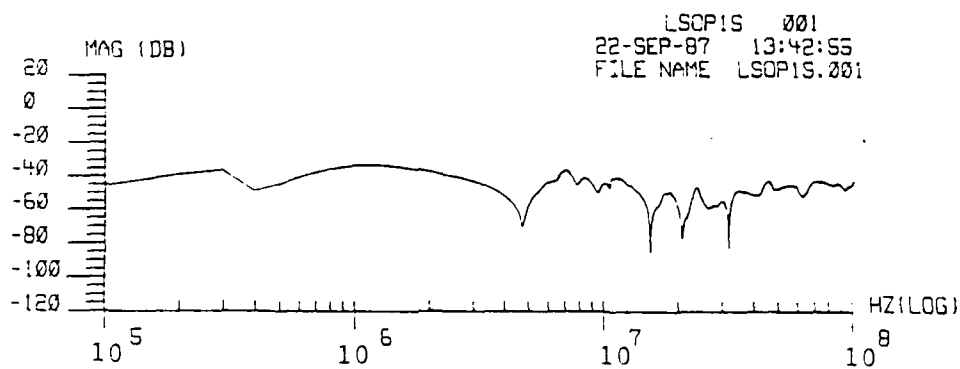
(c)

Figure V-43. SFCW Transfer Functions Made With LTO and Solid Panel. (a) LTO With Short. (b) LTO Terminated With Matched Load. (c) LTO Terminated With Open.

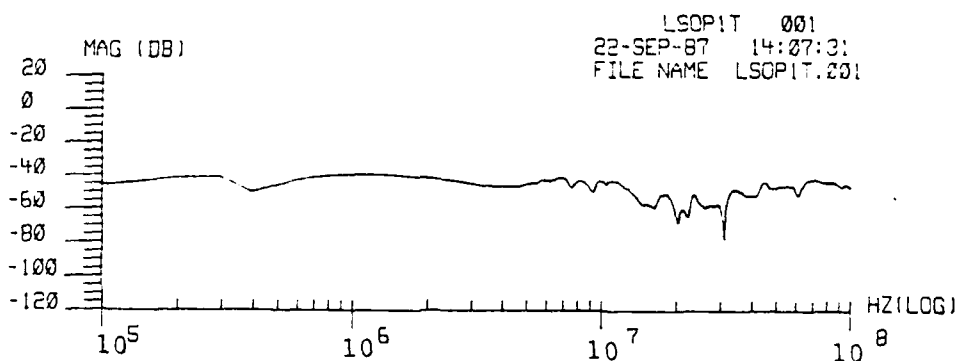
evident. Above 50 MHz, we enter the resonance region and the results in all three cases are identical. It is interesting to note the slope of the curve in the case of the open termination. This is probably caused by the charging of the structure, as it acts like a capacitor in this case.

For the case of the composite panels, Figures V-44 and V-45, similar observations can be made. There are noticeable differences though, in the transition region. These are to be expected, as the structure has been changed, with the change in panels, and the lumped parameters of the panels are different. With composite panels on the LTO, a change in the current distribution on the cylinder will take place, depending upon the type of panel that is in the aperture. Again, the charging effect for the open termination is noticeable.

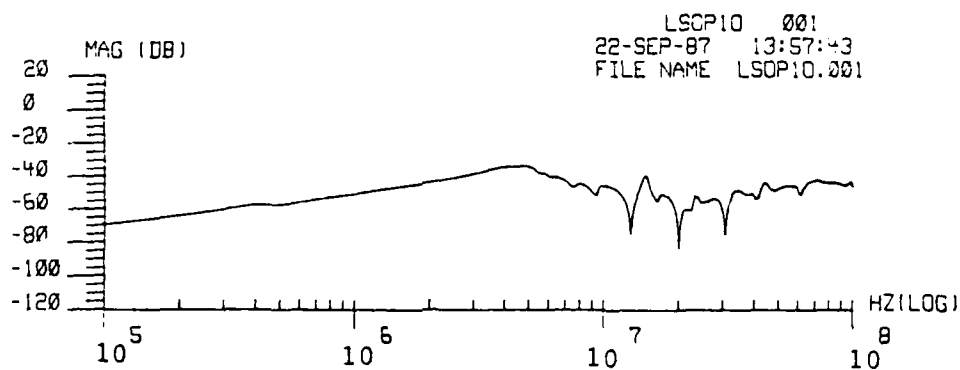
For the open panel configuration, with aperture oriented down (Figure V-46) and up (Figure V-47), we see results that are analogous to those seen with the composite panels. That is, in orienting the aperture up or down, we are introducing a change in the interaction of the object with the configuration, much as changing the composite panel characteristics does. For each case, we see that the results are consistent between the different terminations, outside the transition region. That is, in



(a)

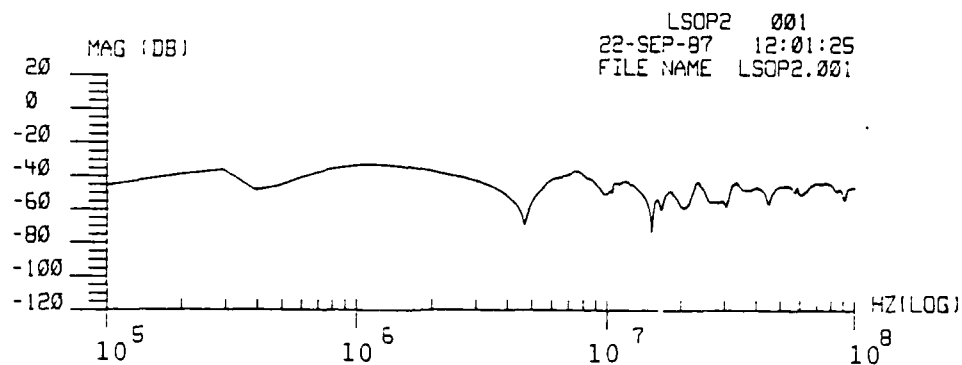


(b)

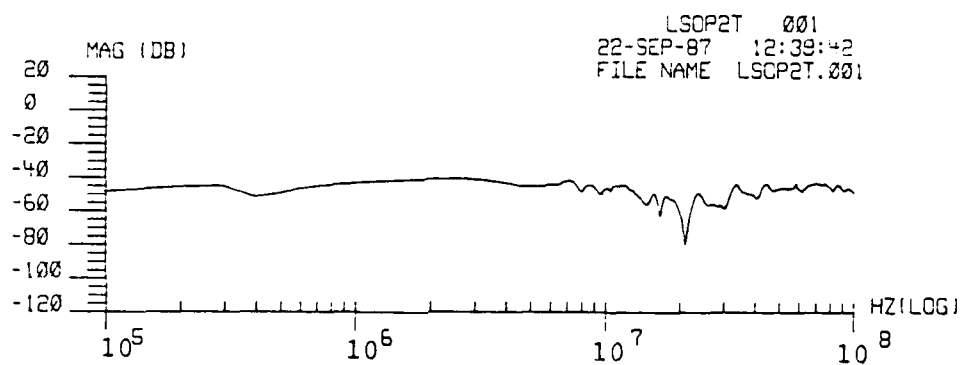


(c)

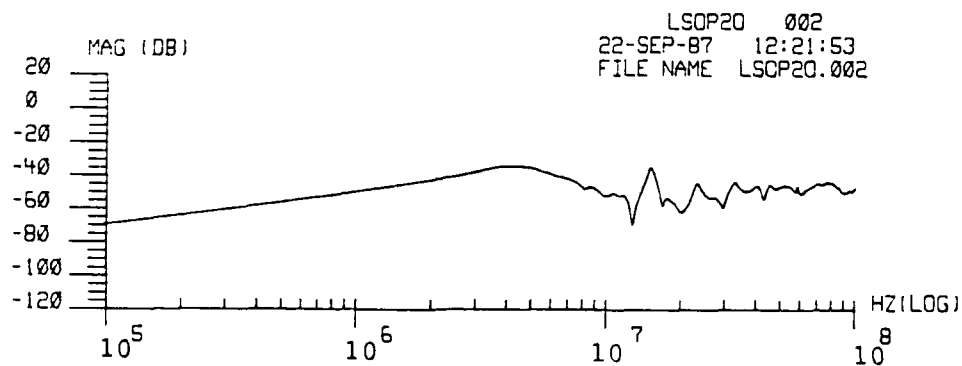
Figure V-44. SFCW Transfer Functions Made With LTO and Composite Panel #1. (a) LTO With Short. (b) LTO Terminated With Matched Load. (c) LTO Terminated With Open.



(a)

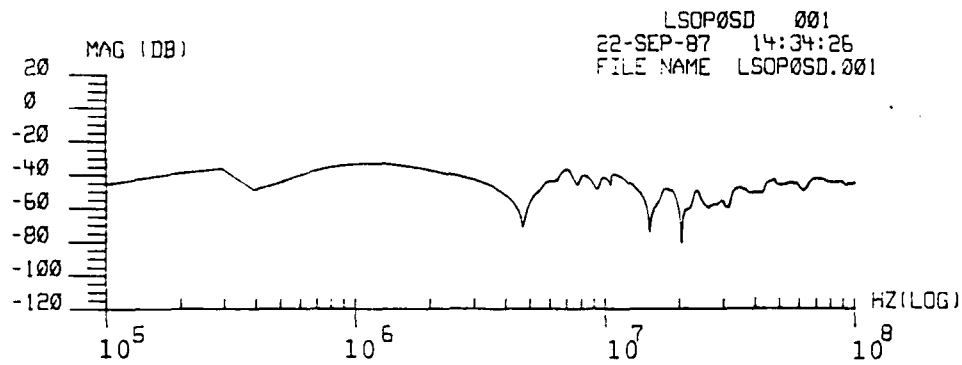


(b)

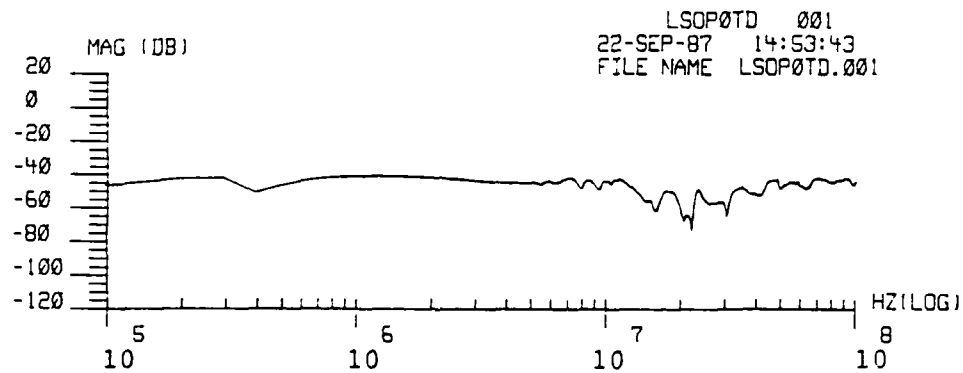


(c)

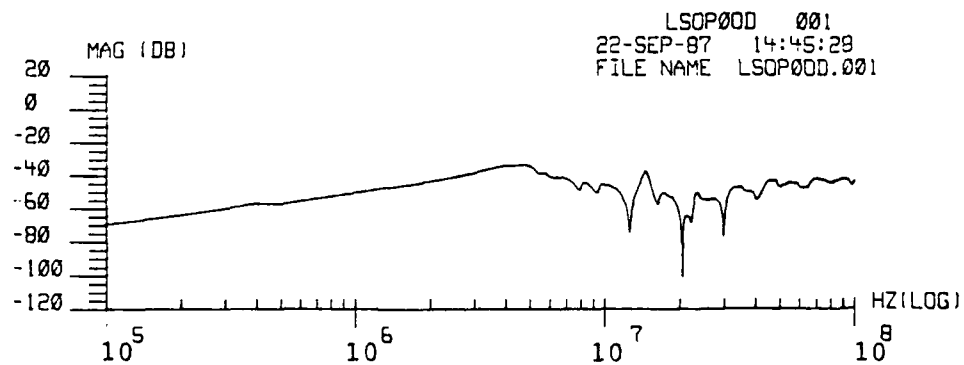
Figure V-45. SFCW Transfer Functions Made With LTO and Composite Panel #2. (a) LTO With Short. (b) LTO Terminated With Matched Load. (c) LTO Terminated With Open.



(a)

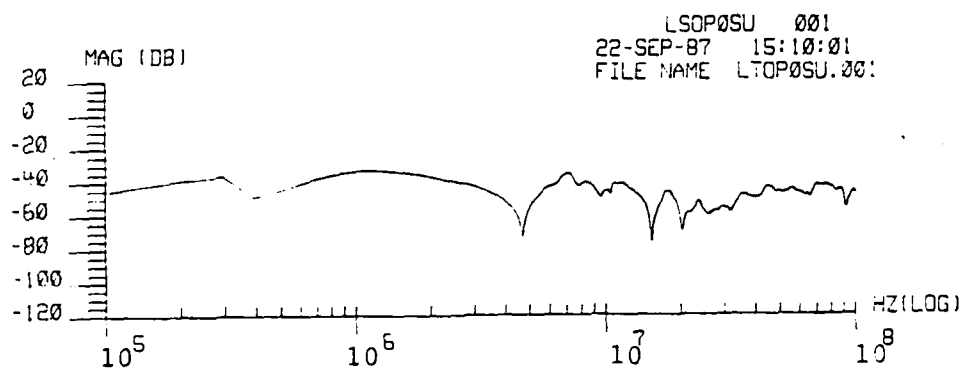


(b)

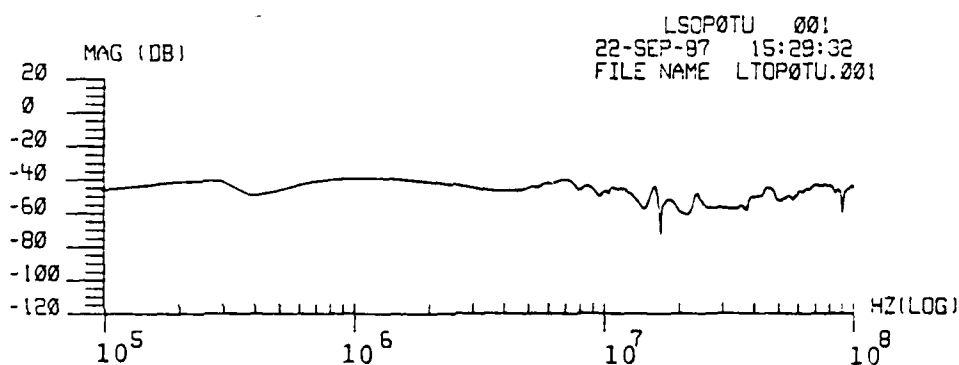


(c)

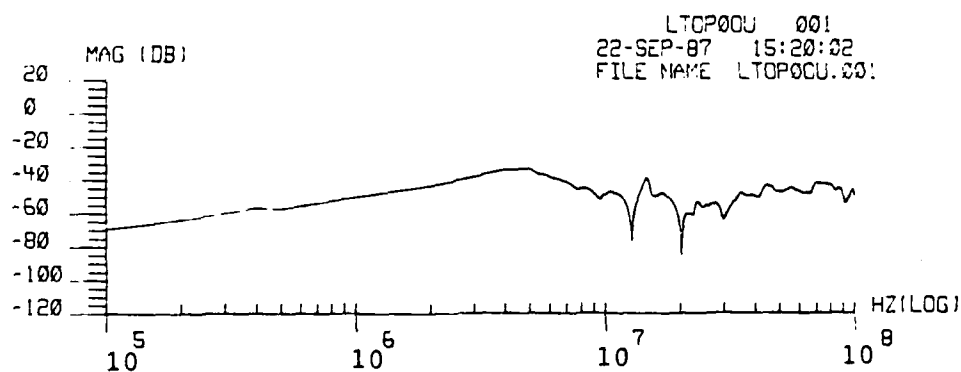
Figure V-46. SFCW Transfer Functions Made With LTO and No Panel, Aperture Down. (a) LTO With Short. (b) LTO Terminated With Matched Load. (c) LTO Terminated With Open.



(a)



(b)



(c)

Figure V-47. SFCW Transfer Functions Made With LTO and No Panel, Aperture Up. (a) LTO With Short. (b) LTO Terminated With Matched Load. (c) LTO Terminated With Open.

Figure V-43, we see that above 50 MHz, the termination does not have much effect on the results, although the matched termination shows a larger effect than the other two. Again, the charging slope is evident in the results.

In Figure V-48, the two composite panels configured with an open termination are shown. It is interesting to note that the SFCW method is sensitive enough to show differences between the two panels. The difference is even more noticeable between the solid panels and one of the composite panels (Figure V-49). Finally, Figure V-50 shows that there are noticeable differences when the same test object, the LTO with no panel, experiences a change in the measurement configuration (ie. is oriented either up or down).

These observable differences indicate that there is much potential in using the SFCW method for vehicle surveillance to verify of continuing vehicle hardness after they have passed their initial qualification. They also point out the need for great care in setting up the measurement configuration, in terms of choosing the type of return path, termination, etc.

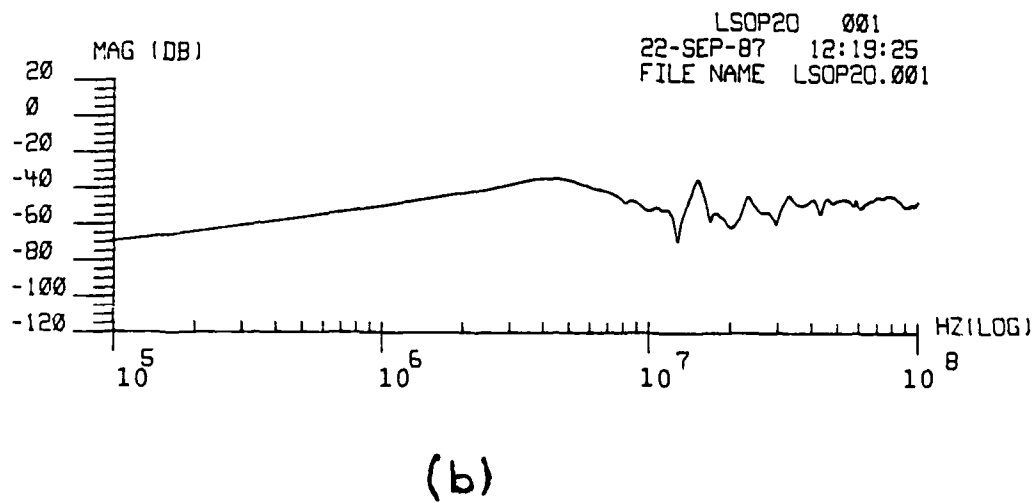
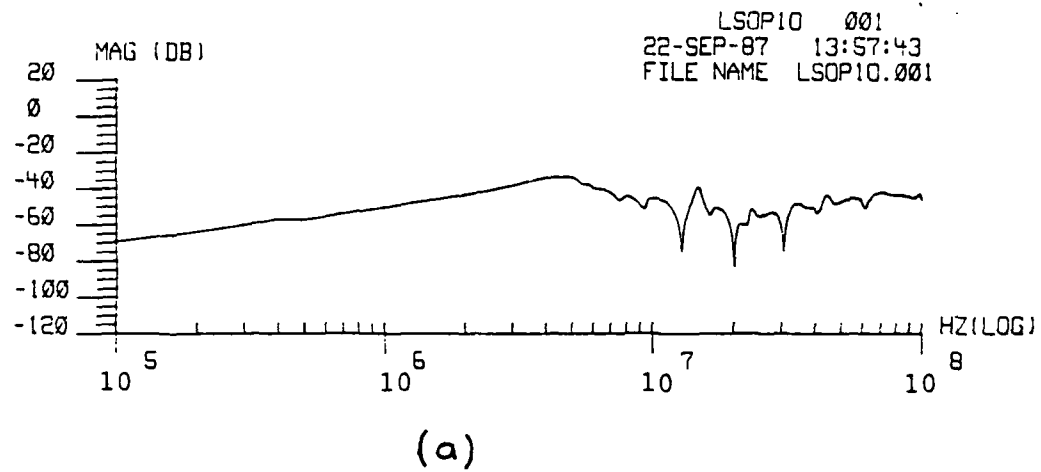


Figure V-48. Comparison of SFCW Transfer Functions Made With LTO Terminated With Open, and Using two Composite Panels. (a) Composite Panel #1. (b) Composite Panel #2.

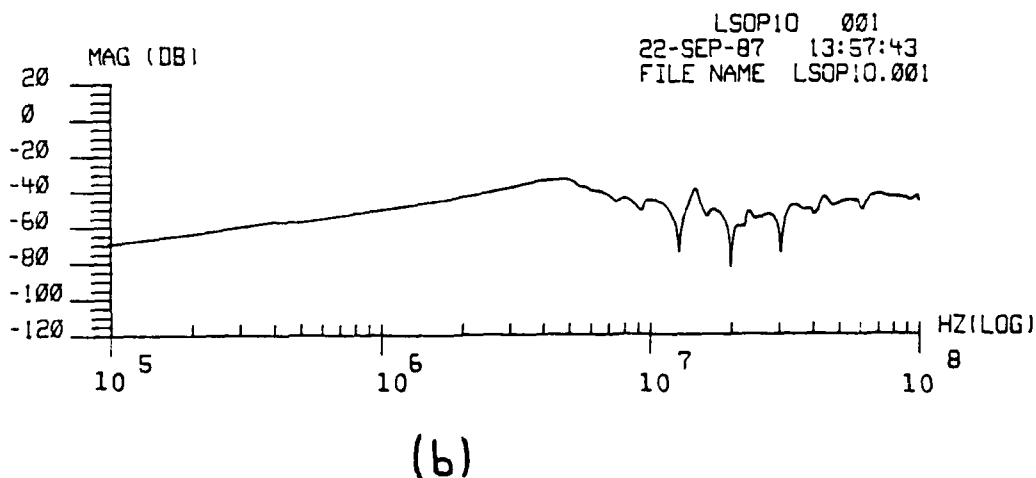
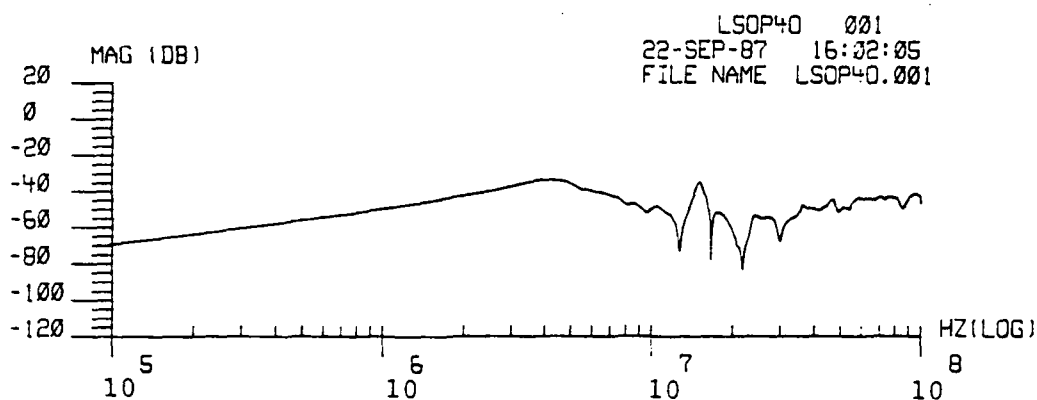


Figure V-49. Comparison of SFCW Transfer Functions Made With LTO Terminated With Open, and Using Solid and Composite Panels. (a) Solid Panel. (b) Composite Panel #1.

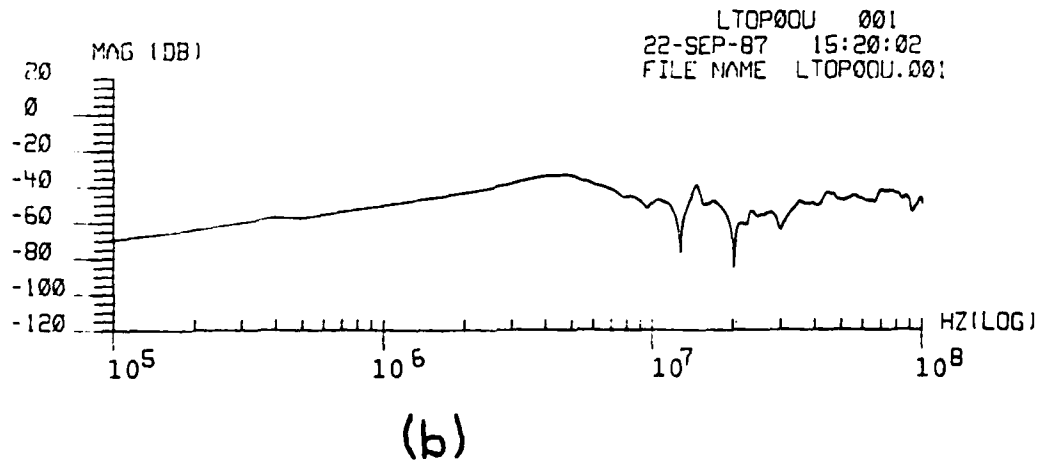
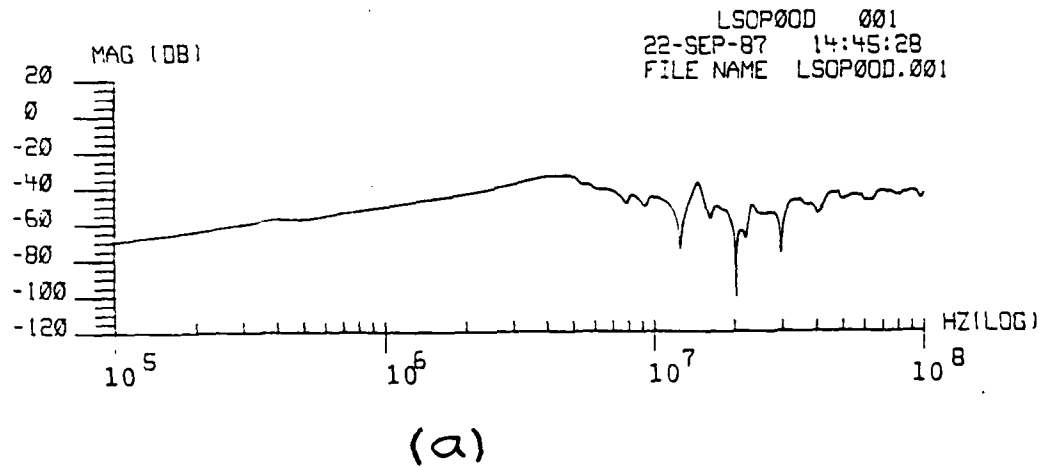


Figure V-50. Comparison of SFCW Transfer Functions Made With LTO Terminated With Open, and Using No Panels in Aperture. (a) Aperture Down. (b) Aperture Up.

Shock-Excitation Tests

This section discusses the configuration effects observed during shock-excitation type ground lightning simulation tests. First, a review of previous experiments done using the shock-excitation test technique will be presented. Then the work done at AFIT investigating configuration effects using the shock-excitation test technique will be presented. The test, objectives of the test, test set-up and configuration, measurement system, measurements and results for each series using the shock-excitation test method are discussed.

Early Work Using Shock-Excitation Test Techniques

The shock-excitation technique was first developed at the McDonnell Aircraft Company, with initial results reported by Clifford and Zeisel [1979] and Lenz, Clifford & Butters [1980]. This technique differs significantly from the current injection technique, with the test body electrically isolated from the generator by spark gaps. Through the use of these spark gaps, the shock-excitation test technique is able to produce charging and discharging transients in the test body. An example of the typical test set-up used by McDonnell Aircraft Company is shown in Figure IV-21.

Some of the results of Clifford and Zeisel's early tests are shown in Figures V-51 through V-53. Figure V-51

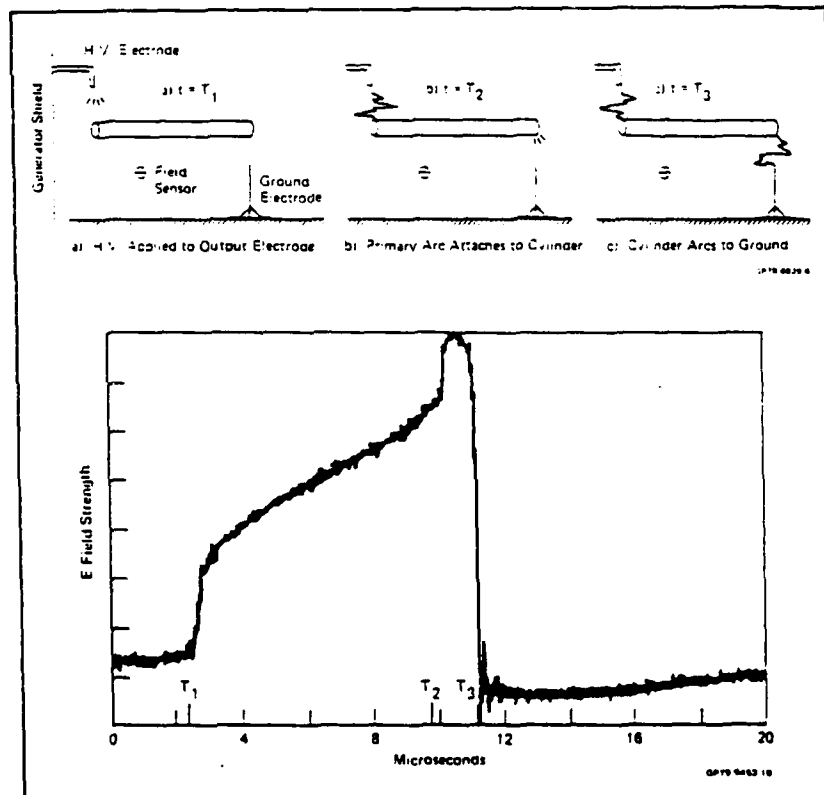


Figure V-51. Relationship of Changes in Electric Field to Arc Attachment Sequence. [Clifford and Zeisel, 1979].

illustrates the sequence of actions that occur during the shock-excitation process and correlates them with the changes in the E-field. The initial, rapid change in the E-field is clearly shown at time T_1 . Between time T_1 and T_2 , the charging of the test body (cylinder) is evident, as well as the rapid change in E-field when the cylinder arcs to ground.

Figure V-52 is an attempt to relate the E-field changes to the input current waveform. During these tests, the voltage induced on a wire located inside the cylinder was monitored. It is clear that the current waveform closely follows the E-field changes. More importantly, potentially significant voltages are induced in the cylinder due to the E-field changes, both at initial attachment and during the discharge of the cylinder potential. This has important implications for the aircraft hardening process, as most of the current effort has focused on the transients induced by the change in the current. For some of the newer aircraft designs, E-dot coupling may play a more important role than previously suspected.

To gain further knowledge about the processes occurring with the spark gaps, the front spark gap was eliminated and only one spark gap was used. In Figure V-53, the waveforms have the same general shape, with the

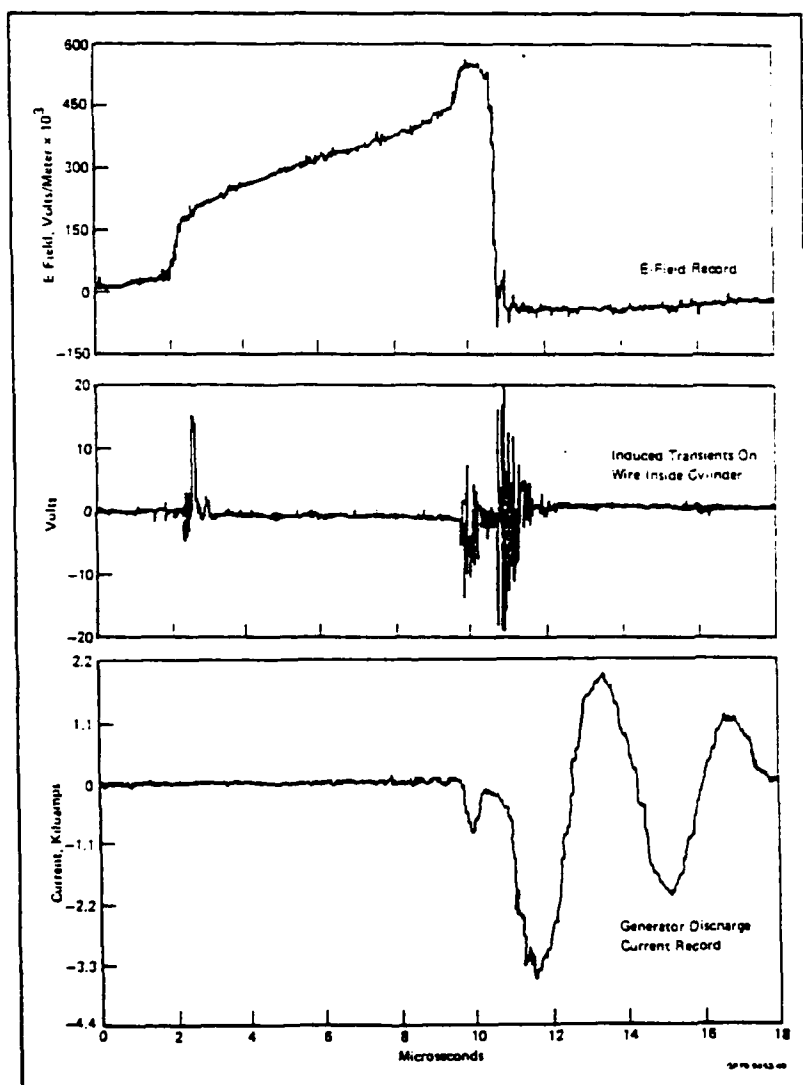


Figure V-52. Comparison of Electric Field, Induced Voltage and Driving Current for the Double Arc Case. [Clifford and Zeisel, 1979].

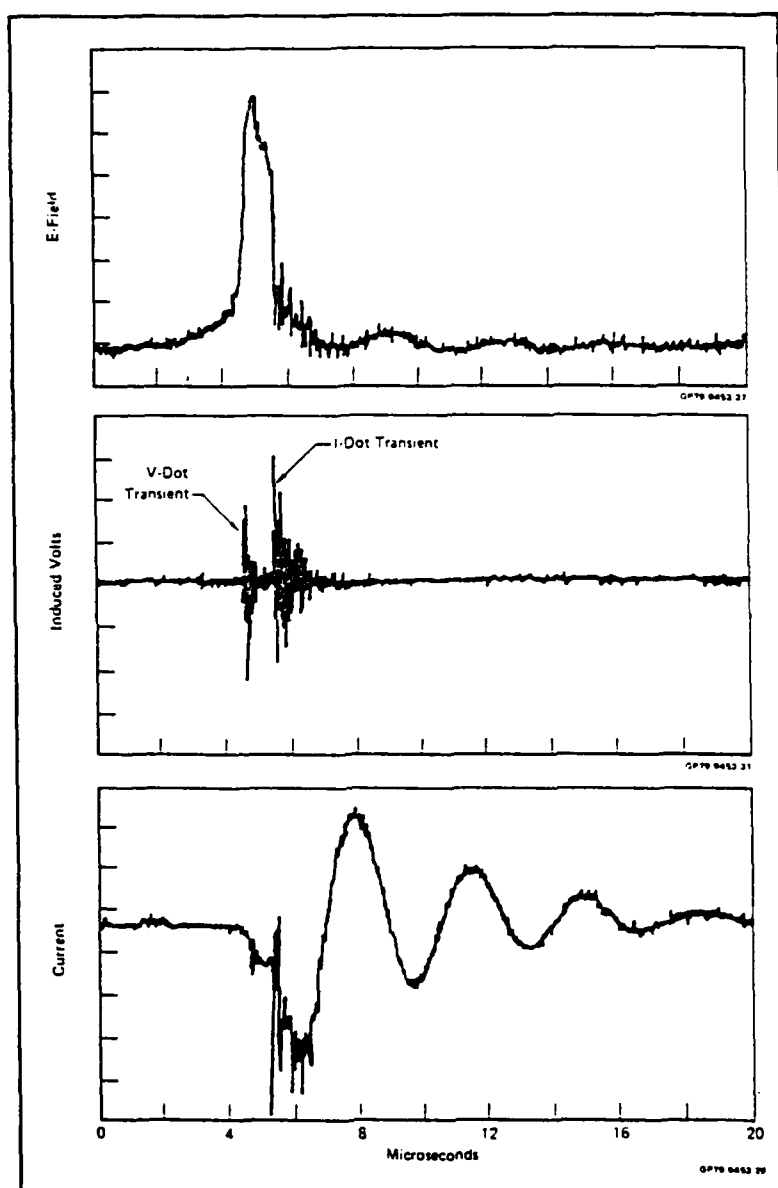


Figure V-53. Comparison of Electric Field, Induced Voltage and Current on the Cylinder.
[Clifford and Zeisel, 1979].

elimination of the initial slow charging taking place in Figure V-52. However, the current monitored has the same shape, indicating that the output spark gap plays an important role in simulating the return stroke current, as it controls the rate of charge transfer off the structure.

These tests were very important in characterizing this test method and indicated the potential utility of this method giving a more realistic result during a lightning simulation test. Because the current generated with this method is relatively low, more information was needed to correlate the results obtained from the shock-excitation tests to test methods that produce higher current levels. For this reason, it was decided to carry out a more detailed study that would form the basis of a comparative study between different simulation test techniques. The AFIT LTO was chosen for the test body, to focus on the test methods instead of the complexities of the test body.

AFIT LTO Shock-Excitation Tests

General. The shock-excitation tests that were performed on the AFIT LTO were the last tests of a comprehensive series of tests investigating the effects of the test set-up configuration on the results of the

measurement taken. These experiments were performed during the last part of the summer of 1987.

Test Objective. The objectives of the shock-excitation tests were: (1) to use shock-excitation results from a simple test object to investigate the effects of various test configurations on measured results, (2) to check the validity of the linear scaling of electric fields to the high levels attained during the shock-excitation test set-up and (3) to correlate the results of the shock-excitation test method to other simulation techniques on a well-behaved test body.

Test Set-up and Configuration. The basic test configuration used in these tests is shown in Figure V-54. For the shock-excitation tests, a flat plate return path was used instead of the coaxial return path. The cylinder was supported above the ground plane by two dielectric stands, with a separation distance between the ground plane and the cylinder of 75 centimeters. At this distance, the characteristic impedance of the cylinder over the ground plane is approximately 56 ohms. This also allows sufficient physical separation between the cylinder and the return path, to prevent arc breakdown from occurring. In addition, it provides another test configuration to explore how the configuration affects the measured data.

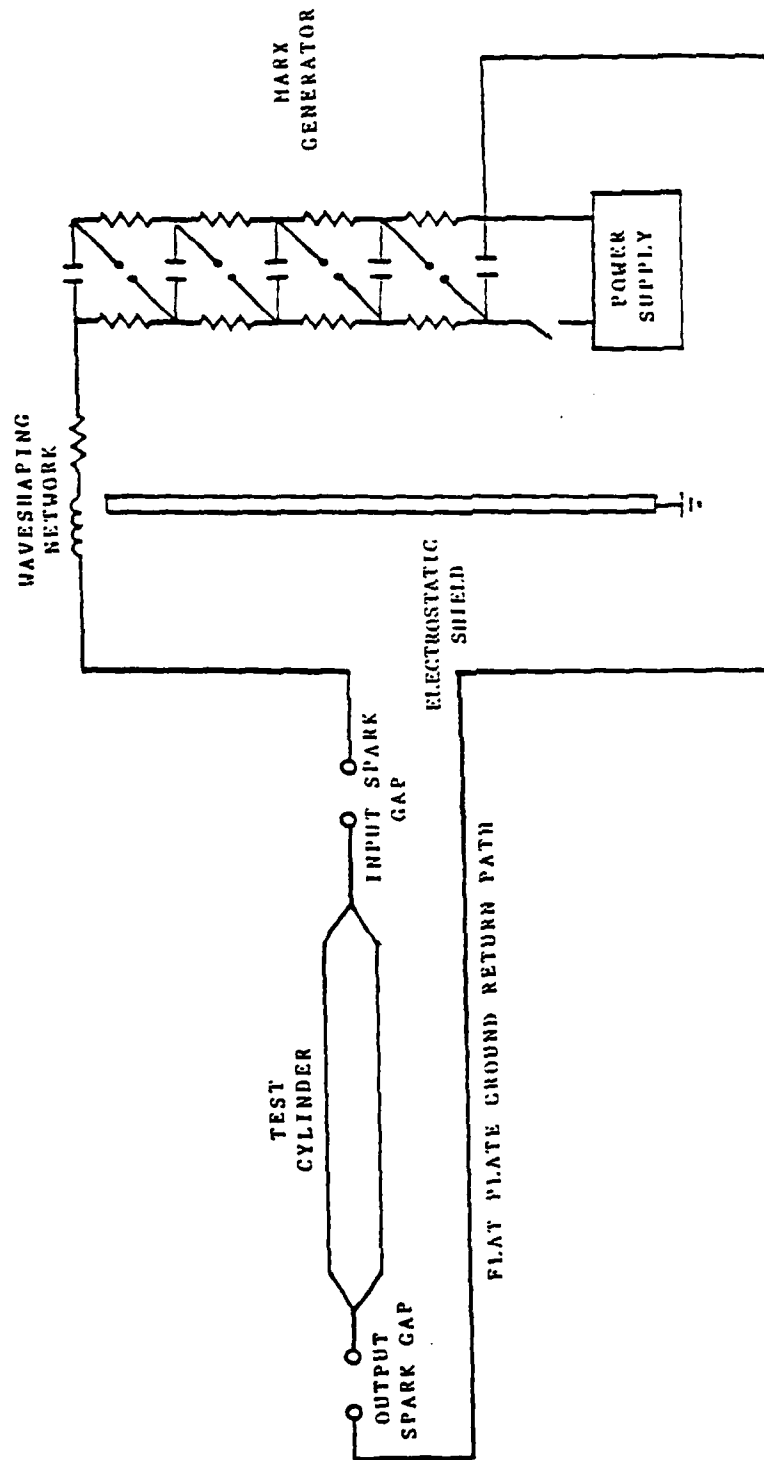


Figure V-54. Basic AFIT Shock-Excitation Test Setup.

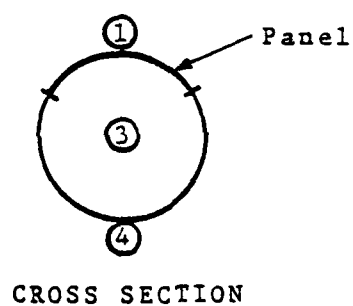
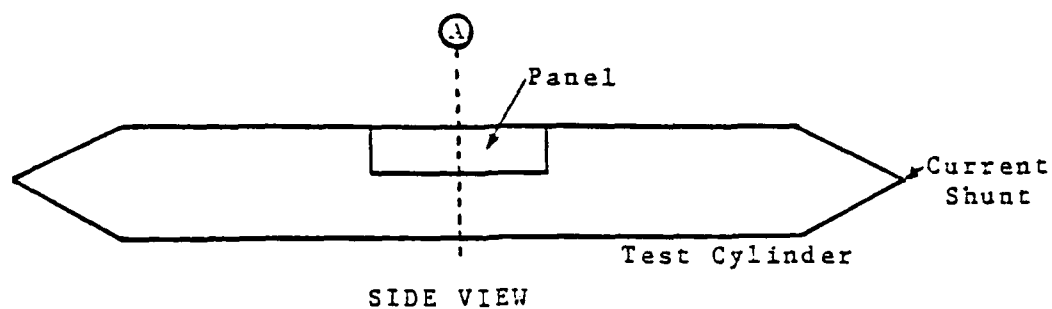
The input and output spark gaps were separated from the cylinder by various distances to examine the effects of separation on charging and discharging transients on the cylinder. The input spark gap was separated by distances of 30 and 60 centimeters, while the output spark gap was separated by distances of 15 and 30 centimeters. Four different spark gap configurations were tested overall. The input-output spark gap combinations studied were: (1) 60-30 cm, (2) 60-15 cm, (3) 30-30 cm and (4) 30-15 cm.

Generator and Measurement System. A Marx generator was used to provide the source of high voltage for this series of tests. The Marx generator consisted of 29 stages of 0.7 microfarad capacitors. Each capacitor could be charged to 50 kV, for a total discharge voltage potential approximately equal to 1.45 MV. For this series of tests, the generator was charged to deliver an output of 1 MV. The wave shaping network between the generator and the cylinder consisted of a total resistance of 1800 ohms in series with an inductor of 116 microhenries. To reduce the electrical noise in the area and shield the cylinder from the fields generated by the generator, a grounded electrostatic screen was placed between the cylinder and generator.

The total current that flowed through the cylinder was measured by a T&M current shunt, which presented a load of 0.005 ohms, and was mounted on the output end of the cylinder. Internal and external field measurements were made with EG&G MGL B-dot and HSD D-Dot sensors, identical to those used during the current injection tests. The external electric field was measured with an EG&G FPD D-dot sensor, mounted in the flat ground plane to minimize the noise pickup of the sensor. Sensor locations are illustrated in Figure V-55. Tests were conducted with no panel, the two composite panels previously described and a solid aluminum panel in the aperture.

The block diagram of the data acquisition system is identical to Figure V-14, the system for the AFIT LTO current injection and SFCW tests. The fiber optic lines were especially useful in this series of tests, due to the spurious electromagnetic noise produced by the Marx generator and the need to isolate the measurement instrumentation from the high voltages on the test object.

Test Data Processing. As before, the time domain data was post-processed to remove the effects of the sensors and fiber optics. Removing the sensor effects from derivative electric field and magnetic field measurements resulted in the integration of these measurements from $dE(t)/dt$ and $dH(t)/dt$ to $E(t)$ and $H(t)$.



Sensor Locations

<u>D-Dot</u>	<u>B-Dot</u>
A1	A1
A3	A3
	A4

Figure V-55. Sensor Locations for Shock-Excitation Tests.

Current transients were measured by current transformers and current shunts and were also corrected by removing sensor effects. However, since these sensors measure current directly, rather than rates-of-change, the data did not require an integration. Figure V-56 shows the typical responses during a shock-excitation test for the current shunt, the external D-dot sensor and an external B-dot sensor.

There is one key difference with the processing of this data with respect to the other simulation tests performed. Unlike the derivative field sensors, the current shunt does not respond during the charging phase of the shock-excitation test. Rather, it responds during the discharge phase after the arc in the output spark gap has been created. Since the current shunt responds to the current flowing on the cylinder after both arcs have been established, using the response of the current shunt as an excitation source to derive transfer functions will result in a noncausal system. This means the electric field and magnetic field responses will occur before any driving function is input to the system.

To account for the field responses occurring during the charging and discharging phases, the magnetic flux density response was used to derive an excitation source. The response of the external B-dot sensor with a solid

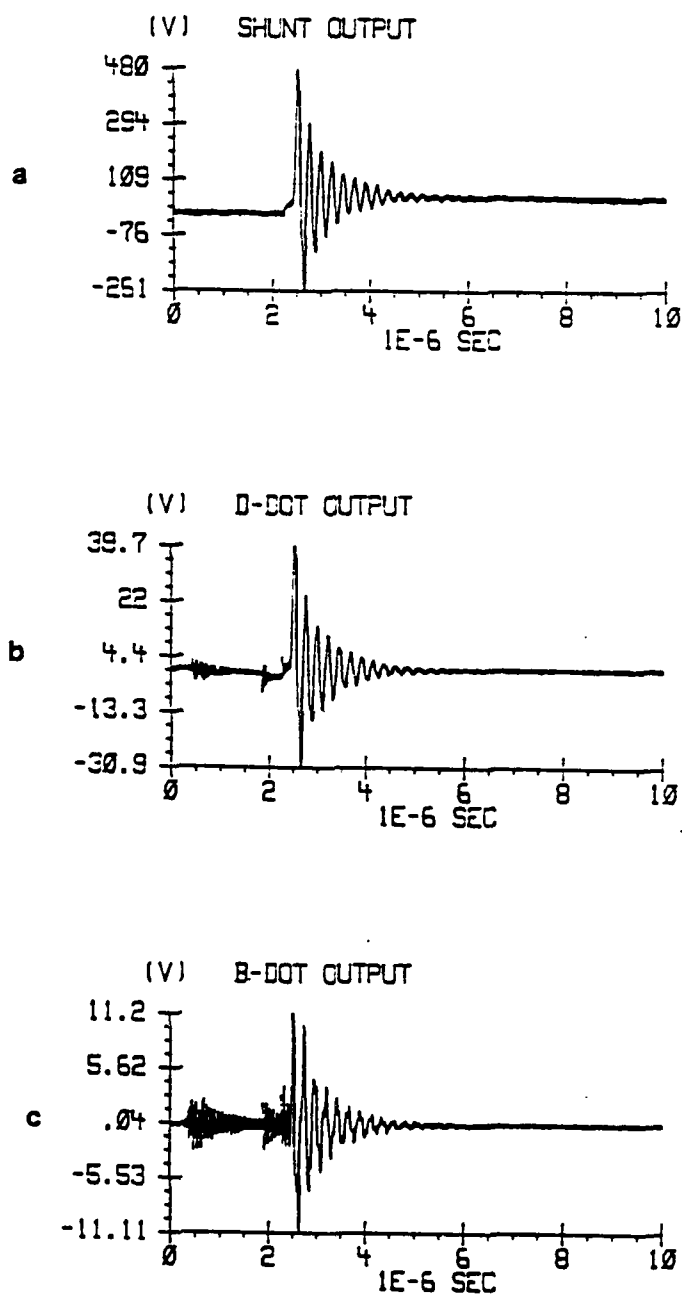


Figure V-56. Typical Shock-Excitation Responses. (a) Current Shunt. (b) External D-Dot Sensor. (c) External B-Dot Sensor.

aluminum panel, shown in Figure V-57, was used for this derivation. Figure V-58 shows the resulting H-field of the sensor after it has been integrated and scaled. This approach can be explained using Maxwell's equation for the curl of the magnetic field, given in differential form as

$$\nabla \times \bar{H} = \sigma \bar{E} + \partial \bar{D} / \partial t$$

The magnetic field is due to a combination of the conduction current density,

$$\bar{J}_c = \sigma \bar{E}$$

and the displacement current density,

$$\bar{J}_d = \partial \bar{D} / \partial t$$

In examining Figure V-56, it appears that the current shunt responds only to the conduction current, occurring during the discharge phase, while the B-dot sensor responds to the effects of both the conduction and displacement current. The displacement current occurs during both phases of the simulation. The displacement current, determined directly by the time rate-of-change of the electric flux density, is proportional to the response of the external D-dot sensor.

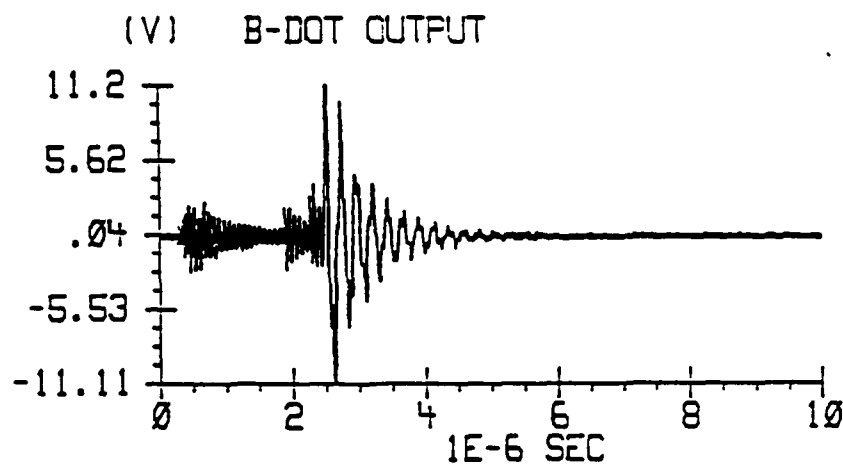


Figure V-57. External B-Dot Sensor Shock-Excitation Response for Solid Panel Configuration.

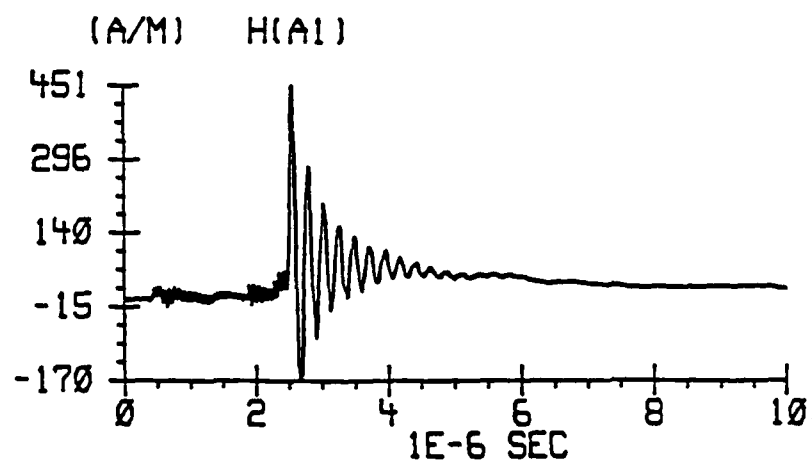


Figure V-58. Resulting Magnetic Field Calculated From the Response of Figure V-57.

Based upon the above, an assumption is made that the magnetic field response is determined by the total current, I_T , which is the sum of the displacement current, I_d , and the conduction current, I_c , on the LTO. An assumption is also made that the displacement and conduction currents generating the measured magnetic field response flow along the longitudinal axis of the LTO. The external B-dot sensor was oriented to respond to the field lines following the circumference of the cylinder. These magnetic field lines, are depicted in Figure V-59, along with the current causing them. Integrating and using Stokes' Theorem, the previous differential form of Maxwell's equation becomes

$$\oint \vec{H} \cdot d\vec{l} = I_d + I_c = I_T$$

Using the circumference of the LTO as a closed circular path, the total current is then given by

$$I_T = H 2\pi r$$

where r is the radius of the LTO. Thus, the total current derived from the magnetic field response provides an excitation source that describes both the charging and discharging phases of the simulation. The response of the current shunt was used to linearly scale the total current to the appropriate levels. Plots of transfer functions were created as before, allowing a comparison to be made

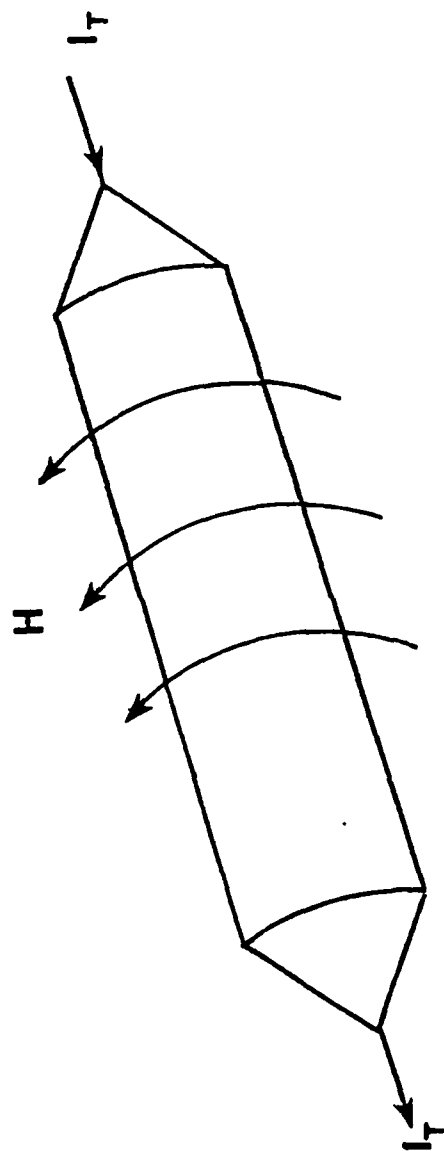


Figure V-59. Magnetic Field Lines Around I_T Due to Current Flowing on the Cylinder.

between the various test methods.

Results. Figure V-60 shows a typical response for the external E-field measured with a solid aluminum panel in the aperture. Note the initial, almost linear, negative increase in the electric field due to the input spark gap breakdown, followed by the charging phase. Once the arc across the output spark gap is established, the electric field immediately oscillates as the excitation current flows on the cylinder.

Figure V-61 shows a corresponding H-field response under the same conditions. During the input spark gap breakdown and charging phase, the magnetic field has a negative rate of change. The magnetic field then experiences a rapid positive change after the output spark gap is established. The magnetic field then follows the source excitation, oscillating as the source current is discharged through the cylinder.

At this time it is instructive to compare transfer functions from the three ground based lightning simulation techniques that we have used in these experiments: the SFCW, current injection and shock-excitation methods. Figure V-62 shows the transfer function for the external magnetic field found by the SFCW method with a coaxial ground path and a solid aluminum panel in the aperture.

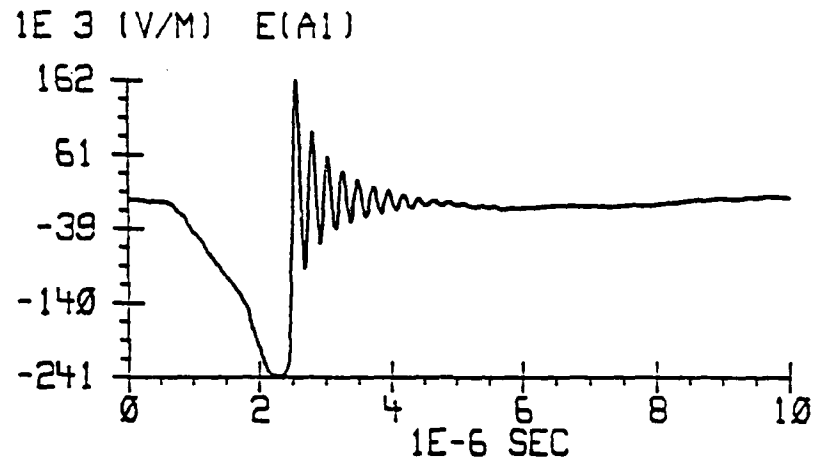


Figure V-60. External Electric Field Response of LTO With Solid Panel Due to Shock-Excitation.

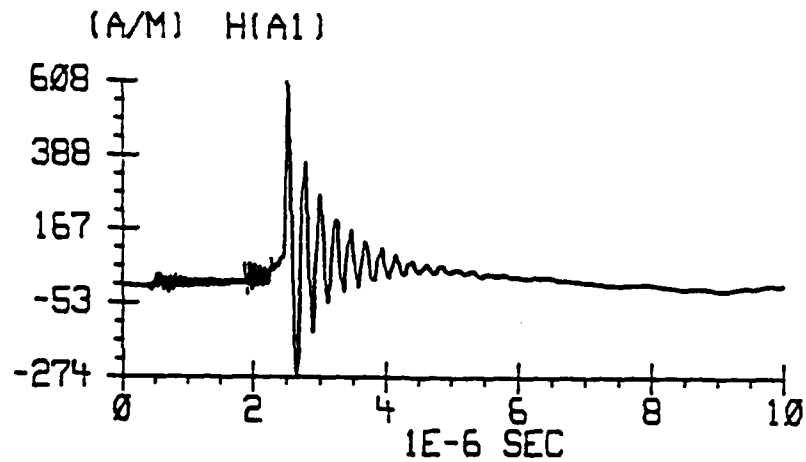


Figure V-61. External Magnetic Field Response of LTO With Solid Panel Due to Shock-Excitation.

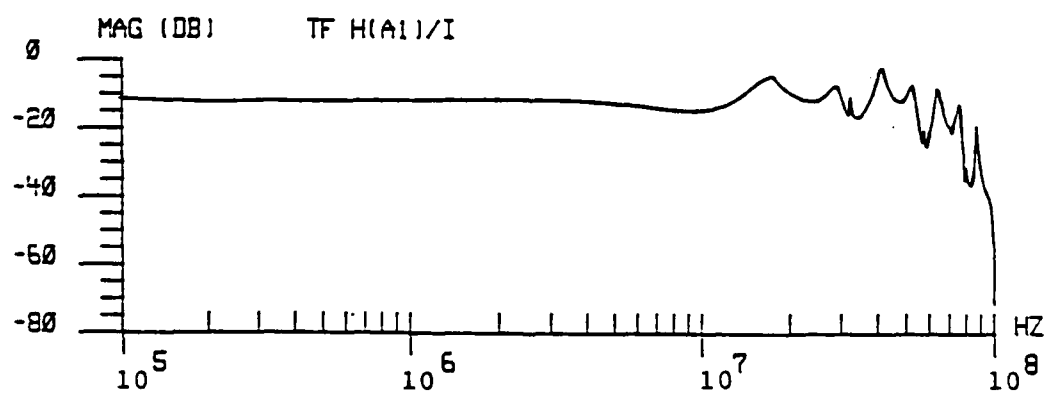
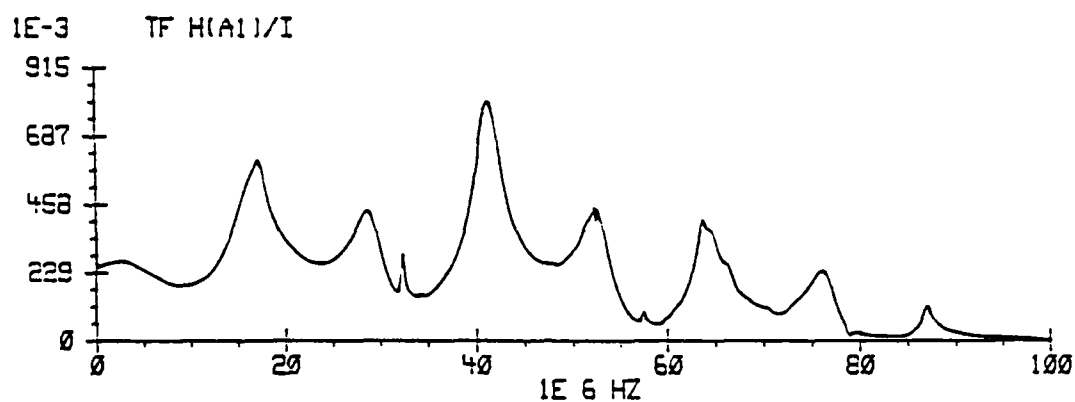


Figure V-62. External Magnetic Field Transfer Function of LTO With Solid Panel Due to SFCW Excitation.

We will compare this waveform to those obtained using the current injection (Figures V-63 through V-65, and V-67 through V-69) and shock-excitation methods (Figures V-66 and V-70).

In the case of the current pulse technique, the magnitude of the transfer function for the external magnetic field response steadily decreases at higher frequencies. This holds true, not only for the unipolar current pulse, (Figure V-63), but also for the oscillatory cases (Figure V-64 and V-65). For these configurations, the oscillatory transfer functions have a faster decrease in magnitude than the unipolar case. This differs from the SFCW case, where the transfer function magnitude is relatively constant until about 80 MHz. For the shock-excitation case, Figure V-66, the transfer function tends to increase in magnitude at higher frequencies.

The linear plots of the transfer function clearly show many distinct peaks. For the SFCW case, spikes occur at 17, 29, 41, 52, 64, 87 MHz. For the current injection case, spikes are evident at 6, 8, 17 and 20 MHz, in addition to a number of lobes between 40 and 60 MHz. The prominent lobes around 17 MHz and between 40 and 60 MHz correlate very strongly with equivalent lobes for the SFCW case. Figure V-66 shows the transfer function resulting from the magnetic field response for the shock-excitation

tests. The resonant coupling at 17 MHz and other frequencies is shown, but distinct, high coupling at 57 and 67 MHz is also shown. This test used a different return path configuration and a different high voltage Marx bank and these spikes are directly related to these differences in the configuration.

The transfer functions for the external electric field measurements are shown in Figures V-67 through V-69 for the current injection technique, and in Figure V-70 for the shock-excitation technique. In all three cases of current injection, there is a large grouping of spikes around 5 MHz, and again at 20 and 40 MHz. In addition, the oscillatory waveforms exhibit additional spikes at higher frequencies, above 80 MHz. In comparing these results with those obtained with the shock-excitation technique, we see large numbers of spikes between 16 and 60 MHz, with additional large spikes at 67, 69 and 72 MHz. We can see that by using multiple simulation techniques, we can identify responses that are due to the test object and those due to the measurement configuration. It is probable that the sharp spikes at 57 and 67 MHz are due to the change in return path and generator.

These results also support the idea of dividing the response up into several regions. For instance, the three electric field response transfer functions are

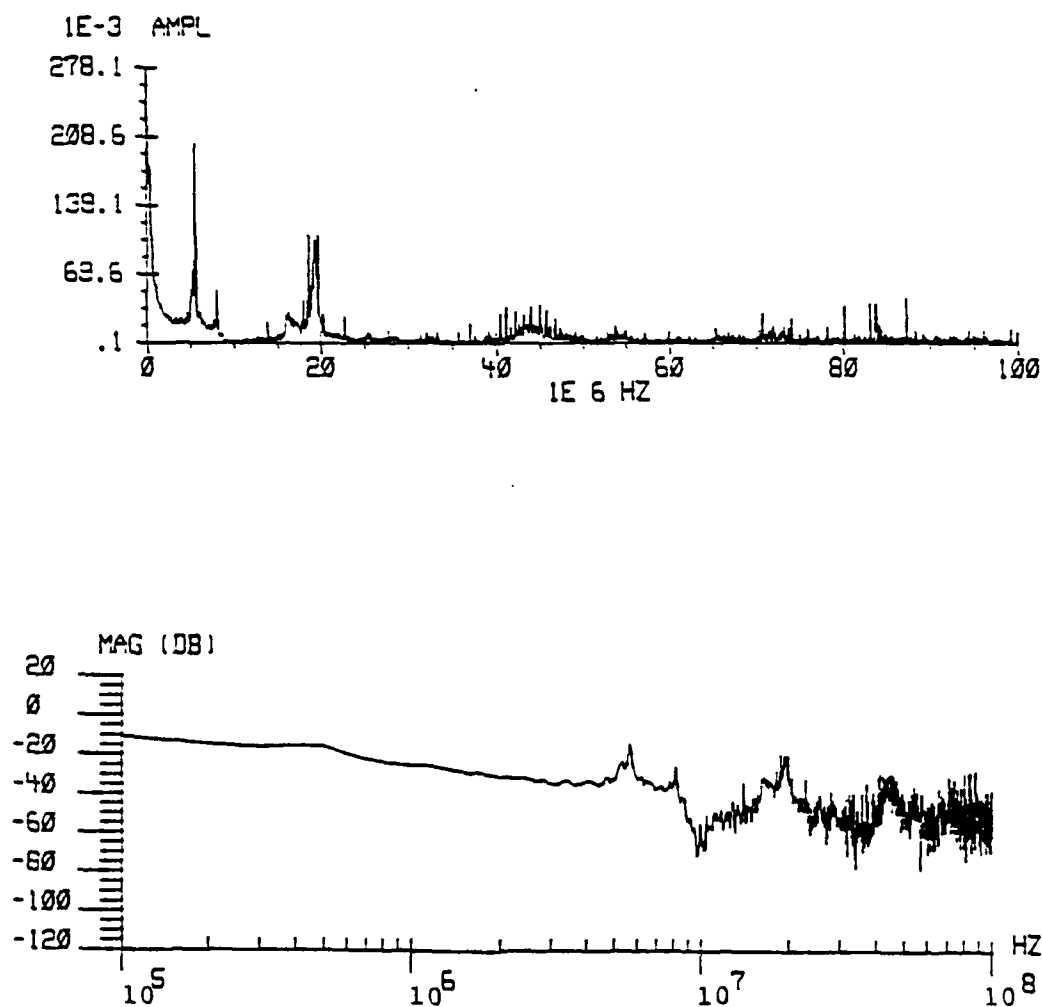


Figure V-63. External Magnetic Field Transfer Function of LTO With Solid Panel Due to 20 kA Unipolar Current Pulse Excitation.

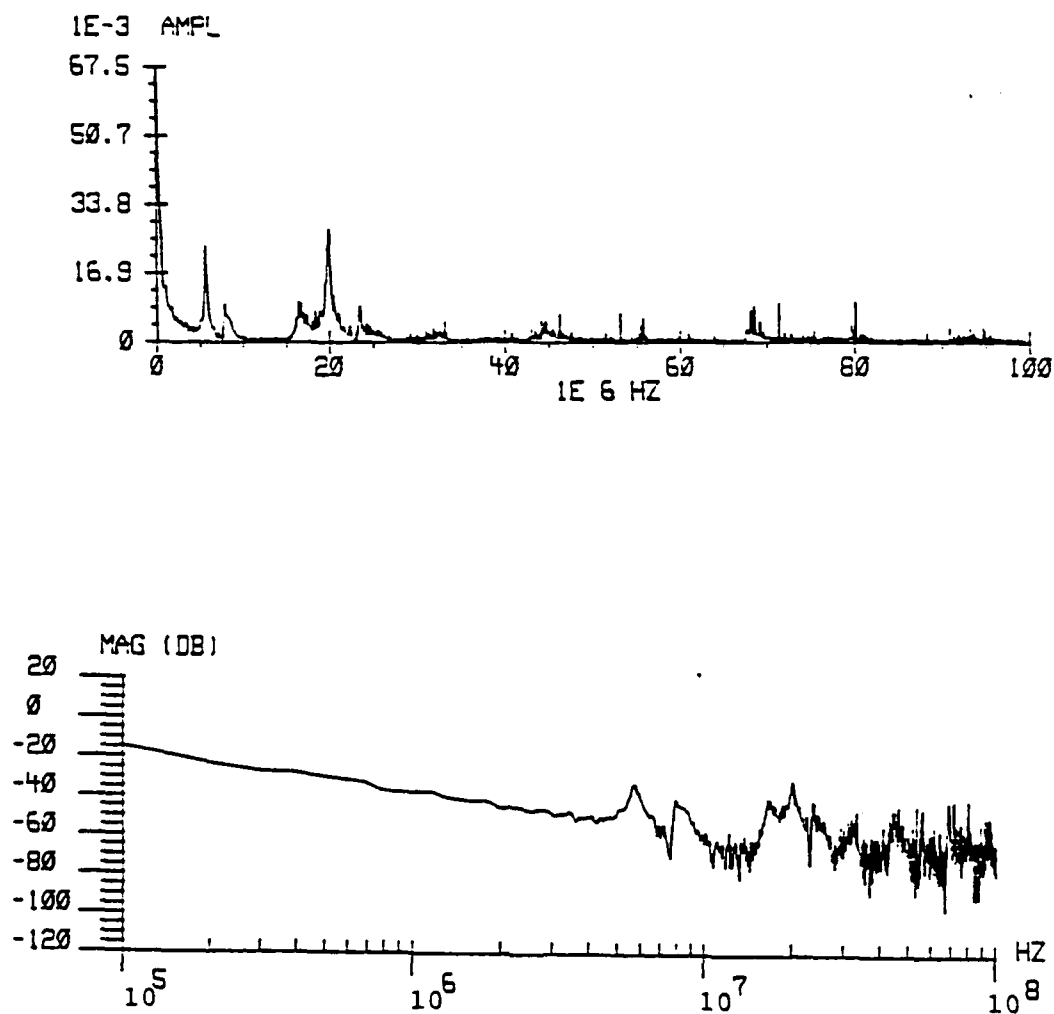


Figure V-64. External Magnetic Field Transfer Function of LTO With Solid Panel Due to 20 kA Oscillatory Current Pulse Excitation.

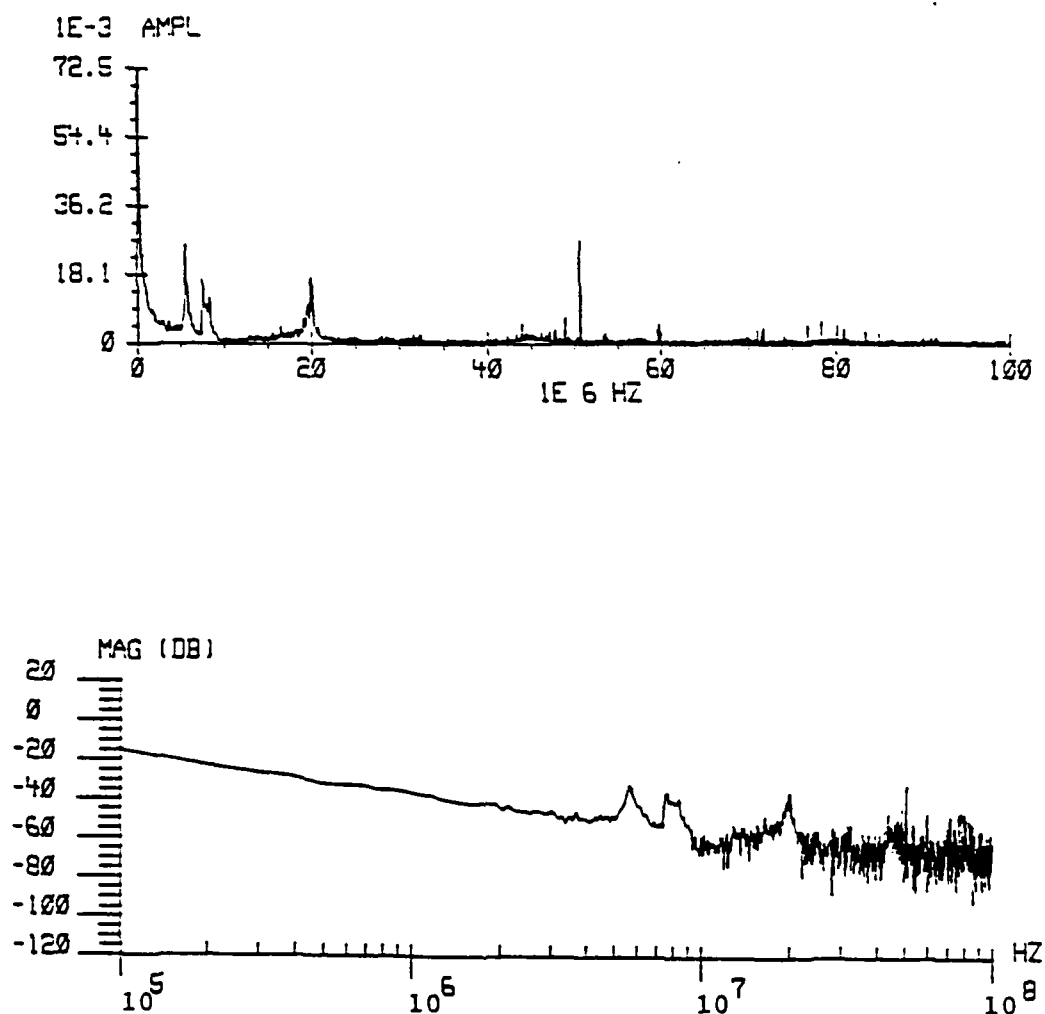


Figure V-65. External Magnetic Field Transfer Function of LTO With Solid Panel Due to 100 kA Oscillatory Current Pulse Excitation.

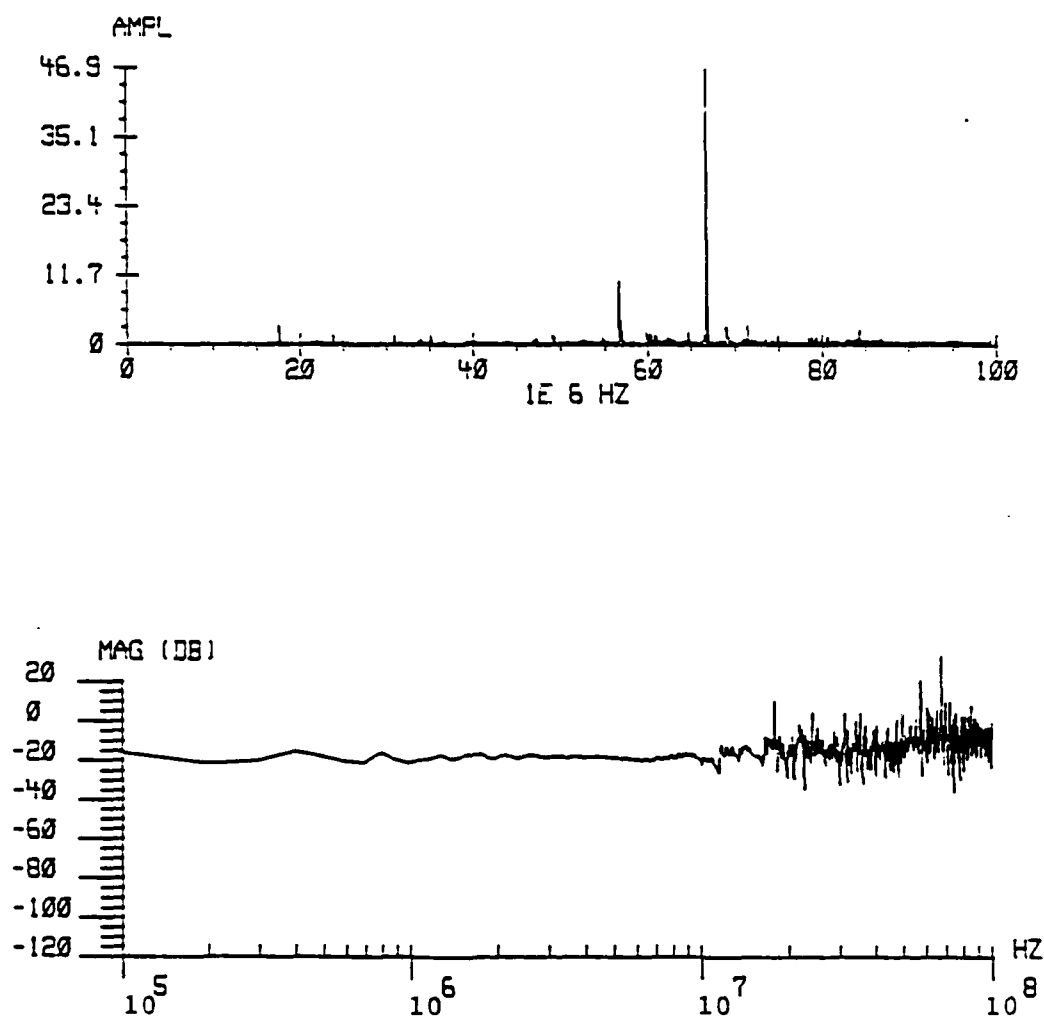


Figure V-66. External Magnetic Field Transfer Function of LTO With Solid Panel Due to Shock-Excitation.

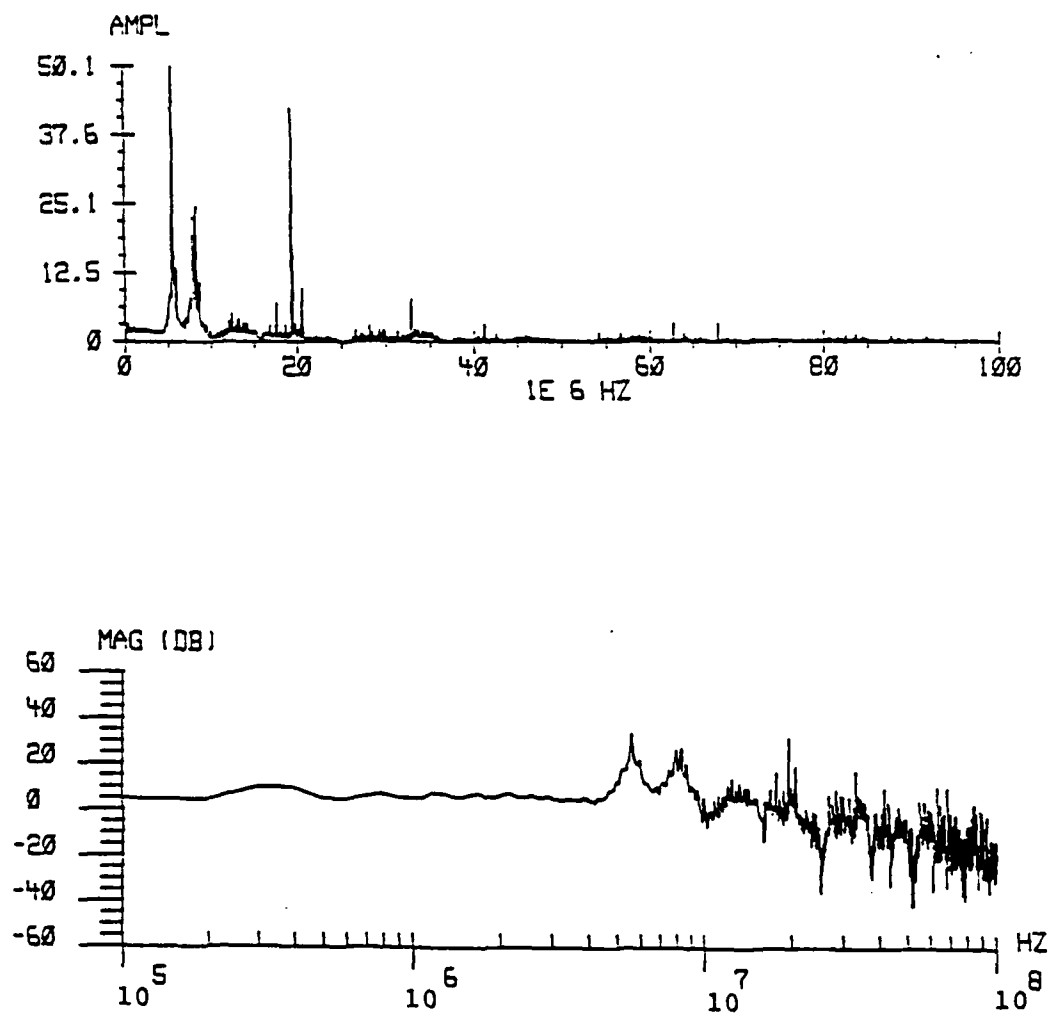


Figure V-67. External Electric Field Transfer Function of LTO With Solid Panel Due to 20 kA Unipolar Current Pulse Excitation.

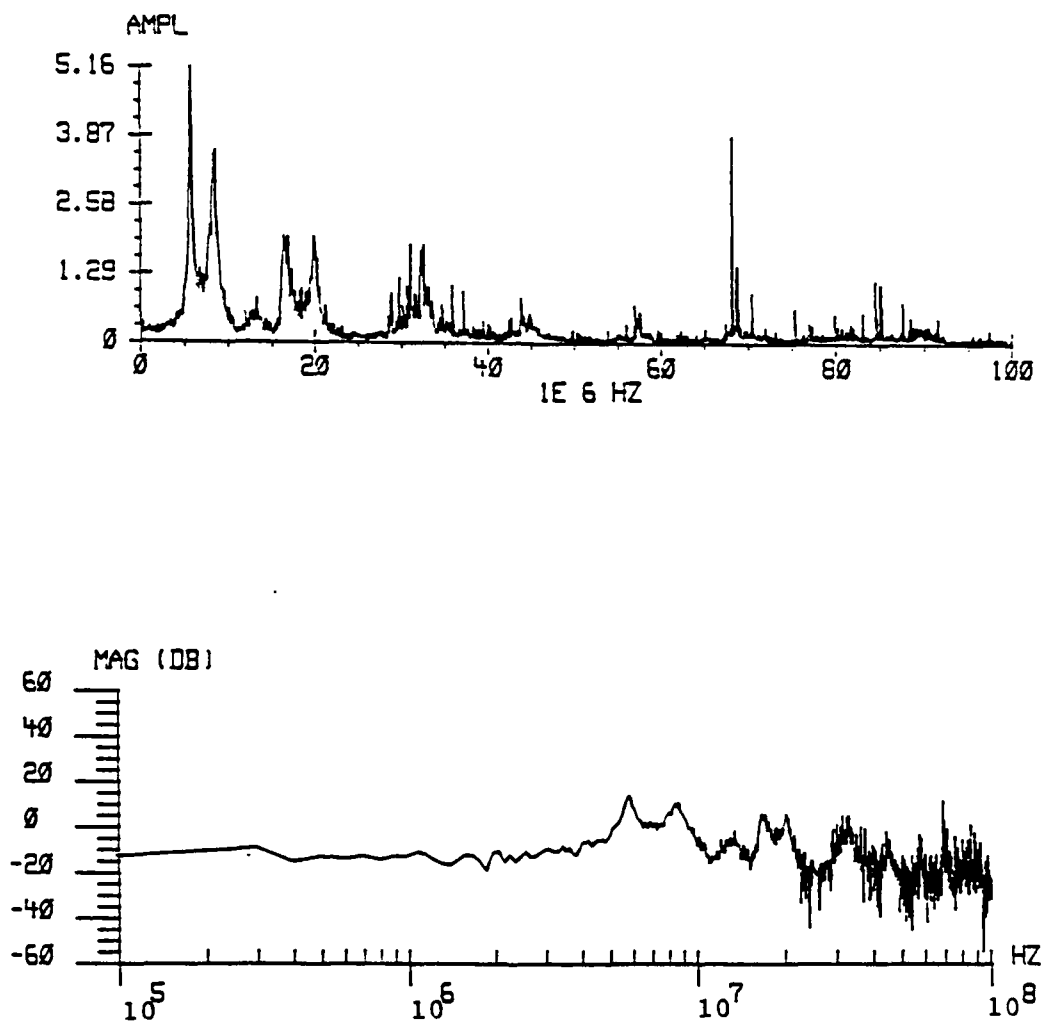


Figure V-68. External Electric Field Transfer Function of LTO With Solid Panel Due to 20 kA Oscillatory Current Pulse Excitation.

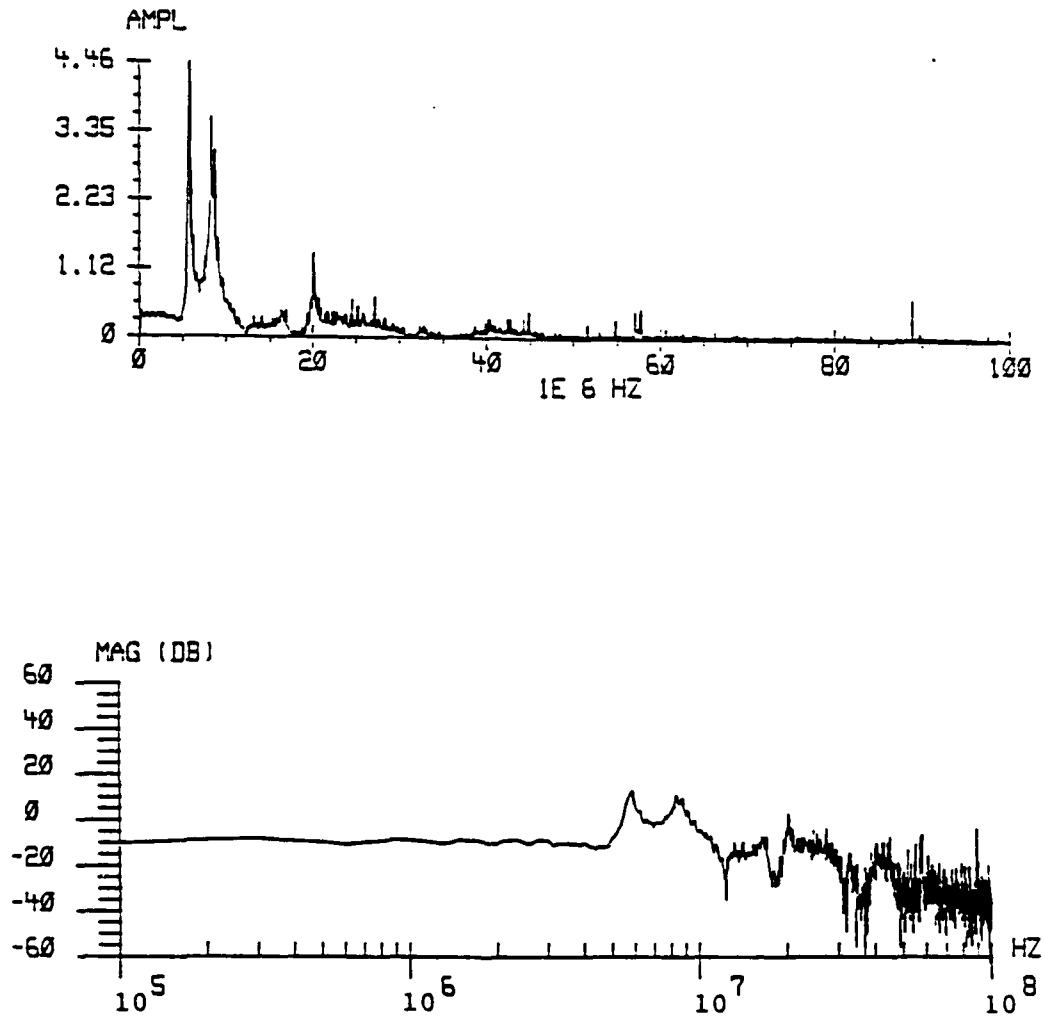


Figure V-69. External Electric Field Transfer Function of LTO With Solid Panel Due to 100 kA Oscillatory Current Pulse Excitation.

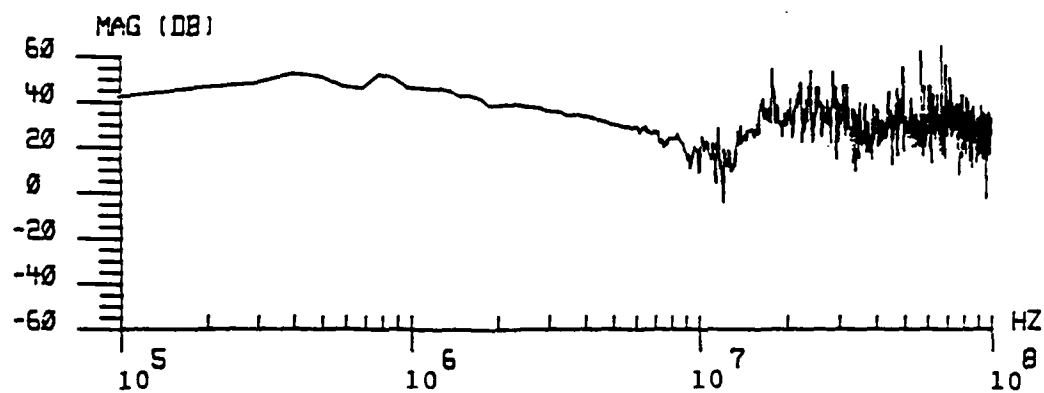
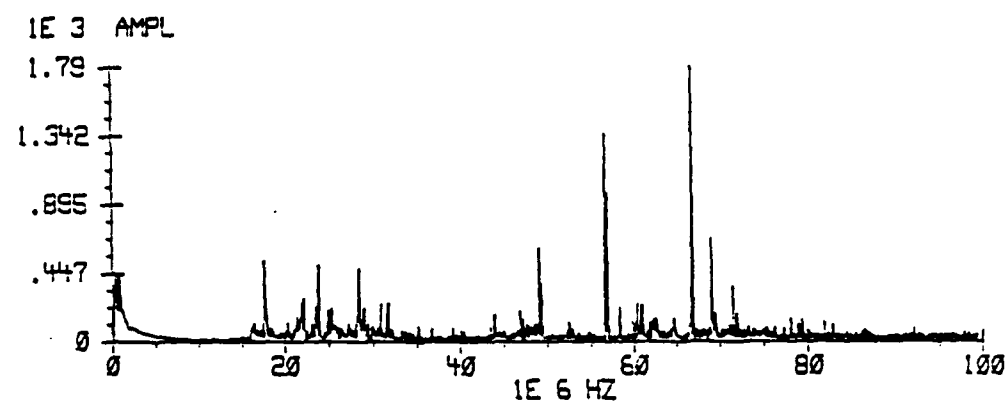


Figure V-70. External Electric Field Transfer Function of LTO With Solid Panel Due to Shock-Excitation.

qualitatively almost identical below 15 MHz, where the quasi-static region would be. Here we would expect to see little effect due to minor variations in the configuration. Above 80 MHz we see only minor variations, again what we would expect for the resonance region. In the transition region between, we do see many variations, indicating the greater sensitivity to the changes in return path, generator, etc.

In the next and final chapter, we will summarize the work done during this research, list the results obtained and present recommendations for further research efforts. As part of the recommendations, a method to utilize these results will be presented.

REFERENCES - CHAPTER V

J.L. Hebert, J.S. Reazer, J.G. Schneider, M.D. Risley, and A.V. Serrano, "Current Levels and Distributions on an Aircraft During Ground Simulation Tests and In-Flight Lightning Attachments," Proceedings of 1986 International Aerospace and Ground Conference on Lightning and Static Electricity, Dayton, OH, June 24-26, 1986, pp.19-1--19-21.

R.M. Braza, "Experimental Comparison of Lightning Simulation Techniques to CV-580 Airborne Lightning Strike Measurements," Masters Thesis, AFIT/GE/ENG/87D-5, School of Engineering, Air Force Institute of Technology (AU), Wright-Patterson AFB, OH, December 1987.

W.G. Butters, D.W. Clifford, K.P. Murphy and K.S. Zeisel, "Assessment of Lightning Simulation Test Techniques," by McDonnell Aircraft Company. Air Force Wright Aeronautical Laboratories Technical Report, AFWAL-TR-81-3075, Part 1, Wright-Patterson AFB, OH, October 1981, p. 107.

J.L. Hebert, "UH-60A Black Hawk Swept Frequency Continuous Wave Lightning EMP Test Plan," Internal Report, Air Force Wright Aeronautical Laboratories, Atmospheric Electricity Hazards Group, AFWAL/FIESL, Wright-Patterson AFB, OH, 12 September 1985.

J.L. Hebert, Personal Communication, November 1987. The majority of SFCW results for the UH-60A Black Hawk are from data provided by Hebert which has not been presented in any previous reports prior to this dissertation. J.L. Hebert is presently with HQ AFSC/SDP, Andrews AFB, 20301.

D.B. Whalen, "Comparison of Low Level Frequency Domain Lightning Simulation Test to Pulse Measurements," Proceedings of 1986 International Aerospace and Ground Conference on Lightning and Static Electricity, Dayton, OH, June 24-26, 1986, pp.9-1--9-8.

D.B. Whalen and M.M. Simpson, "Atmospheric Electricity Hazards Protection Part II: Assessment, Test and Analysis - F14A," by Boeing Military Airplane Company. Air Force Wright Aeronautical Laboratory Technical Report, AFWAL-TR-87-3025, Part II, Wright-Patterson AFB, OH, June 1987.

D.W. Clifford and K.S. Zeisel, "Evaluation of Lightning-Induced Transients in Aircraft Using High-Voltage Shock Excitation Techniques," Proceedings of the 1979 IEEE International Symposium on Electromagnetic Compatibility, San Diego, CA, October 9-11, 1979, pp. 160-166.

J.E. Lenz, D.W. Clifford and W.G. Butters, "Experimental Resolution of System Resonances Produced by Simulated Lightning Excitation," Proceedings of Lightning Technology Symposium, NASA Langley, NASA Conference Publication 2128, FAA-RD-80-30, April 22-24, 1980, pp. 21-37.

CHAPTER VI

SUMMARY, CONCLUSIONS AND RECOMMENDATIONS

Overview

This chapter presents a short summary of the accomplishments of this research effort. The conclusions that can be drawn from this work are discussed. Finally, several recommendations for further efforts in this area of work are presented.

Summary of Accomplishments

During the course of this research, several items of significance were accomplished. One of the goals of this research effort was to better characterize how the measurement configuration affects the ground-based lightning simulation of the airborne lightning-aircraft interaction event. This research shows that the response of an object, even one as simple as a cylinder, is not only dependent upon the particular simulation technique used, but is very dependent upon the configuration used with that technique. For more complex objects, such as an aircraft, there is a high probability that configuration effects may mask some of the resonances introduced by the greater geometrical complexity of the test object.

Evidence gathered during the course of this research clearly indicates that the type of return path and choice of ground plane will affect the results achieved. The purpose of the return path is to create, as much as possible, an electromagnetic field around the test object which is equivalent to the one the object would experience during flight. If sufficient attention is not paid to good return path design, additional resonances between the return path and test object will be introduced. Again, these false resonances may mask the true response of the vehicle to the excitation source.

One idea presented in this work is the concept of characterizing interactions by determining if the interaction falls into one of three regions of interaction. That is, the interactions between the test object and the configuration can be broken up into the quasi-static, transition and resonance regions. In the quasi-static region, the configuration effects are negligible, while in the resonance region the configuration effects are dominated by the distributed electrical parameters of the system. The transition region provides a bridge between the quasi-static and resonance regions. In this region the configuration effects are noticeable and the lumped circuit parameters of the generator, return path, test object, etc., dominate the response. In other words, the configuration effects

can be characterized by the lumped circuit parameters of the measurement configuration.

Conclusions

Several conclusions can be drawn based upon the results of this research. These conclusions are based upon a combination of the literature examined and the experimental data gathered during this research. The conclusions will be presented in an order which mirrors the sequence of background and experimental data presented in this dissertation.

When we want to perform ground-based simulations of the lightning-aircraft interaction event, it is neither feasible nor desirable to design the perfect test setup and simulation generator. At the present time, and for the near-term, there are far too many design factors, especially cost, to consider. Rather, the designer should strive to design a well-characterized test setup that achieves the simulation goals for his particular test series.

Due to a lack of understanding, it is not yet feasible to simulate the nonlinearities of the interaction processes with a high degree of confidence. Much work remains in characterizing the underlying physical causes

of these processes and the importance of their effects. Once the physics is better understood, further development of codes, such as the FDTD codes, should make it possible to create models which can accurately predict the sequence of activities that will occur during those processes.

The results of the CV-580 airborne lightning characterization program indicate that the aircraft interacts with the lightning channel to produce skin current and charge distributions that give a response which is influenced by the complex geometry of the aircraft. Also, these results, as well as those from the UH-60 investigations, indicate that the location of entry and exit points is important in determining the response of the vehicle to lightning excitation. This is important when determining what sort of measurement configuration to construct, as the results from a coaxial configuration will not be the same as a ground plane configuration. While nose-to-tail and wingtip-to-wingtip simulations can be done relatively easily, the results of swept stroke studies would be more difficult to achieve if a coaxial return path was used.

Configuration effects appear to introduce their influence by causing a change in these skin current and charge distributions. This has the effect of shifting and/or masking the actual responses (natural resonances)

of the vehicle to the excitation caused by the lightning, or adding false resonances which would not be present if the measurement configuration was not surrounding the vehicle.

In comparing the magnetic field results from the different simulation techniques, the conclusion can be drawn that scaling should be applied very carefully when extrapolating from low levels. The scaling of the SFCW results to the level of the severe threat tends to significantly overestimate the threat. Extrapolation from the 20 kA simulation yields better results, while the 100 kA simulation is very close. The less extrapolation needed, the more accurate the predicted induced transient will be.

In terms of the electric field transients, the inflight measurements of the CV-580 recorded maximum E-field transients of approximately 200 kV/m. From the results of the peak external E-field responses, only the shock-excitation test method produces a peak E-field transient which exceeds the airborne response. Based upon these results, it appears that the current injection techniques are sufficient to reproduce the effects of the rapidly changing magnetic field caused by lightning, but that the shock-excitation technique is needed if the changes in the electric field are to be accurately

reproduced.

Through the use of frequency domain techniques, many of these configuration effects can be removed, leaving a more accurate and valid representation of the response of the test object to the stimulus employed in the simulation technique. In fact, one could conclude that a combination of validated prediction codes, measured data, and the removal of configuration effects by Fourier transform techniques will yield a simulation of much higher quality than is presently carried out. These enhanced simulation techniques have the potential for reducing the cost of simulator design, while adding flexibility to the simulation process.

The goal of these techniques would be to use this combination of tools to remove the measuring sensors' contributions to the measured transient data and the test setup/generator configuration effects. In essence, this should provide a better prediction and simulated measurement of the circuit transients which systems would experience during an airborne lightning strike. The enhanced simulation techniques would involve three separate, but related, phases: 1) Analytical phase; 2) Test phase; and 3) Post-Test phase.

Analytical Phase. The key to enhanced simulation techniques is the analytical prediction of electric field and skin current distributions on a vehicle during an airborne lightning strike. These predictions, which may result from either time domain or frequency domain analysis, would be used to remove configuration effects in the following manner.

The result needed is a transfer function for each panel which covers circuits or equipment where electromagnetic energy may couple into the interior of the aircraft: an analytically derived electric field transfer function $TF_{EA}(\omega)$ where the strongest coupling mechanism is expected to be capacitive coupling, and an analytically derived skin current transfer function $TF_{JA}(\omega)$ where inductive coupling would be expected. Actually, both of these transfer functions should be derived for each panel of interest. These transfer functions should be analytically derived for each test configuration that the vehicle will be tested in (i.e. wing-to-wing, nose-to-tail, etc.). If time domain codes are utilized, these transfer functions can be easily derived using Fast Fourier Transform techniques.

The two analytical transfer functions are found by dividing the appropriate response by the excitation

source. The first is

$$TF_{E_{Ai}}(\omega) = \frac{E_{Ai}(\omega)}{I_A(\omega)}$$

where

$TF_{E_{Ai}}(\omega)$ = The analytical (A) impedance/meter electric (E) field transfer function at panel i.

$E_{Ai}(\omega)$ = Analytically (A) predicted electric field response at panel i due to the excitation source $I_A(\omega)$.

$I_A(\omega)$ = The current excitation source (a current because this is the excitation source most commonly used in lightning simulation tests.)

The second transfer function is given by

$$TF_{J_{Ai}}(\omega) = \frac{J_{Ai}(\omega)}{I_A(\omega)}$$

where

$TF_{J_{Ai}}(\omega)$ = The analytical (A) skin current (J) redistribution transfer function at panel i.

$J_{Ai}(\omega)$ = The skin currents at panel i produced by $I_A(\omega)$.

$I_A(\omega)$ = The same as above.

Test Phase. The second step is to perform the simulation test, whether current pulse, shock excitation or SFCW, in the same manner as has been performed regularly in recent years, with a few additional measurements. These additional measurements will allow the sensor and configuration effects to later be removed from the data. Record the input currents and electronic

circuit transient responses as usual. The additional measurements are somewhat similar to the E-field measurements performed during EMP testing. During the test, derive the same transfer functions which were derived in the analytical predictions by measuring the current excitation source, I_M , the measured skin current distribution on the panels, J_{Mi} and the E-fields present on the panels, E_{Mi} .

Before calculating the measured transfer functions, remove the sensor effects, as described in frequency domain techniques above, by dividing the sensor's transfer function out of the sensor measurement

$$J_{Mi}(\omega) = \frac{J(\omega) \text{ Actually measured}}{TF(\omega)_{\text{sensor}}}$$

$$E_{Mi}(\omega) = \frac{E(\omega) \text{ Actually measured}}{TF(\omega)_{\text{sensor}}}$$

$$I_M(\omega) = \frac{I(\omega) \text{ Actually measured}}{TF(\omega)_{\text{sensor}}}$$

Note that this will also integrate derivative sensor measurements, that is, $J\text{-dot}$ measurements will become J measurements. This will remove the measurement sensors' effects from the measured data. Then form the appropriate measured transfer functions for each panel which

corresponds to those analytically predicted

$$TF_{EMi}(\omega) = \frac{E_{Mi}(\omega)}{I_M(\omega)}$$

$$TF_{JMi}(\omega) = \frac{J_{Mi}(\omega)}{I_M(\omega)}$$

Post-test Processing. With the circuit transient response measurement, $R(\omega)$, and the input excitation, $I(\omega)$, recorded for each shot, plus the additional measurements described above, post-test processing is used to relate the ground simulation responses to those which would occur with the aircraft in an airborne lightning strike. Post-processing begins by removing the sensors' effects from each response and input waveform using the frequency domain techniques described earlier. For each panel i , closest to to where the internal circuit response is measured, find a difference (D) transfer function for the electric field, $TF_{EDi}(\omega)$, and the skin current distribution, $TF_{JDi}(\omega)$, where

$$TF_{EDi}(\omega) = \frac{TF_{EMi}(\omega)}{TF_{EAI}(\omega)}$$

$$TF_{JDi}(\omega) = \frac{TF_{JMi}(\omega)}{TF_{JAI}(\omega)}$$

These new difference transfer functions describe the difference between the electric field and skin current distributions present during ground simulation tests and those which were analytically predicted for an airborne strike. These are used to relate the ground simulation responses to those which would occur in the airborne case.

Form the total measured transfer function

$$TF_{TOTM}(\omega) = \frac{R(\omega)}{I(\omega)}$$

If the coupling processes are weak between the exterior and interior of the vehicle, then the interior does not affect the exterior electric field or skin current distribution significantly. In this case, the total measured transfer function, $TF_{TOTM}(\omega)$, will be given by

$$TF_{TOTM}(\omega) = TF_{EMi}(\omega) \times [TF_{Ex-In}(\omega) \times TF_{In-Wire}(\omega) \times TF_{etc}(\omega)]$$

where $TF_{EMi}(\omega)$ - Measured transfer function described above.

$TF_{Ex-In}(\omega)$ - Transfer function from exterior to interior of the vehicle.

$TF_{In-Wire}(\omega)$ - Transfer function from interior fields to the circuits where response is measured.

$TF_{etc}(\omega)$ - All other transfer functions which may exist.

Often, by simply examining the responses, it is possible to determine whether the dominant coupling mechanism is capacitive or inductive. Depending on whether it is capacitive or inductive, divide the total circuit response transfer function by $TF_{EDi}(\omega)$ or $TF_{JDi}(\omega)$ respectively. This will essentially change the $TF_{EMi}(\omega)$ part of $TF_{TOTM}(\omega)$ to $TF_{EAI}(\omega)$ and $TF_{JMi}(\omega)$ to $TF_{JAI}(\omega)$, thus relating the rest of the response to the airborne case. The advantage of this procedure is only the configuration effects on the E-field and skin current distributions are corrected, while all the other transfer functions which would be present, whether airborne or in ground simulation, remain the same. The new total transfer function, $TF_{TOT}(\omega)$, may then be used to determine the circuit's response to any threat waveform by frequency domain multiplication, which directly relates to time domain convolution. The response of the circuit $R(\omega)$ to a threat waveform $I(\omega)$ for the airborne case is given by

$$R(\omega) = I(\omega) \times TF_{TOT}(\omega)$$

By taking the inverse transform of $R(\omega)$ and $I(\omega)$ the time domain transient response $r(t)$ to the threat waveform $i(t)$ can be determined.

These enhanced simulation techniques would not only allow the ground measured simulation responses to be related to the airborne case, but also allow determination

of the circuit responses to any threat waveform. This could be done for any level of test, including very low level SFCW, moderate level (20kA-50kA) or full threat level (200 kA) responses. By correcting for configuration effects, it is possible that the difficulties due to extrapolation could be minimized.

Recommendations for Future Work

As with most research efforts, this work raised as many questions as it answered. The following are suggestions for further work to be done in this area.

Much work remains in defining the three regions of interaction and what the limits of applicability are. Currently, this concept is based upon qualitative results from this investigation. If the limits of the regions can be quantified and a determination can be made of the application to other measurements, then this concept has the possibility of focusing characterization efforts in the same way that radar cross-section predictions and measurements tend to be focused in one of three regions.

Investigations into the effects of configuration for more complex geometries and composite structures should be carried out. There is a broad gap between measurements on simple geometries, such as that of a cylinder, and a full-

size vehicle. There would be utility in developing test bodies of intermediate complexity. This would allow a check on the extrapolation of results from simple bodies to complex bodies.

Many of the results obtained must be further quantified and defined. For instance, the question of whether configuration effects mask natural resonances must be addressed. If natural resonances are masked, under what conditions does this masking occur.

There should be a determination of what information is needed to remove configuration effects efficiently. It is suggested that the instrumentation and techniques now available, especially vector network analyzers with time domain capability, can provide the necessary information to analyze and remove many of the unwanted configuration effects. Also, if more accurate prediction models can be developed, then the method for enhanced simulation techniques presented in the previous section should be able to be used. Research should be done to validate this concept and determine the limits of usefulness.

Follow up work is being carried out by many researchers to further characterize and quantify the influence of these configuration effects. Through a combination of better characterization of the measurement

configuration and more accurate configuration diagnostic techniques, it is believed that both the quality of lightning qualification and surveillance testing and prediction capabilities can be improved. With this increased capability will come an improvement in hardening techniques used for the protection of aerospace vehicles.

APPENDIX I

SENSOR DATA SHEETS

The following data sheets are provided to give additional information on the sensors and signal conditioning components discussed in Chapter II. These data sheets also cover the sensors that were used during the experimentation outlined in Chapter V. For additional information on other types of sensors, consult the EG&G Standard EMP and Lightning Instrumentation Catalog, from which these data sheets were extracted.

The equipment covered in this appendix includes:

Multi-Gap Loop (MGL) B-dot Sensor

Cylindrical Moebius Loop (CML) B-dot Sensor

Hollow Spherical Dipole (HSD) D-dot Sensor

Flush Plate Dipole (FPD) D-dot Sensor

Asymptotic Conical Dipole (ACD) D-dot Sensor

Circular Parallel Mutual Inductance (CPM) I-dot Sensor

Parallel Plate Dipole (PPD) E-field Sensor

A typical optical data link data sheet

Passive Integrator (RCI-1B)

Active Integrator (IA)

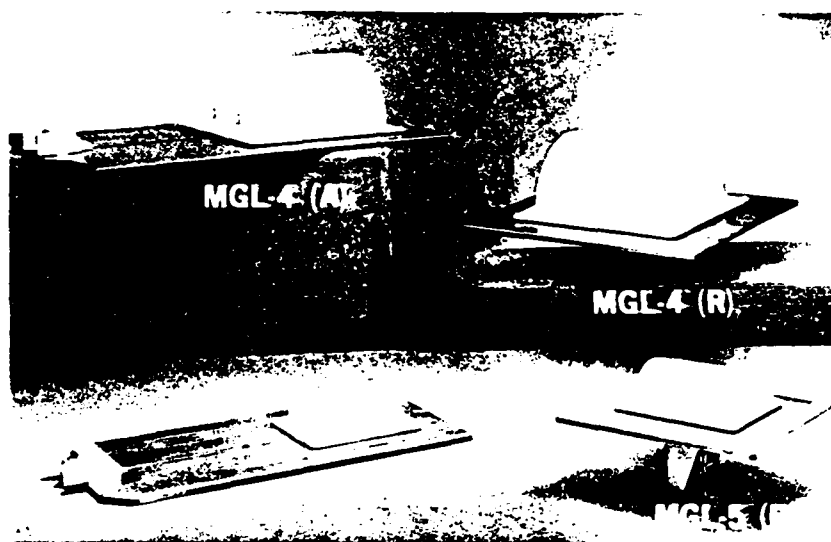


WASHINGTON ANALYTICAL SERVICES CENTER, INC.

DATA SHEET 1103

April 1979

MGL \dot{B} SENSORS (Ground Plane)



The MGL (Multi-Gap Loop) ground plane B-dot sensors (Models 3, 4, 5, 7 and 8) are half cylinder loops mounted on conducting ground plates for positioning on a ground plane to measure the time rate-of-change of incident magnetic fields. These sensors can also be used for surface current density measurements. (Data Sheet 1107 describes J-dot sensors designed especially for skin current measurements.) These sensors are passive devices; they require no external power. Gas fittings allow pressurization to eliminate arcing in intense fields and weather problems. They have been used extensively in EMP simulation programs.

The half cylinder sensors have two symmetrically located gaps which are combined by a series-parallel wiring arrangement to drive the coaxial output connector. The output connector can exit either along the cylinder axis (axial version) or along a radius (radial version) as shown above.

PERTINENT EQUATION

$$V_o = \bar{A}_{eq} \cdot \frac{d\bar{B}}{dt} = \text{sensor output (in volts)}$$

where

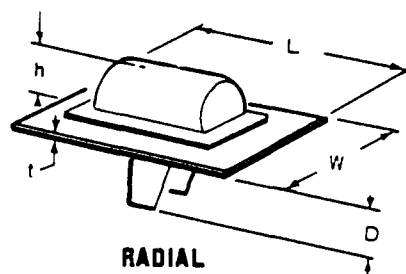
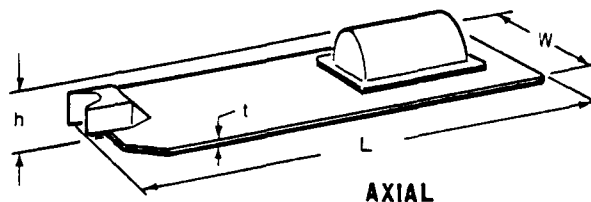
$$\bar{A}_{eq} = \text{sensor equivalent area (in m}^2\text{)}$$

$$\bar{B} = \text{magnetic flux density vector (in teslas)}$$

SPECIFICATIONS

Parameter	MGL-3	MGL-4	MGL-5	MGL-7	MGL-8
A_{eq} m ²	1×10^{-1}	1×10^{-2}	1×10^{-3}	1×10^{-4}	1×10^{-5}
Frequency Response (-3 dB Point)	78 MHz	230 MHz	700 MHz	> 2 GHz	> 3 GHz
Risetime T_r (10-90)	< 4.5 ns	1.5 ns	0.5 ns	< 0.15 ns	< 0.05 ns
Maximum Output (peak)	5 kV	5 kV	5 kV	1.0 kV	150 V
Maximum Field Change	5×10^{-4} tesla/sec	5×10^{-5} tesla/sec	5×10^{-6} tesla/sec	1.0×10^{-7} tesla/sec	1.5×10^{-8} tesla/sec
Output Connector	GR874L-50	GR874L-50	GR874L-50	ARM 1054-0000	APMM 4052-0000
Mass	25.9 kg	4.5 kg	2.7 kg	50 g	15 g
Dimensions (cm)	Axial* Radial*		Axial* Radial*		Axial* Radial*
L	37.5	37.5	35.2	28.6	10.4
W	32.7	32.7	25.4	25.4	5.6
h	16.6	16.6	13.2	13.2	2.3
t	0.47	0.47	0.25	0.35	0.25
D	--	1.0	--	9.1	--

Note: Axial or Radial Output Specified by Designations MGL-N-A and MGL-N-R*, Respectively, where N=3, 4, 5, 7 or 8.



(Data and Specifications Subject to Change without Notice)

ORDERING INFORMATION

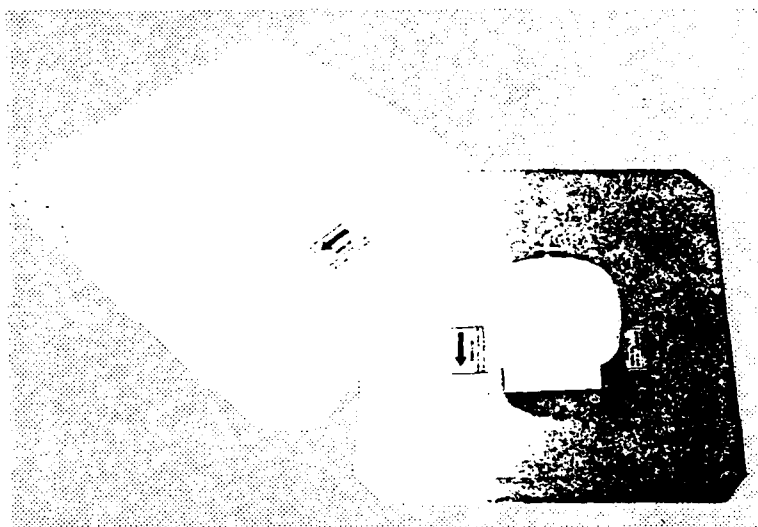
For Price, Availability, or Further Information, Contact

 **EG&G** WASHINGTON ANALYTICAL SERVICES CENTER, INC.
ELECTROMAGNETICS

2450 Alamo Avenue, S.E., P.O. Box 9100, Albuquerque, New Mexico 87119
phone (505) 243-2233, TWX No. 910-989-1684

CML \dot{B} SENSORS (Full Loop)

AIRBORNE LIGHTNING MEASUREMENTS



The CML (Cylindrical Moebius Loop) B-dot sensors (Model 7) are used to measure the currents on an aircraft surface caused by a direct or nearby lightning stroke. These probes are passive devices requiring no external power.

These sensors are cylindrical loops with one gap and the pickoff cables wired in a Moebius configuration. The voltage signal developed across the gap by the changing magnetic field associated with the skin currents is sensed in the differential mode by the pickup cables. The Moebius configuration and the differential output provide for common mode rejection of unwanted signals generated in the sensor by electric field components. The output cables of these CML sensors can exit in a variety of ways as shown on the reverse, and the ground plate is sufficiently flexible to conform to a surface with large ($\geq 1\text{m}$) curvature radius.

PERTINENT EQUATION

$$V_o = \bar{A}_{eq} \cdot \frac{d\vec{B}}{dt} = \text{sensor output (in volts)}$$

where

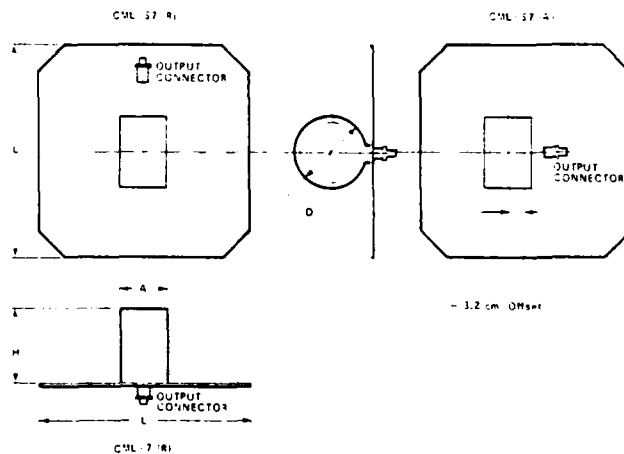
$$\bar{A}_{eq} = \text{sensor equivalent area (in m}^2\text{)}$$

$$\vec{B} = \text{magnetic flux density vector (in teslas)}$$

SPECIFICATIONS

Parameter	CML-7 or CML-S7
A_{eq} (m ²)	2×10^{-2}
Frequency Response (3 dB point)	38 MHz
Risetime (10-90%)	9 ns
Maximum Output	4 kV (with TCC)
Maximum Field Change	2×10^5 tesla sec
Output Connector	TCC*
Mass	1.0 kg
Dimensions (cm)	
L	35.6
D	11.9
H	12.4
A	6.4

*100-ohm twinaxial connector (Data Sheet 1340); Two 50-ohm SMA connectors optional.



(Data and Specifications Subject to Change without Notice)

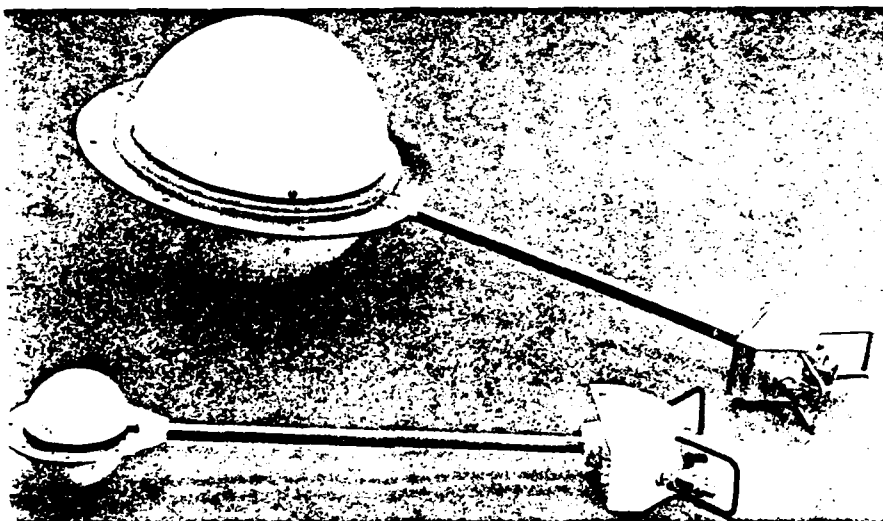
ORDERING INFORMATION

For Price, Availability, or Further Information, Contact

EG&G WASHINGTON ANALYTICAL SERVICES CENTER, INC.
ELECTROMAGNETICS

2450 Alamo Avenue, S.E., P.O. Box 9100, Albuquerque, New Mexico 87119
phone (505) 243-2233, TWX No. 910-989-1684

HSD \vec{D} SENSORS (Free Field)



The free-field HSD (Hollow Spherical Dipole) sensors (Models 2 and 4) measure the normal component of the displacement current ($d\vec{D}/dt$). They consist of two hemispherical shells symmetrically attached to a metal conducting surface by dielectric rings. A pressurizing stem and pressure relief valve, located on opposite sides of the output connectors, allow sensor pressurization with high dielectric strength gas (such as SF_6 or N_2) to prevent arcing in intense EMP fields. Free-field HSD sensors are available only in a radial version (see photo), and require no power. Signal output is on 100-ohm twinaxial cable.

PERTINENT EQUATION

$$I_o = \bar{A}_{eq} \cdot \frac{d\vec{D}}{dt}$$

or

$$V_o = R A_{eq} \frac{dD}{dt} \cos \theta$$

where

I_o = sensor output (in amps)

V_o = sensor output (in volts)

R = sensor characteristic load impedance 100 ohms

A_{eq} = sensor equivalent area (in m^2)

D = magnitude of electric displacement vector $\vec{D} = \epsilon_0 \vec{E}$, in Coul m^2

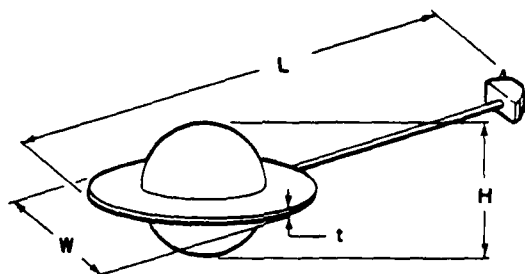
θ = angle between E and vector normal to sensor ground plate

SPECIFICATIONS

Parameter	HSD-2 (R)	HSD-4 (R)
A_{eq} (m^2)	1×10^{-1}	1×10^{-2}
Frequency Response (3 dB Point)	> 45 MHz	> 150 MHz
Risetime (T_r 10-90)	≤ 7.4 ns	≤ 2.3 ns
Maximum Output	5 kV	5 kV
Output Connector	TCC - 100 ohm*	TCC - 100 ohm*
Mass	2.15 kg	0.59 kg
Dimensions (cm)		
L	62.5	44.7
W	28.5	8.9**
H	20.6	6.9
t	0.3	0.16

*100-ohm Twinaxial Connector (EG&G Data Sheet 1340)

**Connector width is greater than W on Model 4 (11.7 cm)



NOTES:

- (1) During use, this sensor must be supported by dielectric materials and positioned at least two sensor diameters from any conducting surfaces.
- (2) A DLT-96 balun (EG&G Data Sheet 1300) can be used to transform 100-ohm balanced output to 50-ohm unbalanced output for telemetry and recording.

(Data and Specifications Subject to Change without Notice)

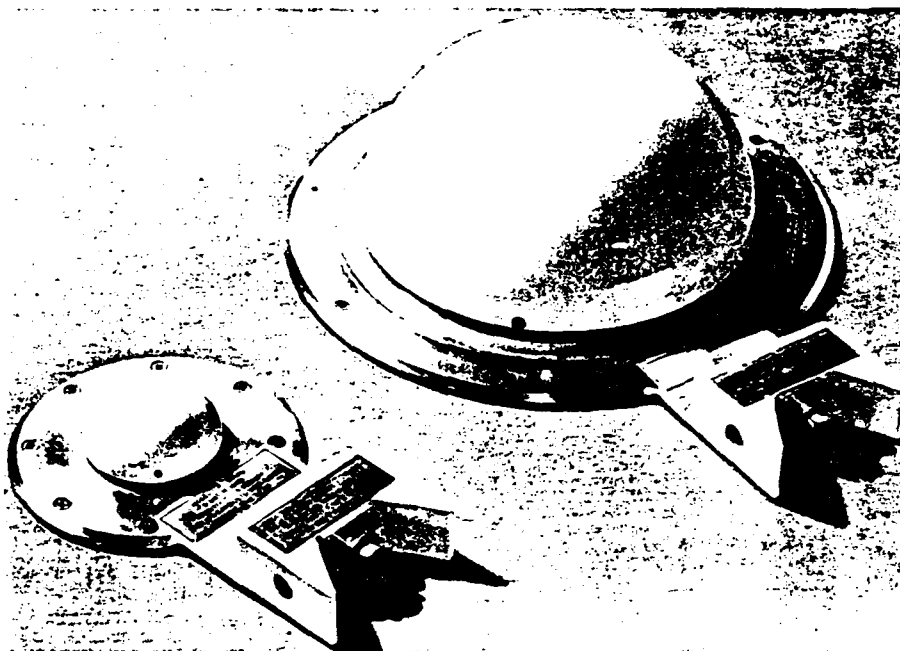
ORDERING INFORMATION:

For Price, Availability, or Further Information, Contact:

EG&G WASHINGTON ANALYTICAL SERVICES CENTER, INC.
ELECTROMAGNETICS

2450 Alamo Avenue, S.E., P.O. Box 9100, Albuquerque, New Mexico 87119
phone (505) 243-2233, TWX No. 910-989-1684

HSD (\dot{q}_s) SENSORS



These HSD (Hollow Spherical Dipole) Sensors are mounted on a conducting surface and used to measure the time rate-of-change of surface charge density ($\frac{dq_s}{dt}$). They are identical to the standard HSD D-dot ground plane sensors with the exception of shorter baseplates, which facilitates mounting on curved surfaces. The proximity of the output connector makes them slightly less accurate than the standard models for D-dot measurements. These sensors are passive devices and require no power. Fittings are provided to fill the interior of the sensor with a high dielectric strength gas, such as N_2 or SF_6 , for use in high field regions where internal arcing could become a problem.

PERTINENT EQUATION

$$I_o = A_{eq} \frac{dq_s}{dt}$$

or

$$V_o = R A_{eq} \frac{dq_s}{dt}$$

where

I_o = sensor output (in amps)

V_o = sensor output (in volts)

R = load resistance (50 ohms)

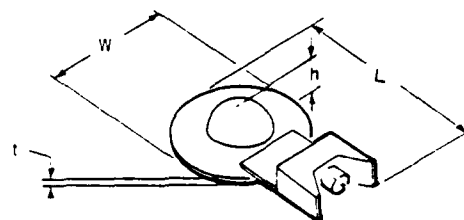
q_s = surface charge density (coul m^{-2})

A_{eq} = sensor area (in m^2)

SPECIFICATIONS

Parameter	HSD-S1	HSD-S3
$A_{eq} (m^2)$	1×10^{-1}	1×10^{-2}
Frequency Response (3 dB Point)	≥ 45 MHz	≥ 150 MHz
Risetime ($T_{r 10-90}$)	≤ 7.4 ns	≤ 2.3 ns
Maximum Output	5 kV	5 kV
Output Connector	GR874L-50 Ω	GR874L-50 Ω
Mass	1.6 kg	1.4 kg
Dimensions (cm)	<u>Radial</u> *	<u>Radial</u> *
L	36.8	22.1
W	28.2	13.7
h	10.4	3.6
t	0.3	0.2

* Only the Radial version of these sensors is available, designated as HSD-SN(R) where N=1 or 3. A standard HSD-N(A) can be used where a connector below the ground plane is needed



(Data and Specifications Subject to Change without Notice)

ORDERING INFORMATION

For Price, Availability, or Further Information, Contact

 **EG&G** WASHINGTON ANALYTICAL SERVICES CENTER, INC.
ELECTROMAGNETICS

2450 Alamo Avenue, S.E., P.O. Box 9100, Albuquerque, New Mexico 87119
phone (505) 243-2233, TWX No. 910-989-1684

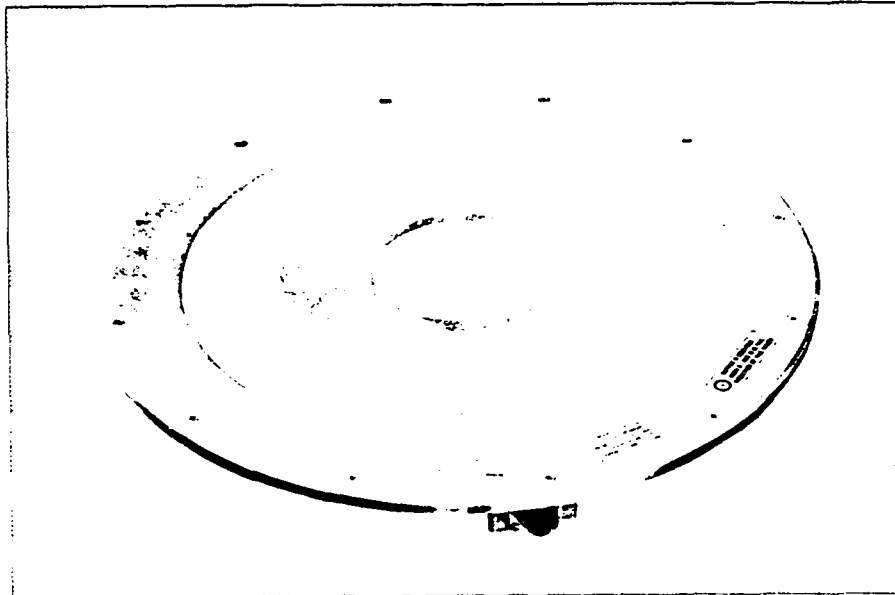

EG&G

WASHINGTON ANALYTICAL SERVICES CENTER, INC.

DATA SHEET 1116

September 1980

FPD \dot{D} SENSOR



The FPD (Flush Plate Dipole) sensor is mounted in a conducting surface (ground plane, aircraft wing, etc.) and used to measure the normal component of the displacement current ($d\bar{D}/dt$). It can also be used to measure the time rate-of-change of surface charge density ($d\dot{q}_s/dt$). (Data Sheet 1117 describes special \dot{q}_s sensors.) The FPD sensor is extremely useful in EMP or lightning fields of high electric stress or where minimum perturbation is required. A special version adapts to the wing tip of a C-130 aircraft used for in-flight lightning measurements. The sensor is a passive device and requires no power.

PERTINENT EQUATION

$$I_o = \bar{A}_{eq} \cdot \frac{d\bar{D}}{dt}$$

or

$$V_o = R A_{eq} \frac{dD}{dt} \cos \theta$$

where

 I_o = sensor output (in amps)

 V_o = sensor output (in volts)

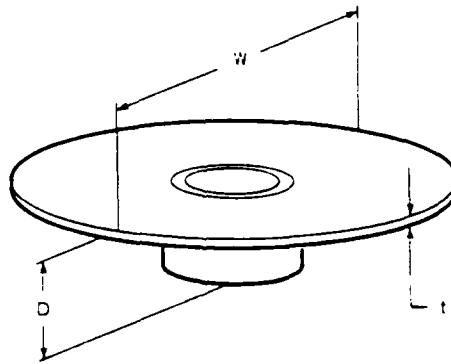
 R = sensor characteristic load impedance (50 ohms)

 A_{eq} = sensor equivalent area (in m^2)

 D = magnitude of electric displacement vector $\bar{D} = \epsilon_0 \bar{E}$, in Coul m^2
 θ = angle between E and vector normal to sensor ground plate

SPECIFICATIONS:

	FPD-1	FPD-2
$A_{eq} (m^2)$	1×10^{-2}	2×10^{-2}
Frequency Response (3 dB point)	> 350 MHz	> 70 MHz
Risetime (T_r 10-90)	< 1 ns	< 5 ns
Maximum Output	5 kV	5 kV
Output Connector	GR874L (50 ohms)	GR874L (50 ohms)
Mass	4 kg	2 kg
Dimensions (cm)		
W	43.2	28.3
t	1.0	0.5
D	5.4	5.2



(Data and Specifications Subject to Change without Notice)

ORDERING INFORMATION

For Price, Availability, or Further Information, Contact


EG&G WASHINGTON ANALYTICAL SERVICES CENTER, INC.
 ELECTROMAGNETICS

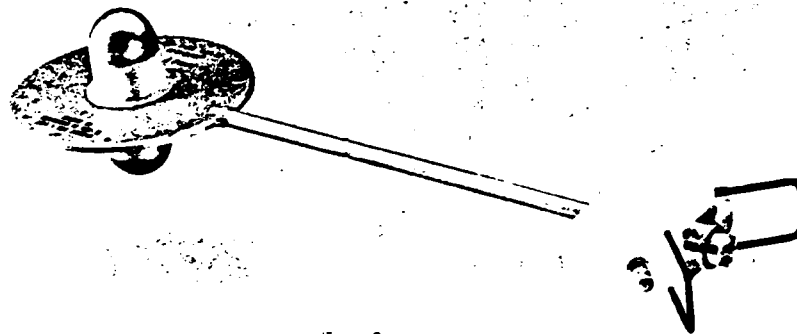
 2450 Alamo Avenue, S.E., P.O. Box 9100, Albuquerque, New Mexico 87119
 phone (505) 243-2233, TWX No. 910-989-1684


EG&G

WASHINGTON ANALYTICAL SERVICES CENTER, INC.

 DATA SHEET 1118
 September 1987

ACD \dot{D} SENSOR (Free Field)



The free - field ACD (Asymptotic Conical Dipole) sensors are used to measure a single component of the displacement current ($d\vec{D}/dt$). The asymptotic cone design exhibits less capacitance than the HSD design and extends the upper frequency limit for the same value of equivalent area (A_{eq}). EG&G has developed a shape for the sensing elements which optimizes the bandwidth and pulse response of these sensors.

PERTINENT EQUATION

$$I_O = \vec{A}_{eq} \cdot \frac{d\vec{D}}{dt}$$

or
$$V_O = R A_{eq} \frac{dD}{dt} \cos \theta$$

where

I_O = sensor output (in amps)

V_O = sensor output (in volts)

R = sensor characteristic load impedance (100 ohms)

A_{eq} = sensor equivalent area (in m^2)

D = magnitude of electric displacement vector ($\vec{D} = \epsilon_0 \vec{E}$, in $Coul.m^2$)

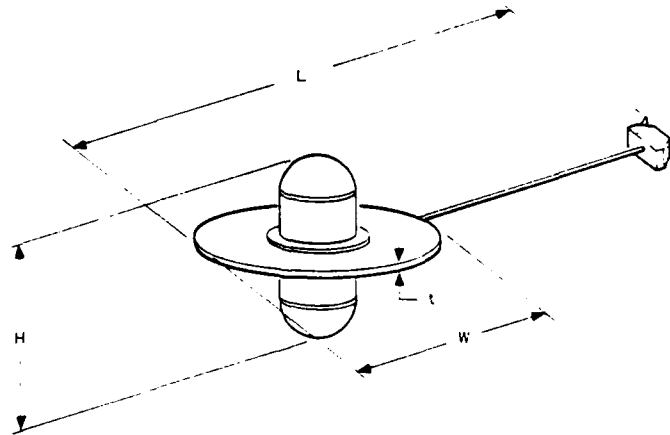
θ = angle between E and vector normal to sensor ground plate

SPECIFICATIONS

	ACD-2(R)	ACD-4(R)	ACD-7(R)	ACD-10(R)
$A_{eq} (m^2)$	1×10^{-4}	1×10^{-2}	1×10^{-3}	1×10^{-1}
Frequency Response (3 dB point)	>10 GHz	>1.0 GHz	>3.3 GHz	>330 MHz
Risetime (T_{r10-90})	<0.033 ns	<0.33 ns	<0.11 ns	<1.1 ns
Maximum Output	125 V	5 kV**	250 V	5 kV**
Output Connector	Dual SMA	TCC-100 Ω *	Dual SMA	TCC-100 Ω *
Mass (nominal)	30 g	780 g	120 g	2.6 kg
Dimensions (cm)				
L	11.12	49.53	18.50	62.20
W	2.54	13.97	6.50	28.20
H	1.12	9.96	3.30	31.12
t	0.20	0.32	0.25	0.64

* 100-ohm Twinaxial Connector (EG&G Data Sheet 1340)

** when filled with SF₆; 2 kV otherwise



(Data and Specifications Subject to Change without Notice)

ORDERING INFORMATION

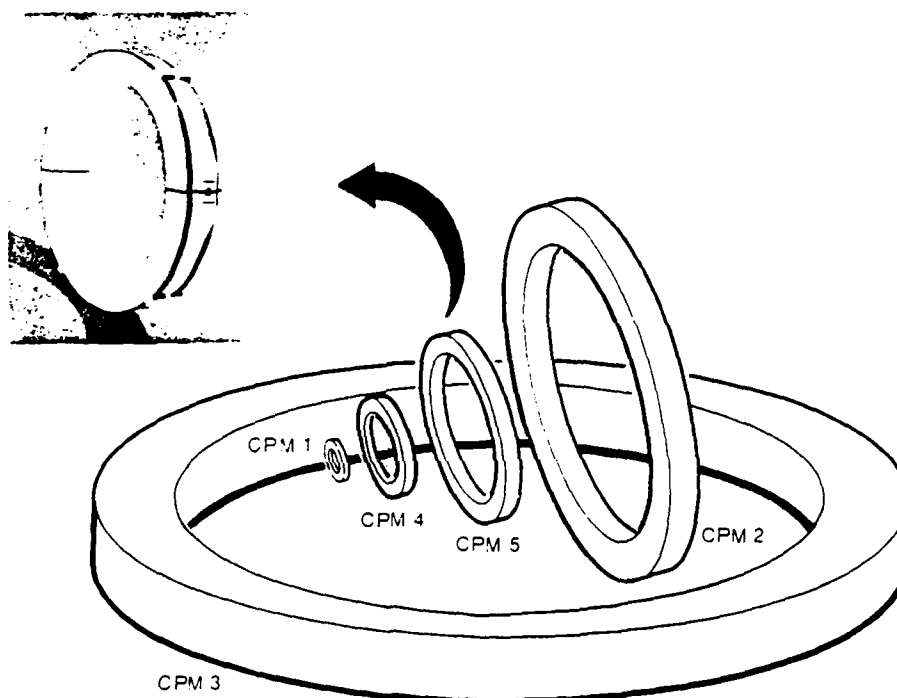
For Price, Availability, or Further Information, Contact



EG&G WASHINGTON ANALYTICAL SERVICES CENTER, INC.
ELECTROMAGNETICS

2450 Alamo Avenue, S.E., P.O. Box 9100, Albuquerque, New Mexico 87119
FAX No. (505) 243-1021, phone (505) 243-2233, TWX No. 910-989-1684

CPM I SENSORS



The CPM (Circular Parallel Mutual Inductance) sensor is an inductive current probe used to measure the time rate-of-change of the total current through its aperture. It is designed for rugged field use in high EMP environments, and it is split into two halves to facilitate installation and transportation. The halves are held together by a circumferential belt having a quick release clasp. The available sensor apertures range from 10 to 200 cm allowing current measurements on individual signal cables or complete test objects like a missile.

PERTINENT EQUATION

$$V_o = M \frac{dI}{dt} = \text{sensor output (in volts)}$$

where

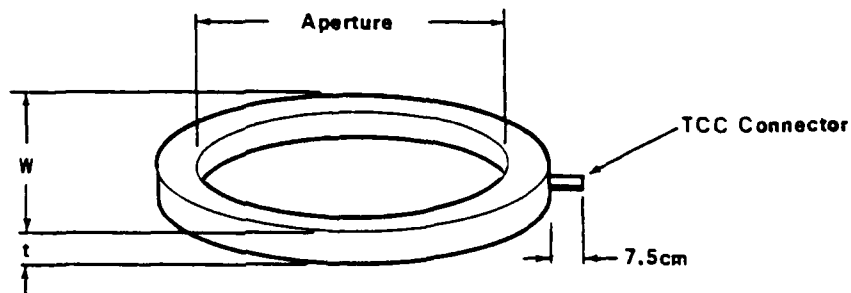
M = mutual inductance (in Henries)

I = total current through aperture (in Amps)

SPECIFICATIONS

Model (CPM-X)	M (henries)	No. of Turns	Frequency Response (upper 3 dB pt)	Risetime (T _r 10-90)	Maximum Output	Output Connector	Mass (kg)	W (cm)	t (cm)	Aperture Dia. (cm)
1	1×10^{-3}	2	700 MHz	0.5 ns	5 kV	TCC*	2.3 kg	20.3	8.2	10
2	1×10^{-8}	4	350 MHz	1 ns	5 kV	TCC*	68 kg	117.3	15.5	100
3	1×10^{-8}	4	350 MHz	1 ns	5 kV	TCC*	136 kg	224.5	20	200
4	1×10^{-8}	2	700 MHz	0.5 ns	5 kV	TCC*	4.3 kg	32	9.9	20
5	1×10^{-8}	4	350 MHz	1 ns	5 kV	TCC*	10 kg	63.5	10.9	50
6	1×10^{-9}	2	350 MHz	1 ns	5 kV	TCC*	118 kg	212.7	6.4	200

*Ref. DATA SHEET 1340



(Data and Specifications Subject to Change without Notice)

ORDERING INFORMATION:

For Price, Availability, or Further Information, Contact

EG&G WASHINGTON ANALYTICAL SERVICES CENTER, INC.
ELECTROMAGNETICS

2450 Alamo Avenue, S.E., P.O. Box 9100, Albuquerque, New Mexico 87119
phone (505) 243-2233, TWX No. 910-989-1684

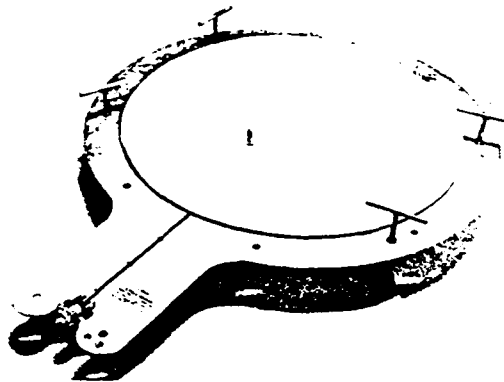
**EG&G**

WASHINGTON ANALYTICAL SERVICES CENTER, INC.

DATA SHEET 1140

December 1975

PPD E-FIELD SENSORS



The PPD E-field Sensor (Parallel Plate Dipole, Model 1, 2, and 3) is used to measure the strength of E-fields. While Models 1 and 3 are placed on the ground plane and measure the E-fields normal to the ground plane, Model 2 is used to measure fields above a ground plane or in free space.

The sensor is housed in a fiberglass radome that provides protection and can contain gas, such as SF_6 , which is used to enhance the voltage standoff capability.

Model 2 is available with a radial output only while Models 1 and 3 are configured for both axial and radial applications. The sensor is a passive device and does not require a source of power.

PERTINENT EQUATION

$$V_o = Eh \left(\frac{R_L}{R_L + R_S} \right) - \frac{1}{(R_L - R_S)} C \int_0^t V_o dt,$$

where

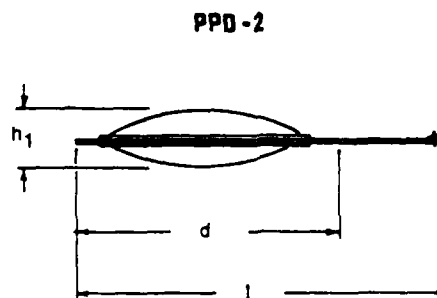
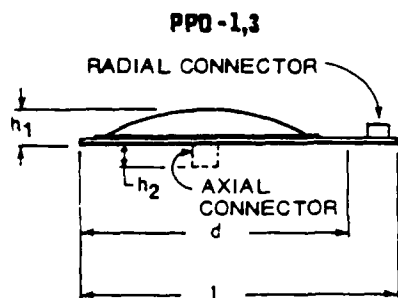
- V_o = sensor output (in volts),
- E = field strength (in volts per meter),
- h = equivalent height (in meters),
- R_L = load resistance (50 ohms or 100 ohms)
- R_S = sensing resistance (in ohms)
- C = sensor capacity (in farads)
- t = time (in seconds)

SPECIFICATIONS

Parameter	PPD-1	PPD-2	PPD-3
Equivalent Height (m)	0.01	0.01 (each side)	0.01
Capacitance (F)	1×10^{-9}	2×10^{-10}	2×10^{-2}
Risetime (ns)	< 1	≤ 1	≤ 1
Frequency Response (3 dB Point)	~ 350 MHz	~ 350 MHz	~ 350 MHz
Peak Field Strength (kV/m)			
Rs = 5 kohms	-	200	200
10 kohms	200	-	-
50 kohms	-	500	500
100 kohms	1000	-	-
500 kohms	-	1000	1000
Output Connector	GR874L, 50 Ω	TCC-2A, $< 100\Omega$	GR874L, 50 Ω
Mass (kg)	57	36	12
Dimensions (m)	<u>Axial*</u> <u>Radial*</u>	<u>Radial*</u>	<u>Axial*</u> <u>Radial*</u>
d	1.42 1.42	0.77	0.77 0.77
l	1.42 1.70	1.04	0.77 1.04
h ₁	0.17 0.17	0.22	0.10 0.11
h ₂	0.02 -	-	0.02 -

* Axial or Radial Output Specified by Designations
PPD-N(A) and PPD-N(R), Respectively where N=1, 2, or 3.

**See Data Sheet 1340



ORDERING INFORMATION:

For Price, Availability, or Further Information, Contact

EG&G WASHINGTON ANALYTICAL SERVICES CENTER, INC.
ELECTROMAGNETICS

2450 Alamo Avenue, S.E., P.O. Box 9100, Albuquerque, New Mexico 87119
phone (505) 243-2233, TWX No. 910-989-1684

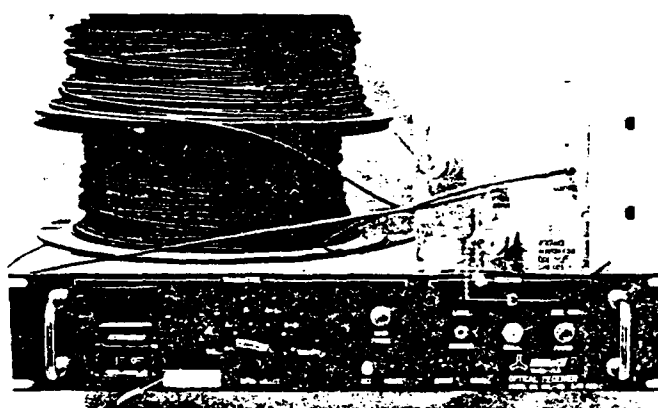


WASHINGTON ANALYTICAL SERVICES CENTER, INC.

DATA SHEET 1223

January 1984

ODL-5B REMOTE CONTROLLED WIDEBAND OPTICAL DATA LINK



The ODL-5B fiber optic data link provides a nonconducting telemetry path for wideband, bipolar data originating in an isolated test environment. Fiber optics data links are well suited for penetrating electromagnetic shields or maintaining electric isolation of a test object during EMP or electrical testing.

The data link consists of a battery-powered transmitter hardened to operate in EMP fields up to 100 kV m, a low-loss 100-meter fiber link, and a receiver powered by either 115 V, 50 60 Hz or 220V, 50 60 Hz. The emitting source is a LED which provides long term stability and reliability. The receiver output impedance is 50 ohms, and the system has a gain of -20dB. Signal input can be either 50 ohms unbalanced or 100 ohms balanced with a built-in DMB-1 balun (Data Sheet 1300) to transform the balanced input for data telemetry. The ODL-5 transmitter can also be supplied with an internal active integrator (Data Sheet 1315), or this option is field upgradable. The transmitter contains an internal remotely controlled attenuator providing 0 to 79 dB of input attenuation. An internal bipolar calibration pulse generator for system test is provided in the transmitter.

The transmitter is remotely controlled by a second fiber optic cable. Control is provided both through receiver front panel mounted switches and through an IEEE 488 bus computer interface. Different parallel computer interfaces, e.g., DEC DR11-C or DRV11, may also be provided as an option if so desired.

The transmitter battery pack is externally removable and is identical to the MDL-3 transmitter battery pack. Charging is accomplished by either of two battery chargers provided in the receiver. The battery pack design provides protection against deep discharge, overvoltage and short-circuit of the batteries, and a minimum of 4 hours continuous operation. To further maximize battery life, the transmitter automatically switches to a low-current drain stand-by mode whenever the transmitter power switch on the receiver is placed in the OFF position or whenever the receiver AC power is turned off.

SPECIFICATIONS

Electrical Characteristics:

System Gain	20 dB (nominal)
Dynamic Range @ 10 MHz	30 dB (1 -dB gain compression to tangential noise) 42 dB (peak-to-peak signal to RMS noise)
Bandwidth (3-dB Points)	Lower Limit: 10 kHz Upper Limit: 130 MHz
Bandpass Ripple	±1 dB from 120 kHz to 100 MHz
Video Input Sensitivity	±1.3 mV peak
Signal Attenuation	Remotely controlled, 0-79 dB, 1-dB steps
Transmitter Input Impedance	50 ohms unbalanced (GR 874) and 100 ohms balanced (TCT)
Balun Insertion Loss	3dB (see Data Sheet 1300)
Peak Signal Level (With Maximum Attenuation)	Linear Operation 50Ω Input: 350V 100Ω Input: 700V
Risetime (Nominal)	Transmitter Protection: 0.5 watt continuous 50Ω Input: 500V peak, 50 ns single pulse 100Ω Input: 1 kV peak, 50 ns single pulse
Transmitter Power	3 nanoseconds 4-hour (continuous operation without IA-200) externally-removable battery with internal protection, rechargeable by receiver supply
Calibration Pulse	±100 mV, bipolar pulse, 200 ns width at 10 kpps rate
Transmitter Control	From receiver front panel switches and IEEE-488 Buss computer interface - input selector (OFF, CAL, A, B, A+I, B-I, 50Ω terminator) and attenuator
Receiver Output Impedance	50 ohms unbalanced (BNC)
Receiver Power	115 Vac, 50/60 Hz; 220 Vac, 50/60 Hz on request

Physical Characteristics:

Transmitter (cm)	27 high x 14 wide x 12.5 long; 3.4 kg w/Battery
Receiver (cm)	9 high x 48 wide x 41 long; 8 kg (standard 19-inch rack slide-mount chassis)
Fiber Optics Length	2 ea. 100 meters (single fiber, step index)

OPTIONS/ACCESSORIES AVAILABLE ON REQUEST

1. IA-200 Active Integrator (see Data Sheet 1315)
2. Controls Compatible with DEC DR11-C or DRV11 in place of IEEE-488 Bus Interface

(Data and Specifications Subject to Change Without Notice)

ORDERING INFORMATION:

For Price, Availability, or Further Information, Contact

**EG&G**WASHINGTON ANALYTICAL SERVICES CENTER, INC.
ELECTROMAGNETICS

2450 Alamo Avenue, S.E., P.O. Box 9100, Albuquerque, New Mexico 87119
phone (505) 243-2233, TWX No. 910-989-1684

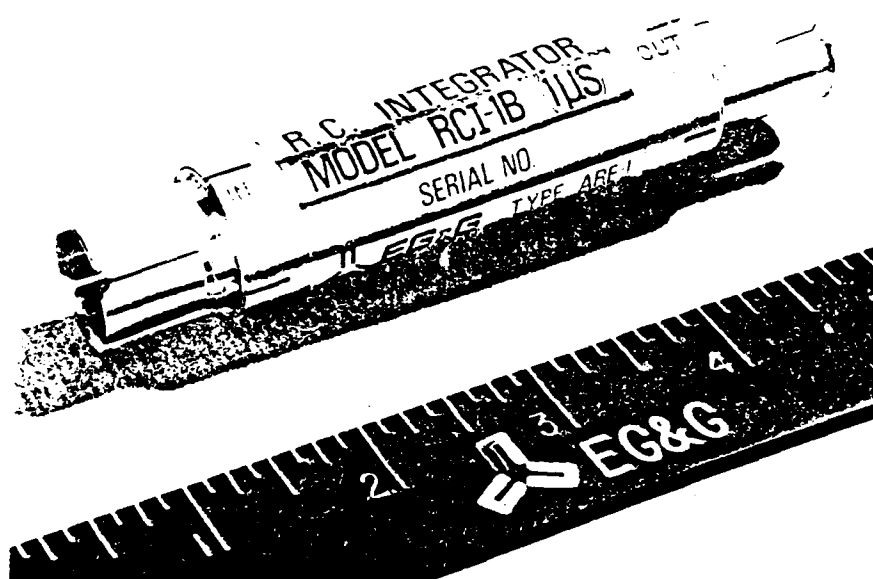


WASHINGTON ANALYTICAL SERVICES CENTER, INC.

DATA SHEET 1310

October 1975

RCI-1B PASSIVE INTEGRATOR



The RCI-1B Integrator is a passive resistor - capacitor integrator available with standard RC time constants of 1, 5, 10, or 100 microseconds.

The transfer function of the RCI-1B Integrator is:

$$\frac{V_{out}(S)}{V_{in}(S)} = \frac{1}{SRC + 1}$$

where $S = j\omega$ = Laplace operator. This transfer function is that of an integrator for sinusoidally varying voltages if the frequency is large compared to $1/(2\pi RC)$; or for transient voltages for times small compared to RC .

The load impedance connected to the output of the RCI-1B should have high input resistance and low input capacity.

SPECIFICATIONS

Input Impedance	50-ohms
Load Impedance	>1-megohm, <10 pF
Maximum Input Voltage	5 kV peak for 100 nsec. max.
Maximum CW Input Power	1-watt

Transfer Function Accuracy

1 μ sec	5% to 100 MHz 3 dB to 200 MHz
5 μ sec	5% to 75 MHz 3 dB to 150 MHz
10 μ sec	5% to 75 MHz 3 dB to 150 MHz
100 μ sec	5% to 20 MHz 3 dB to 40 MHz

Input and Output Connectors General Radio Type 874

(Data and Specifications Subject to Change without Notice)

ORDERING INFORMATION

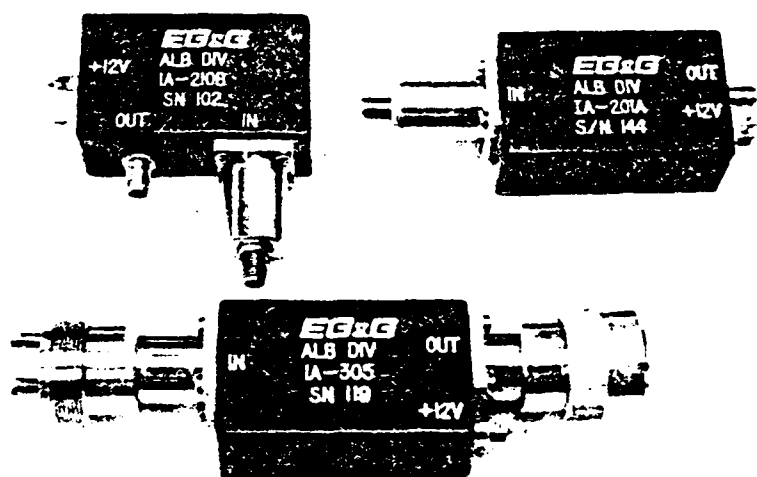
For Price, Availability, or Further Information, Contact



EG&G WASHINGTON ANALYTICAL SERVICES CENTER, INC.
ELECTROMAGNETICS

2450 Alamo Avenue, S.E., P.O. Box 9100, Albuquerque, New Mexico 87119
phone (505) 243-2233, TWX No. 910-989-1684

IA-200 and IA-300 ACTIVE INTEGRATORS



The EG&G Series IA-200 and IA-300 integrators consist of a passive resistor-capacitor integrator available with standard RC time constants of 1 or 10 microseconds followed by an active FET amplifier section to provide a high impedance load for the integrator and to provide a 50-ohm output impedance.

The Series IA-200 integrators (with SMA connectors) are designed for installation inside EG&G optical transmitter packages and use power from the transmitter battery pack. Integrators equipped with internal voltage regulator (when specified) may use either Tektronix or Hewlett Packard probe power (-15 Vac) to eliminate the need for an additional supply.

SPECIFICATIONS

Integration Time Constant:

IA201 or IA301

IA210 or IA310

 $1\mu s \pm 0.1\mu s$ $10\mu s \pm 1.0\mu s$

Bandwidth (see plot below)

 ± 1.0 dB of Ideal Integrator ± 1.0 dB of Integrator Equation ± 3 dB of Integrator Equation $1\mu s$ $10\mu s$

500 kHz-200 MHz

50 kHz-200 MHz

400 Hz-200 MHz

400 Hz-200 MHz

100 Hz-400 MHz

100 Hz-400 MHz

Insertion Loss:

 6.0 ± 0.5 dB

Input Impedance:

50 ohms nominal

Load Impedance:

50 ohms nominal

Input Power:

 -12 V ($\pm 10\%$); < 20 mA w/o internal regulator -15 - 30 V; 25 mA w/ internal regulator

Input Connector:

GR874 or BNC (IA-300); SMA (IA-200)

Output Connector:

GR874 or BNC (IA-300); SMA (IA-200)

Range:

Device is saturated when $V_{out} \geq -600$ mV

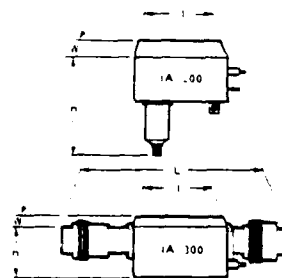
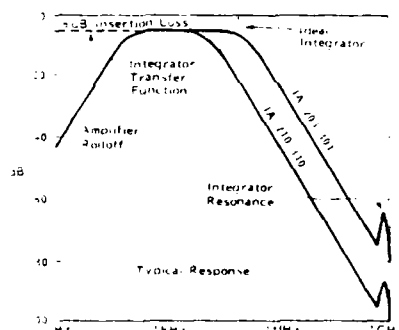
Dimensions (cm):

IA-200

IA-300

L	l	W	h
-	5.1	1.9	5.9
13.9	5.1	1.9	3.3

PERFORMANCE & EQUIVALENT CIRCUIT - The typical response curves and equivalent circuit for the $1\mu s$ and $10\mu s$ time constant integrators are shown below:



TRANSFER FUNCTION. The transfer function of the integrator is given by: $\frac{V_{out}(s)}{V_{in}(s)} = \frac{0.5}{sRC-1}$

where s = Laplace operator. The transfer function is that of an integrator for sinusoidally varying voltage if the frequency is large compared to $1/2\pi RC$, or for transient voltages for times small compared to RC . The 6dB loss is due to the amplifier gain of 0.5, which permits a low power supply current.

(Data and Specifications Subject to Change without notice)

ORDERING INFORMATION

For Price, Availability, or Further Information, Contact



EG&G

WASHINGTON ANALYTICAL SERVICES CENTER, INC.
ELECTROMAGNETICS

2450 Alamo Avenue, S.E., P.O. Box 9100, Albuquerque, New Mexico 87119
phone (505) 243-2233, TWX No. 910-989-1684

BIBLIOGRAPHY

BOOKS

C.A. Balanis, Antenna Theory: Analysis and Design. New York: Harper & Row, 1982.

Bell Laboratories, EMP Engineering and Design Principles. Whippany, New Jersey: Bell Laboratories Technical Publication Department, 1975.

J.A. Chalmers, Atmospheric Electricity. 2nd ed. Oxford: Pergamon Press, 1967.

R.E. Collin, Field Theory of Guided Waves. New York: McGraw-Hill Book Co., 1960.

EG&G Standard EMP and Lightning Instrumentation Catalog, EG&G Washington Analytical Services Center, Inc., Albuquerque, NM, January 1988.

L.B. Felsen, ed., Topics in Applied Physics, Vol. 10: Transient Electromagnetic Fields, Berlin, Germany: Springer-Verlag, 1976.

F.A. Fisher and J.A. Plumer, Lightning Protection of Aircraft. NASA Reference Publication 1008, NASA RP-1008, Washington, D.C.: Government Printing Office, October 1977.

T.J. Gallagher and A.J. Pearmain, High Voltage - Measurement, Testing and Design. Chichester, England: John Wiley & Sons, 1983.

H.B. Garrett and C.P. Pike, eds., Space Systems and Their Interactions with Earth's Space Environment. In Vol 71 of Progress in Astronautics and Aeronautics. New York: American Institute of Aeronautics and Astronautics, 1980.

R.H. Golde, Lightning Protection. New York: Chemical Publishing Co., Inc., 1975.

R.H. Golde, ed., Lightning. Vol. 1: The Physics of Lightning. New York: Academic Press, 1977.

R.H. Golde, ed., Lightning. Vol. 2: Lightning Protection. New York: Academic Press, 1977.

A. Greenwood, Electrical Transients in Power Systems. New York: John Wiley & Sons, 1971.

R.F. Harrington, Field Computation by Moment Methods. New York: MacMillan, 1968.

V. Hartel, Optoelectronics, Theory and Practice. New York: McGraw-Hill Book Co., 1978.

J.D. Jackson, Classical Electrodynamics. 2nd ed. New York: John Wiley & Sons, 1975.

E. Kamen, Introduction to Signals and Systems. New York: Macmillan Publishing Co., 1987.

H. Knoepfel, Pulsed High Magnetic Fields. New York: American Elsevier Publishing Co., 1970.

J.D. Kraus, Antennas, 2nd ed. New York: McGraw-Hill Book Co., 1988.

E. Kuffel and W.S. Zaengl, High Voltage Engineering - Fundamentals. Oxford: Pergamon Press, 1984.

K.S.H. Lee, ed., EMP Interaction: Principles, Techniques and Reference Data. New York: Hemisphere Press, 1986.

D.J. Malan, Physics of Lightning. London: English Universities Press, 1963.

E.K. Miller, ed., Time-Domain Measurements in Electromagnetics. New York: Van Nostrand Reinhold Company, 1986.

R. Morrison, Grounding and Shielding Techniques in Instrumentation. New York: John Wiley & Sons, 1986.

J.A. Stratton, Electromagnetic Theory. New York: McGraw-Hill Book Co., 1941.

W.L. Stutzman and G.A. Thiele, Antenna Theory and Design. New York: John Wiley & Sons, 1981.

M.A. Uman, Lightning. New York: McGraw-Hill, 1969.

P.L.E. Uslenghi, ed., Electromagnetic Scattering. New York: Academic Press, 1978.

L. Wahlin, Atmospheric Electrostatics. New York: John Wiley & Sons, 1986.

W.E. Waters, Electrical Induction from Distant Current Surges. Englewood Cliffs, NJ: Prentice-Hall, 1983.

PERIODICALS AND REPORTS

- E. Arvas and T.K. Sarkar, "TM Transmission Through Dielectric-Filled Slots in a Conducting Cylindrical Shell of Arbitrary Cross Section," IEEE Transactions on Electromagnetic Compatibility, Vol. EMC-29, May 1987.
- C.E. Baum, "Parameters for Some Electrically-Small Electromagnetic Sensors," Sensor and Simulation Note 38, Air Force Weapons Laboratory, Kirtland AFB, NM, March 1967.
- C.E. Baum, "An Equivalent-Charge Method for Defining Geometries of Dipole Antennas," Sensor and Simulation Note 72, Air Force Weapons Laboratory, Kirtland AFB, NM, January 1969.
- C.E. Baum, "The Singularity Expansion Method," in Topics in Applied Physics, Vol. 10: Transient Electromagnetic Fields, edited by L.B. Felsen. Berlin, Germany: Springer-Verlag, 1976.
- C.E. Baum, "Toward an Engineering Theory of Electromagnetic Scattering: The Singularity and Eigenmode Expansion Methods," in Electromagnetic Scattering, edited by P.L.E. Uslenghi, New York: Academic Press, 1978.
- C.E. Baum, E.L. Breen, J.C. Giles, J.P. O'Neill and G.D. Sower, "Sensors for Electromagnetic Pulse Measurements Both Inside and Away from Nuclear Source Regions," IEEE Transactions on Antennas and Propagation, AP-26, No. 1, January 1978 and IEEE Transactions on EMC, No. 1, February 1978.
- C.E. Baum, "EMP Simulators for Various Types of Nuclear EMP Environments: An Interim Categorization," IEEE Transactions on Antennas and Propagation, AP-26, No. 1, January 1978 and IEEE Transactions on EMC, No. 1, February 1978.
- C.E. Baum, E.L. Breen, J.P. O'Neill, C.B. Moore and G.D. Sower, "Electromagnetic Sensors for General Lightning Application," Proceedings of Lightning Technology Symposium, NASA Conference Publication 2128, FAA-RD-80-30, NASA Langley, Hampton, VA, April 22-24, 1980.
- C.E. Baum, "Simulation of Electromagnetic Aspects of Lightning" Proceedings of Lightning Technology Symposium, NASA Conference Publication 2128, FAA-RD-80-30, NASA Langley, Hampton, VA, April 22-24, 1980.

C.E. Baum, "Sensors for Measurement of Intense Electromagnetic Pulses," Proceedings of 3rd IEEE International Pulsed Power Conference, Albuquerque, NM, June 1981.

C.E. Baum, E.L. Breen, F.L. Pitts, G.D Sower and M.E. Thomas, "The Measurement of Lightning Environmental Parameters Related to Interaction with Electric Systems," IEEE Transaction on Electromagnetic Compatibility, EMC-24, No. 2, May 1982.

K. Berger, et al., "Parameters of Lightning Flashes," Electra, Vol. 80, 1975.

H.A. Bethe, "Theory of Diffraction by Small Holes," The Physical Review, Vol. 66, October 1944.

C.L. Blake and J.C. Corbin, "Electrical/Electromagnetic Concerns Associated with Advanced Composite Materials in Aerospace Systems," AGARD Conference Proceedings No. 283, AGARD CP-283, June 1980.

C.F. Boyce, "Protection of Telecommunication Systems," in Lightning. Vol. 2: Lightning Protection, ed. R.H. Golde, (New York: Academic Press, 1977).

R.M. Braza, "Experimental Comparison of Lightning Simulation Techniques to CV-580 Airborne Lightning Strike Measurements," Masters Thesis, AFIT/GE/ENG/87D-5, School of Engineering, Air Force Institute of Technology (AU), Wright-Patterson AFB, OH, December 1987.

R.M. Braza, R.J. Jost and J.L. Hebert, "Comparison of the Swept Frequency Continuous Wave, Current Pulse and Schock-Excitation Lightning Simulation Techniques," Proceedings of the 1988 International Aerospace and Ground Conference on Lightning and Static Electricity, Oklahoma City, OK, 18-22 April 1988.

C.E.R. Bruce and R.H. Golde, "The Lightning Discharge," Journal of Institution of Electrical Engineers, Part II, Vol. 88, 1941.

H. Burket, "Comparison of Electromagnetic Measurements on an Aircraft from Direct Lightning Attachment and Simulated Nuclear Electromagnetic Pulse," Proceedings of 1986 International Aerospace and Ground Conference on Lightning and Static Electricity, Dayton, OH, June 24-26, 1986.

C.M. Butler and K.R. Umashankar, "Electromagnetic Excitation of a Wire through an Aperture-Perforated, Conducting Screen," IEEE Transactions on Antennas and Propagation, Vol. AP-24, July 1976.

C.M. Butler, Y. Rahmat-Samii and R. Mittra, "Electromagnetic Penetration Through Apertures in Conducting Surfaces," IEEE Transactions on Antennas and Propagation, Vol. AP-26, January 1978.

W.G. Butters and D.W. Clifford, "Lightning Induced Electrical Transient Testing on Aircraft Wiring System," Proceedings of the 1977 IEEE International Symposium on Electromagnetic Compatibility, Seattle, WA, 2-4 August, 1977.

W.G. Butters, D.W. Clifford, K.P. Murphy and K.S. Zeisel, "Assessment of Lightning Simulation Test Techniques," by McDonnell Aircraft Company. Air Force Wright Aeronautical Laboratories Technical Report, AFWAL-TR-81-3075, Part 1, Wright-Patterson AFB, OH, October 1981.

R.L. Carney and G.J. Von Bokern, Final Report, Atmospheric Electricity Hazards Protection Program, Part V. Design Guide for Air Vehicles, by Boeing Military Airplane Company. Air Force Wright Aeronautical Laboratory Technical Report, AFWAL-TR-87-3025, Part IV, Wright-Patterson AFB, OH, June 1987.

N. Cianos and E.T. Pierce, "A Ground Lightning Environment for Engineering Usage," Stanford Research Institute Technical Report 1, August 1972.

D.W. Clifford and K.S. Zeisel, "Evaluation of Lightning-Induced Transients in Aircraft Using High-Voltage Shock Excitation Techniques," Proceedings of the 1979 IEEE International Symposium on Electromagnetic Compatibility, San Diego, CA, October 9-11, 1979.

D.W. Clifford, "Aircraft Mishap Experience From Atmospheric Electricity Hazards," AGARD Lecture Series No. 110, Atmospheric Electricity-Aircraft Interaction, AGARD LS-110, June 1980.

D.W. Clifford and H.W. Kasemir, "Triggered Lightning," IEEE Transaction on Electromagnetic Compatibility, EMC-24, No. 2, May 1982.

D.W. Clifford, K.E. Crouch and E.H. Schulte, "Lightning Simulation and Testing," IEEE Transaction on Electromagnetic Compatibility, EMC-24, No. 2, May 1982.

D.H. Colvin, "Computationally Efficient Method of Calculations Involving Lumped-Parameter Transmission-Line Models," IEEE Transactions on Electromagnetic Compatibility, Vol. EMC-27, February 1985.

J. Corbin, "Protection/Hardening of Aircraft Electronic Systems Against the Indirect Effects of Lightning," Federal Aviation Administration - Florida Institute of Technology Workshop on Grounding and Lightning Technology, FAA Report No. FAA-RD-79-6, Melbourne, FL, March 6-8, 1979.

J. Corbin, "An Overview of the Electrical/Electromagnetic Impact of Advanced Composite Materials on Aircraft Design," from A Compendium of Lightning Effects on Future Aircraft Electronic Systems, N. Rasch, ed. Department of Transportation, Federal Aviation Administration, Report No. DOT/FAA/CT-82/30, February 1982.

J.C. Corbin, "Lightning Interaction with USAF Aircraft," Proceedings of 1983 International Aerospace and Ground Conference on Lightning and Static Electricity, Fort Worth, TX, June 21-23, 1983.

J.C. Corbin, "The Risk Factor in Aircraft Lightning Protection," Proceedings of 1984 International Aerospace and Ground Conference on Lightning and Static Electricity, Orlando, FL, June 26-28, 1984.

P.B. Corn, "Lightning as a Hazard to Aviation," Proceedings of American Meteorological Society's 11th Conference on Severe Local Storms, Kansas City, MO, October 2-5, 1979.

K.E. Crouch and J.A. Plumer, "Improved Test Methods for Determining Lightning-Induced Voltages in Aircraft," by Lightning Technologies, Inc., National Aeronautics and Space Administration, Contractor Report NASA CR-3329, September, 1980.

A.S. Dennis and E.T. Pierce, "The Return Stroke of the Lightning Flash to Earth as a Source of VLF Atmospherics," Radio Science, Journal of Research of the National Bureau of Standards, 68D, 1964.

J. Eckert, "RFI and the Black Hawks," EMC Technology & Interference Control News, Vol. 7, No. 1, Jan-Feb 1988.

F.S. Edwards, A.S. Husbands and F.R. Perry, "The Development and Design of High-Voltage Impulse Generators," Proceedings of the IEE, Vol. 98, Part I, No. 111, May 1951.

F. Eriksen, T. Rudolph and R. Peralá, "Atmospheric Electricity Hazards Analytical Model Development and Application, Vol. III: Electromagnetic Coupling Modeling of the Lightning/Aircraft Interaction Event," by Electro Magnetic Applications, Inc. Air Force Wright Aeronautical Laboratory Technical Report, AFWAL-TR-81-3084, Volume III, Wright-Patterson AFB, OH, August 1981.

A. Eriksson, "Lightning and Tall Structures," Transactions of South African Institute of Electrical Engineers, Vol. 69, Pt. 8, August, 1978.

Federal Aviation Administration. "Protection of Aircraft Fuel Systems Against Fuel Vapor Ignition Due to Lightning," FAA Advisory Circular AC 20-53A, 1983.

B. Fisher and J. Plumer, "Lightning Attachment Patterns and Flight Conditions Experienced by the NASA F-106B Airplane," Proceedings of 1983 International Aerospace and Ground Conference on Lightning and Static Electricity, Fort Worth, TX, June 21-23, 1983.

B. Fisher, P. Brown and J. Plumer, "Summary of NASA Storm Hazards Lightning Research, 1980-1985," Proceedings of 1986 International Aerospace and Ground Conference on Lightning and Static Electricity, Dayton, OH, June 24-26, 1986.

F.A. Fisher, "Analysis and Calculations of Lightning Interactions with Aircraft Electrical Circuits," by General Electric Company, Air Force Wright Aeronautical Laboratory Technical Report, AFFDL-TR-78-106, Wright-Patterson AFB, OH, August 1978.

E. Garbagnati and G. Lopipard, "Lightning Parameters - Results of 10 Years of Systematic Investigation in Italy," Proceedings of 1982 International Aerospace and Ground Conference on Lightning and Static Electricity, Oxford, England, March 24-26, 1982.

H. Garrett, "Spacecraft Charging: A Review," in Space Systems and Their Interactions with Earth's Space Environment, Edited by H. Garrett and C. Pike, Progress in Astronautics and Aeronautics, Vol 71, pp. 167-226, 1980.

W.P. Gerren, "Calibration of C-130 Lightning Characterization Sensors," by Boeing Military Airplane Company. Air Force Wright Aeronautical Laboratories Technical Report, AFWAL-TR-82-3095, Wright-Patterson AFB, OH, December 1982.

R.H. Golde, "The Frequency of Occurrence and the Distribution of Lightning Flashes to Transmission Lines," Transactions of the American Institute of Electrical Engineers, Vol 64, 1945.

R.H. Golde, "Lightning Surges on Overhead Distribution Lines Caused by Indirect and Direct Lightning Strokes," Transactions of the American Institute of Electrical Engineers, Vol 73, Part III-A, June 1954.

S.B. Griscom, R.W. Caswell, R.E. Graham, H.R. McNutt, R.H. Schlomann and J.K Thorton, "Five-Year Field Investigation of Lightning Effects on Transmission Lines," IEEE Transactions on Power Apparatus and Systems, PAS-84, No. 4, April 1965.

E. Hansson and S.K. Waldorf, "An Eight-Year Investigation of Lightning Currents and Preventive Lightning Protection on a Transmission System," Transactions of the American Institute of Electrical Engineers, Vol. 63, May 1944.

J.L. Hebert, "UH-60A Black Hawk Swept Frequency Continuous Wave Lightning EMP Test Plan," Internal Report, Air Force Wright Aeronautical Laboratories, Atmospheric Electricity Hazards Group, AFWAL/FIESL, Wright-Patterson AFB, OH, 12 September 1985.

J.L. Hebert, J.S. Reazer, J.G. Schneider, M.D. Risley, and A.V. Serrano, "Current Levels and Distributions on an Aircraft During Ground Simulation Tests and In-Flight Lightning Attachments," Proceedings of 1986 International Aerospace and Ground Conference on Lightning and Static Electricity, Dayton, OH, June 24-26, 1986.

J.L. Hebert and C. Sanchez-Castro, Implementation of a Three-Dimensional Finite Difference Electromagnetic Code for Analysis of Lightning Interaction with a FAA CV-580 Aircraft," Air Force Wright Aeronautical Laboratory Technical Report, AFWAL-TR-86-3008, Wright-Patterson AFB, OH, May 1987.

J.L. Hebert, Personal Communications, June, 1987 - July, 1988.

R. Holland, "THREDE: A Free-Field EMP Coupling and Scattering Code," IEEE Transactions on Nuclear Science, Vol. NS-24, December 1977.

R. Holland, L. Simpson and R.H. St. John, "Code Optimization for Solving Large 3D EMP Problems," IEEE Transactions on Nuclear Science, Vol. NS-26, No. 6, December 1979.

IEEE Power Engineering Society, Substations Committee, Transmission Substation Subcommittee. "Bibliography of Publications Pertaining to Lightning Protection," IEEE Transactions on Power Apparatus and Systems, PAS-94, No. 4, July/August, 1975.

T. James and J. Phillpott, "Simulation of Lightning Strikes to Aircraft," Culham Laboratory Report CLM-R111, Abingdon, Oxfordshire, U.K. 1971.

R.J. Jost, F.G. Tomko and J.L. Hebert, "Initial Validation of GEMACS for Aircraft Lightning Interaction Analysis," Proceedings of 1987 IEEE International Symposium on Electromagnetic Compatibility, Atlanta, GA, August 25-27, 1987.

R.J. Jost and J.L. Hebert, "Characterization of Configuration Effects on Lightning Simulation/Qualification Testing," Proceedings of the 1988 International Aerospace and Ground Conference on Lightning and Static Electricity, Oklahoma City, OK, April, 18-22 1988.

R.J. Jost, M.P. Hebert and J.L. Hebert, "An Assessment of Analytical Methods and Lightning Simulation Test Techniques Used in Lightning Qualification and Surveillance Testing," Proceedings of the 1988 International Aerospace and Ground Conference on Lightning and Static Electricity, Oklahoma City, OK, April, 18-22 1988.

G. Ketterling, Final Report, Atmospheric Electricity Hazards Protection Program, Part V. Qualification and Surveillance Test and Analysis Procedures, by Boeing Military Airplane Company. Air Force Wright Aeronautical Laboratory Technical Report, AFWAL-TR-87-3025, Part V, Wright-Patterson AFB, OH, June 1987.

K.S. Kunz, H.G. Hudson and J.K. Breakall "A Shielding-Effectiveness Characterization for Highly Resonant Structures Applicable to System Design," IEEE Transactions on Electromagnetic Compatibility, Vol. EMC-28, February 1986.

K.S. Kunz and H.G. Hudson, "Experimental Validation of Time-Domain Three-Dimensional Finite-Difference Techniques for Predicting Interior Coupling Responses," IEEE Transactions on Electromagnetic Compatibility, Vol. EMC-28, February 1986.

J.E. Lee, W.G. Butters and R.J. Lauber, "Laboratory Simulation of Near-by Lightning Induced Electrical Transients," FAA Report No. FAA-RD-79-6, Federal Aviation Administration - Florida Institute of Technology Workshop on Grounding and Lightning Technology, Melbourne, FL, March 6-8, 1979.

J.E. Lenz, D.W. Clifford and W.G. Butters, "Experimental Resolution of System Resonances Produced by Simulated Lightning Excitation," Proceedings of Lightning Technology Symposium, NASA Langley, NASA Conference Publication 2128, FAA-RD-80-30, April 22-24, 1980.

R.W. Leonard and D.R. Mulville, "Current and Projected Use of Carbon Composites in United States Aircraft," AGARD Conference Proceedings No. 283, AGARD CP-283, June 1980.

P.F. Little, A.W. Hanson and B.J.C. Burrows, "Test Techniques for Simulating Lightning Strikes to Carbon (Graphite) Fibre Composite Structures," Federal Aviation Administration - Florida Institute of Technology Workshop on Grounding and Lightning Technology, FAA Report No. FAA-RD-79-6, Melbourne, FL, March 6-8, 1979.

T.K. Liu, K.S.H. Lee and L. Marin, "Broadband Responses of Deliberate Aircraft Antennas, Part I," Interaction Notes, Note 228, Air Force Weapons Laboratory, Kirtland AFB, NM, May 1975.

K.J. Lloyd, J.A. Plumer and L.C. Walko, "Measurements and Analysis of Lightning-Induced Voltages in Aircraft Electrical Circuits," by General Electric. National Aeronautics and Space Administration, Contractor Report NASA CR-1744, February 1971.

D.S. Mabey, "Validation of GEMACS for Modeling Lightning-Induced Electromagnetic Fields," Masters Thesis, AFIT/GE/ENG/87D-39, School of Engineering, Air Force Institute of Technology (AU), Wright-Patterson AFB, OH, December 1987.

D.S. Mabey, R.J. Jost, J.L. Hebert and M.P. Hebert, "Validation of GEMACS for Prediction of Lightning-Induced Electromagnetic Fields," Proceedings of the 1988 International Aerospace and Ground Conference on Lightning and Static Electricity, Oklahoma City, OK, 18-22 April 1988.

D.L. Mangan and R.A. Perala, "SGEMP Low-Level Simulation of the FLTSATCOM," Mission Research Corp., AMRC-R-49, August, 1975.

V. Mazur, B. Fisher and J. Gerlach, "Conditions conducive to Lightning Striking an Aircraft in a Thunderstorm," Proceedings of 1983 International Aerospace and Ground Conference on Lightning and Static Electricity, Fort Worth, TX, June 21-23, 1983.

V. Mazur, L.H. Ruhnke, and T. Rudolph, "Effect of E-Field Mill Location on Accuracy of Electric Field Measurements with Instrumented Airplane," Proceedings of the 1986 International Aerospace and Ground Conference on Lightning and Static Electricity, Dayton, OH, June 24-26, 1986.

W. McCormick, K.J. Maxwell and R. Finch, "Analytical and Experimental Validation of the Lightning Transient Analysis Technique," by Technology Incorporated. Air Force Flight Dynamics Laboratory Technical Report, AFFDL-TR-78-47, Wright-Patterson AFB, OH, March 1978.

B.G. Melander, "Effects of Tower Characteristics on Lightning Arc Measurements," Proceedings of 1984 International Aerospace and Ground Conference on Lightning and Static Electricity, Orlando, FL, June 26-28, 1984.

B.G. Melander, "Atmospheric Electricity Hazards Threat Environment Definition," by Boeing Military Airplane Company. Air Force Wright Aeronautical Laboratory Technical Report, AFWAL-TR-85-3052, Wright-Patterson AFB, OH, August 1985.

D.E. Merewether, "Transient Currents Induced on a Metallic Body of Revolution by an Electromagnetic Pulse," IEEE Transactions on Electromagnetic Compatibility, Vol. EMC-13, May 1971.

E.K. Miller, "Some Computational Aspects of Transient Electromagnetics," Lawrence Livermore Laboratory, Report UCRL-51276, 1972. Also, Interaction Note 143, Air Force Weapons Laboratory, Kirtland AFB, NM, September 1972.

E.K. Miller and A.J. Poggio, "Moment Method Techniques in Electromagnetics from an Applications Viewpoint," in Electromagnetic Scattering, edited by P.L.E. Uslenghi, New York: Academic Press, 1978.

R. Mittra, "Integral Equation Method for Transient Scattering," in Topics in Applied Physics, Vol. 10: Transient Electromagnetic Fields, edited by L.B. Felsen. Berlin, Germany: Springer-Verlag, 1976.

J.E. Nanevicz, "Static Charging Effects on Avionic Systems," AGARD Lecture Series No. 110, Atmospheric Electricity-Aircraft Interaction, AGARD LS-110, June 1980.

J.L. O'Neil, "Analysis of Lightning Induced Magnetic Field Penetration Through Protective Metal Screens Using an Equivalent Dipole Moment Representation of an Array of Elliptic Apertures," Masters Thesis, AFIT/GE/ENG/86D-30, School of Engineering, Air Force Institute of Technology (AU), Wright-Patterson AFB, OH, December 1986.

C.R. Paul, "Applications of Multiconductor Transmission Line Theory to the Prediction of Cable Coupling, Vol. I, Multiconductor Transmission Line Theory," Rome Air Development Center Technical Report, RADC-TR-76-101, Vol. I, Griffiss AFB, NY, April 1976.

C.R. Paul, "Frequency Response of Multiconductor Transmission Lines Illuminated by an Electromagnetic Field," IEEE Transactions on Electromagnetic Compatibility, Vol. EMC-18, November, 1976.

R. Pengelly and A. Ezzeddine, "GaAs MMIC Module Tunes High Gain from 50 MHz to 4 GHz," Microwaves & RF, Vol. 27, No. 4, April 1988.

R.A. Perala and J.D. Robb, "The Experimental Verification of Circuit Modeling Techniques Used to Determine Lightning Current Distribution as Applied to the NASA Space Shuttle Vehicle," Proceedings of the 1977 IEEE International Symposium on Electromagnetic Compatibility, Seattle, WA, August 2-4, 1977, pp. 278-281.

R.A. Perala, T. Rudolph and F. Eriksen, "Electromagnetic Interaction of Lightning with Aircraft," IEEE Transaction on Electromagnetic Compatibility, EMC-24, No. 2, May 1982.

J.A. Plumer, "Data From the Airlines Lightning Strike Reporting Project," Proceedings of 1972 International Aerospace and Ground Conference on Lightning and Static Electricity, Las Vegas, NV, December 12-15, 1972.

J.A. Plumer, , F.A. Fisher and L.C. Walko, "Lightning Effects on the NASA F-8 Digital-Fly-By-Wire Airplane," by General Electric. National Aeronautics and Space Administration, Contractor Report NASA CR-2524, March 1975.

J.A. Plumer, "Further Thoughts on Location of Lightning Strike Zones on Aircraft," Supplement to NASA Conference Publication 2128, Proceedings of Lightning Technology Symposium, Hampton, VA, April 22-24, 1980.

J.R. Pressley and G.D. Sower, "Instrumentation for Time-Domain Measurements," in Time-Domain Measurements in Electromagnetics, edited by E.K. Miller, New York: Van Nostrand Reinhold Co., 1986.

N.O. Rasch, "User's Manual for AC-20-53A Protection of Aircraft Fuel Systems Against Fuel Vapor Ignition Due to Lightning," U.S. Dept. of Transportation, Report No. DOT/FAA/CT-83/3, October 1984.

N.O. Rasch and M.S. Glynn, "Lightning Interaction with Commercial Air Carrier Type Aircraft," Proceedings of 1984 International Aerospace and Ground Conference on Lightning and Static Electricity, Orlando, FL, June 26-28, 1984.

J. Reazer and A. Serrano, "Spatial and Temporal Description of Strikes to the FAA CV-580 Aircraft," Proceedings of 1986 International Aerospace and Ground Conference on Lightning and Static Electricity, Dayton, OH, June 24-26, 1986.

M.D. Rymes, T3DFD User's Manual: Final Technical Report, August 1979--June 1981. Prepared for Air Force Flight Dynamics Laboratory, Wright-Patterson AFB, OH. Contract number F33615-79-C-3412, by Electro Magnetic Applications, Inc., (EMA-81-r-24), Denver, CO, April 1981.

J. Robb, "Atmospheric Electricity Hazards Analytical Model Development and Application, Vol. II: Simulation of the Lightning/Aircraft Interaction Event," by Lightning and Transients Research Institute. Air Force Wright Aeronautical Laboratory Technical Report, AFWAL-TR-81-3084, Volume II, Wright-Patterson AFB, OH, August 1981.

S. Rusck, "Protection of Distribution Lines," in Lightning. Vol. 2: Lightning Protection, ed. R.H. Golde, New York: Academic Press, 1977.

P. Rustan and P. Axup, "Analysis of Lightning Current Measurements," Proceedings of 1984 International Aerospace and Ground Conference on Lightning and Static Electricity, Orlando, FL, June 26-28, 1984.

P. Rustan and J. Hebert, "Lightning Measurements on an Aircraft Flying at Low Altitude," Proceedings of the Second International Conference on the Aviation Weather System, June 19-21, 1985.

D.B. Seidel, D.G. Dudley and C.M. Butler, "Aperture Excitation of a Wire in a Rectangular Cavity," Interaction Note 345, Air Force Weapons Laboratory, Kirtland AFB, NM, June 1977.

T.B.A. Senior, "Electromagnetic Field Penetration into a Cylindrical Cavity," IEEE Transactions on Electromagnetic Compatibility, Vol. EMC-18, May 1976.

Society of Automotive Engineers. "Lightning Test Waveforms and Techniques for Aerospace Vehicles and Hardening," Report of the SAE Committee AE4L, June 20, 1978.

Society of Automotive Engineers, "Recommended Draft Advisory Circular, Protection of Aircraft Electrical/Electronic Systems Against the Indirect Effects of Lightning," Report of the SAE Committee AE4L, Report AE4L-87-3, February 4, 1987.

Spacecraft Charging Technology - 1976, NASA Technical Memorandum TM-X-73537, U.S Air Force Academy, Colorado Springs, CO, Oct 27-29, 1976.

Spacecraft Charging Technology - 1978, NASA Conference Publication 2071, U.S Air Force Academy, Colorado Springs, CO, Oct 31-Nov 2, 1978.

Spacecraft Charging Technology - 1980, NASA Conference Publication 2182, U.S Air Force Academy, Colorado Springs, CO, Nov 12-14, 1980.

Spacecraft Charging - Proceedings of the Air Force Geophysics Laboratory Workshop on Natural Charging of Large Structures in Near Earth Polar Orbit, AFGL-TR-83-0046, Sept 14-15, 1982.

Spacecraft Environmental Interaction Technology, NASA Conference Publication 2359, U.S Air Force Academy, Colorado Springs, CO, Oct 4-6, 1983.

Space Shuttle Program Lightning Protection Criteria Document, JSC-07636, Revision A, National Aeronautics and Space Administration, Lyndon B. Johnson Space Center, Houston, TX, November 4, 1975.

I.S. Stekolnikov, "The Parameters of the Lightning Discharge and the Calculation of the Current Waveform," Elektrichestvo. 3, 1941.

A. Taflove, "Application of the Finite-Difference Time-Domain Method to Sinusoidal Steady-State Electromagnetic Penetration Problems," IEEE Transactions on Electromagnetic Compatibility, Vol. EMC-22, No. 3, August, 1980.

C.D. Taylor, D.H. Lam and T.H. Shumpert, "Electromagnetic Pulse Scattering in Time-Varying Inhomogeneous Media," IEEE Transactions on Antennas and Propagation, Vol. AP-17, September 1969.

C.D. Taylor, "Electromagnetic Pulse Penetration Through Small Apertures," IEEE Transactions on Electromagnetic Compatibility, Vol. EMC-15, February 1973.

F.G. Tomko, "GEMACS Frequency Domain Analysis to Determine the Lightning Induced Electromagnetic Skin Current Distribution on Aircraft," Masters Thesis, AFIT/GE/ENG/86D-10 School of Engineering, Air Force Institute of Technology (AU), Wright-Patterson AFB, OH, December 1986.

M.A. Uman and E.P. Krider, "A Review of Natural Lighting: Experimental Data and Modeling," IEEE Transaction on Electromagnetic Compatibility, EMC-24, No. 2, May 1982.

K.R. Umashankar and C.E. Baum, "Transient Electromagnetic Characterization of Arbitrary Conducting Bodies Through an Aperture-Perforated Conducting Screen," Interaction Note 343, Air Force Weapons Laboratory, Kirtland AFB, NM, March 1978.

L.C. Walko, "A Test Technique for Measuring Lightning-Induced Voltages on Aircraft Electrical Circuits," by General Electric. National Aeronautics and Space Administration, Contractor Report NASA CR-2348, February 1974.

L.C. Walko and J.G. Schneider, "Full Scale Lightning Test Technique," Proceedings of Lightning Technology Symposium, NASA Conference Publication 2128, FAA-RD-80-30, NASA Langley, Hampton, VA, April 22-24, 1980.

L.C. Walko and J.L. Hebert, "Lightning Simulation Tests on FAA CV-580 Lightning Research Aircraft," Proceedings of the 10th International Aerospace and Ground Conference on Lightning and Static Electricity, Paris, France, 10-13 June 1985.

D.B. Whalen, "Comparison of Low Level Frequency Domain Lightning Simulation Test to Pulse Measurements," Proceedings of 1986 International Aerospace and Ground Conference on Lightning and Static Electricity, Dayton, OH, June 24-26, 1986, pp.9-1--9-8.

D.B. Whalen and M.M. Simpson, "Atmospheric Electricity Hazards Protection Part II: Assessment, Test and Analysis - F14A," by Boeing Military Airplane Company. Air Force Wright Aeronautical Laboratory Technical Report, AFWAL-TR-87-3025, Part II, Wright-Patterson AFB, OH, June 1987.

E.R. Whitehead, "Protection of Transmission Lines," in Lightning. Vol. 2: Lightning Protection, ed. R.H. Golde, New York: Academic Press, 1977.

C.F. Williford, "Comparison of Absorption and Radiation Boundary Conditions Using a Time-Domain Three-Dimensional Finite Difference Electromagnetic Computer Code," Masters Thesis, AFIT/GE/ENG/85D-53, School of Engineering, Air Force Institute of Technology (AU), Wright-Patterson AFB, OH, December 1985.

C.F. Williford, R.J. Jost and J.L. Hebert, "Comparison of Absorption and Radiation Boundary Conditions in 3DFD Code," Proceedings of 1986 International Aerospace and Ground Conference on Lightning and Static Electricity, Dayton, OH, June 24-26, 1986.

K.S. Yee, "Numerical Solution of Initial Boundary Value Problems Involving Maxwell's Equation in Isotropic Media," IEEE Transactions on Antennas and Propagation, AP-14, May 1966.

D.E. Young and L.D. Piszker, "The Use of CW Test and Analysis Techniques in Lightning Vulnerability Assessment of Aircraft Systems," Federal Aviation Administration - Georgia Institute of Technology Workshop on Grounding and Lightning Protection, FAA Report No. FAA-RD-78-83, Atlanta, GA, May 2-4, 1978.

Vita

Randy J. Jost [REDACTED]

[REDACTED]. After graduation from high school in 1974, he attended the United States Military Academy at West Point, New York. In 1976 he transferred to the University of Missouri-Columbia and received his B.S. in Electrical Engineering in 1978 and the MSEE in 1980.

From January 1981 to May 1982 he was a Lecturer for the Department of Electrical Engineering, University of Missouri-Columbia. After attending Officer Training School, he was commissioned a Second Lieutenant in the United States Air Force in August 1982, and returned to the University of Missouri for doctoral studies.

From June 1984 to May 1988 Captain Jost was an Instructor for the Department of Electrical and Computer Engineering at the Air Force Institute of Technology, Wright-Patterson AFB, Dayton, Ohio. Since May 1988, he has been assigned to the Air Force Wright Aeronautical Laboratories, located at Wright-Patterson AFB. He is married to the former [REDACTED], [REDACTED], and they have four children.